

**A Kinetic and Mechanistic Study into
the Substitution Behaviour of Platinum(II)
Polypyridyl Complexes with a Series of
Azole Ligands**

By

AISHATH SHAIRA

MASTER OF SCIENCE



School of Chemistry

Pietermaritzburg

January 2010

**A Kinetic and Mechanistic Study into the Substitution
Behaviour of Platinum(II) Polypyridyl Complexes
with a Series of Azole Ligands**

By

AISHATH SHAIRA

BSc. (Hons) (UKZN)

Submitted in fulfilment of the academic requirements for the degree of
Master of Science
in the Faculty of Science & Agriculture
School of Chemistry
University of KwaZulu-Natal
Pietermaritzburg
January 2010

"Patience is the companion of wisdom"

- St Augustine -

This work is dedicated to my loving:

Mom and Dad

*Thank you for all your endless and unconditional love, prayers, support and encouragement.
Without your wisdom and guidance I would never have been where I am today. Thank you both.*

DECLARATION

I A. Shaira declare that:

1. The research reported in this thesis, except where otherwise indicated, is my original research.
2. This thesis has not been submitted for any degree or examination at any other university.
3. This thesis does not contain other persons' data, pictures, graphs or other information, unless specifically acknowledged as being sourced from other persons.
4. This thesis does not contain other persons' writing, unless specifically acknowledged as being sourced from other researchers. Where other written sources have been quoted, then:
 - a. Their words have been re-written but the general information attributed to them has been referenced
 - b. Where their exact words have been used, then their writing has been placed in italics and inside quotation marks, and referenced.
5. This thesis does not contain text, graphics or tables copied and pasted from the Internet, unless specifically acknowledged, and the source being detailed in the thesis and in the References sections.

Signed: **A. Shaira)**

Date:

We hereby certify that this is correct, and as the candidates' supervisors we have approved this thesis for submission

Signed: **Professor D. Jaganyi (supervisor)**

Date:

Signed: **Dr. D. Reddy (co-supervisor)**

Date:

Declaration

The work presented in this thesis is carried out in the School of Chemistry, University of KwaZulu-Natal, Pietermaritzburg, under the supervision of Professor Deogratius Jaganyi, Dr. Desigan Reddy and Dr. Joanne Perils.

The research reported in this thesis, except where otherwise indicated, is the author's original research and has not been submitted for any degree of examination at any other university. Where use has been made of work of others, it is duly accredited in the text.

A. Shaira

As the candidate's supervisors we hereby certify that this statement is correct.

Professor D. Jaganyi
(Supervisor)

Dr. D. Reddy
(Co-Supervisor)

Dr. J. Perils
(Co-Supervisor)

School of Chemistry
University of KwaZulu-Natal

Table of Contents

| | |
|---|-----------|
| <i>Abstract</i> | i |
| <i>Acknowledgements</i> | iii |
| <i>Conference</i> | iv |
| <i>List of Abbreviations</i> | v |
| <i>List of Figures</i> | viii |
| <i>List of Schemes</i> | xii |
| <i>List of Tales</i> | xiii |
| | |
| Chapter 1: Introduction to Platinum Chemistry | 1 |
| | |
| 1.1. Overview | 1 |
| 1.2. The Anticancer Activity of Platinum Complexes | 3 |
| 1.2.1. The Mechanism of Action of Cisplatin | 4 |
| 1.2.2.1. Reactivity of Cisplatin | 6 |
| 1.2.2. Cisplatin Resistance | 10 |
| 1.3. Current Findings on Anticancer Platinum(II) drugs | 12 |
| 1.3.1. Mononuclear Platinum(II) Complexes | 12 |
| 1.3.2. Multinuclear Platinum(II) Complexes | 14 |
| 1.4. Current Research on Platinum(II) Terpy and Polypyridine Complexes | 14 |
| 1.4.1. Biological Importance | 15 |
| 1.4.1.1. DNA Intercalation | 15 |
| 1.4.1.2. Substitution of Platinum(II) Terpy with Biologically Active Nucleophiles | 19 |
| 1.4.2. Current Study on Substitution Reactions on Platinum(II) Polypyridyl and Platinum(II) Terpy complexes | 21 |
| 1.5. Aims of This Study | 25 |
| 1.6. References | 26 |
| | |
| Chapter 2: Substitution Reactions | 31 |
| | |
| 2.1. Introduction to substitution reactions | 31 |
| 2.2. Mechanisms of Substitution Reactions | 32 |
| 2.2.1. Dissociative Mechanism | 33 |
| 2.2.2. Dissociatively Activated Interchange Mechanism | 33 |

| | | |
|--|--|-----------|
| 2.2.3. | Associative Mechanism | 33 |
| 2.2.4. | Associatively Activated Interchange Mechanism | 35 |
| 2.3. | Substitution Reactions of Square Planar Complexes | 35 |
| 2.3.1. | Mechanisms of Substitution Reaction Kinetics | 36 |
| 2.4. | Factors Influencing the Rate of Substitution Reactions | 39 |
| 2.4.1. | The Spectator Ligand | 39 |
| 2.4.1.1. | The <i>trans</i> Effect | 39 |
| | (a) The π -Bonding Theory | 43 |
| | (b) The Polarization Theory | 44 |
| 2.4.1.2. | The Molecular Orbital Theory | 45 |
| | (a) The σ - <i>trans</i> effect | 45 |
| | (b) The π - <i>trans</i> effect | 47 |
| 2.4.2. | The Effect of the Entering Nucleophile | 48 |
| 2.4.3. | The <i>cis</i> -Effect | 52 |
| 2.4.4. | The Steric Effect | 53 |
| 2.4.5. | The Effect of Solvent | 55 |
| 2.4.6. | The Effect of Leaving Group | 56 |
| 2.5. | Dissociative Mechanisms of Square Planar Complexes | 58 |
| 2.6. | References | 60 |
| Chapter 3: Kinetic Theory and Associated Techniques | | 63 |
| 3.1. | Introduction | 63 |
| 3.2. | Rate Laws | 64 |
| 3.3. | Integrated Rate Expressions | 65 |
| 3.3.1. | Irreversible First-Order Reactions | 65 |
| 3.3.2. | Reversible First-Order Reactions | 66 |
| 3.3.3. | Consecutive First-Order Reactions | 68 |
| 3.3.4. | Irreversible Second-Order Reactions | 70 |
| 3.3.5. | Reversible Second-Order Reactions | 72 |
| 3.4. | Activation Parameters | 75 |
| 3.4.1. | The Arrhenius Equation | 75 |
| 3.4.2. | The Transition-State Theory | 76 |
| 3.5. | Techniques Associated with the Study of Chemical Kinetics | 78 |
| 3.5.1. | UV/Visible Spectrophotometry | 79 |
| 3.5.2. | Flow Methods | 83 |

| | |
|--|-----|
| 3.6. References | 85 |
| Chapter 4: Experimental: Synthesis and Kinetic Analysis of Platinum(II) Complexes | 87 |
| 4.1. Materials and Methodology | 87 |
| 4.2. Synthesis | 88 |
| 4.2.1. Synthesis of the Ligand Precursors and the Polypyridyl Ligand | 88 |
| 4.2.1.1. Synthesis of 3-acetylisquinoline | 88 |
| 4.2.1.2. Synthesis of 1-(3'-isoquinolyl)-3-(<i>o</i> -tolyl)-prop-2-en-1-one | 89 |
| 4.2.1.3. Synthesis of 4-(<i>o</i> -tolyl)-6-(3''-isoquinoyl)-2,2'-bipyridine | 90 |
| 4.2.2. Synthesis of Platinum(II) Complexes | 92 |
| 4.2.2.1. Synthesis of [Pt{4-(<i>o</i> -tolyl)-6-(3''-isoquinoyl)-2,2'-bipyridine}Cl]SbF ₆ | 92 |
| 4.2.2.2. Synthesis of Dichloro(1,5-cyclooctadiene) Platinum(II) | 93 |
| 4.2.2.3. Synthesis of 2,2':6',2''-terpyridine Platinum(II) (Pt1) | 94 |
| 4.2.2.4. Synthesis of [Pt{4'-(<i>o</i> -tolyl)terpy}MIm](CF ₃ SO ₃) ₂ | 95 |
| 4.3. Single Crystal X-ray Diffraction Studies | 96 |
| 4.3.1. Crystal Structure of 4-(<i>o</i> -tolyl)-6-(3''-isoquinoyl)-2,2'-bipyridine Ligand | 96 |
| 4.3.2. Crystal Structure of [Pt{4'-(<i>o</i> -tolyl)terpy}MIm](CF ₃ SO ₃) ₂ | 97 |
| 4.4. Instrumentation and Physical Measurements | 101 |
| 4.4.1. Characterisation | 101 |
| 4.4.2. Computational Modelling | 102 |
| 4.5. Kinetic Analyses | 102 |
| 4.5.1. Preparation of Platinum Complexes for Kinetic Analyses | 103 |
| 4.5.2. Preparation of Nucleophile Solutions for Kinetic Analysis | 103 |
| 4.5.3. Preliminary Kinetic Investigations | 103 |
| 4.5.4. Kinetic Measurements | 104 |
| 4.6. References | 106 |
| Chapter 5: Results and Discussion | 108 |
| 5.1. Synthesis and Characterisation of the Complexes | 108 |
| 5.2. Kinetic Results | 111 |
| 5.3. Computational Analysis | 119 |
| 5.4. Discussion | 128 |

| | |
|---|------------|
| 5.4.1. Kinetic Study of the Displacement of Chloride by Nitrogen Donors | 128 |
| 5.4.2. Accounting for the Reverse Reactions | 143 |
| 5.5. References | 148 |
| | |
| Chapter 6: Conclusions and Future Work | 151 |
| 6.1. Conclusions | 151 |
| 6.2. Future Work | 152 |
| 6.3. Supporting Information | 153 |
| 6.4. References | 154 |
| | |
| Appendix A- Selected Spectra of the Platinum(II) Complexes Synthesised | 155 |
| Appendix B- Kinetic Investigation: Data and Selected Spectra | 181 |

Abstract

A novel platinum(II) complex, [Pt{4-(*o*-tolyl)-6-(3''-isoquinoyl)-2,2'-bipyridine}Cl]SbF₆ (**Pt4**) was synthesized and characterised by means of infrared, elemental analysis, mass spectroscopy, and NMR spectroscopy.

Substitution kinetics of chloride ligand from square planar platinum(II) complexes namely; [Pt(2,2':6',2''-terpyridine)Cl]Cl·2H₂O (**Pt1**), [Pt{2-(2'-pyridyl)-1,10-phenanthroline}Cl], (**Pt2**), [Pt{4'-(*o*-tolyl)-2,2':6',2''-terpyridine}Cl]CF₃SO₃ (**Pt3**) and [Pt{4'-(*o*-tolyl)-6-(3''-isoquinoyl)-2,2'-bipyridine}Cl]SbF₆ (**Pt4**) were studied using a series of five-membered heterocyclic neutral nitrogen donor nucleophiles, *viz.* pyrazole (**Pz**), triazole (**Tz**), imidazole (**Im**), 1-methylimidazole (**MIm**) and 1,2-dimethylimidazole (**DMIm**) under *pseudo* first-order conditions in methanol. The kinetics of the substitution reactions were studied as a function of concentration of the nucleophiles at different temperatures using UV/Visible spectrophotometry and conventional stopped-flow techniques. The observed second-order rate constants, k_2 followed a two term rate law $k_{obs} = k_2[\text{Nucleophile}] + k_{-2}$ except for 1,2-dimethylimidazole with **Pt1**, **Pt3**, **Pt4** and **Pz** and **Tz** with **Pt1**. The observed second-order rate constants along with the negative entropies of activation support an associative mode of substitution behaviour.

The results obtained indicate that increasing the π -conjugation in the *cis* and *cis/trans* position influences the rate of substitution reactions. Increasing the π -conjugation in the *cis* position decreases the rate of the substitution reactions by decreasing the π -acceptor property of the terpy moiety. On the other hand, increasing the π -conjugation in the *cis/trans* position increases the rate of substitution reaction by enhancing the π -acceptor property within the ligand framework. This in turn increases the electronic communication, which consequentially decreases the frontier orbital energy gap between HOMO and LUMO and hence increases the reactivity of the metal centre. Thus the observed trend for the reactivity was **Pt2** > **Pt1** > **Pt3** > **Pt4**. The observed kinetic trend was further supported by DFT-calculations obtained from the computational analysis carried out for the complexes.

The substitution kinetics was influenced by the basicity of the incoming nucleophiles. Except for the sterically hindered nucleophile, **DMIm**, the pK_a of the entering nucleophiles followed a Linear Free Energy Relationship (LFER) indicating an increase in the substitution reactions with increase in the basicity of the nucleophile. The general trend observed for the reactivity of the nucleophiles is **MIm** > **Im** > **DMIm** > **Pz** > **Tz**.

In the reverse reactions the replacement of the azoles by the chloride was controlled by the strength of the Pt—N(azole) bond which is dependent on the strength of the extent of the π -back-bonding between the platinum centre and the azole.

Acknowledgements

I would like to express my sincere gratitude to my supervisor Professor Deogratius Jaganyi for his guidance, encouragement and feedback for this work. I also gratefully acknowledge the financial help from him.

I wish to extend my sincere gratitude to my co-supervisor:

- ✓ *Dr. D. Reddy, without whose help I would not have been able to accomplish this work. His diligent help, guidance and never-ending support in every possible way were an inspiration. His input for this work has been invaluable.*

I would also like to acknowledge the following people:

- ✓ *Dr. J. Perils for her contribution for my synthesis and proof reading. Prof. J. S. Field for his enthusiasm, support and input for my synthetic and crystallographic work. His inspiration, readily offered assistance and expertise made this work possible.*
- ✓ *Mr. M. P. Akerman and Dr. Kirsty Stewart for their contribution in X-ray crystal structure determinations. Mr. C. Grimmer for his expertise in running and analysing the NMR spectra. Mr. M. Sonopo for the help with the NMR spectra. Mrs. Caryl. J. van Rensburg for her help in doing the mass spectra.*
- ✓ *All the academic and technical staff in the School of Chemistry who readily offered help, support and assistance at all times.*
- ✓ *All my friends and colleagues at the School of Chemistry in Pietermaritzburg Campus for all their support and inspiration, especially my friends in the kinetic department for making my work a pleasant experience.*
- ✓ *Finally I am indebted to my family for their endless love, encouragement, support and prayers. This work would not have been possible if it was not for them. Thank you for believing in me.*
- ✓ *Above all, I would like to thank the Almighty God for watching over me throughout my life.*

Conference

- ✓ 39th Inorganic Reaction Mechanisms Group (IRMG) Meeting, Kloster-Banz, Germany, 7th-10th January 2010. Paper presented: D. Reddy, D. Jaganyi, J. Perils, K. J. Gillham, **A. Shaira** & M. P. Akerman, "A detailed Kinetic and Mechanistic Study of the Reactions of Platinum(II) Polypyridyl Complexes with a Series of Azole ligands."

List of abbreviations and symbols

| | |
|------------------------------------|---|
| A | Associative mechanism |
| A | Arrhenius pre-exponential factor |
| aaa | [Pt(diethylenetriamine)OH ₂] ²⁺ |
| aap | [Pt(N-(pyridyl-2-methyl)-1,2diamino-ethane)OH ₂] ²⁺ |
| apa | [Pt(2,6-bis-aminomethylpyridine)OH ₂] ²⁺ |
| AET | aminoethanethiol |
| AgCl | Silver chloride |
| AgSbF ₆ | Silver hexafluoroantimonate |
| app | [Pt(2,2'-bipyridine)(NH ₃)(OH ₂)] ²⁺ |
| BBR3464 | [{ <i>trans</i> -PtCl(NH ₃) ₂] ₂ { μ - <i>trans</i> -Pt(NH ₃) ₂ -(HN ₂ (CH ₂) ₆ NH ₂) ₂ }] ⁴⁺ |
| ^t Bu | <i>tert</i> -butyl |
| bipy | 2,2'-bipyridine |
| bp | base pair |
| Cys | cysteine |
| cisplatin | <i>cis</i> -diaminedichloroplatinum(II) |
| D | dissociative |
| DFT | Density functional theory |
| DMIm | 1,2-dimethylimidazole |
| DMSO | Dimethyl sulfoxide |
| DMTU | dimethylthourea |
| DNA | Deoxyribonucleic acid |
| dppz | dipyridophenazine |
| E_a | Activation energy |
| ϵ | Molar absorptivity coefficient |
| e | exponential |
| eq | Equilibrium |
| $\Delta G^\ddagger/\Delta G^\circ$ | Gibbs free energy of activation |
| 5'-GMP | guanine-5'-monophosphate |
| GSH | glutathione |
| h | Planck constant (6.626 x 10 ⁻³⁴ Js ⁻¹) |
| ΔH^\ddagger | Activation enthalpy |
| HET | 2-hydroxyethanethiol |
| His | histidine |

| | |
|---|--|
| HMG | high-mobility group proteins |
| HOMO | Highest occupied molecular orbital |
| <i>I</i> | Ionic strength |
| I | interchange |
| I _A | Associatively activated |
| I _D | Dissociatively activated |
| 5'IMP | inosine-5'-monophosphate |
| Im | imidazole |
| INO | inosine |
| IR | infrared |
| <i>k</i> ₁ , <i>k</i> ₋₁ , <i>k</i> ₂ , <i>k</i> ₋₂ | rate constants |
| <i>k</i> _b | Boltzmann constant (1.3807 x 10 ⁻²³ JK ⁻¹) |
| K | Kelvin |
| <i>k</i> _{expt} | Experimental pseudo first-order constant |
| <i>k</i> _{obs} | observed pseudo first-order constant |
| L | ligand |
| LACVP | Los Alamos Core Valence Potential |
| LFER | Linear free energy relationship |
| LUMO | Lowest unoccupied molecular orbital |
| M | Molarity (mol dm ⁻³) or metal |
| MeCN | acetonitrile |
| MLCT | Metal to ligand charge transition |
| 5MESS | [5-methyl-1,10-phenanthraline)(1S,2S-diaminocyclohexane)platinum(II)] ²⁺ |
| 56MESS | [(5,6-dimethyl-1,10-phenonthraline)(1S,2S-diaminocyclohexane)platinum(II)] ²⁺ |
| MIm | 1-methylimidazole |
| MO | Molecular orbital |
| NBO | Natural bond orbital |
| NER | Nucleotide excision repair |
| nm | nanometer |
| NMR | nuclear magnetic resonance |
| Nu | nucleophile |
| <i>o</i> -tolyl | ortho toluene |
| pap | [Pt(bis(2-pyridylmethyl)amine) OH ₂] ²⁺ |
| phen | 1,10-phenanthraline |

| | |
|------------------------------|--|
| PHENSS | [(1,10-phenanthraline)(1S,2S-diaminocyclohexane)platinum(II)] ²⁺ |
| PPI | N-{1-(2'-pyridyl)-1-oxo-2-ethyl}pyridinium iodide |
| ppm | Parts per million |
| ppp | [Pt(terpy)OH ₂] ²⁺ |
| Pt1 | [Pt(2,2':6',2''-terpyridine)Cl]Cl·2H ₂ O |
| Pt2 | [Pt{2-(2'-pyridyl)-1,10-phenanthroline}Cl] |
| Pt3 | [Pt{4'-(<i>o</i> -tolyl)-2,2':6',2''-terpyridine}Cl]CF ₃ SO ₃ |
| Pt4 | [Pt{4-(<i>o</i> -tolyl)-6-(3''-isoquinoyl)-2,2'-bipyridine}Cl]SbF ₆ |
| Pz | pyrazole |
| R | universal gas constant (8.3145 JK ⁻¹ mol ⁻¹) |
| RNA | ribonucleic acid |
| s | nucleophilic discrimination factor |
| s | singlet or strong |
| ΔS [‡] | Activation entropy |
| SAR | structure activity relationship |
| T | temperature |
| <i>T.cruzi</i> | <i>Trypanasoma cruzi</i> |
| terpy | 2,2':6',2''-terpyridine |
| TMTU | 1,1,3,3-tetramethyl-2-thiourea |
| Tu | thiourea |
| Tz | triazole |
| UV | Ultraviolet |
| X | Leaving group (unless otherwise mentioned) |
| Y | Incoming group (unless otherwise mentioned) |
| <i>ν</i> | frequency |
| <i>n</i>_{pt} | nucleophilicity |

List of Figures

| Figure | Title | Page |
|-------------|---|------|
| Figure 1.1 | Structure of <i>cis</i> -diaminedichloroplatinum(II). | 3 |
| Figure 1.2 | Structure of platinum complexes initially studied for antitumor activities. | 3 |
| Figure 1.3 | Suggested reaction pathway for cisplatin in the cell and binding to DNA. | 5 |
| Figure 1.4 | The sequence of cisplatin binding to DNA and the structurally different adducts formed. The <i>k</i> values and $t_{1/2}$ values were obtained from a kinetic study of hydrolysis of cisplatin by short lengths of single- or double-strand DNA containing adjacent guanosines using ^{15}N NMR at pH 7.1 in water containing 10 mol dm^{-3} sodium phosphate. | 8 |
| Figure 1.5 | Some possible cisplatin-DNA binding modes. | 9 |
| Figure 1.6 | Platinum complexes in worldwide clinical use and as well as those with regionally limited approval: nedaplatin, lobaplatin and SK12053R. | 11 |
| Figure 1.7 | Some platinum(II) complexes which deviate from the proposed structural-activity relation, yet have shown antitumor activity in line with cisplatin. | 13 |
| Figure 1.8 | Some polynuclear platinum complexes which have shown potential anticancer activity. | 14 |
| Figure 1.9 | Structure of some of the well studied platinum(II) terpyridine complexes which have shown cytotoxicity and DNA intercalation against tumor cells (anions are omitted for simplicity). | 16 |
| Figure 1.10 | Structure of 1,10-phenanthroline and phenanthroline-based platinum(II) intercalating complexes. Complexes (30), (31) and (32) are the three best platinum(II) based DNA intercalators studied by Wheate <i>et al.</i> Complex (33) is from Ref. The anions are omitted for simplicity. * Indicates a chiral centre (either <i>R</i> or <i>S</i> , <i>R</i> complexes are found to be more effective). | 18 |
| Figure 1.11 | Some of the platinum(II) terpy complexes and biologically active nucleophiles studied by Bugarčić <i>et al.</i> | 20 |
| Figure 1.12 | Platinum(II) complexes studied by van Eldik <i>et al.</i> | 22 |
| Figure 1.13 | Platinum(II) polypyridyl complexes studied by van Eldik <i>et al.</i> to investigate the Pt—C <i>cis</i> and <i>trans</i> σ -donation on the rate of substitution behaviour. | 23 |
| Figure 1.14 | Platinum(II) terpy complexes studied by Jaganyi <i>et al.</i> | 24 |
| Figure 2.1 | The relationship between the mechanism of substitution and its energy profile and the classifications of Langford-Gray and Hughes-Ingold. | 32 |
| Figure 2.2 | Energy profiles for the A mechanism for the substitution, showing the relationship between the intermediate and the bond-breaking transition states: (a) the bond breaking transiting state at higher energy (b) the bond-making transition state at higher energy. | 34 |

| | | |
|--------------------|---|----|
| Figure 2.3 | Schematic representation of the energy profile and possible steric changes during an associative substitution of leaving group, X by the entering group, Y of a square planar complex: energies at 2, 4, 6, and 8 represent the transition states and the reaction intermediates would have energies shown at 3, 5 and 7. | 36 |
| Figure 2.4 | Schematic representation for substitution in d^8 four coordinate square planar complexes showing the alternative D and A or I_a solvolysis to account for the $k_1k_Y[Y]/(k_X[X]+k_Y[Y])$ or (k_1 limit) term. | 37 |
| Figure 2.5 | Rates of reaction of <i>trans</i> -[Pt(Py) ₂ Cl ₂] as a function of concentration of different nucleophiles in methanol at 30° C. | 38 |
| Figure 2.6 | Schematic representation of the R ₃ P—Pt double bond. If ligands PR ₃ and X are in the <i>xy</i> plane, then the <i>d</i> orbitals shown are either d_{xz} or d_{yz} . | 43 |
| Figure 2.7 | Activated trigonal bipyramidal complex for the <i>trans</i> - PtA ₂ LXY. | 44 |
| Figure 2.8 | Distribution of Charge induced dipoles in the L—Pt —X coordinate of <i>trans</i> -PtA ₂ LX. | 45 |
| Figure 2.9 | Molecular orbital representation showing the relative orbital energies in PtCl ₄ ²⁻ . | 46 |
| Figure 2.10 | Representation of L— Pt—X bonding using σ_x MO (a) The σ bond strength of L and X are almost equal. (b) Strong σ donor ligand L, the σ bond strength of L is much greater than that of X. | 46 |
| Figure 2.11 | The σ - <i>trans</i> effect due to the stabilization of the trigonal bipyramidal intermediate. (a) Only one <i>p</i> orbital is available for σ -bond formation of L and X. (b) Two <i>p</i> orbitals are available for the σ -bonding of L, X and Y. | 47 |
| Figure 2.12 | Correlation of the rates of reaction of platinum(II) complexes with the standard <i>trans</i> - Pt(py) ₂ Cl ₂ for different nucleophiles: •, <i>trans</i> -Pt(PEt ₃) ₂ Cl ₂ in methanol at 30 °C; ▲, Pt(en)Cl ₂ in water at 35 °C. | 51 |
| Figure 2.13 | The steric effect of the aryl square planar complex showing the steric bulk for the <i>cis</i> isomer blocking the attacking site. | 54 |
| Figure 2.14 | Representation of the non-stereospecific substitution of dissociation mechanism of a platinum(II) square planar complex due to the intermolecular rearrangements. | 59 |
| Figure 3.1 | A summary of reaction techniques and their corresponding time scales. | 79 |
| Figure 3.2 | Schematic diagram of a UV/Visible spectrophotometry setup. | 80 |
| Figure 3.3 | Spectrum obtained from Cary UV/Visible spectrophotometer for the substitution of Cl ⁻ from [Pt{4'-(<i>o</i> -tolyl)-2,2':6',2''- terpyridine}Cl]CF ₃ SO ₃ (2.50 x 10 ⁻⁵ mol dm ⁻³) with 1-methylimidazole (5.00 x 10 ⁻⁴ mol dm ⁻³) in methanol solution (<i>I</i> = 0.10 M (0.09 M LiCF ₃ SO ₃ + 0.01 M NaCl)) at 333 nm and 298.15 K. | 82 |

| | | |
|--------------------|---|-----|
| Figure 3. 4 | Diagrammatic representation of a continuous flow kinetic system. The letter <i>d</i> represents the distance from the mixture to the point of observation. | 83 |
| Figure 3. 5 | Diagrammatic representation of stopped-flow apparatus. | 84 |
| Figure 4.1 | Perspective view showing the molecular geometry and atom numbering scheme for the 4-(<i>o</i> -tolyl)-6-(3'-isoquinoyl)-2,2'-bipyridine ligand. Non-H atoms are drawn as 50% thermal ellipsoids and the H atoms as spheres of arbitrary radius. | 96 |
| Figure 4.2 | Perspective view of the dication in [Pt{4'-(<i>o</i> -tolyl)-2,2':6',2"-terpyridine}MIm](CF ₃ SO ₃) ₂ showing the molecular geometry and atom numbering scheme. Non-H atoms are drawn as 50% thermal ellipsoids and the H atoms as spheres of arbitrary radius. | 97 |
| Figure 5.1 | Structures of platinum(II) complexes and the nucleophiles used in kinetic investigations. Anions are omitted for simplicity. | 110 |
| Figure 5.2 | Absorbance change for the reactions of Pt3 ((2.50 x 10 ⁻⁵ M) with triazole 10 x 2.50 x 10 ⁻⁵ M and 50 x 2.50 x 10 ⁻⁵ M) in methanol solution (<i>I</i> = 0.1 M, (0.09 M LiCF ₃ SO ₃ + 0.01 M NaCl)) at 298.15 K. | 112 |
| Figure 5.3 | Spectrum obtained from Cary UV/Visible spectrophotometer for the reaction of Pt3 (2.50 x 10 ⁻⁵ M) with triazole (1.25 x 10 ⁻³ M) in methanol solution (<i>I</i> = 0.10 M (0.09 M LiCF ₃ SO ₃ + 0.01 M NaCl)) at 333 nm at 308.15 K. | 112 |
| Figure 5.4 | First-order exponential fit and residuals (lower part) for the reaction of Pt2 (1.53 x10 ⁻⁵ M) with 1-methylimidazole (4.59 x 10 ⁻⁴ M) in methanol solution (<i>I</i> = 0.10 M (0.09 M LiCF ₃ SO ₃ + 0.01 M NaCl)) at 311 nm and 298.15 K. | 113 |
| Figure 5.5 | Dependence of the <i>pseudo</i> first-order rate constants (<i>k</i> _{obs}) on the concentrations of the nucleophiles for the chloride substitution from Pt1 in methanol solution (<i>I</i> = 0.10 M (0.09 M LiCF ₃ SO ₃ + 0.01 M NaCl)) at 298.15 K. | 114 |
| Figure 5.6 | Plots of ln(<i>k</i> ₂ / <i>T</i>) against 1/ <i>T</i> for the reactions of Pt2 with the nucleophiles at various temperatures in the range 15-40 °C. | 117 |
| Figure 5.7 | Plots of ln(<i>k</i> ₂ / <i>T</i>) against 1/ <i>T</i> for the reactions of Pt3 with the nucleophiles at various temperatures in the range 15-40 °C. | 117 |
| Figure 5.8 | Numbering scheme employed for the atoms around the platinum centre for the platinum(II) complexes investigated. X represents Cl in the forward reactions and N4 (from azole) in the reverse reactions. The bond angles, bond lengths and atomic charges are referred according to the numbering scheme shown. | 119 |
| Figure 5.9 | HOMO and LUMO energy gap for the platinum(II) complexes investigated. | 124 |
| Figure 5.10 | The HUMO and LUMO energy gap for the N-donor substituted platinum(II) complexes. | 128 |
| Figure 5.11 | Absorption spectrum of Pt3 , Pt4 and the ligand of Pt4 , (4-(<i>o</i> -tolyl)-6-(3'-isoquinoyl)-2,2'-bipyridine) in acetonitrile solution. | 132 |

| | | |
|--------------------|---|-----|
| Figure 5.12 | Plot of variation of $\log k_2$ obtained for the substitution reactions against the pK_a values of the nucleophiles studied. | 135 |
| Figure 5.13 | Putative representation of the interaction of the α -methyl group on the DMIm with the pyridine hydrogen of $[\text{PtCl}]^+$ showing the steric congestion in the trigonal bipyramidal intermediate. | 136 |
| Figure 5.14 | Structure of the nucleophiles investigated indicating the different nitrogen atoms. | 138 |
| Figure 5.15 | Geometry-optimised structures of the nucleophiles investigated and distribution of the electrons on the nucleophiles. The blue area indicates the most electropositive areas and the red region indicates the most electronegative areas. Given on the diagram are the NBO charges for the nitrogen atoms and the potential energy of the electron density with respect to the electron distribution. | 139 |
| Figure 5.16 | Plot of DFT-calculated potential energy at the pyridinic nitrogen centres (<i>Figure 5.15</i>) against the pK_a of the azoles. | 142 |
| Figure 5.17 | Plots for the DFT-calculated $r_{\text{Pt-N}}$ bond lengths against the pK_a of the leaving groups for the replacement of azole by chloride. | 145 |
| Figure 5.18 | Movement of electrons from the filled $5d$ orbitals of platinum to the antibonding orbitals of the azole ligand and the π , σ -donation from azole to the platinum centre in the ground state. | 146 |

List of Schemes

| Scheme | Title | Page |
|-------------------|---|-------------|
| Scheme 1.1 | Changes in oxidation states of platinum by oxidative addition or reductive elimination. | 1 |
| Scheme 1.2 | Schematic diagram representing hydrolysis of cisplatin and attack of cisplatin to DNA. The k values and $t_{1/2}$ values were obtained from a ^{195}Pt NMR platination kinetic study of platination of cisplatin to chicken erythrocyte DNA at 37 °C and pH 6.5. | 7 |
| Scheme 1.3 | Reaction of platinum(II) (terpy) with guanosine (1:1) showing the N7 binding of guanosine with platinum(II) (terpy). | 19 |
| Scheme 1.4 | Substitution reaction of $[\text{Pt}(\text{terpy})\text{Cl}]^+$ with histidine (His) to form $[\text{Pt}(\text{terpy})\text{His}]^{2+}$. | 21 |
| Scheme 5.1 | The possible resonance structures for the electrophilic attack and the possible resonance structures for the formation of energetically most favourable complex. | 140 |
| Scheme 5.2 | Tautomeric resonance structures of imidazole. | 140 |

List of Tables

| Table | Title | Page |
|------------------|---|------|
| Table 1.1 | Binding constants for some of the platinum(II) terpy complexes studied by Lippert and co-workers. | 17 |
| Table 2.1 | Estimated relative σ - and π - <i>trans effects</i> of some ligands. | 48 |
| Table 2.2 | Some nucleophilic constants given for Pt(py) ₂ Cl ₂ with different nucleophiles of donor atoms. | 50 |
| Table 2.3 | The effect of <i>trans</i> ligand, L on the rate of reaction of <i>cis</i> -Pt(PEt ₃) ₂ LCl with py. | 52 |
| Table 2.4 | Steric effects on the rates of substitution of <i>cis</i> - and <i>trans</i> - Pt(PEt ₃) ₂ LCl by pyridine | 53 |
| Table 2.5 | The rate constants for the reactions of steric <i>cis</i> -effect of <i>ortho</i> -methylation of an aryl ligand at 30 °C. | 55 |
| Table 2.6 | Effect of solvent on the chloride exchange reaction (<i>Equation 2.26</i>) at 25 °C. | 56 |
| Table 2.7 | Effects of leaving group on the rates of reaction of Pt(dien) complexes in water at 25 °C. | 57 |
| Table 4.1 | Crystal structure, data collection and refinement details for 4-(<i>o</i> -tolyl)-6-(3''-isoquinolyl)-2,2'-bipyridine (ligand) and [Pt{4'-(<i>o</i> -tolyl) terpy}MIm](CF ₃ SO ₃) ₂ (complex) | 100 |
| Table 4.2 | Selected bond lengths and angles for [Pt{4'-(<i>o</i> -tolyl)terpy}MIm](CF ₃ SO ₃) ₂ | 101 |
| Table 5.1 | Summary of second-order rate constants and their standard deviations for the displacement of the chloride from the platinum(II) complexes by Pz , Tz , Im , MIm and DMIm in methanol, (<i>I</i> = 0.10 M (0.09 M LiCF ₃ SO ₃ + 0.01 M NaCl)) at 298.15. | 115 |
| Table 5.2 | Relative rates of the complexes based on <i>k</i> ₂ ; Pt1 , Pt2 , Pt3 and Pt4 with Pz , Tz , Im , MIm and DMIm with Pt1 taken as the basis. | 116 |
| Table 5.3 | Relative rates based on <i>k</i> ₂ of the complexes; Pt1 , Pt2 , Pt3 and Pt4 with Pz , Tz , Im , MIm and DMIm with Im taken as the basis. | 116 |
| Table 5.4 | Summary of activation parameters for the forward and the reverse reactions with their corresponding standard deviations for the chloride substitution reactions of the platinum(II) complexes studied with Pz , Im , MIm , DMIm and Tz in methanol (<i>I</i> = 0.10 M (0.09 M LiCF ₃ SO ₃ + 0.01 M NaCl)). | 118 |
| Table 5.5 | Geometry-optimised structures of the platinum complexes investigated and distribution of the electron density on the platinum complexes. The blue area indicates the most electropositive areas and the red region indicates the most electronegative areas. Included in this <i>Figure</i> is a nucleophile substituted complex for the product of the kinetic reaction of Pt3 with MIm , ([Pt{4'-(<i>o</i> -tolyl)terpy}MIm](CF ₃ SO ₃) ₂)(Pt3-MIm). | 120 |

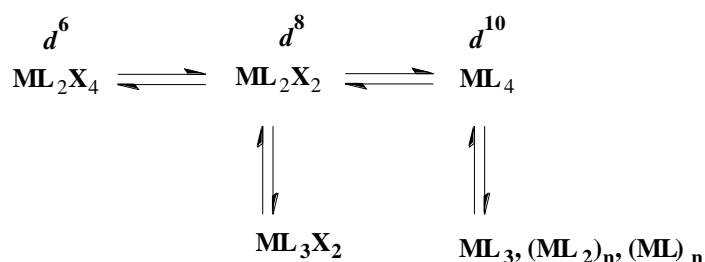
| | | |
|-------------------|--|-----|
| Table 5.6 | Selected bond lengths (Å) for the platinum complexes Pt1 , Pt2 , Pt3 , Pt4 and (Pt-3MIm) obtained from the computational studies, literature and the X-ray crystal structure. | 121 |
| Table 5.7 | Summary of selected Bond Angles(°) for Pt1 , Pt2 , Pt3 , Pt4 , (Pt3-MIm) obtained from DFT-calculations, X-ray crystal structure and from literature. | 121 |
| Table 5.8 | DFT-calculated (B3LYP/LACVP+**) molecular orbitals, <i>i.e.</i> HOMO's and LUMO's for the platinum complexes investigated. | 123 |
| Table 5.9 | Energies of HOMO-LUMO obtained for the platinum(II) complexes studied. Geometry optimised studies done using the B3LYP/LACVP+** level of theory. | 124 |
| Table 5.10 | The DFT-calculated NBO charges on the central Pt, the donor nitrogen atoms and the leaving group, Cl. | 124 |
| Table 5.11 | Selected bond lengths (Å) for the N-donor substituted platinum(II) complexes Pt1 , Pt2 , Pt3 and Pt4 obtained from the computational studies. | 125 |
| Table 5.12 | The DFT-calculated NBO charges on the central Pt, the donor nitrogen atoms and the leaving group, (N-donor azole). Geometry optimised studies done using the B3LYP/LACVP+** level of theory. | 126 |
| Table 5.13 | Energies of HOMO-LUMO obtained for the substituted platinum(II) complexes. Geometry optimised studies done using the B3LYP/LACVP+** level of theory. | 127 |
| Table 5.14 | The logarithm of second-order rate constants, k_2 for the forward reactions of the platinum complexes studied and the pK_a of the nucleophiles studied. | 134 |

Chapter 1

Introduction to Platinum Chemistry

1.1. Overview

Platinum is one of the most versatile transition metals having a variety of oxidation states.^[1, 2] This metal is mainly extracted from naturally occurring ores such as PtAs₂ and PtS. Platinum is distinctive from the other transition metals due to its ability to form a wide range of complexes and the ease with which it takes part in different chemical reactions.^[2] The most common oxidation states of platinum are platinum(0), platinum(II) and platinum(IV), particularly, platinum(II) and platinum(IV) which forms a wide range of kinetically and thermodynamically stable complexes. The change in oxidation states often results in a change in the coordination chemistry of the metal centre either by *oxidative addition* or by *reductive elimination* (Scheme 1.1).^[2]



L = neutral ligand, X = anionic ligand

Scheme 1.1 Changes in oxidation states of platinum by oxidative addition or reductive elimination.^[2]

Of all the oxidation states of platinum, the +2 species is the most well studied. Platinum(II) forms a range of stable mononuclear complexes with neutral ligands (Group IV, V or VI donor atoms) and anionic monodentate ligands such as chlorides, sulphides and nitrites.^[2, 3] Formation of isomers with these ligands led to the discovery of the *trans effect* in the early twentieth century.^[2] Details of the *trans effect* are given in *Chapter 2, Section 2.4.1.1*. With bidentate ligands such as **SS**, **NN**, **NO** or **PN**, platinum(II) often forms mono- or dinuclear bridged complexes.^[2] With tridentate ligands such as 2,2':6',2''-terpyridine (**NNN**-donor) four-coordinate mononuclear complexes are often obtained.

The chemistry of d^8 platinum(II) complexes is versatile and is recognised for its distinctive features. These include:^[2]

- ✓ a coordinatively unsaturated nature
- ✓ the presence of filled vacant p_z orbitals for nucleophilic attack
- ✓ the ability to form π -complexes and Pt—C σ -bonded complexes
- ✓ the presence of filled d_{z^2} orbitals for electrophilic attack by oxidative addition
- ✓ the ability to undergo reductive elimination.

When dealing with bonding properties, platinum(II) has eight electrons in the $5d$ orbital. This d^8 system has a total of nine orbitals available for bonding which are the $5d$, $6s$ and $6p$ orbitals. Out of the nine orbitals, the $5d_{x^2-y^2}$, $6p_x$, $6p_y$ orbitals and a combination of $6s$ and $5d_{z^2}$ are used to form σ -bond formation.^[2] The resulting dsp^2 orbitals have mainly s character.^[2] The orbitals appropriate for π -bonding are d_{xy} , d_{xz} , d_{yz} , p_x , p_y and p_z orbitals.^[2] To form the metal-ligand π interactions, these orbitals interact with the ligand mainly *via* three different mechanisms each using a different orbital:^[2]

- I. In the first type the d_{xy} overlaps with four π_h ligand orbitals (where π_h is the ligand orbitals which are in the same plane as the complex and possess suitable symmetry to undergo π interactions) which results in the formation of the in-plane π -system
- II. In the second type both d_{xz} and d_{yz} orbitals interact with two *trans* π_v ligand orbitals (where π_v is the ligand orbitals perpendicular to the plane of complex and have suitable symmetry to undergo π interactions) which forms the *trans*- π -system
- III. In the third type the p_z orbitals interact with the four π_v ligand orbitals forming the ring π -system

Apart from these three mechanisms, interactions of p_x and p_y orbitals with two π_h ligand orbitals is also possible. An appropriate energy-level diagram showing these interactions is given in Chapter 2, Section 2.4.1.2., Figure 2.9.

Important uses of platinum chemistry include photoluminescent applications and catalysis. However, the greatest achievement of platinum chemistry was the discovery of the biologically active platinum antitumor complex, *cis*-diaminedichloroplatinum(II) (cisplatin).^[4] Cisplatin was first synthesised in 1844 and was called Peyrone's Chloride.^[5]

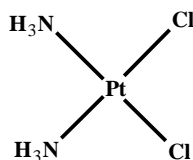


Figure 1.1 Structure of *cis*-diaminedichloroplatinum(II) (cisplatin).^[4]

1.2. The Anticancer Activity of Platinum Complexes

The use of platinum in the pharmaceutical industry has gained a considerable interest with the discovery of cisplatin in 1969 by Barnett Rosenberg.^[4-8] Today platinum compounds comprise of a distinct class of chemotherapeutic agents which are widely used as antitumor and antiviral agents.^[5]

The antitumor activity of cisplatin was serendipitously discovered during an investigation of the effects of electric field on *Escherichia coli* (*E. coli*) bacteria growth in ammonium chloride solution using a platinum electrode.^[9] It was found that during electrolysis, the bacteria stopped cell division in ammonium chloride solution when sunlight was passed through it. Further investigations showed that in the presence of ultraviolet light, traces of platinum present in the solution caused a series of reactions in the ammonium chloride solution and formed some platinum complexes namely; *cis*-[Pt(NH₃)₂Cl₂], *trans*-[Pt(NH₃)₂Cl₂], *cis*-[Pt(NH₃)₂Cl₄] and *trans*-[Pt(NH₃)₂Cl₄] (Figure 1.2). After several tests it was found that only the *cis* complexes were active against the growth of bacteria cells.^[4]

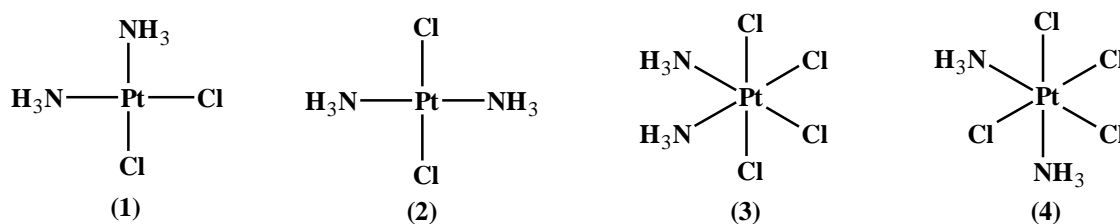


Figure 1.2 Structure of platinum complexes initially studied for antitumor activities.^[4]

Both the *trans* and the *cis* isomers of platinum(II) and platinum(IV) complexes in Figure 1.2 contain two non-leaving neutral ammonia ligands along with two labile anionic chloride ligands that can be substituted by any other ligands or nucleophiles. Based on the results obtained by screening a large number of cisplatin related complexes, Cleare and Hoeschele, had proposed some early structural-activity relationships, (SAR), on which the synthesis of platinum anticancer drugs are based.^[10, 11] These include:^[10-13]

- ✓ The complexes must have anionic leaving groups with moderate binding strength to platinum and should possess a weak *trans effect* to avoid labilisation of the amine moiety, eg. Cl^- or SO_4^{2-} . Complexes with other leaving groups are found to be either toxic (NO_3^-) or inactive (inert) ligands.
- ✓ The complexes must have a *cis* geometry with the general formulae, *cis*- $[\text{Pt}(\text{am})_2\text{X}_2]$ or *cis*- $[\text{Pt}(\text{am}_2\text{R}_2)_2\text{X}_4]$, where am is the amine ligand, R is an alkyl group and X is the leaving group. *Cis* geometry is preferred because reactivity of *trans* chloro compounds often involves side reactions with other species which hinder the antitumor activity.^[14]
- ✓ The amine group must possess at least one N—H group, which is thought to play a role in the hydrogen bond formation with the DNA. The nature of the amine group also affects the solubility of the drug in the lipid medium. The size and the shape of the substituents on the amine ligand influences the reactivity and the toxicity of the drug.^[12]
- ✓ The complex must be neutral.^[15] Neutral complexes are found to be more active since they are more lipophilic and thus can easily pass through the cell membrane.

In the past few years, the development of new platinum anticancer drugs has achieved very little success. However, one recent achievement in platinum anticancer research is the successful elucidation of the mechanism of action of cisplatin and the causal drug resistance to it. This understanding of the existing drugs, would be an important insight to the development of effective and cell targeted platinum drugs with less toxicity.^[16]

1.2.1. The Mechanism of Action of Cisplatin

The development of cisplatin in the 1960s led to a tremendous amount of research activity trying to understand how the drug destroys cancer cells in the human body. Despite its simplicity in structure, it is one of the most potent drugs developed for anticancer chemotherapy during the last thirty years.^[5, 15, 17, 18] Since the beginning of its clinical trials in 1971,^[4, 19] the drug has been used as an effective treatment against a wide range of cancerous

cells such as bladder, head, neck, ovarian and testicular cancer.^[4, 5, 20-25] However, the effectiveness of the drug is limited due to its severe side effects such as vomiting/nausea,^[26-28] nephrotoxicity and neurotoxicity,^[29-39] frequent development of drug resistance in certain tumor cells^[39-46] and limited water solubility.^[5] In spite of the large number of research initiatives in the past, the actual mechanism of its action has still not been fully understood.^[47, 48] However, over thirty years of laboratory studies have revealed a considerable amount of information about how the drug kills certain tumor cells and becomes resistant to others.

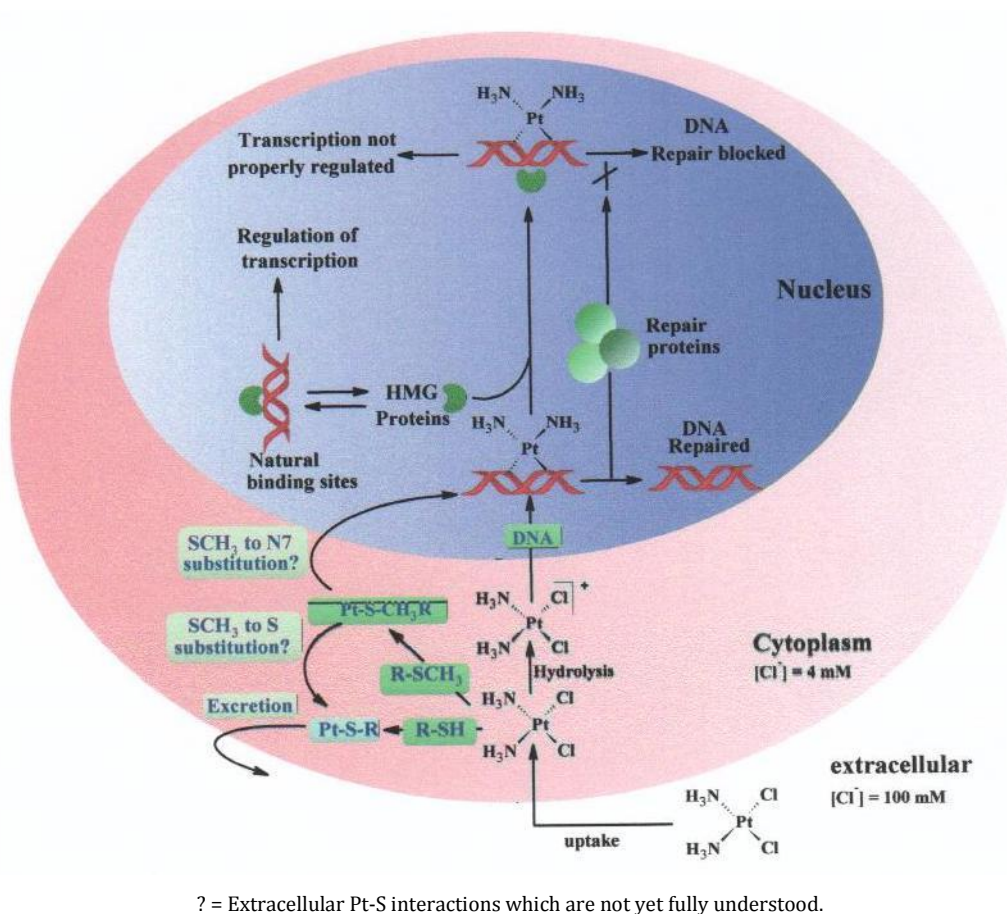


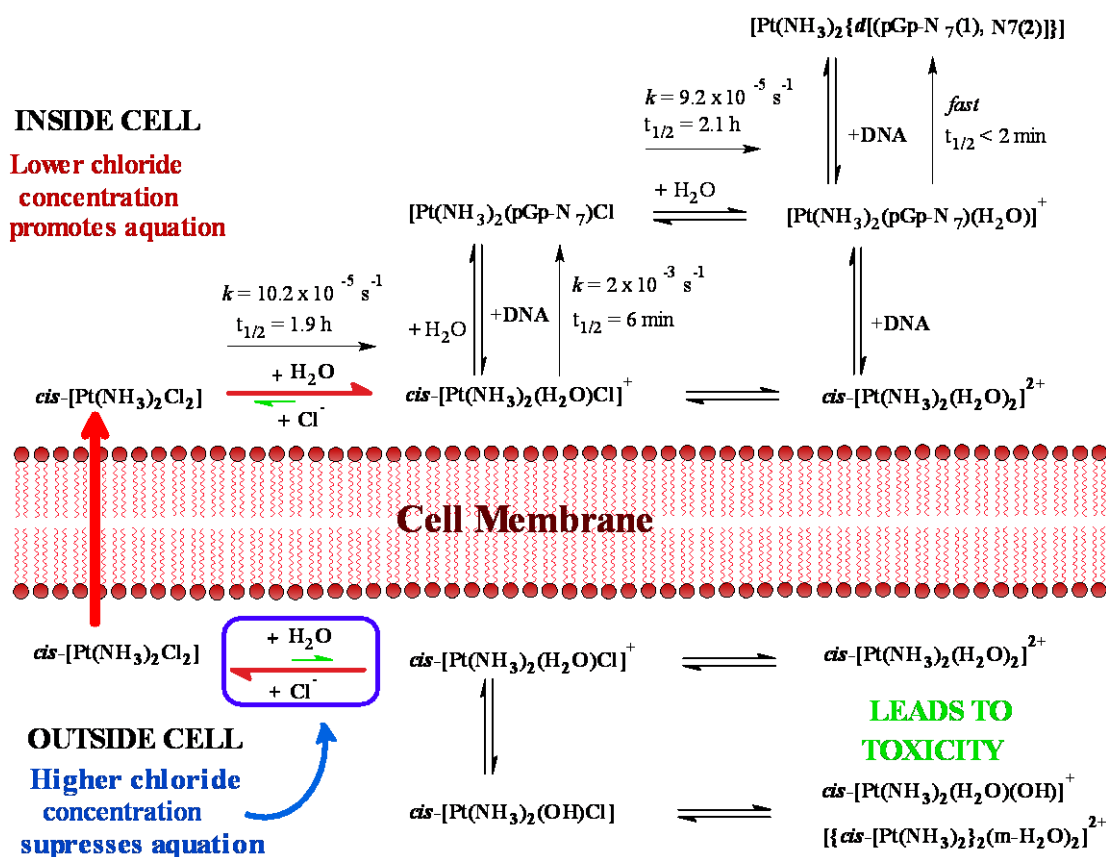
Figure 1.3 Suggested reaction pathway for cisplatin in the cell and binding to DNA.^[5, 9, 49]

Experimental evidence suggests that the main target of cisplatin is DNA^[5, 50-52] and the antitumor activity of cisplatin is mediated by detection of platinated DNA adducts by the high-mobility group proteins (HMG) or other repair protein groups.^[5] These HMG groups play an important role in DNA transcription during cell division. In the DNA, HMG and other proteins bind to the cisplatin modified DNA adducts and prevent cisplatin adducts from DNA transcription (*Figure 1.3*). However, it was found that coordination of certain sulfur containing proteins and amino acids^[53, 54] to the platinum drug leads to some toxic side

effects such as neuro- and nephrotoxicity^[53, 55] and also affects the biodistribution of the drug and its pharmacokinetics resulting into decreased drug accumulation and reduced formation of the required Pt—DNA adducts.^[53, 56] Since sulfur is a strong *trans* influencing donor atom, coordination of certain sulfur compounds of thioethers^[53] or methionine derivatives^[55] to square planar *cis*-diamineplatinum(II) core results in the removal of the *trans* amine ligand by the incoming sulfur ligand prior to DNA.^[53, 55] This consequently effects the actual mechanism of action of the drug since *cis*-diamineplatinum(II) core is the active fragment of the metal complex that binds to DNA resulting the cytotoxicity.^[53]

1.2.1.1. Reactivity of Cisplatin with DNA

Cisplatin is administered into human body intravenously as a sterile saline solution at a dose (phase one) of about 50-120 mg/m² (m² = body surface area) per course over 0.5 to 2 hours.^[4, 23] The drug is often used in combination with other adjuvants to minimise the side effects. Once the drug enters into the blood stream, it is subjected to other compounds in the blood such as sugars, proteins, salts and water. High chloride concentration (~100 mM) in the bloodstream suppresses the hydrolysis of the molecule thus most of it remains unchanged.^[12, 23] The neutral compound enters the cell by passive diffusion or active uptake. Inside the cell, due to the low chloride concentration (*ca.* 20 mM), the neutral cisplatin molecule undergoes hydrolysis producing a charged species (*Scheme 1.2*).^[5, 9, 12] Since water is a better leaving group than chloride, the resulting charged species are more reactive towards biomolecules.^[57] This hydrolysis of cisplatin lowers the p*K*_a of the complex. When comparing the p*K*_a values at 25 °C, the monoaqua complex has a p*K*_a of 6.49 and the p*K*_{a1} and p*K*_{a2} of the diaquatic complex are 5.39 and 7.1 respectively.^[4] Research has shown that the rate of reaction of cisplatin with DNA depends on the hydrolysis of the drug.^[58] Any side reactions of *cis*-Pt(NH₃)₂²⁺ other than to DNA leads potential deactivation or resistance of the drug and increased toxicity^[53] (*Scheme 1.2*).



Scheme 1.2 Schematic diagram representing hydrolysis of cisplatin and attack of cisplatin to DNA. The k values and $t_{1/2}$ values were obtained from a ^{195}Pt NMR platination kinetic study of platination of cisplatin to chicken erythrocyte DNA at 37 °C and pH 6.5.^[12]

The hydrated species then bind to the DNA in multiple steps (Figure 1.4). The steps involved are:^[59]

- Aquation:** The binding of cisplatin to DNA starts with the formation of the mono aquated species. Experimental evidence shows that this aquation step follows a first-order kinetics and this was assumed to be the rate determining step.^[56, 60] However, there is a degree of uncertainty about this since the aquation involves many species.^[61]
- Preassociation:** This involves an irreversible binding of platinum to DNA and is therefore kinetically controlled.^[62]
- Monofunctional adduct formation:** Irreversible monofunctional Pt-DNA adducts are formed in this step. The cross-links are formed mainly between 1,2 adjacent guanine-guanine (60-65%)^[58] while the cross-link between adjacent adenine-guanine was found to be 20-25%^[63] and this binding unwinds DNA by 13°. Minor bindings involve 1,3-intrastrand bindings which unwind DNA by 23°.

- d. **Second aquation:** Hydrolysis of the second chlorine. This diaqua species has double reactivity towards DNA in comparison to the mono aqua species.
- e. **Ring closure and formation of bifunctional adduct:** Binding of the second DNA strand to the platinum complex. There is some degree of uncertainty about the formation of the bifunctional adduct being directly from the monochloro complex or whether it is *via* aquation.
- f. **DNA distortion** and recognition of DNA distortion by a variety of proteins

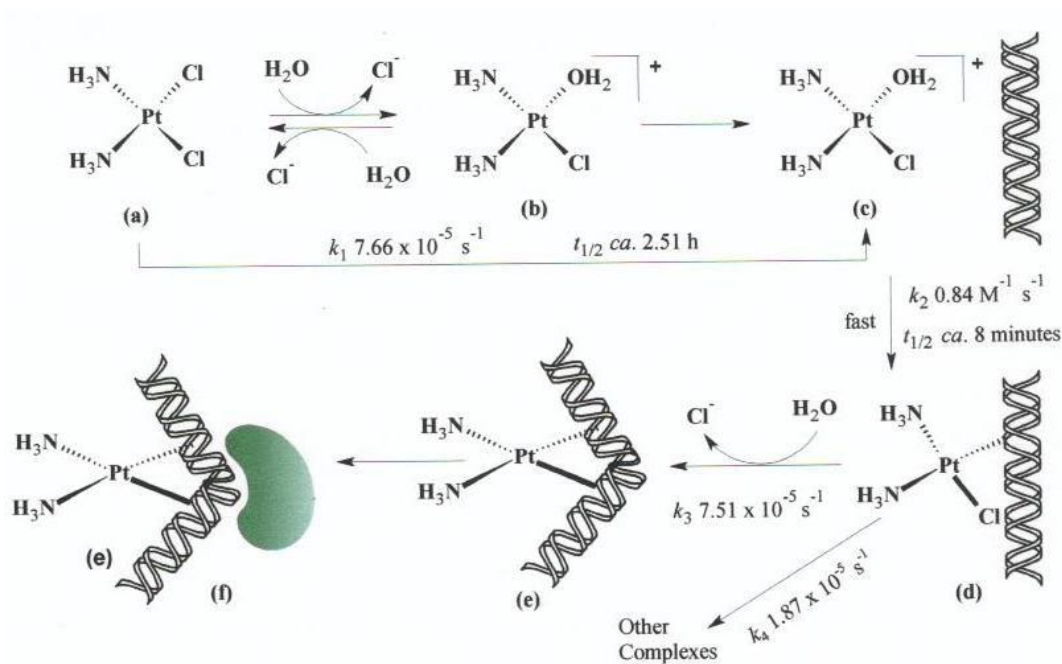


Figure 1.4 The sequence of cisplatin binding to DNA and the structurally different adducts formed.^[59] The k values and $t_{1/2}$ values were obtained from a kinetic study of hydrolysis of cisplatin by short lengths of single- or double-strand DNA containing adjacent guanosines using ¹⁵N NMR at pH 7.1 in water containing 10 mol dm⁻³ sodium phosphate.^[12]

Although inside the cell, cisplatin can react with many cellular components such as proteins, RNA and sulphur donor groups (*Figure 1.3*), it was proven that the binding involves the coordination of cisplatin with the DNA bases *viz.* cytosine (C), adenine(A), thymine(T) and guanine(G), showing a preference for the N7-position of guanine.^[4, 9, 12, 19, 53, 63-70] This is because the N7 position of the imidazole ring in guanine is more accessible for platinum binding as it is located in the major groove of DNA. Also the binding of N7 with cisplatin is enhanced due to the high nucleophilicity of the N7 centre. The basicity of guanine N7 allows to form hydrogen bonding with the ligands of platinum complex.^[65]

As can be seen from *Figure 1.4*, the binding of the complexes may form mono- or di- Pt-DNA adducts. Often the monofunctional adducts react to form either interstrand or intrastrand adducts which can then stop DNA multiplication resulting in antitumor activity.^[71] However, the di-Pt-DNA adducts are assumed to be the major contributor to the cisplatin anticancer activity.^[65] The possible modes of cisplatin binding to DNA are shown in *Figure 1.5*.

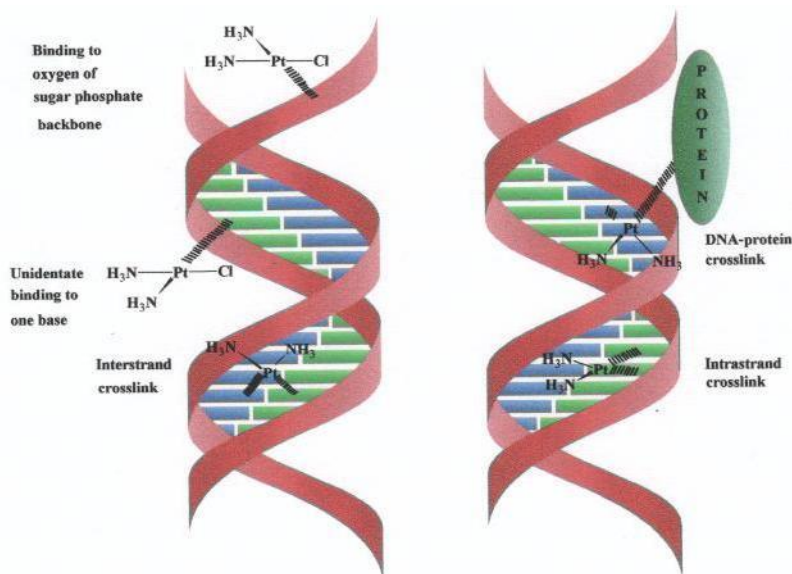


Figure 1.5 Some possible cisplatin-DNA binding modes.^[12]

In DNA, the main target of cisplatin is the telomeric regions of chromosomes.^[23] The telomeric region lies at the ends of eukaryotic chromosomes and consists of 5'-TTAGGG-3' tandem repeat units.^[72] These telomeric units are rich in guanosines and their main function is to protect the ends of chromosomes from degradation and to transfer the genetic information during cell division.^[23, 73] On average, during one cell division, the telomeres get shortened by 50-200 bp (where bp = base pairs).^[74] Cell death occurs when they get critically shortened. In over 90% of the tumor cell lines, the telomeric length is maintained by telomerase.^[75] Cisplatin degrades the telomeric regions in the chromosomes and suppresses cell division. With low doses of cisplatin, telomere degradation was reported to be 61% effective.^[23] Consequences of telomeres degradation are significant damages in the DNA and DNA replication by apoptosis, often known as “programmed cell death”.^[23]

The binding of cisplatin to DNA alters the DNA conformation and brings distortion to the structure. This results in DNA unwinding, bending and flattening of the minor grooves in the DNA helix.^[4, 67] Research has shown that cisplatin binding at adjacent guanine-guanine sequence causes the bending of DNA by 32-40°.^[76, 77] These changes result in the inhibition

of DNA transcription which is an important step for protein synthesis and cell division. Synthesis of anticancer drugs which can inhibit the telomerase activity is therefore important.

1.2.2. Cisplatin Resistance

Resistance of certain tumor cells to cisplatin is one of the major drawbacks of the drug. It was found that some tumor cells have intrinsic resistivity to the drug while others develop resistance to the drug during the treatment. Research has shown that the loss of function of tumor suppressor protein p53, through its regulations of other proteins can influence the resistance of cisplatin to certain cancer cells.^[23] Development of resistance to cisplatin are thought to be due to a number of reasons such as:^[12]

- ✓ Low intracellular accumulation due to the slow uptake and release rate of the drug.
- ✓ Binding of the drug to other complexing agents such as thiols which compete with DNA.
- ✓ Nucleotide excision repair (NER). This involves stimulation of DNA repair in the lesions of platinated DNA region. It was assumed that NER is the major contributor to cisplatin resistance.^[23, 63]

As a result, numerous platinum(II) complexes have been developed to improve the clinical inconveniences with less tumor resistance and toxicity.^[4, 29-31, 46] Unfortunately, out of thousands of platinum complexes that have been synthesised and clinically screened, only a few have been approved for clinical administration, including carboplatin, [cis-diaminecyclobutanedicarboxylatoplatinum(II)], oxaliplatin, {[[(1*R*,2*R*-diaminocyclohexane)oxalatoplatinum(II)](1,2-diaminocyclohexane, DACH)}nedaplatin, [cis-diammineglycolatoplatinum(II)] and lobaplatin^[5, 63] (*Figure 1.6*).^[38, 78]

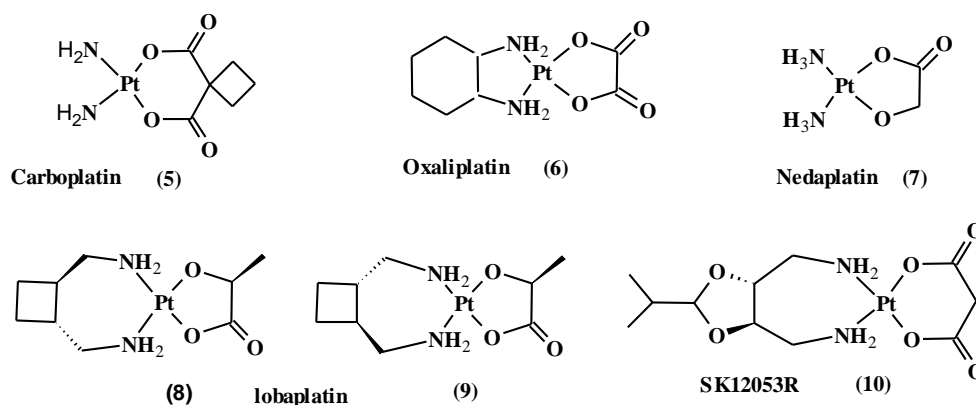


Figure 1.6 Platinum complexes in worldwide clinical use and as well as those with regionally limited approval: nedaplatin, lobaplatin and SK12053R.^[38, 78]

Of the five platinum complexes (5), (6), (7), (8) and (9), carboplatin was found to be less toxic^[4, 5, 79] and administered at higher doses (2000 mg/dose)^[80] than standard regimes (900 mg/m²).^[4, 81] This is due to its different pharmacokinetic profile where the leaving group of carboplatin is a less labile cyclobutanedicarboxylate ligand^[56, 69] which undergoes a slower aquation^[79, 82] compared to the chloride ligands in cisplatin.^[4, 5, 56] However, due to the similarities in its structure and the mechanism of action to cisplatin, carboplatin exhibits similar kind of cross-resistance to cisplatin and thus has not demonstrated many significant advantages over cisplatin.^[45, 83]

Therefore, the search for new platinum drugs which do not exhibit cross-resistance with cisplatin and carboplatin is ongoing. After thousands of platinum compounds were tested clinically, it was found that the structure of the leaving group appears to influence the distribution and the coordination of the platinum complex to the tumor cells. Recent studies have shown active platinum(II) complexes containing bidentate leaving groups with lower toxicity.^[12] This led to the synthesis of 1,2-diaminocyclohexane, (DACH) platinum analogues, oxaliplatin. Oxaliplatin was found to be active in combination with 5-fluorouracil and leucovorin for the treatment of colorectal cancer, a disease where cisplatin and carboplatin showed no significant activity.^[4, 5, 84] This drug has been approved for clinical use by France^[22] Europe, China and United states.^[5, 85, 86] Another platinum complex, nedaplatin, registered in Japan is in use for head, neck, lung and oesophageal cancer.^[22] However, clinical trials of this drug have shown cross-resistance similar to cisplatin but is less toxic.^[5] Lobaplatin has been approved in China while SK12053R is under phase(II) clinical trials.^[22]

Since most of these drugs are structural analogues of cisplatin, they exhibit a similar kind of cross-resistance and hence did not show as a fundamental breakthrough in the pharmaceutical industry.

1.3. Current Findings on Anticancer Platinum(II) Drugs

Current research on the development of anticancer drugs focuses on the synthesis of structurally different analogues of cisplatin derivatives with altered pharmacokinetic and pharmacodynamic properties which can exhibit effective antitumor activity with less side effects and tumor resistance. As a result, a number of active mono- and multi-nuclear platinum(II) complexes have been discovered with various structural modifications. However, focus here will be given mainly on the mononuclear platinum(II) N-donor complexes.

1.3.1. Mononuclear Platinum(II) Complexes

The early structural-activity relationships played an important role in the development of active platinum anticancer drugs. However, structural-activity relationships have been proven to be invalid with the recent findings of active platinum complexes which do not conform to these structural-activity features. Recent studies have found mononuclear platinum(II) complexes which are active against tumor cells and are:^[15]

- ✓ *Trans* configuration
- ✓ Charged complexes
- ✓ Non-H-amine neutral ligands

Research has shown *in vitro* toxicity for some platinum(II) *trans* compounds (*Figure 1.7*) with the general formula, $[\text{PtCl}_2\text{LL}']$ where L = L' = pyridine (**14**), L = quinoline, L' = ammonia (**15**), L = L' = *N*-methylimidazole (**16**).^[15, 22]

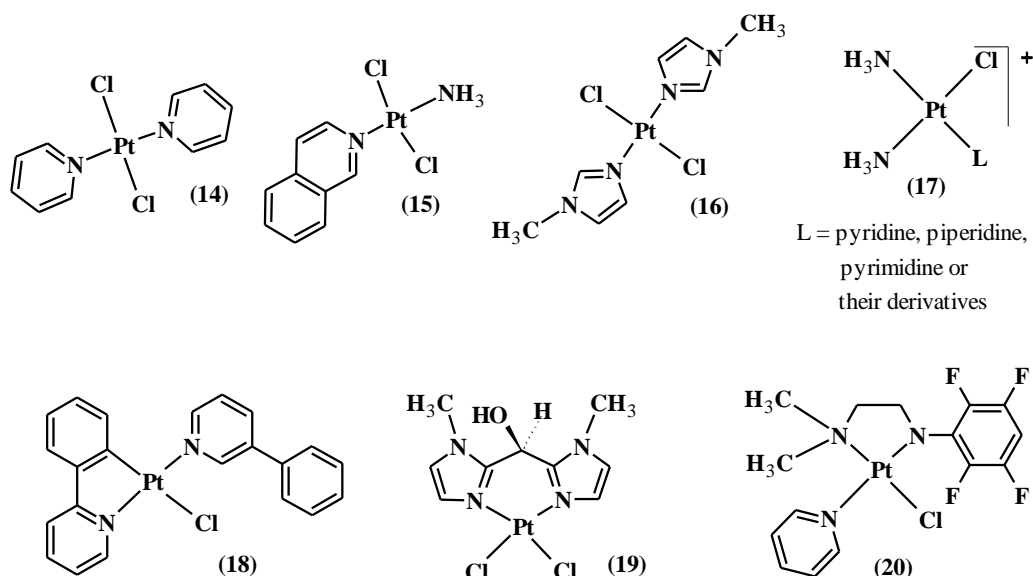


Figure 1.7 Some platinum(II) complexes which deviate from the proposed structural-activity relation, yet have shown antitumor activity in line with cisplatin. [12, 15, 87]

Since neutral complexes are more lipophilic, early studies have shown that neutrality is an essential feature for antitumor activity. However, several active platinum(II) complexes of the general formula $cis\text{-[Pt(NH}_3\text{)}_2\text{(L)Cl]}^+$ (L = pyridine, purine, pyrimidine, piperidine or a saturated amine) **(17)** have recently been reported.^[12, 15] In addition, non-H-amine platinum(II) complexes such as complexes **(18)**, **(19)** and **(20)** were also found to be active towards tumor cell lines exhibiting *in vivo* cytotoxicity. Furthermore, complex **(18)** was discovered to be active against cisplatin resistant mouse sarcoma 180 cell line due to its high efficiency in cellular uptake.^[88]

Another approach of synthesis of effective mononuclear anticancer platinum(II) drugs involves attaching a biologically active carrier group to an active platinum(II) complex which results in a platinum(II) complex with more than one active centre known as ditopic molecules.^[12] Such compounds have greater cell targeting properties and are expected to have improved cellular uptake.^[12] However, details of ditopic molecules will not be focussed on in this dissertation.

1.3.2. Multinuclear Platinum Complexes

Multinuclear platinum complexes are an important class of platinum compounds which has gained a considerable research interest. Examples of these compounds include flexible diaminoalkane chains^[89] and rigid multinuclear complexes^[90] (Figure 1.8).

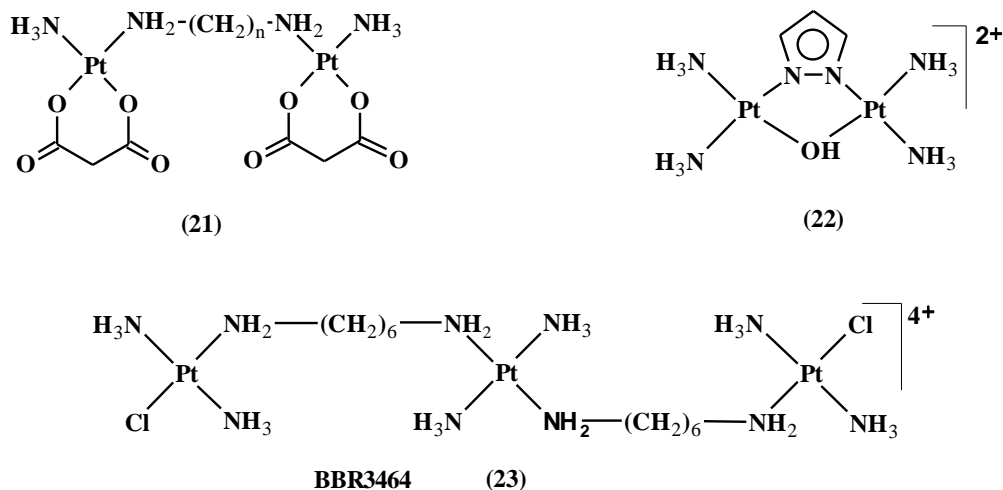


Figure 1.8 Some polynuclear platinum complexes which have shown potential anticancer activity.^[45, 90-92]

The dinuclear platinum complexes **(21)** ($n = 4 - 9$), was found to have desirable anticancer activities against human tumor cells.^[45] A different type of dinuclear complex with a rigid linkage group **(22)** has shown higher intrastrand cross-linkage with DNA, causing changes in the double helix. This compound was found to be highly active against tumor cells including renal and breast cancer.^[93] Recent studies have reported trinuclear platinum complexes such as BBR3464 **(23)** which are retained within the same cell lines as cisplatin and are active against melanoma, pancreatic cancer, lung cancer.^[90, 91] This compound was found to bind to the N7 site of guanine in DNA to form long-range interstrand and intrastrand DNA cross-links^[90, 92] with higher cellular uptake and no cross-resistance to cisplatin resistance cells.^[22]

1.4. Current Research on Platinum(II) Terpy and Polypyridine Complexes

Platinum(II) 2,2':6',2''-terpyridine (terpy) complexes have the basic form $[\text{PtY}(\text{terpy})\text{X}]^{n+}$, where **Y** is the substituent on the terpy ligand and **X** is the ligand in the fourth coordination

site.^[8] These complexes were first synthesized in 1934.^[8] Platinum(II) terpy and polypyridine complexes have a wide range of chemical applications including photophysical applications and biological activities. However, our focus will be only the biological importance and the substitution reactions of mononuclear platinum(II) terpy and some of its analogous complexes.

1.4.1. Biological Importance

Recently the coordination chemistry of platinum(II) chromophores such as terpy and 1,10-phenanthroline complexes have gained a considerable interest due to their tendency to selectively bind to DNA.^[75, 94-97] Cationic, planar aromatic platinum(II) terpy and polypyridyl derivatives are proven to inhibit the telomerase activity by binding with the G-quadruplex of DNA.^[75] Complexes with extended π -conjugation of the terpy ligands such as phenanthroline allows a better σ -bonding framework and increases the strength of the ligand and the π -stacking with DNA.^[98] Such complexes can interact with the DNA either by intercalating with the base pairs of DNA or *via* covalent bonding.^[8, 96]

1.4.1.1. DNA Intercalation

DNA intercalation is a non-covalent association between the platinum molecules and base pairs of DNA.^[8, 99] Interaction of platinum(II) terpy and polypyridine complexes with DNA depends on number of factors such as:^[8, 100]

- ✓ Planarity of the complex
- ✓ Aromaticity and the surface extension of the terpy moiety to overlap the π system with DNA base pairs
- ✓ Size and the bulkiness of the complex
- ✓ The charge on the complex
- ✓ The ability of the **X** ligand to form hydrogen bonds with DNA base pairs.

Intercalation of platinum(II) terpy with DNA dates back to 1974 with the cationic $[\text{Pt}(\text{terpy})\text{Cl}]^+$ complex.^[94] To avoid complications due to chloride ligand displacement reactions, $[\text{Pt}(\text{terpy})(\text{HET})]^+$ (HET = 2-hydroxyethanethiol) (*Figure 1.9*, complex **(24)**), was often used in initial studies. Investigations of $[\text{Pt}(\text{terpy})(\text{HET})]^+$ and calf thymus DNA had shown interactions of the compound with DNA with a binding constant of $1.2 \pm 0.2 \times 10^6 \text{ M}$ at a pH of 6.8 in 0.003 M sodium chloride solution.^[8] Studies of the X-ray crystal structure of

this complex with DNA has shown that the complex adds between the DNA base pairs where the compound binds to every other base-pair space in DNA. Thus the results of this study led to the discovery of the nearest neighbour exclusion effect.^[101, 102]

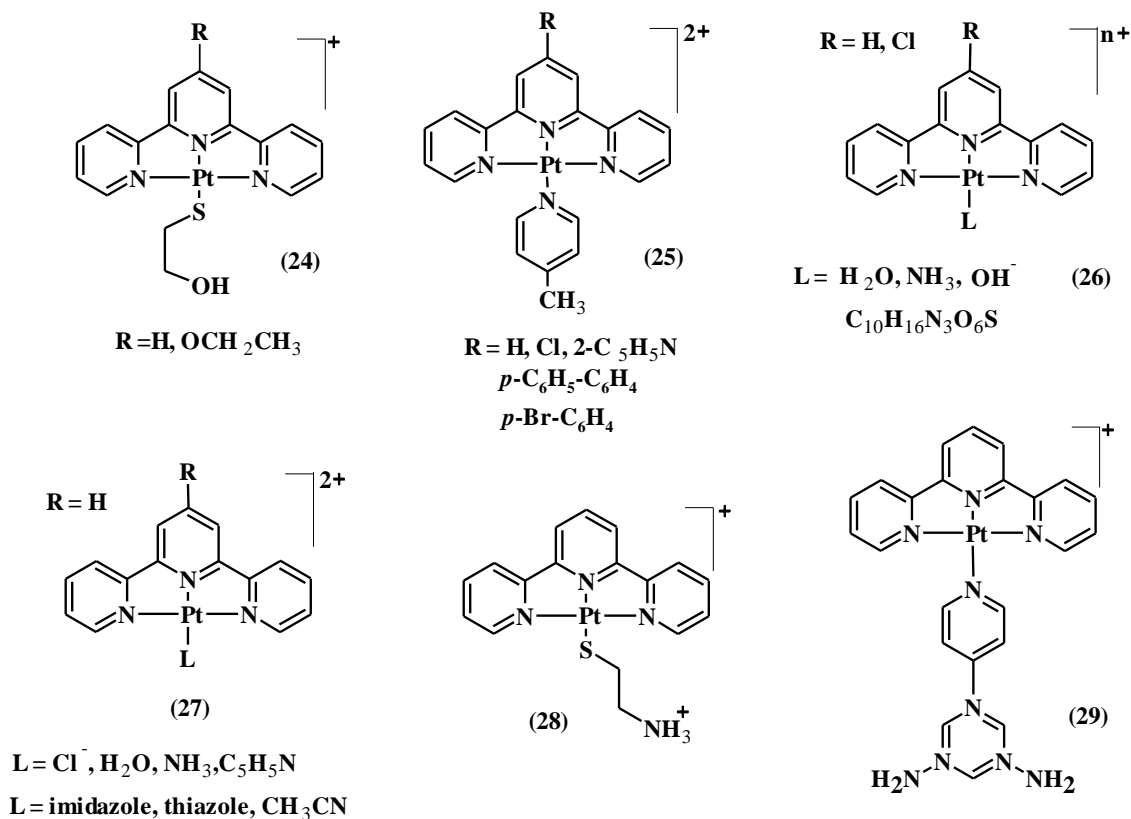


Figure 1.9 Structure of some of the well studied platinum(II) terpyridine complexes which have shown cytotoxicity and DNA intercalation against tumor cells (anions are omitted for simplicity).^[8, 75, 95, 103-106]

Investigations on the analogous complexes such as, $[Pt(terpy)(4\text{-picoline})]^{2+}$ (**25**, $R = H$) were found to bind with DNA even stronger ($1.8 \pm 0.5 \times 10^7 M^{-1}$) while $[Pt(terpy)(OH)]^+$ (**26**, $R = H$) was found to have a binding constant of $\approx 7 \times 10^4 M^{-1}$.^[104] The observed binding abilities of the complexes with DNA is due to their significant π -bonding ability with the DNA base pairs and the orientation of the molecules which points the positive centre towards the minor groove of DNA while the ligands in the fourth coordination site directs to the major groove.^[8] *In vitro* tests for the complexes, (**24**, **25**) and (**26**, $R = Cl$, $L = OH, NH_3, C_{10}H_{16}O_6S$) with *Trypanosoma cruzi* Trypanothione Reductase (*T. cruzi* TR) has shown effective inhibition of the TR parasite from *T. cruzi*.^[105] This effective binding was thought to be partly due to the irreversible binding or substitution of the ligand in the fourth coordination site by DNA bases. Complexes (**27**) and (**28**) were found to be effective against human ovarian cancer cells.^[95] The reaction of the complex (**29**) with human DNA, showed potent anticancer

activity towards nasopharyngeal carcinoma (CNE3 and its cisplatin variant, CNE1) with comparable cytotoxicity with IC_{50} values of ~ 10 IM.^[107] The higher reactivity was thought to be due to its ability to form hydrogen bonding with the DNA base pairs.

Research has shown that the charge on the complex affects the biological activity of the platinum drug with DNA.^[8] Lippert and co-workers have studied a number of $[Pt(terpy)X]^{n+}$ (for $n = 1$, $X = Cl^-$, HET, Cysteine (Cys) and $n = 2$, $X =$ aminoethanethiol (AET)). In this study the observed high binding constant for the AET complex was found to be due to its high charge (*Table 1.1*).^[8]

Table 1.1 Binding constants for some of the platinum(II) terpy complexes studied by Lippert and co-workers.^[8]

| Complex | DNA medium | Binding constant, K (M^{-1}) | Reference |
|-------------------------|-----------------------------------|------------------------------------|-----------|
| $[Pt(terpy)Cl]^+$ | ct-DNA; Tris buffer | 3.9×10^5 | [108] |
| $[Pt(terpy)(HET)]^+$ | ct-DNA; pH 7.5, 0.2 M NaCl | 1.2×10^5 | [109] |
| $[Py(terpy)(AET)]^{2+}$ | ct-DNA; pH 7.5, 0.2 M NaCl | 4.3×10^5 | [109] |
| $[Pt(terpy)Cys]^+$ | ct-DNA; pH 7.5, 0.2 M NaCl | 1.0×10^5 | [109] |
| $[Pt(terpy)(OH)]^+$ | st-DNA; pH 9.0, 0.5 M EPSS buffer | 7×10^4 | [104] |

Furthermore, research done by Cusumano *et al.*^[110] had shown that the steric hindrance in the fourth coordination sphere reduces the binding strength of platinum complexes with DNA. Two complexes, $[Pt(terpy)(2-CH_3py)]^{2+}$ ($py =$ pyridine) and $[Pt(terpy)(py)]^{2+}$ with similar aromatic surfaces when subjected to DNA binding, showed a higher binding constant for the latter complex. The methyl group on the second position of $[Pt(terpy)(2-CH_3py)]^{2+}$ reduces the stacking surface which causes more destabilization of the resulting complex thus reducing the binding constant.

Considerable research efforts are currently focused on other platinum(II) DNA intercalators such as derivatives of platinum(II) phenanthroline complexes. Recent studies done by Wheate *et al.*^[97, 111] had investigated the cytotoxicity and DNA intercalation for a number of platinum(II) phenanthroline complexes with different chiral and achiral ancillary groups (*Figure 1.10*). Based on the *in vitro* cytotoxicity, the best DNA intercalating activity was shown for [(5,6-dimethyl-1,10-phenanthroline)(1*S*,2*S*-diaminocyclohexane)platinum(II)]²⁺ (**56MESS**) (**30**), [5-methyl-1,10-phenanthroline)(1*S*,2*S*-diaminocyclohexane)platinum(II)]²⁺ (**5MESS**) (**31**) and [(1,10-phenanthroline)(1*S*,2*S*-diaminocyclohexane)platinum(II)]²⁺ (**PHENSS**) (**32**).^[97] The activity of the complexes towards the L1210 murine leukaemia cell

line, **(30)** was found to be about 100-fold more cytotoxic than cisplatin.^[97] Furthermore, **(32)** has shown potent cytotoxicity towards various human cancer cell lines *viz.* lung, bladder, oesophageal, cervical, breast and ovarian cancer including some of the tumor cells which have shown resistance to cisplatin.^[97] *In vitro* cytotoxicity of **(30)** is under clinical trials. The high cytotoxicity and improved resistance was observed for the complexes which have:^[97]

- ✓ a methyl group either at fifth or fifth and sixth position
- ✓ the *R,R* configuration
- ✓ chiral ancillary ligands

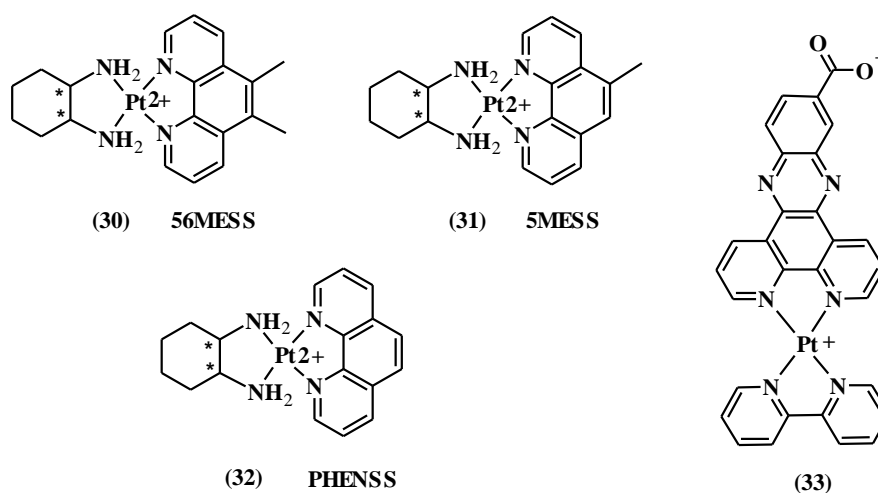


Figure 1.10 Structure of 1,10-phenanthroline and phenanthroline-based platinum(II) intercalating complexes. Complexes **(30)**, **(31)** and **(32)** are the three best platinum(II) based DNA intercalators studied by Wheate *et al.*^[97] Complex **(33)** is from Ref.^[75] The anions are omitted for simplicity. * Indicates a chiral centre (either *R* or *S*, *R* complexes are found to be more effective).

Even though the exact mechanism of intercalation was not understood, from the studies it was found that DNA intercalation is either *via* the phenanthroline or the ancillary ligand. Also it was found that the DNA binding of these complexes is independent of the way that they exhibit their cytotoxicity or induced apoptosis but it is based on the intracellular transport factors such as structural changes of the molecule.^[97]

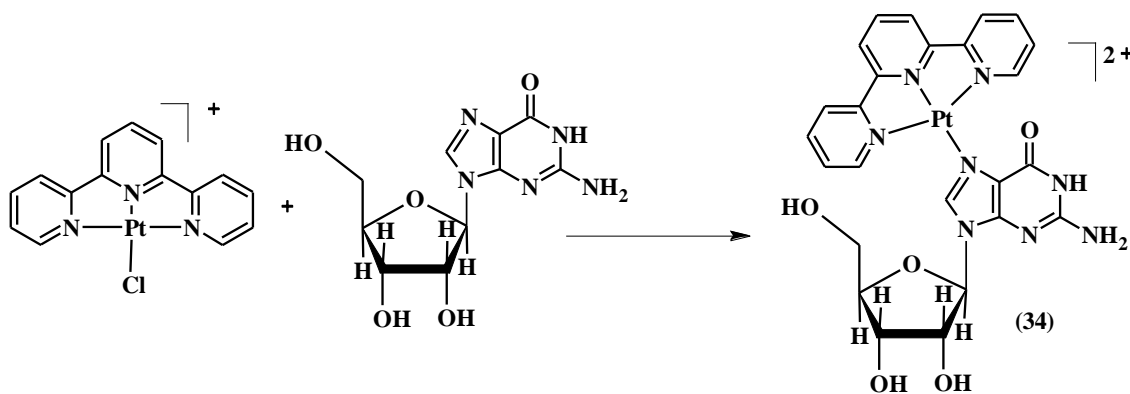
Further investigation done by Ma *et al.*^[75] on the binding of phenanthroline derivatives to G-quadruplex DNA involved a number of platinum(II) complexes having dipyrrophenazine (dppz) and C-deprotonated 2-phenylpyridine ($N^{\wedge}CH$) ligands. From this study the complex **(33)** was found to bind with G-quadruplex DNA with a binding affinity of 10^7 M. The *in vitro* telomerase activity of this compound using a biotinylated-primer extension telomerase

assay, showed the compound is an effective telomerase inhibitor with $^{tel}IC_{50}$ value of 760 nM.^[75]

The consequences of the intercalation results the unwinding of the closed circular DNA backbone and increase in the helix length and its rigidity. It also results in changes in the physical properties such as an increase in the melting point^[8]

1.4.1.2. Substitution of Platinum(II) Terpy with Biologically Active Nucleophiles

Apart from the non-covalent binding to DNA, $[PtY(terpy)X]^{n+}$ (where X = a labile group such as chloride, hydroxide, water or pyridine derivatives and Y = H, Cl, OCH₃, CH₃ and 2-C₅H₅N, Figure 1.9, (25), (26) and (27)) can also undergo ligand substitution reactions, covalent binding to the donor atoms of nucleobases of DNA. This is one of the main areas where the kinetic and mechanistic studies of substitution reactions of platinum(II) terpy analogues are important to understand the mechanisms of platinum anticancer drugs with DNA. Scheme 1.3 shows a reaction of $[Pt(terpy)Cl]^+$ with guanosine.^[8, 103]



Scheme 1.3 Reaction of platinum(II) (terpy) with guanosine (1:1) showing the N7 binding of guanosine with platinum(II) (terpy). Structure (34) from Reference.^[8, 103]

The success of such reactions depends on both thermodynamic factors such as the stability of the Pt—N bond formed in relation to the Pt—X bond, and kinetic factors such as the rate of replacement of X by the incoming ligand.^[8] In such instances the reaction can be forced to completion by using excess concentration of nucleophile (under *pseudo conditions*). Studies done by Lowe *et al.*^[103] support the platinum(II) (terpy)(guanosine) structure (34) indicating the binding of the terpy complex with the N7 position of guanosine. However, at

low pH, substitution at N1 is possible since at low pH the N7 position might get protonated. Therefore, controlling the pH of the reaction medium is necessary in such reactions.

An equilibrium kinetic study done by Bugarčić *et al.*^[112, 113] on $[\text{Pt}(\text{terpy})\text{Cl}]^+$ at pH 6, with some biologically active nucleophiles, inosine (INO), inosine-5'-monophosphate (5'-IMP) and guanosine-5'-monophosphate (5'-GMP) (Figure 1.11) have shown the higher reactivity towards the studied nucleophiles, particularly 5'-GMP and GSH.^[112] Similarly work done by van Eldik and co-workers^[113] showed that at lower pH of 2.5, $[\text{Pt}(\text{terpy})(\text{OH}_2)]^{2+}$ coordinates rapidly to 5'-GMP, INO and IMP *via* their N1 positions. In addition, reactions of platinum(II) terpy complexes with other DNA bases such as adenosine and 1-methylcytosine (Hmcyt) were found to form di- and tri-cationic complexes depending on the reaction stoichiometry.^[8]

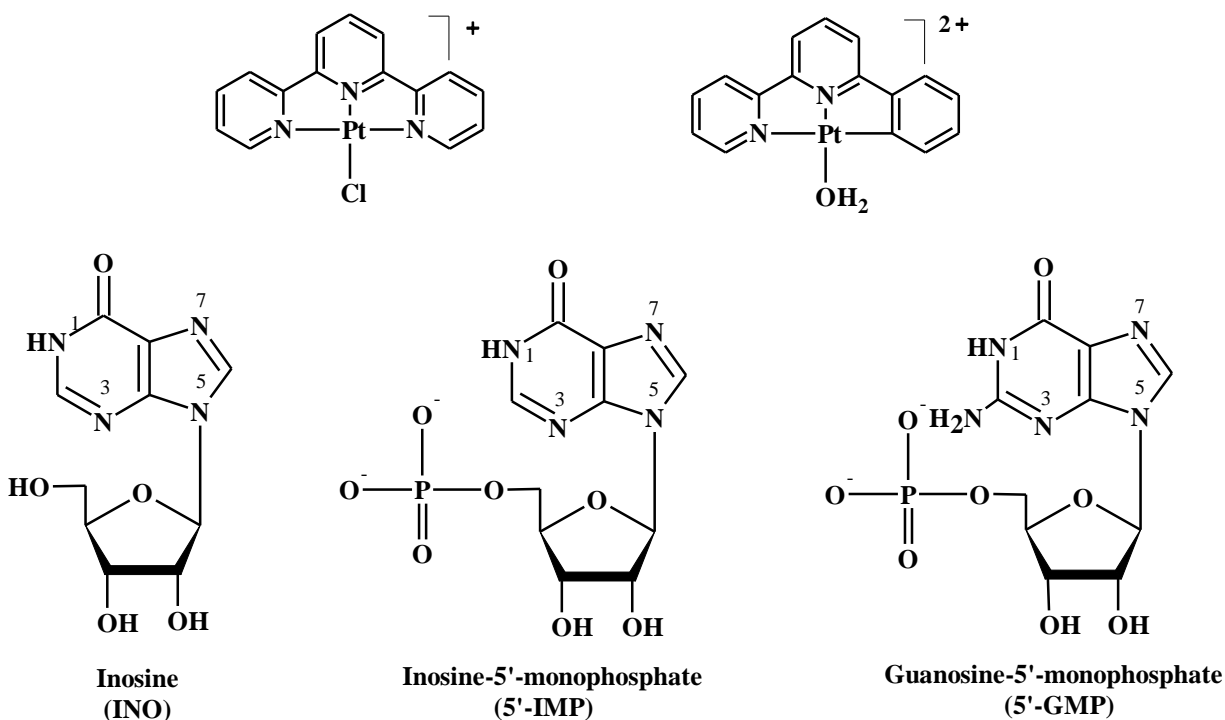
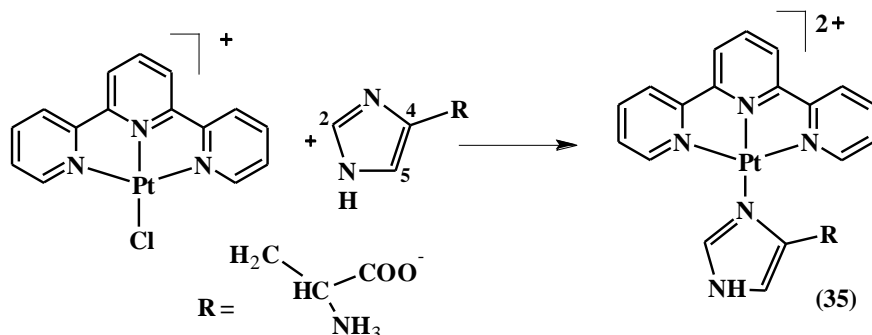


Figure 1.11 Some of the platinum(II) terpy complexes and biologically active nucleophiles studied by Bugarčić *et al.*^[112, 113]

Furthermore, kinetic studies of *pseudo* first-order ligand substitution reactions of $[\text{Pt}(\text{terpy})\text{Cl}]^+$ at pH 3 with nitrogen donor ligands, *viz.* histidine (His) and cysteine (Cys) showed dependence of reactivity towards the nature of the nucleophiles. The higher reactivity for Cys ($k_{\text{obs}} = 1.3 \times 10^{-2} \text{ s}^{-1}$) compared to His ($k_{\text{obs}} = 8.5 \times 10^{-5} \text{ s}^{-1}$)^[114] explained in

terms of the stability of the $[\text{Pt}(\text{terpy})(\text{His})]^+$ cation in aqueous medium compared to the Cys complex.^[8] Interestingly, the substituted complex, $[\text{Pt}(\text{terpy})(\text{His})]^+$ was found to have enzyme inhibition activity when bound to the Histidine-630 residue of the active site.^[56]



Scheme 1.4 Substitution reaction of $[\text{Pt}(\text{terpy})\text{Cl}]^+$ with histidine (His) to form $[\text{Pt}(\text{terpy})\text{His}]^{2+}$.^[8]

Therefore, due to the irreversible binding of platinum(terpy) complexes with biological nucleophiles such as guanosine, histidine, cysteine and their cytotoxic behaviour, platinum(II) terpy derivatives can be used as probes for anticancer drugs.^[8]

1.4.2. Current Study on Substitution Reactions on Platinum(II) Polypyridyl and Platinum(II) Terpy complexes

Of the large number of platinum complexes synthesized and tested for anticancer activity, platinum(II) terpy and its analogues as anticancer probes have become one of the main research targets. To design more effective anticancer drugs, a clear understanding of the factors which influence the substitution behaviour of such complexes is important.^[115] The knowledge of kinetic and mechanistic substitution behaviour of such complexes would be an important tool in the synthesis of new platinum anticancer drugs.

Investigation of substitution reactions of platinum(II) terpy complexes with neutral nitrogen donors have seldom been studied. Pitteri *et al.*^[116] has investigated the kinetics of $[\text{Pt}(\text{terpy})\text{Cl}]^+$ with neutral five membered heterocycles such as, thiazole, oxazoles, imidazole, pyrazole and 3,5-dimethylpyrazole of different basicities. The results of this study had shown an increase in the rate of substitution reactions with increase in the basicity of the nucleophiles whereas increase in the steric hindrance has decreased the substitution rate.

To understand the substitution behaviour of platinum complexes, studies were focused on different aspects. van Eldik *et al.*^[117] studied the effect of increasing the π -acceptor pyridine ligands on the substitution rates of aqua platinum(II) tri(N-donor) complexes *viz.* [Pt(diethylenetriamine)OH₂]²⁺ (**aaa**), [Pt(2,6-bis-aminomethylpyridine)OH₂]²⁺ (**apa**), [Pt(N-(pyridyl-2-methyl)-1,2diamino-ethane)OH₂]²⁺ (**aap**), [Pt(bis(2-pyridylmethyl)amine)OH₂]²⁺ (**pap**), [Pt(2,2'-bipyridine)(NH₃)(OH₂)]²⁺ (**app**) and [Pt(terpy)OH₂]²⁺ (**ppp**) (Figure 1.12) with some neutral and anionic nucleophiles namely; thiourea (**TU**), dimethylthiourea (**DMTU**), trimethylthiourea (**TMTU**), thiocyanate (**SCN⁻**) and iodide (**I⁻**) respectively.

Results of this study have shown an increase in the rate of the substitution reactions with an increase in the π -acceptor pyridine ligands on the metal centre.^[117] The increase in these ligands increases the electrophilicity of the metal centre.^[117] The observed trend for the reactivity of the complexes was **aaa** < **apa** < **aap** < **pap** < **app** < **ppp**. This was explained in terms of the increase in the electronic communication due to the increase in the π -acceptance pyridine rings in the spectator chelate ring.^[117] This results in a decrease in the frontal orbital energy resulting in a smaller gap between HOMO and LUMO energy level. The π -antibonding orbitals on the pyridine ligands accept electron density from the platinum centre making the metal centre more electrophilic. Furthermore, the increase in the aromaticity around the platinum centre helps to stabilise the five coordinate transition state by spreading the electron density over the aromatic system thereby resulting in an increase in the substitution reaction.^[117]

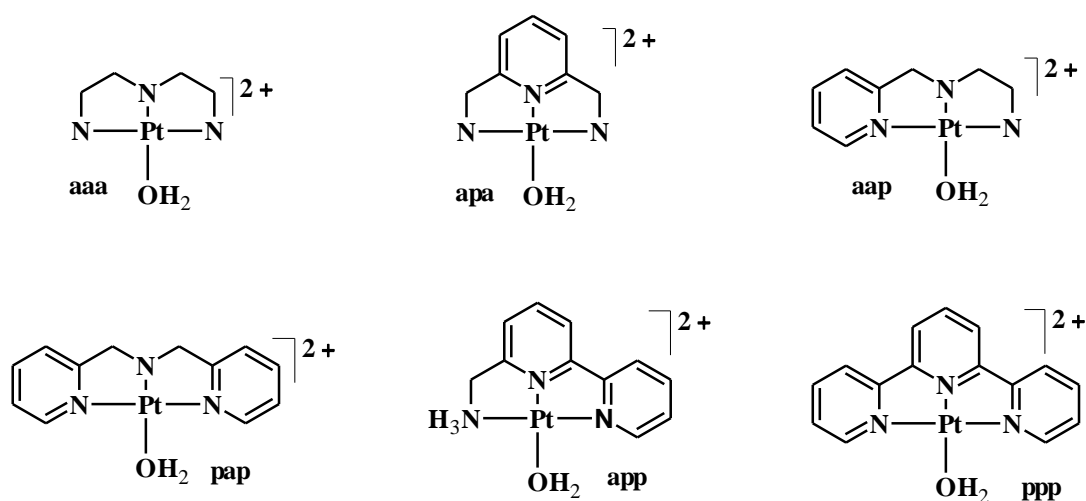


Figure 1.12 Platinum(II) complexes studied by van Eldik *et al.*^[117]

van Eldik *et al.*^[118] further, investigated the effect of *cis* and *trans* Pt—C σ -donor effect on the substitution reaction in the presence of a π -acceptor backbone. In this study, kinetics of [Pt(NNC)Cl] (NNCH = 6-phenyl-2,2'-bipyridine), [Pt(NCN)Cl] (NCHN = 1,3-di(2-pyridyl)benzene), and [Pt(NNN)Cl] (NNN = 2,2':6',2''-terpyridine)(Figure 1.13) with nucleophiles **TU**, **DMTU**, **TMTU** Br^- and I^- were investigated.

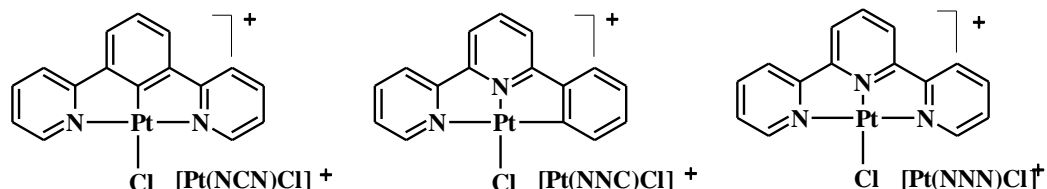


Figure 1.13 Platinum(II) polypyridyl complexes studied by van Eldik *et al.* to investigate the Pt—C *cis* and *trans* σ -donation on the rate of substitution behaviour.^[118]

The results showed that the reactivity of [Pt(NCN)Cl] was much higher than the reactivity of the other two complexes. The higher reactivity of [Pt(NCN)Cl] was due to the strong *trans* labilizing effect of the carbon donor which increases the intrinsic reactivity.^[118] When the stronger π -accepting pyridine in [Pt(NNN)Cl] is replaced by a phenyl ring in [Pt(NCN)Cl], the π -accepting ability of the chelate ligand is partially decreased by the σ -donor effect of the Pt—C bond in [Pt(NCN)Cl].^[118]

When comparing the reactivity of [Pt(NNC)Cl] with [Pt(NNN)Cl], the influence of *cis* σ -donicity of Pt—C was significant. The stronger σ -donor Pt—C in the *cis* position slows down the substitution reactions. The reason or the slower reactivity of [Pt(NNC)Cl] is due to the decrease in the nucleophilic discrimination of *cis* σ -donor in comparison to the *trans* σ -donor. This is in agreement with the findings of Romeo *et al.* where the strong σ -donors when placed in *cis* position dominates over the electron withdrawing effect of π -acceptors.^[119]

The influence of the chelate substituent^[115, 120], the *cis* σ -effect^[120] and the extent of π -back-bonding on the ligand substitution behaviour was further studied by Jaganyi *et al.*^[121] A series of platinum(II) complexes, [PtL(terpy)Cl]⁺ (where L = H or tri-*tert*-butyl), [Pt{4'-phenyl-terpy}Cl]⁺, [Pt{4'-(*o*-R-phenyl)-terpy}Cl]⁺ (where R = CF₃, CH₃ and Cl⁻) and [Pt{4'-(*o*-CF₃-phenyl)-6-phenyl-bipy}Cl]⁺ were studied using anionic and neutral nucleophiles, *viz.* I^- , SCN^- and **TU**, **DMTU**, **TMTU** respectively. Results obtained from the studies support the finding of van Eldik *et al.* indicating that the Pt—C *cis* σ -effect decelerates

the substitution reaction by 'pumping' electron density onto the metal centre which in turn destabilises the transition state thus decreasing reactivity.

When comparing the substituent on the terpy fragment, studies showed that substitution of the chloride ligand is controlled by the electrophilicity of the metal centre which is dependent on the properties of the terpy fragment.^[120] The presence of electron donating groups on the ancillary position of the terpy moiety slows down the substitution reaction whereas the presence of electron withdrawing group on the *ortho* position of the ancillary phenyl ring increases the reactivity by enhancing the π -back-bonding ability of the terpy fragment.^[121]

When comparing the reactivity of $[\text{Pt}(\text{terpy})\text{Cl}]^+$ with $[\text{Pt}(\text{tBu}_3\text{terpy})\text{Cl}]^+$ (Figure 1.14), the slower reactivity of the latter is due to the presence of electron donating groups on the ancillary position of terpy ligand which reduces the π -acceptor property of the ligand and hence reduces the electrophilicity of the metal centre. The same is true for $[\text{Pt}\{4\text{'-phenyl-terpy}\}\text{Cl}]^+$ where the phenyl ring on the 4' position being an electron donating group, reduces the reactivity of the complex compared to $[\text{Pt}(\text{terpy})\text{Cl}]^+$.

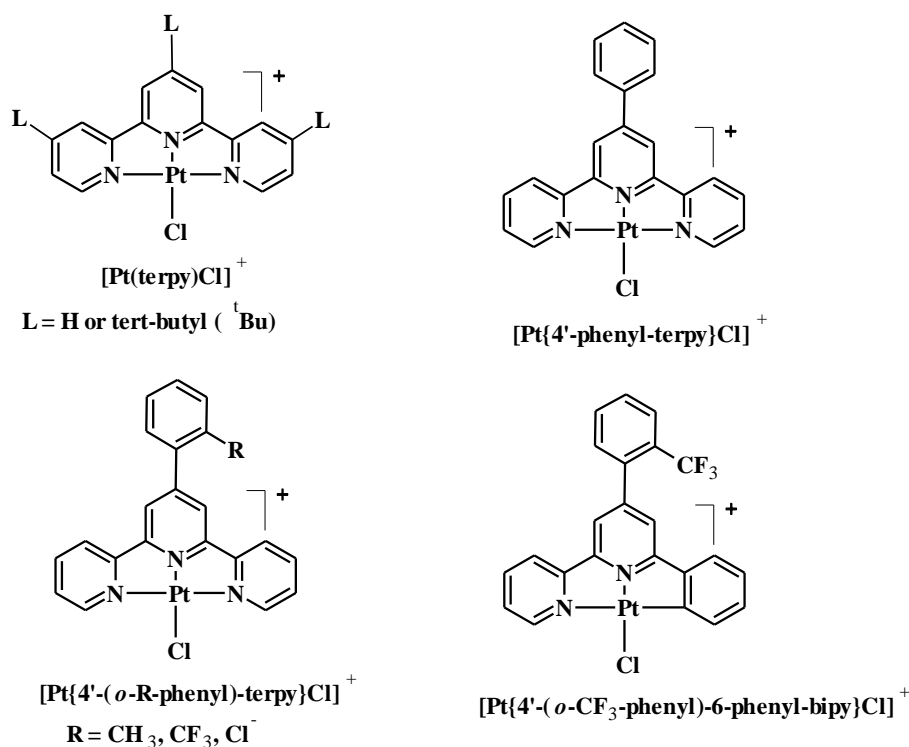


Figure 1.14 Platinum(II) terpy complexes studied by Jaganyi *et al.*,^[115, 117, 120, 121]

The presence of substituents on the *ortho* position of the ancillary phenyl ring alters the reactivity either by enhancing or reducing the π -back-bonding ability of the terpy moiety.

The substitution rate of the $[\text{Pt}\{4'-(o\text{-CH}_3\text{-phenyl})\text{-terpy}\}\text{Cl}]^+$ is lower when compared with that of $[\text{Pt}\{4'-(o\text{-CF}_3\text{-phenyl})\text{-terpy}\}\text{Cl}]^+$ due to the presence of an electron withdrawing group on the *ortho* position of the phenyl ring which increases the π -back-bonding ability of the terpy ring system. This increases the electrophilicity of the platinum centre which in turn increases the reactivity of the metal centre. The opposite is true for the former complex where CH_3 on the *ortho* phenyl group is an electron donor.

1.5. Aims of This Study

Since anticancer platinum(II) drugs such as cisplatin shows more preference to the binding of N7 guanine of DNA, understanding the kinetic and mechanistic substitution behaviour of potential platinum(II) complexes with heterocyclic nitrogen donors which possess similar binding sites to guanine and other biologically active ligands such as histidine is important to elucidate the mechanism of action of these drugs with DNA. Since platinum(II) terpy derivatives are potential antitumor agents, the study of kinetic and mechanistic substitution behaviour of platinum(II) terpy derivatives with biologically relevant nitrogen donors such as pyrazole and imidazole derivatives is of great importance to the development of effective platinum antitumor drugs.

Previous research in our laboratories had reported the kinetic studies of platinum(II) terpy and substituted platinum(II) terpy complexes with different ionic and neutral sulphur donor nucleophiles especially; iodide, chloride, bromide, thiocyanide and thiourea, dimethylthiourea and trimethylthiourea respectively.^[115, 117, 120, 121] No kinetic studies have yet been done to investigate the effect of increasing the conjugation in the *cis* and *cis/trans* positions between π -acceptor ligands of platinum(II) terpy and its analogous complexes with heterocyclic nitrogen donors.

Therefore, the aim of this work is to investigate the effect of increased π -conjugation in the *cis* and *cis/trans* between π -acceptor ligands has on the rate of platinum(II) substitution reactions using neutral five-membered nitrogen donor ligands namely; pyrazole (**Pz**), imidazole (**Im**), 1-methylimidazole (**MIm**), 1,2-dimethylimidazole (**DMIm**) and triazole (**Tz**). These nucleophiles are chosen because of their relevance to the biologically active ligands such as histidine.^[8] The experimental data were supported by modelled DFT-calculations for the platinum(II) complexes in order to explain the observed reactivity trend. The structure of complexes and the nucleophiles used in this study are given in *Figure 5.1*.

1.6 References

1. R. B. Heslop and P. L. Robinson, *Inorganic Chemistry: A Guide to Advance Study*, 2nd Ed., Elsevier Publishing Company, New York, **1963**, p. 501-511.
2. U. Belluco, *Organometallic Coordination Chemistry of Platinum*, Academic Press, London, **1974**, p. 1, 19-50, 220-221.
3. C. E. Housecroft and A. G. Sharpe, *Inorganic Chemistry*, 2nd Ed, Pearson Prentice Hall, London, **2005**, p. 684-689.
4. B. Lippert, *Cisplatin: Chemistry and Biochemistry of a Leading Anticancer Drug*, Wiley-VCH, New York, **1999**, p. 1-100, 184-190.
5. M. Gieleng and E. R. T. Tiekink, *Metallotherapeutic Drugs and Metal-Based Diagnostic Agents: The Use of Metals in Medicine*, John Wiley and Sons, Ltd, Canada, **2005**, p. 489-502.
6. B. Rosenberg, L. Van Camp, J. E. Trosko and V. H. Mansour, *Nature*, **1969**, 222, 385.
7. B. Rosenberg, L. Van Camp and T. Krigas, *Nature*, **1965**, 205, 698.
8. S. C. Cummings, *Coord. Chem. Rev.*, **2009**, 253, 1495.
9. R. R. Crichton, *Biological Inorganic Chemistry: An Introduction*, Elsevier, New York, p. 1, 341-344.
10. M. J. Cleare and J. D. Hoeschele, *Plat. Met. Rev.*, **1973**, 17, 3.
11. M. J. Cleare and J. D. Hoeschele, *Bioinorg. Chem.*, **1973**, 2, 187.
12. C. J. Jones and J. R. Thornback, *Medicinal Application of Coordination Chemistry*, Royal Society of Chemistry, Cambridge, **2007**, p. 1, 218-257.
13. P. S. Sengupta, R. Sinha, S. K. Bera and G. S. De, *Ind. J. Chem., Sect. A*, **2002**, 41A, 712.
14. M. Coluccia and G. Natile, *Anti-Cancer Agents Med. Chem.*, **2007**, 111.
15. T. W. Hambley, *Coord. Chem. Rev.*, **1997**, 166, 181.
16. W. Zhen, J. C. Link, M. P. O'Connor, A. Reed, R. Parker, S. B. Howell and V. Bohr, *Mol. Cell. Biol.*, **1992**, 12, 3689.
17. S. Komeda, G. V. Kalayda, M. Lutz, A. L. Spek, Y. Yamanaka, T. Sato, M. Chikuma and J. Reedijk, *J. Med. Chem.*, **2003**, 46, 1210.
18. C. M. Sorenson and a. Eastman, *Cancer Res.*, **1988**, 48, 4484.
19. C. Avendano and J. C. Menendez, *Medicinal Chemistry of Anticancer Drugs*, 1st Ed., Elsevier, New York, **2008**, p. 169-173.
20. D. C. Ash, *J. Clin. Hemat. Oncol.*, **1980**, 10, 55.
21. G. Chu, *J. Biol. Chem.*, **1994**, 269, 787.
22. E. Wong and C. M. Giandomenico, *Chem. Rev.*, **1999**, 99, 2451.
23. E. R. Jaimeson and S. J. Lippard, *Chem. Rev.*, **1999**, 99, 2467.

24. I. Lakomska, *Inorg. Chim. Acta*, **2009**, 362, 669.
25. F. Arnesano and G. Natile, *Pure Appl. Chem.*, **2008**, 80, 2715.
26. P. Di Blasi, A. Bernareggi, L. Beggiolin, L. Piazzoni and E. Menta, *Anticancer Res.*, **1998**, 18, 3113.
27. F. Huq, H. Daghriri, J. Q. Yu, H. Tayyem, P. Beale and M. Zhang, *Eur. J. Med. Chem.*, **2004**, 39, 947.
28. P. J. Loehrer and L. H. Einhorn, *Ann. Intern. Med.*, **1984**, 100, 704-713.
29. R. S. Goldstein, B. Noordewier, J. T. Bond, J. B. Hook and G. H. Mayor, *Toxicol. Appl. Pharmacol.*, **1981**, 60, 163.
30. S. Komeda, M. Lutz, A. L. Spek, M. Chikuma and J. Reedijk, *Inorg. Chem.*, **2000**, 39, 4230.
31. D. D. Von Hoff, R. Schilsky, C. M. Reichert, R. L. Reddick, M. Rozenzweig, R. C. Young and F. M. Muggia, *Cancer Treat Rep*, **1979**, 63, 1527.
32. K. Lemma, T. Shi and L. I. Elding, *Inorg. Chem.*, **1999**, 39, 1728.
33. D. Petrovic, B. Stojimirovic, B. Petrovic, Z. M. Bugarcic and Z. D. Bugarcic, *Bioorg. Med. Chem.*, **2007**, 15, 4203.
34. S. M. Cohen and S. J. Lippard, *Prog. Nucleic Acid Res. Mol. Biol.*, **2001**, 67, 93.
35. D. S. Alberts and J. K. Noel, *Anticancer Drugs*, **1995**, 6, 369.
36. M. P. Goren, R. K. Wright and M. E. Horowitz, *Cancer Chemother. Pharmacol.*, **1986**, 18, 69.
37. D. V. Thurston, *Chemistry and Pharmacology of Anticancer Drugs*, CRC Press Taylor and Francis Group, London, **2006**, p. 61.
38. Y. Yu, L.-G. Lou, W.-P. Liu, H.-J. Zhu, Q.-S. Ye, X.-Z. Chen, W.-G. Gao and S.-Q. Hou, *Eur. J. Med. Chem.*, **2008**, 43, 1438.
39. S. K. Bera, P. S. Sengupta and G. S. De, *Inorg. React. Mech.*, **2003**, 5, 65.
40. R. W. Hay and S. Miller, *Polyhedron*, **1998**, 55, 528.
41. P. Perego, C. Caserini, L. Gatti, N. Carenini, S. Romanelli, R. Supino, D. Colangelo, I. Viano, R. Leone, S. Spinelli, G. Pezzoni, C. Manzotti, N. Farrell and F. Zunino, *Mol. Pharmacol.*, **1999**, 55, 528.
42. J. H. Burchenal, K. Kalaher, K. Dew, L. Lokys and G. Gale, *Biochimie*, **1978**, 60, 961.
43. A. Eastman and E. Bresnick, *Biochem. Pharmacol.*, **1981**, 30, 2721.
44. S. Komeda, H. Yamane, M. Chikuma and J. Reedijk, *Eur. J. Inorg. Chem.*, **2004**, 4828.
45. A. J. Kraker, J. D. Hoeschele, W. L. Elliott, H. D. Showalter, A. D. Sercel and N. P. Farrell, *J. Med. Chem.*, **1992**, 35, 4526.
46. M. Galanski, M. A. Jakupec and B. K. Keppler, *Curr. Med. Chem.*, **2005**, 12, 2075.

47. N. A. Kas'yanenko, E. E. E. Aia, A. A. Bogdanov, Y. V. Kosmotynskaya and K. I. Yakovlev, *Mol. Biol.*, **2002**, *36*, 745.
48. A. A. Tulub and V. E. Stefanov, *Int. J. Biol. Macromol.*, **2001**, *28*, 191.
49. J.-M. Teuben, M. R. Zubiri and J. Reedijk, *J. Chem. Soc., Dalton Trans.*, **2000**, 369.
50. J. Reedijk, *Proc. Natl. Acad. Sci. U.S.A.*, **2003**, *100*, 3611.
51. N. P. Johnson, J.-L. Butour and V. e. a. G., *Prog. Clin. Biochem. Med.*, **1989**, *10*, 1.
52. P. S. Sengupta, R. Sinha and G. S. De, *Indian J. Chem., Sect. A.*, **2001**, *40A*, 509.
53. S. E. Crider, R. J. Holbrook and K. J. Franz, *Metallomics.*, **2010**, *2*, 74.
54. T. Peleg-Shulman, Y. Najajreh and D. Gibson, *J. Inorg. Biochem.*, **2002**, *91*, 306.
55. X. Wang and Z. Guo, *Anti-Cancer Agents Med. Chem.*, **2007**, *7*, 19.
56. J. Vinje and E. Sletten, *Anti-Cancer Agents Med. Chem.*, **2007**, *7*, 35.
57. S. E. Miller and H. D. A., *Inorg. Chim. Acta*, **1991**, *187*, 125.
58. J. Kozelka, F. Legendre, F. Reeder and J.-C. Chottard, *Coord. Chem. Rev.*, **1999**, *190-192*, 61.
59. T. W. Hambley, *J. Chem. Soc., Dalton Trans.*, **2001**, 2711.
60. N. P. Johnson, J. D. Hoeschele and R. O. Rahn, *Chem.-Biol. Interact.*, **1980**, *30*, 151.
61. S. J. Berners-Price, T. A. Frenkiel, U. Frey, J. D. Ranford and P. J. Sadler, *J. Chem. Soc., Chem. Commun.*, **1992**, 789.
62. H. Su, P. Williams and M. Thompson, *Anal. Chem.*, **1995**, *67*, 1010.
63. M. A. Fuertes, C. Alonso and J. M. Perez, *Chem. Rev.*, **2003**, *103*, 645.
64. A. Zenker, M. Galanski, T. L. Bereuter, B. K. Keppler and W. Lindner, *J. Chromatogr., B*, **2000**, *745*, 211.
65. M. Meroueh, J. Kjellstrom, K. S. Margareta Martensso, A. K. C. Elmroth and C. S. Chow, *Inorg. Chim. Acta*, **2000**, *297*, 145.
66. J. Reedijk, *Chem. Rev.*, **1999**, *99*, 2499.
67. M.-H. Baik, R. A. Friesner and S. J. Lippard, *Inorg. Chem.*, **2003**, *42*, 8615.
68. U. Bierbach and N. Farrel, *Inorg. Chem.*, **1997**, *36*, 3657.
69. K. J. Mellish, Y. Qu, N. Scarsdale and N. P. Farrell, *Nucleic Acids Res.*, **1997**, *25*, 1265.
70. A. Zenker, M. Galanski, T. L. Bereuter, B. K. Keppler and W. Lindner, *J. Chromatogr., A*, **1999**, *852*, 337.
71. P. J. Bednarski, F. S. Mackay and P. J. Sadler, *Anti-Cancer Agents Med. Chem.*, **2007**, *7*, 75.
72. R. K. Moyzis, J. M. Buckingham, L. S. Cram, M. Dani, L. L. Deaven, M. D. Jones, J. Meyne, R. L. Ratliff and J.-R. Wu, *Proc. Natl. Acad. Sci. U.S.A.*, **1988**, *85*, 6622.
73. C. M. Counter, *Mutat. Res.*, **1996**, *366*, 45.
74. C. B. Harley, A. B. Futcher and C. W. Greider, *Nature*, **1990**, *345*, 458.

75. D.-L. Ma, C.-M. Che and S.-C. Yan, *J. Am. Chem. Soc.*, **2009**, *131*, 1835.
76. J. A. Rice, D. M. Crothers, A. L. Pinto and S. J. Lippard, *Proc. Natl. Acad. Sci. U.S.A.*, **1988**, *85*, 4158.
77. S. F. Bellon and S. J. Lippard, *Biophys. Chem.*, **1990**, *35*, 179.
78. M. Galanski and B. K. Keppler, *Anti-Cancer Agents Med. Chem.*, **2007**, *7*, 55.
79. W.-C. Su, S.-L. Chang, T.-Y. Chen, J.-S. Chen and C.-J. Tsao, *Jpn. J. Clin. Oncol.*, **2000**, *12*, 562.
80. J. Reedijk, *J. Chem. Soc., Chem. Commun.*, **1996**, 801.
81. M. Bower, E. S. Newlands, L. Holden, G. J. S. Rustin and R. H. J. Begent, *Ann. Oncol.*, **1997**, *8*, 447.
82. I. H. Hamelers and A. I. P. M. de Kroon, *J. Liposome. Res.*, **2007**, *17*, 183.
83. J. Lokich, *Cancer Invest.*, **2001**, *19*, 756.
84. F. Levi, G. Metzger, C. Massari and G. Milano, *Clin. Pharmacokin.*, **2000**, *38*, 1.
85. L. R. Wiseman, J. C. Adkins, G. L. Plosker and K. L. Goa, *Drugs and Aging*, **1999**, *14*, 459.
86. J. Lokich, *Cancer Invest.*, **2001**, *19*, 756.
87. M. V. Beusichem and N. Farrel, *Inorg. Chem.*, **1992**, *31*, 634.
88. G. Zhao and H. Lin, *Curr. Med. Chem.-Anti-Cancer Agents.*, **2005**, *5*, 137.
89. F. Huq, H. Daghiri, J. Q. Yu, H. Tayyem, P. Beale and M. Zhang, *Eur. J. Med. Chem.*, **2004**, *39*, 947.
90. J. Reedijk, *Proc. Natl. Acad. Sci. U. S. A.*, **2003**, *100*, 3611.
91. N. Farrell, Y. Qu, L. Feng and B. Van Houten, *Biochemistry*, **1990**, *29*, 9522.
92. A. Maisonia, P. Serafin, M. Traikia, E. Debiton, V. Thery, D. J. Aitken, P. Lemoine, B. Viossat and A. Gautier, *Eur. J. Inorg. Chem.*, **2008**, 298.
93. S. Komeda, S. Bombard, S. Perrier, J. Reedijk and J. Kozelka, *J. Inorg. Biochem.*, **2003**, *96*, 357.
94. K. W. Jennette, S. J. Lippard, G. A. Vassiliades and W. R. Bauer, *Proc. Natl. Acad. Sci. U. S. A.*, **1974**, *71*, 3839.
95. G. Lowe, A. S. Droz, T. Vilaivan, G. W. Weaver, L. Tweedale, J. M. Pratt, P. Rock, V. Yardley and S. L. Croft, *J. Med. Chem.*, **1999**, *42*, 999.
96. J. J. Moore, J. J. Nash, P. E. Fanwick and D. R. McMillin, *Inorg. Chem.*, **2002**, *41*, 6387.
97. N. J. Wheate, R. I. Talen, A. M. Krause-Heuer, R. L. Cook, S. Wang, V. J. Higgins and J. R. Aldrich-Wright, *Dalton Trans.*, **2007**, 5055.
98. Y.-Z. Hu, M. H. Wilson, R. Zong, C. Bonnefous, D. R. McMillin and R. P. Thummel, *Dalton Trans.*, **2005**, 354.
99. D. M. Neville and D. R. Daves, *J. Mol. Biol.*, **1966**, *17*, 805.
100. M. Cusumano, M. L. Di Pietro and A. Giannetto, *Inorg. Chem.*, **1999**, *38*, 1754.

101. Y. Wong and S. J. Lippard, *J. Am. Chem. Soc.*, **1977**, 824.
102. P. J. Bond, R. Langridge, K. W. Jennette and S. J. Lippard, *Proc. Natl. Acad. Sci. U.S.A.*, **1975**, 72, 4825.
103. G. Lowe, J. A. McCloskey, J. Ni and T. Vilaivan, *Bioorg. Med. Chem.*, **1996**, 4, 1007.
104. C. S. Peyratout, T. K. Aldridge, D. K. Crites and D. R. McMillin, *Inorg. Chem.*, **1995**, 34, 4484.
105. S. Bonse, J. M. Richards, S. A. Ross, G. Lowe and R. L. Krauth-Siegel, *J. Med. Chem.*, **2000**, 43, 4812.
106. A. McCoubrey, H. C. Latham, P. R. Cook, A. Rodger and G. Lowe, *FEBS Lett.*, **1996**, 380, 73.
107. R. W.-Y. Sun, D.-L. Ma, E. L.-M. Wong and C.-M. Che, *Dalton Trans.*, **2007**, 4884.
108. L. Messori, G. Marcon, A. Innocenti, E. Gallori, M. Franchi and P. Orioli, *Bioinorg. Chem. Appl.*, **2005**, 3, 239.
109. M. Howe-Grant, K. C. Wu, W. R. Bauer and S. J. Lippard, *Biochemistry*, **1976**, 15, 4339.
110. M. Cusumano, M. L. Di Pietro and A. Giannetto, *Inorg. Chem.*, **1999**, 38, 1754.
111. S. Kemp, N. J. Wheate, D. P. Buck, M. Nikac, J. G. Collins and J. R. Aldrich-Wright, *J. Inorg. Biochem.*, **2007**, 101, 1049.
112. Ž. D. Bugarčić, T. Soldatovic, R. Jelic, B. Alguero and A. Grandas, *Dalton Trans.*, **2004**, 3869.
113. Ž. D. Bugarčić, F. W. Heinemann and R. van Eldik, *Dalton Trans.*, **2004**, 279.
114. H. M. Brothers and N. M. Kostic, *Inorg. Chem.*, **1988**, 27, 1761.
115. D. Jaganyi, K. L. De Boer, J. Gertenbach and J. Perils, *Int. J. Chem. Kinet.*, **2008**, 40, 808.
116. B. Pitteri and M. Bortoluzzi, *Polyhedron*, **2006**, 25, 2698.
117. A. Hofmann, D. Jaganyi, O. Q. Munro, G. Liehr and R. van Eldik, *Inorg. Chem.*, **2003**, 42, 1688.
118. A. Hofmann, L. Dahlenburg and R. van Eldik, *Inorg. Chem.*, **2003**, 42, 6528.
119. R. Romeo, Plutino.M.R, L. M. Scolaro, S. Stoccoro and G. Minghetti, *Inorg. Chem.*, **2000**, 39, 4749.
120. D. Jaganyi, D. Reddy, J. A. Gertenbach, A. Hofmann and R. van Eldik, *Dalton Trans.*, **2004**, 299.
121. D. Reddy and D. Jaganyi, *Dalton Trans.*, **2008**, 6724.

Chapter 2

Substitution Reactions

2.1. Introduction to substitution reactions

A substitution reaction can be defined as the replacement of an ion or a molecule from the coordination sphere of a reactive centre by another molecule or an ion in the reaction medium.^[1] The two major aspects of a simple substitution reaction involves the breaking of bonds and formation of new bonds with the reactive centre and the incoming species which results in an intermediate with a different coordination number.^[2]

Ingold and Hughes^[3] were the first people who classified the substitution reactions at carbon centres in terms of bond breaking between the leaving group and the reactive centre.^[3] Substitution reactions of carbon are often classified as homolytic or heterolytic, depending on the type of the bond breaking.^[1] Heterolytic reactions can be subdivided into either electrophilic or nucleophilic reactions. When the electron pair departs with the leaving group, it is called nucleophilic heterolysis and in electrophilic heterolysis the electron pair remains in the reactive centre when the leaving group departs.^[1] These reactions can be represented as follows:^[1, 2]



Inorganic reactions can be divided into electrophilic substitution (S_E) or nucleophilic substitutions (S_N), and the latter could be represented by S_{N1} or S_{N2} depending on the molecularity of the rate determining step of the mechanism.^[1, 4] Often most kinetic substitution reactions are based on S_{N1} or S_{N2} mechanisms.^[4] However, since this method is based on the substitution on carbon centres, it may not be sufficient for the classification of detailed inorganic reaction mechanisms.^[2]

2.2. Mechanisms of Substitution Reactions

A reaction mechanism is a detailed process which involves all the step by step elementary reactions which culminates the observed overall reaction.^[5] Langford and Gray^[6] attempted to classify the inorganic reactions based on the concepts of stoichiometric mechanism and intimate mechanisms.^[2] The stoichiometric mechanism can be classified in one of the three forms described below.^[2, 7-9]

- Limiting dissociative (D)**- intermediate with lower coordination number.
The D term replaces the older S_N1 term.
- Limiting associative (A)**- intermediate with higher coordination number.
The A term replaces the older S_N2 term.
- Interchange (I)**- no observable intermediate forms here.

Since the activation mechanism is related to the mode of activation step, the stoichiometric interchange mechanism is further classified into its **intimate** mechanism. They are:^[1, 2]

- Dissociatively activated (I_D)** - there is no direct interaction between the reactive centre and the entering group in the transition state
- Associatively activated (I_A)** - there is bonding between the incoming group and the reactive centre in the transition state.

In intimate mechanism the bond-breaking and the bond-formation take place in a pre-formed aggregate. The incoming group, **Y**, and the leaving group, **X**, are interchanged in the inner and the outer coordination sphere of the metal centre. Therefore, the rate is independent of the incoming nucleophile and the relationship from dissociative to associative can be represented as in *Figure 2.1*.^[1, 10]

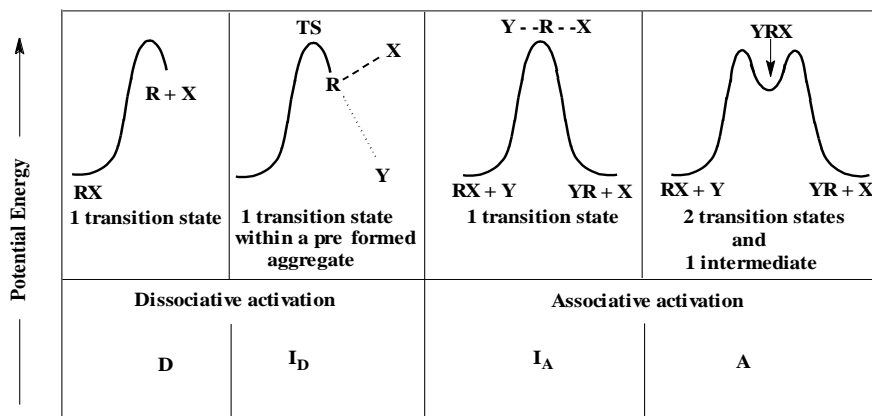


Figure 2. 1 The relationship between the mechanism of substitution and its energy profile and the classifications of Langford-Gray and Hughes-Ingold.^[1, 10]

2.2.1. Dissociative Mechanism

In this mechanism, the **R—X** bond breaks (*Figure 2.1*) completely before incoming group attaches to the metal centre. This results into an intermediate with lower coordination number which is assumed to live long enough allowing the intermediate to discriminate the potential ligands in the surrounding medium before it reacts with the entering group.^[14] The leaving group moves from the coordination shell to the solvation. This results in the favouring of solvent attack as the solvent is present in large access. However, the entering group dominates if it is present in a large excess. The formation of the product will therefore occur while the leaving group is in close proximity to the intermediate. Thus the rate of reaction depends on the nature of the leaving group and is not sensitive to the nature and the concentration of the incoming group.^[8]

2.2.2. Dissociatively Activated Interchange Mechanism

In this reaction mechanism the leaving group is moving from the inner coordination sphere to the outer coordination sphere while the entering group moves from the outer coordination sphere to the inner coordination sphere. The metal-leaving group bond gets weakened before the entering group tightly binds to the metal centre. In this mechanism, if there is a reagent whose concentration is much less than that of the solvent which is already in the inner coordination sphere when the dissociation takes place, then the probability of the solvent attaching to the reactive metal centre is higher.

2.2.3. Associative Mechanism

In this mechanism the **R—Y** bond formation (*Figure 2.1*) takes place before the **R—X** bond breaks resulting in an increase in the coordination number around the metal centre. Here the bond making transition state is more distinct than the bond breaking transition state. When the entering group, **Y**, and the leaving group, **X**, are chemically identical, the bond making and the bond breaking transition states have the same energy. But, when there is a net chemical change, one will be at a higher energy level and the more stable transition state will have a deeper potential energy well. A typical energy profile diagram for the associative mechanism is shown in *Figure 2.2*.^[10, 11]

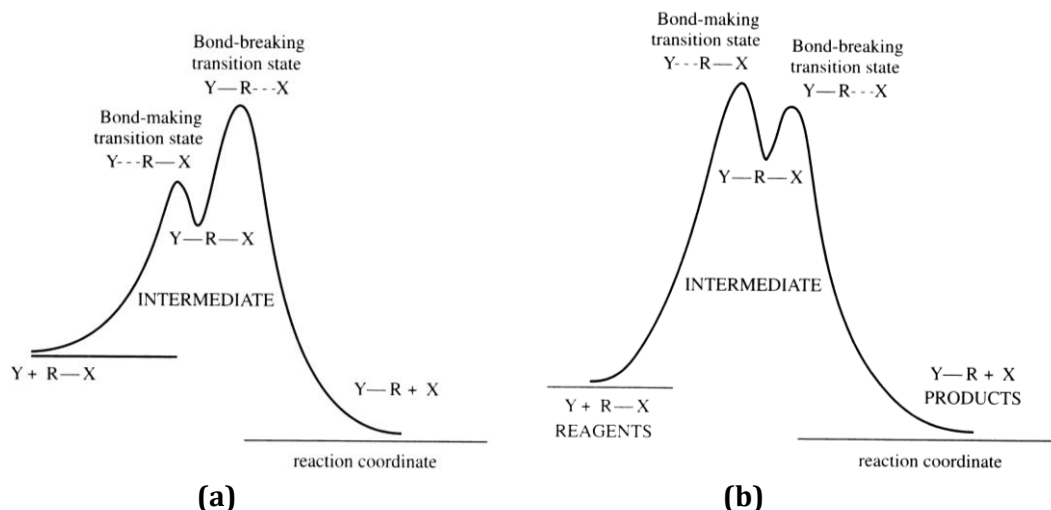
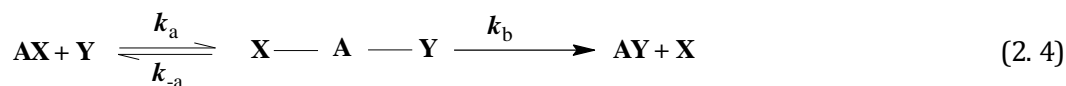


Figure 2.2 Energy profiles for the A mechanism for the substitution, showing the relationship between the intermediate and the bond-breaking transition states: (a) the bond breaking transition state at higher energy (b) the bond-making transition state at higher energy.^[10, 11]

In an associative mechanism bond making is an important step for the transition states. For a reaction that goes to completion: ^[2]



The steady-state approximations can be used if the concentration of the intermediate is small and constant^[9, 12] and thus assumed to be negligible so that:

$$-\frac{d[AX]}{dt} = \frac{d[AX]}{dt} = \frac{k_a k_b}{k_{-a} + k_b} [AX][Y] = k_2 [AX][Y] \quad (2.5)$$

where $k_2 = (k_a k_b)/(k_{-a} + k_b)$.

When $k_b \ll k_{-a}$, the second-order rate constant simplifies to $k_2 = (k_a k_b)/k_{-a}$ and hence the second-order rate constant not only depends on breaking the bond with the leaving group, but also is sensitive to the nature of the incoming group, Y .^[2] This is indicative of the relative stability of the intermediate with the higher coordination number (k_a/k_{-a}). When $k_b \gg k_{-a}$ the second-order rate constant, k_2 is equal to k_a which is the case of rate-limiting bond formation.^[2]

2.2.4. Associatively Activated Interchange Mechanism

In this mechanism the reaction rate is more dependent on the nature of the entering group since there is a bond formation between the entering group and the reactive centre in the transition state. The leaving group leaves the reactive centre only once the incoming group fully binds to the reactive centre.^[13]

2.3. Substitution Reactions of Square Planar Complexes

Square planar complexes are generally of the form d^8 low-spin type.^[10, 11] These include the four coordinate complexes of nickel(II), palladium(II), gold(III), rhodium(I) and platinum(II).^[10] Substitution reactions of square planar complexes are most well studied and understood in inorganic reaction mechanisms.^[12, 14-18] The beginning of four coordinate substitution reactions dates back to 1950s^[13] and were dominated by platinum(II) complexes due to their stable redox behaviour and relatively low reactivity.^[10, 11] This allows the synthesis of specifically designed platinum complexes and the study of mechanistic and kinetic behaviour of the complexes.^[2, 10, 13, 14] In the past few decades an appreciable amount of research has been done on the kinetic and the mechanistic behaviour of substitution reactions of platinum(II) complexes.^[6, 8, 13, 14] Due to the similarity of the reaction mechanisms of platinum(II) complexes with the other square planar complexes, the information collected on platinum(II) complexes can therefore be applied to the other square planar complexes. For example, the substitution behaviour of palladium(II) complexes are known to be very similar to platinum(II). However, their reaction rates are often five order of magnitude faster than the platinum(II) analogues.^[19]

Square planar d^8 metal complexes often follow an associative mechanism as they are coordinatively unsaturated with sixteen valence shell electrons. The reactions proceed *via* a five coordinate transition state which has eighteen electrons in the valence shell.^[20] Platinum(II) d^8 systems have relatively low energy level vacant p_z orbitals which allow the accommodation of electrons from the entering nucleophile.^[2] A large amount of kinetic and thermodynamic data available confirms this.^[2, 10, 14] Since the four coordinate square planar complexes are not sterically hindered, the incoming ligand can attack the metal centre both from above and below the plane (*Figure 2.3*).^[8]

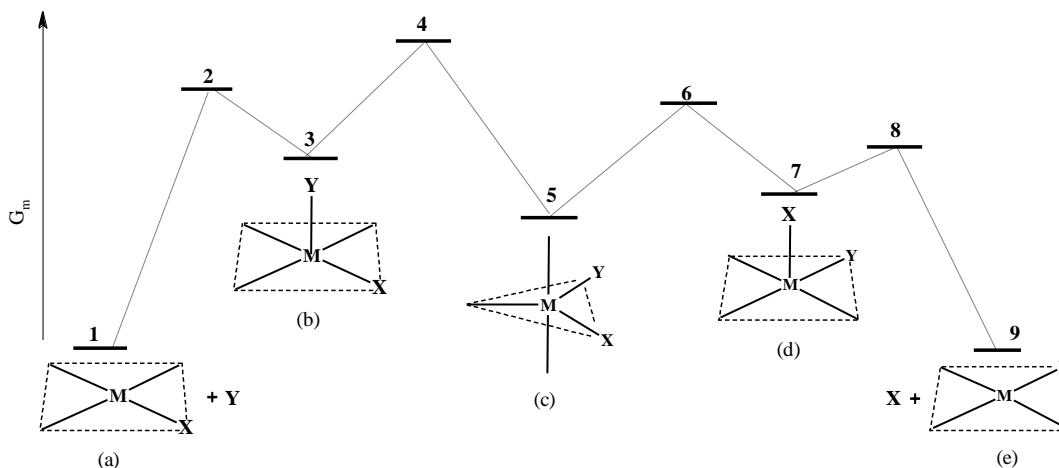


Figure 2.3 Schematic representation of the energy profile and possible steric changes during an associative substitution of leaving group, X by the entering group, Y of a square planar complex: energies at 2, 4, 6, and 8 represent the transition states and the reaction intermediates would have energies shown at 3, 5 and 7.^[8]

Therefore, for square planar complexes, ligand substitution occurs with increase in the coordination number from four to five in the transition state since the incoming ligand binds to the metal centre before the leaving group leaves, thus resulting in the formation of a trigonal bipyramidal geometry^[8, 10, 13] (c) (Figure 2.3). Even though, associative mechanism is more favourable for square planar complexes, recent studies have shown some dissociative mechanisms for square planar complexes.^[21-24] This is further discussed in Section 2.5.

2.3.1. Mechanism of Substitution Reaction Kinetics

Depending on the nature of the reactants and the solvent, the substitution kinetics of square planar reactions may take place in any one of the three pathways shown in Figure 2.4.^[2] This involves either:^[2]

- I. An associative pathway involving a direct attack of the incoming ligand
- II. An associative pathway involving a solvated complex
- III. A dissociative pathway involving a three coordinate intermediate

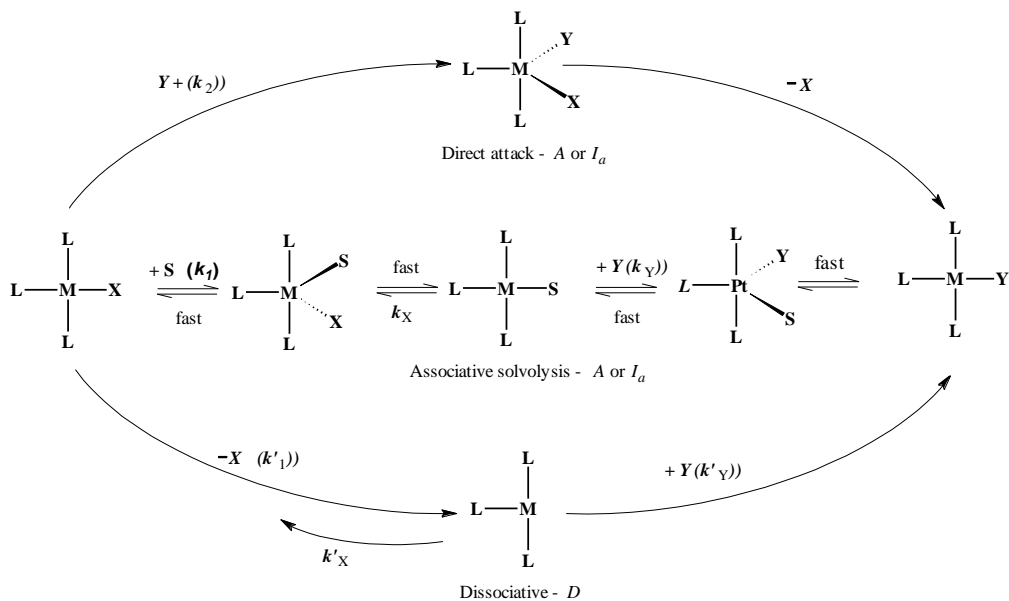
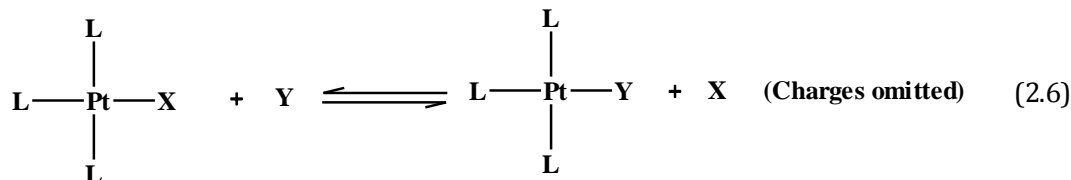


Figure 2.4 Schematic representation for substitution in d^8 four coordinate square planar complexes showing the alternative D and A or I_a solvolysis to account for the $k_1k_Y[Y]/(k_X[X]+k_Y[Y])$ or (k_1 limit) term.^[2]

However, most of the substitution reactions of square planar platinum(II) systems often involve a direct displacement of a ligand by the incoming nucleophile. This can be represented as follows:^[4, 8, 12]



The substitution can be described by the rate law:

$$-\frac{d[\text{PtL}_3\text{X}]}{dt} = k_1[\text{PtL}_3\text{X}] + k_2[\text{PtL}_3\text{X}][\text{Y}]$$

$$\text{Rate} = (k_1 + k_2[\text{Y}])[\text{PtL}_3\text{X}] \quad (2.7)$$

where k_1 and k_2 represents the first-order and the second-order rate constant respectively.

The above equation explains a typical bimolecular displacement mechanism for a square planar complex which is dependent on both the metal complex and the incoming nucleophile.^[12] However, kinetic substitution reactions are usually done under *pseudo* first-order conditions, *i.e.* the entering nucleophile concentration is at least 10 fold greater than

the metal complex in order to force the reaction to go to completion while the kinetics remains the first-order. Thus the rate equation simplifies to a first-order form:

$$= k_{\text{obs}}[\text{PtL}_3\text{X}] \quad (2.8)$$

$$k_{\text{obs}} = k_1 + k_2[\text{Y}] \quad (2.9)$$

Where k_{obs} = observed first-order or observed pseudo first-order rate constant.

A plot of k_{obs} versus concentration of Y will give the intercept (equal to k_1) and the slope will yield the value of k_2 . Figure 2.5 represents a typical example of such a plot for the substitution reaction of *trans*-Pt(py)₂Cl₂ with different nucleophiles.^[4, 10-12]

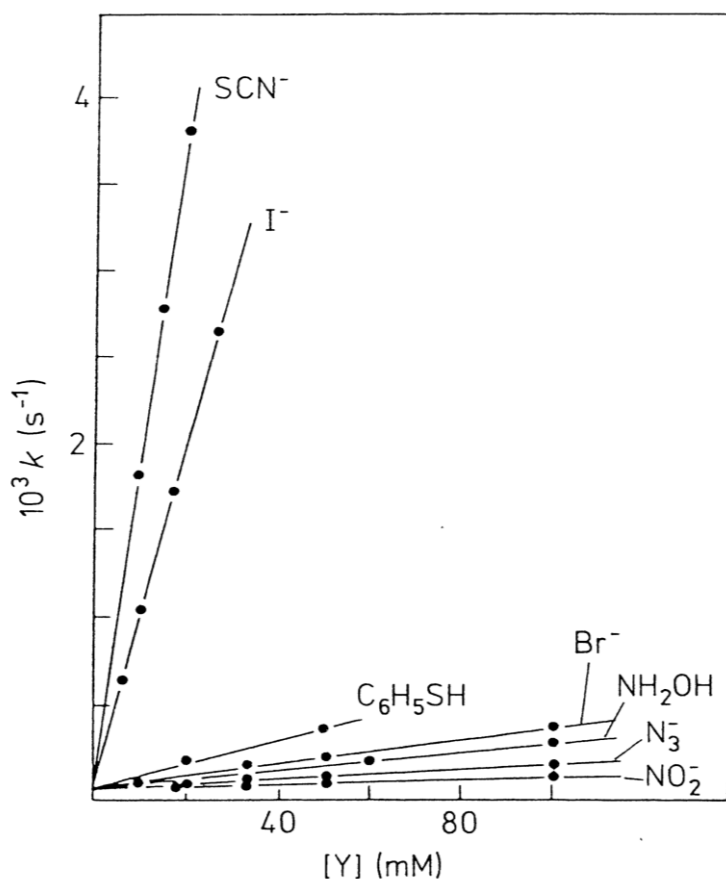


Figure 2.5 Rates of reaction of *trans*-[Pt(Py)₂Cl₂] as a function of concentration of different nucleophiles in methanol at 30° C.^[4, 10-12, 25]

From Figure 2.5, it can be seen that the value of k_1 is same for all the nucleophiles with the same metal complex while k_2 is sensitive to the nature of the entering nucleophile as this is a nucleophile dependent path.^[12] It is worth noting that a positive intercept may not always

mean to be k_1 (Equation 2.9). A positive intercept might also reflect the rate for the back reaction (Equation 2.6) or a parallel solvolysis.^[26, 27]

Kinetic studies are often carried out in coordinating solvents^[2, 19] such as water and methanol. If the reaction is carried in a coordinating solvent, then k_1 becomes a measure of the pathway.^[10, 13, 14]

2.4. Factors Influencing the Rate of Substitution Reactions

The rate of substitution reactions of square planar complexes is depended upon a number of factors. Since the associative mechanisms depend on the formation of a five coordinate intermediate, all the ligands present in the transition state therefore can affect the stability and the activation energy of the process. This section will highlight some of the factors which influence the rate of substitution reactions of square planar complexes.

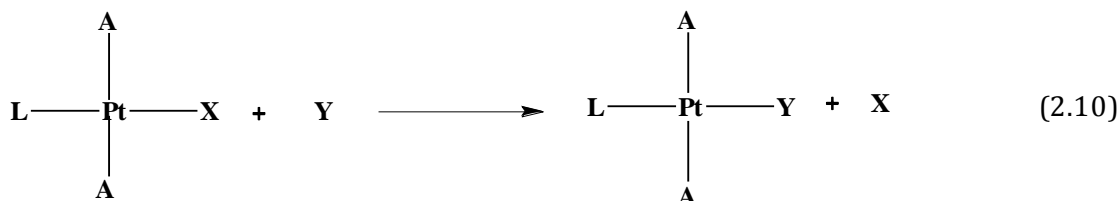
2.4.1. The Spectator Ligand

Substitution reactions of square planar complexes are hugely influenced by the ligand *trans* to the leaving group. A lot of research has been done by changing the properties such as the π and σ -bond strengths, the steric factors and also changing the ligands *trans* and *cis* to the leaving group.^[28, 29] In an associative type mechanism, in the transition state the leaving group, **X**, the entering group, **Y** and the *trans* ligand, **L** are in the same trigonal plane. Due to the T-shaped relationship between the *trans* ligand and the two *cis* ligands, the *cis* ligands remain symmetrically distinct (Figure 2.4). The *cis* ligands to the leaving group occupy the axial positions thus the stereochemistry is retained in the final complex. However, the influence due to the *trans* ligand is much stronger than the two *cis* ligands.^[16]

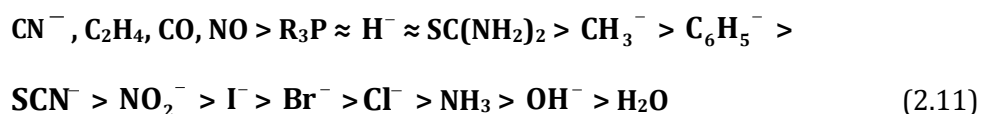
2.4.1.1. The *trans* Effect

The influence of *trans* ligand on the rate of substitution of the leaving group was first observed by Werner in the early 20th century.^[10, 30, 31] However, the observation was not generally understood until 1926, when Chernyaev introduced the concept of *trans effect* to some of the platinum(II) complexes.^[12] The *trans effect* is taken as being the influence a non-labile group has on the rate of displacement of the ligand opposite to it in a metal complex.^[4] In other words it is the tendency of the spectator ligand to direct the incoming ligand, **Y** to

the place *trans* to itself.^[14] For example, the reaction in *Equation 2.10*, the ligand, **L** can affect the lability of the leaving group, **X** as **L** is *trans* to **X**.

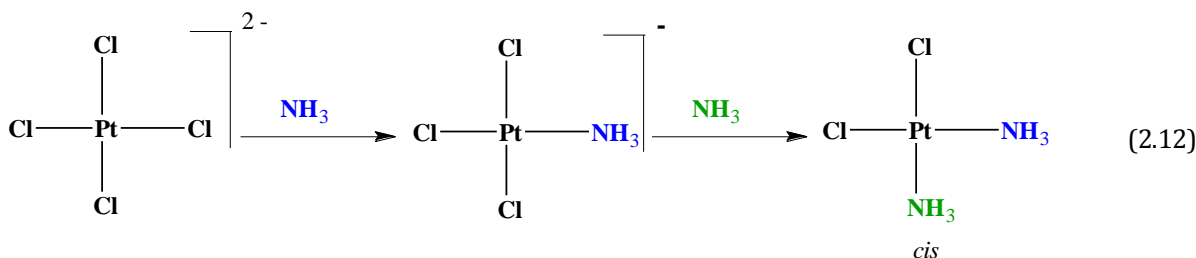


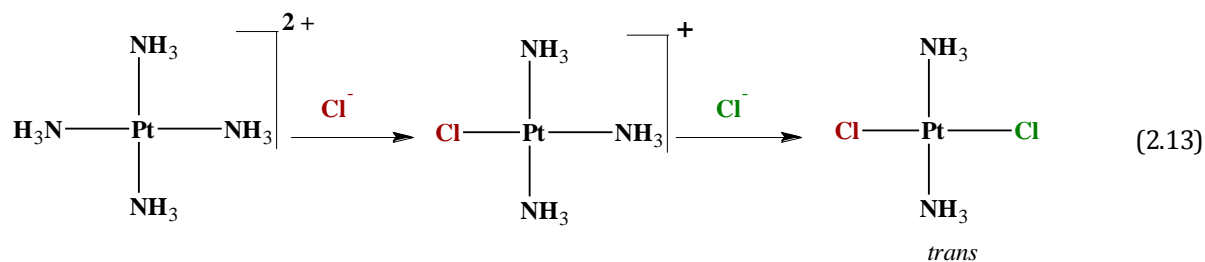
The greater *trans effect* is said to be associated with larger rate constants for the substitution reactions of square planar complexes. According to Chernyaev^[12] unlike a neutral, non π -bonding ligand, a negative ligand such as Cl^- has a greater labilizing effect on the ligand *trans* to it than it does on a group in the *cis* position.^[12] Thus a ligand can be assigned according to its *trans effect* which indicates its tendency to direct an incoming group *trans* to itself.^[14] In platinum(II) complexes the approximate order of decreasing the *trans effect* is as follows:^[2, 10, 12, 14]



It is noteworthy that kinetically the effect can be large. Research has shown that a factor of 10^6 or more in the rate for complexes which contain a good *trans* labilizing ligand.^[12]

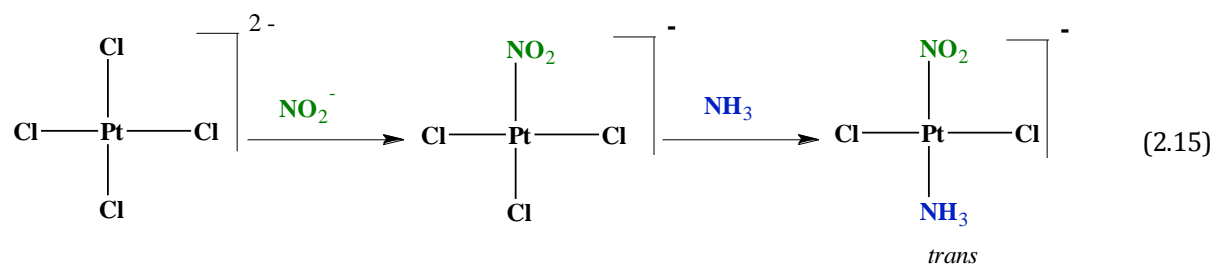
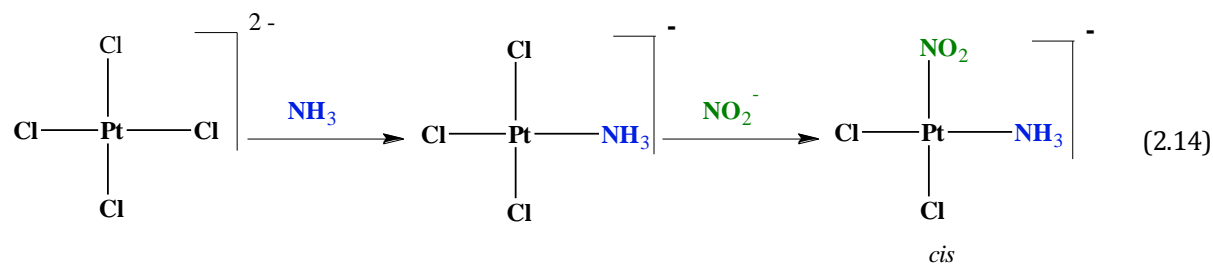
The *trans effect* has played an important role in the synthesis of platinum(II) complexes of the desired geometry.^[14] For example, in the synthesis of *cis* and *trans* isomers of $\text{Pt}(\text{NH}_3)_2\text{Cl}_2$, the second NH_3 (*Equation 2.12*), is substituted in the *cis* position because the *trans effect* of negatively charged Cl^- is larger than the neutral NH_3 ligand. So the least reactive chloride group in $[\text{Pt}(\text{NH}_3)\text{Cl}_3]^-$ is the Cl ligand opposite to the NH_3 group.



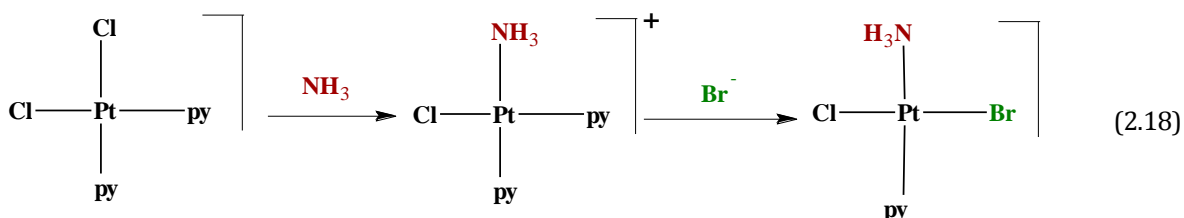
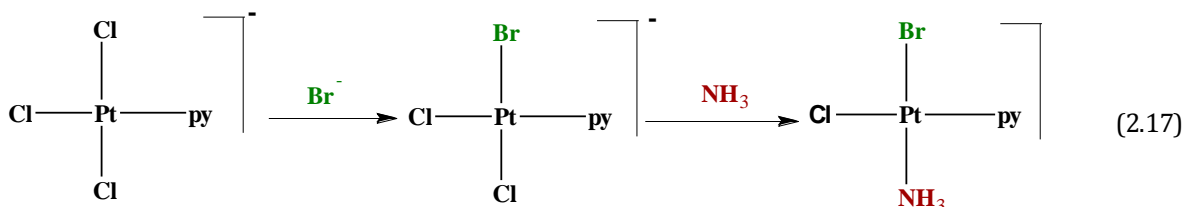
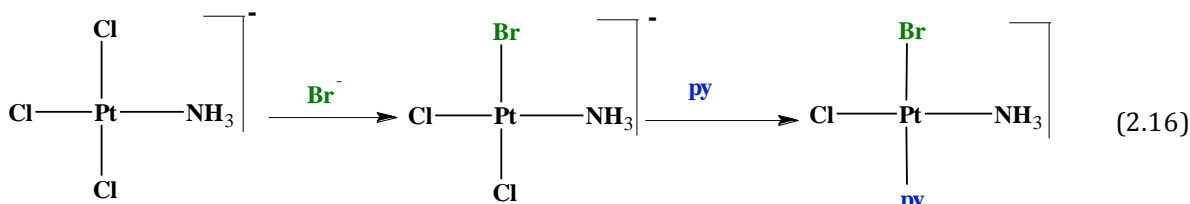


In Equation 2.13, the chloride group replaces the most labile ligand in $[\text{Pt}(\text{NH}_3)_3\text{Cl}_2]^+$ which is the NH_3 ligand opposite to the chloride ligand there by forming the *trans*- $\text{Pt}(\text{NH}_3)_2\text{Cl}_2$.

In Equation 2.14 and Equation 2.15, synthesis of *cis*- and *trans*- $\text{Pt}(\text{NH}_3)(\text{NO}_2)\text{Cl}_2$ is done by reversing the order at which the ligands are introduced to PtCl_4^{2-} .^[12] Equation 2.15 illustrates that the *trans* direction effect of nitrite is greater than that of chloride, thus directs the incoming NH_3 group to the *trans* to nitrite. Therefore, the *trans* labilizing effect of the ligands follow the order $\text{NO}_2^- > \text{Cl}^- > \text{NH}_3$.



Another such example is the synthesis of $\text{Pt}(\text{py})(\text{NH}_3)\text{BrCl}$ (Equation 2.16 – Equation 2.18).^[12] Since the strength of the $\text{Pt}-\text{N}$ bond is stronger than the strength of $\text{Pt}-\text{Cl}$ bond, the incoming bromide ligand was substituted *trans* to chloride ligand.



To understand the *trans effect* better it is important to know both σ - and π -bonding effects. These effects involve the ground state orbitals shared by the metal **M**, the leaving group **X** and the *trans* ligand **L**^[9]. Thus, the *trans effect* provides information about the *trans* ligand on ground state as well as the transition state. The effect of *trans* ligand to ground state properties such as bond lengths are known as *trans influence* whereas the *trans effect* is the influence of the *trans* ligand to the transition state complex.^[9, 10, 32] If there were no transition state differences, the *trans influence* order and the *trans effect* order would be the same.

A good π -accepting *trans* ligand can stabilise the five coordinate transition state intermediate by accepting the electron density from the filled orbitals on the metal centre.^[12] The π orbital in the metal centre is a filled d_{xy} , d_{zy} or d_{yz} orbital and hence electrons are donated from this orbital to the empty p orbitals on the *trans* ligand, **L** and leaving group, **X**. This “back donation” strengthens the **L—M** bond if the *trans* ligand **L** is a better π -acceptor.^[12] Thus, in the transition state, the increase in the electron density due to the increase in the coordination number on the metal centre is reduced. Hence the activation energy is lowered and the rate of substitution is increased.

In the five coordinate transition state, the *trans* ligand and the leaving group do not directly share the same p orbital. Thus the σ -donicity is the ground state stabilization of the **M—X** bond. In the past several studies have been conducted to explain *trans effect* ^[33-35]. The

π -bonding theory and the polarisation theory are the two very common theories that are used to explain the *trans effect*.^[4]

a. The π -Bonding Theory

The effect of π -bonding in metal complexes was first introduced by Pauling^[36] to account for the short Ni—C bond distances in Ni(CO)₄. This theory deals only with the ligands which are high in the *trans effect* series.^[12] Such ligands, C₂H₄, PR₃ and CO have stronger π -acceptor abilities and are considered as strong *trans* directors, thus stabilises the transition state complex by accepting the electron density from the metal centre.^[12, 32] In *Figure 2.6*, a pair of electrons is donated from phosphorous to platinum to form the σ -bond and the corresponding π -bond is formed by the overlap of electrons from the filled d orbital of platinum with the vacant d orbital of phosphorous.^[12, 32]

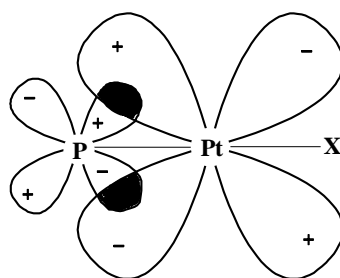


Figure 2.6 Schematic representation of the R₃P—Pt double bond. If ligands PR₃ and X are in the xy plane, then the d orbitals shown are either d_{xz} or d_{yz} .^[12, 32, 37]

The removal of electron density from the platinum centre to the empty d orbital of the ligand weakens the **M—X** bond with an exception of olefins, in which their electron donating property to form σ -bond is more important than the electron removal property to form the π -bond.^[12] However, it is not always clear if the bond weakening in the ground state is always sufficient enough to account for the effect of good *trans* activation.

Chatt *et al.*^[38] and Orgel^[39] independently proposed a π -bonding stabilization of the activated complex for the reaction of *trans*-PtA₂LX with Y to form *trans*-PtA₂LY where Y is the entering group, X is the leaving group and L is the *trans* π -bonding ligand (*Figure 2.7*). They related *tran effect* with the π -accepting ability of the ligand from the metal centre in the trigonal bipyramidal intermediate complex.

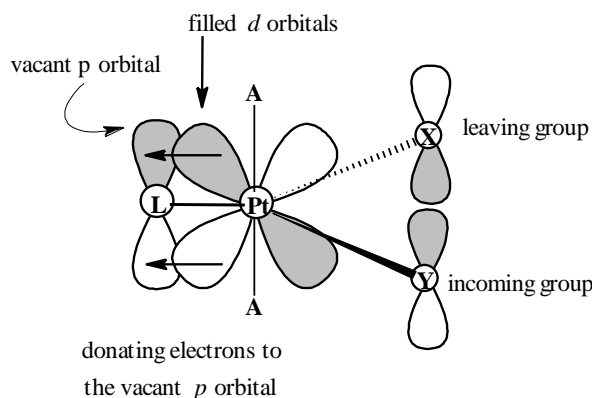


Figure 2.7 Activated trigonal bipyramidal complex for the *trans*-PtA₂LXY.^[12, 32]

In relation to the explanation given by Chatt *et al.*, strong *trans* directing ligands enhances the substitution reactions by accepting the added electron density from the metal centre.^[38] The overlap of d_{xz} and p_z metal orbitals produces two dp -hybrid orbitals in which one overlaps with the empty p -orbital on the *trans* ligand.^[32] Thus the other two orbitals readily accept the electron from the incoming ligand and favour a more rapid reaction.^[2, 12] An analogous π -acceptor mechanism proposed by Orgel^[39] shows that the presence of the π -acceptor ligand in the five coordinate transition state lowers the energy of the intermediate because the electron density on the platinum(II) is reduced along the **Pt—X** and **Pt—Y** directions and hence, **Y** and **L** would have a similar influence to the rate of the reaction.^[12]

b. The Polarization Theory

The influence of ligand polarization on the rate of substitution was first studied in detail and used by Meerwein.^[40] This theory is based on weakening of the **Pt—X** bond due to the strong *trans* effect caused by **L** in PtA₂LX.^[12] Grinberg^[41] suggested this hypothesis before any experimental evidence. The charge on the platinum(II) induces a dipole in **L**, which in turn induces a dipole in the platinum metal which repels the negative charge in **X**.^[12] Thus, the force of attraction of **X** and platinum is reduced which results in the weakening of the **Pt—X** bond. A greater effect is predicted if the central metal is polarisable.^[12] A diagrammatic representation of charge induced dipoles in **L—Pt—X** coordinate is shown in *Figure 2.8*.

However, there are some contradictions to this theory. The induced dipole on platinum(II) should depend on the overall charge of the *trans* ligand, **L** more than the induced moment.^[12] The effect will be greater if the **Pt—L** bond is shorter. However, this explanation contradicts

the position of Cl^- and I^- in the *trans effect* series. Thus, the effect of covalent bonding in such systems needs to be considered. Ligands of high polarisability are expected to form the most covalent bonds with platinum(II).

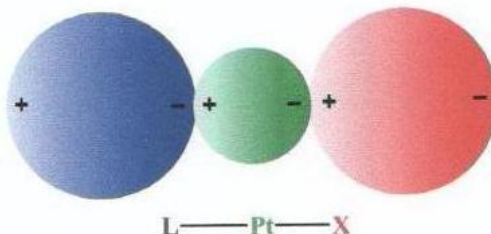


Figure 2.8 Distribution of Charge induced dipoles in the L—Pt—X coordinate of *trans*-PtA₂LX.^[12]

2.4.1.2. The Molecular Orbital Theory

The explanation for σ - and π -*trans effect* is best described in the molecular orbital theory (MO theory).^[12]

a. σ -*trans effect*

Figure 2.9 shows a simplified MO diagram for PtCl_4^{2-} . The most stable σ -bonding orbitals are located mostly on the chloride groups and the next most stable orbital is the π -bonding orbital followed by the anti-bonding orbitals of the σ and π orbitals.^[32] These orbitals are derived from the 5d orbitals of platinum(II) and have four probable MO of which the π_{xy}^* is the most stable and the $\sigma_{x^2-y^2}^*$ is relatively the least stable MO.^[12, 32] The higher energy p_z valence orbitals are not involved in the σ -bond formation and the higher energy anti-bonding σ orbitals; σ_s^* , σ_x^* and σ_y^* are relatively the least stable from all.^[12]

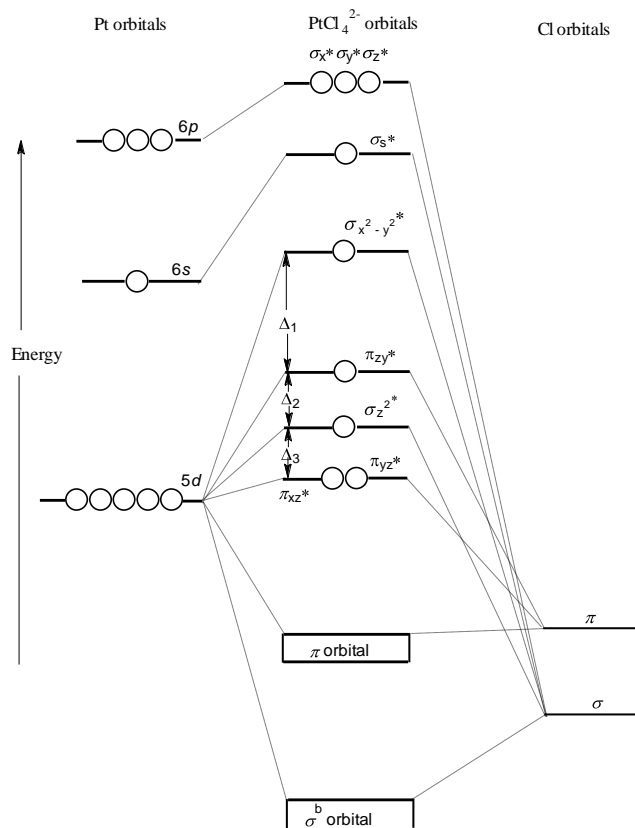


Figure 2.9 Molecular orbital representation showing the relative orbital energies in PtCl_4^{2-} .^[12, 32]

In a square planar complexes, $d_{x^2-y^2}$, s , p_x , p_y and $5d_{z^2}$ metal valence orbitals are used for the σ -bond formation.^[32] However, out of the four orbitals, only the two p orbitals have the right geometry for the *trans* directing properties. Therefore, in *trans*- PtA_2LX , the *trans* ligand, **L** and the leaving group, **X** must share the same σ_x orbital in the overall MO arrangements.^[12] If the σ -donor ability of ligand, **L**, is large, then it strengthens the **Pt—L** bonding which in turn results in the weakening of the **Pt—X** bond due to the smaller share of the electrons available for the bonding (*Figure 2.10*).^[12] Hence increases the rate of substitution of **X**.

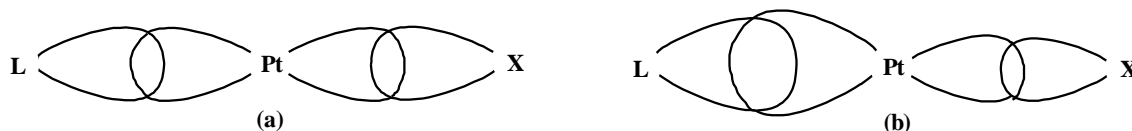


Figure 2.10 Representation of **L—Pt—X** bonding using σ_x MO (a) The σ bond strength of **L** and **X** are almost equal. (b) Strong σ donor ligand **L**, the σ bond strength of **L** is much greater than that of **X**.^[10, 12]

A good σ -donor (covalent ligand), such as H^- , will donate a large amount of electron density to the p_x orbital of the metal.^[12] This creates repulsion between the σ electrons of the *trans* ligand and the electrons of the metal in the same p_x orbital. Langford and Gray^[42] explained

this with respect to the increase in the stabilization of the trigonal bipyramidal intermediate since the five coordinate intermediate has more orbitals for σ -bonding. In a square planar complex, the same p_x orbital in the x axis is used to form the bond with the *trans* ligand, **L** and the leaving group, **X** in **L—Pt—X**.^[12] Addition of the incoming group, **Y** from above the xy plane shifts **X** out of plane which results in two suitable p orbitals (p_x and p_z) for the formation of a trigonal plane containing **Pt**, **L**, **X** and **Y** (Figure 2.11).^[12] Good σ -bonding ligands such as H^- and CH_3 can therefore use the extra p character to increase the σ structure in the trigonal bipyramidal intermediate and thus will have higher *trans* effect.^[12]

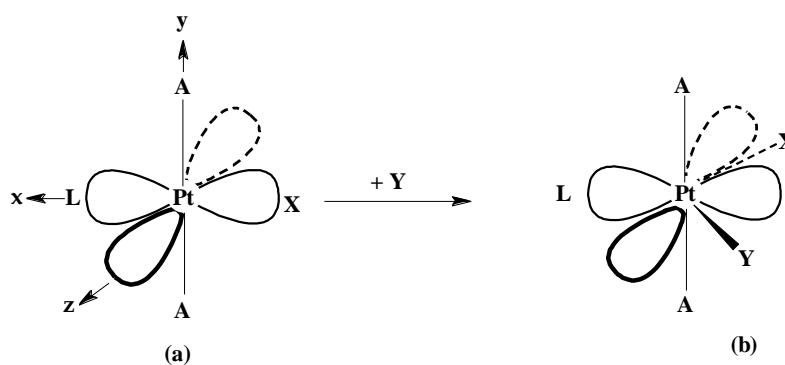


Figure 2.11 The σ -*trans* effect due to the stabilization of the trigonal bipyramidal intermediate. (a) Only one p orbital is available for σ -bond formation of **L** and **X**. (b) Two p orbitals are available for the σ -bonding of **L**, **X** and **Y**.^[12]

b. π -*trans* effect

Good *trans* directing groups form strong π -bonds. In a square planar complex, the three MO's, π_{xz}^* , π_{yz}^* , and π_{xy}^* have suitable symmetries for π -bonding.^[12] Addition of the incoming group, **Y**, results in the formation of a trigonal bipyramidal structure with four MO's of the right symmetries for π -bond formation, that is, π_{xz}^* , π_{yz}^* , π_{xy}^* and $\pi_{x^2-y^2}^*$.^[12] In the trigonal plane, the four orbitals are shared in π -bonding with the three ligands, **L**, **X** and **Y**. This stabilises the trigonal bipyramidal transition state if *trans* ligand, **L**, can form bonds with the π^* orbitals which results in the delocalization of the electronic charge to the ligands and lowers the energy of the system.^[12] Thus, a good *trans* ligand lowers the activation energy of the reaction.^[10, 12] Recent studies done by Jaganyi *et al.*^[29, 43] have shown that *trans* π -accepting ligands can cause the increase in the substitution reaction of platinum(II) complexes. The *trans* effect was related to the π -accepting ability of the ligands which can withdraw the electron density from the metal centre thereby stabilising the five coordinate intermediate in an associative mechanism.

A number of studies have been done to study the σ - and the π -*trans* effects of several ligands. Some of the qualitative results reported are given in Table 2.1.^[12] Good *trans* directing ligands are either strong or moderate σ and π bonding ligands.^[12]

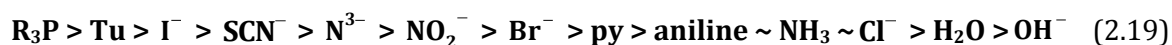
Table 2.1 Estimated relative σ - and π - *trans* effects of some ligands.^[12]

| Ligand | σ effect* | π effect* |
|-------------------------------|------------------|---------------|
| C ₂ H ₄ | w | vs |
| CO | m | vs |
| CN ⁻ | m | s |
| PR ₃ | s | m |
| H ⁻ | vs | vw |
| I ⁻ | m | m |
| CH ₃ ⁻ | s | w |
| Pyridine | w | w |

* vs, very strong; s, strong; m, medium; w, weak; vw, very weak

2.4.2. The Effect of the Entering Nucleophile

An associative substitution reaction mechanism depends on the nucleophilicity of the entering nucleophile. In order to discuss the nucleophilicity of the entering nucleophile, it is important to define the species interacting with the nucleophile.^[10] Studies done on the platinum(II) complexes showed that the nucleophilic reactivity order is:^[12, 15, 44]



It is important to note that the nucleophilicity of the reagents is independent of their base strength. However, the softness or the polarizability of the nucleophile plays an important role and the reactivity of the nucleophile.^[10, 12]

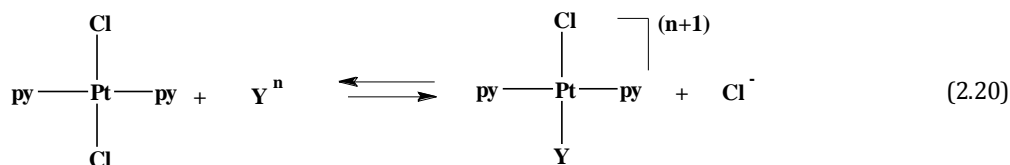
The nucleophilicity of the ligand is often influenced by several factors:^[8]

- Basicity:** The pK_a often determines the nucleophilicity of the entering nucleophile. The basicity also correlates the ligand nucleophilicity towards the metal centre.
- Polarisability:** Polarisability of the nucleophile is an important consideration for the rates than for equilibria.^[12] This was often explained by using Peason's "Hard Soft Acid Base" (HSAB) theory discovered in

1963.^[45, 46] Hard acids (metal ions) are small and highly charged (eg: Li^+ and Mg^{2+}) and possess a valence electron shell which is not easily distorted while soft acids (metal ions) are large and possess low charge and have a valence electron shell which is easy to distort or remove.^[8] Polarisability refers to the “softness” of the nucleophile. “Hard” nucleophiles prefer “hard” metal centres and “soft” nucleophiles prefer “soft” substrates or metal centres.^[8, 9, 47] Platinum(II) being a soft metal centre prefers to be with soft donors. Thus, platinum(II) is more effective towards large donors.

- c. Oxidability: Ligands that are readily oxidised are considered as good nucleophiles. The oxidability of the ligands can be characterised by their electrode reduction potential.
- d. Solvation Energy: Easily solvated ligands are considered as weak nucleophiles. The ligand has to desolvate before it gets coordinated with the metal centre.
- e. Metal Centre: Nucleophilicity depends much on the nature of the metal centre. Heavier elements are better polarised in the transition state.

Earlier work had established the nucleophilic reactivity for platinum(II) with different nucleophiles.^[15, 44] The most detailed study on the relative reactivity and nucleophilicity was done by Bellucco^[25] for *trans*- $\text{Pt}(\text{py})_2\text{Cl}_2$ in methanol at 30 °C (Equation 2.20).^[2]



Trans- $\text{Pt}(\text{py})_2\text{Cl}_2$ was used as the standard and the nucleophilic reactivity constants, n_{pt} was defined as follows:^{[12] [10]}

$$\log \frac{k_Y}{k_S} = n_{\text{pt}} \quad (2.21)$$

where k_Y = the rate constant for the reaction of the entering nucleophile

k_S = the rate constant for attack of the solvent (methanol).

Some of the experimental results obtained are presented in *Table 2.2*.

Table 2.2 Some nucleophilic constants given for Pt(py)₂Cl₂ with different nucleophiles of donor atoms.^[12, 25, 48]

| Nucleophile | n_{Pt} | Donor atom | Nucleophile | n_{Pt} | Donor atom |
|---|-----------------|------------|--|-----------------|--------------|
| CH ₃ O ⁻ | <2.4 | O | I ⁻ | 5.42 | I (Halogen) |
| C ₆ H ₅ NH ₂ | 3.02 | N | Br ⁻ | 4.18 | Cl (Halogen) |
| NH ₃ | 3.06 | N | ³⁶ Cl ⁻ | 3.04 | Br (Halogen) |
| C ₅ H ₅ N | 3.13 | N | (C ₆ H ₅)P | 8.79 | P |
| H ₂ N- NH ₂ | 3.85 | N | (C ₂ H ₅) ₃ P | 8.85 | P |
| (C ₆ H ₅) ₂ S | 4.38 | S | (C ₆ H ₅ CH ₂) ₂ Se | 5.39 | Se |
| S=C(NH ₂) ₂ | 7.17 | S | (CH ₃) ₂ Se | 5.56 | Se |
| (CH ₃) ₂ S | 4.73 | S | (C ₆ H ₅) ₃ As | 6.75 | As |
| SCN ⁻ | 6.65 | S | (C ₂ H ₅) ₃ As | 7.54 | As |

The nucleophilicity constant refers to the reactivity of the nucleophile towards platinum(II) and correlates with the other properties of the ligand.^[12] This type of correlation is the linear free energy relationship (LFER). Brønsted^[49] successfully applied the LFER to displacement reactions at hydrogen in various compound and a linear correlation between the log of the rate constant for the proton transfer and the log of the base strength of the reagent was found.^[12]

For the platinum(II) complexes, plots of log k_Y verses n_{Pt} were observed to be linear (*Figure 2.12*). The linear free energy relationship is given by:^[10, 12]

$$\log k_Y = s n_{\text{Pt}} + \log k_S \quad (2.22)$$

where the slope, s is complex specific and is called the *nucleophilic discrimination factor*. It is a measure of the sensitivity of the metal centre to the nucleophilicity of the incoming ligand.^[12] If the value of s is large then that means the reaction is more sensitive to the changes in the nucleophilic character. For *trans*-Pt(py)₂Cl₂, s is assigned to be 1. The y-intercept, log k_S is the intrinsic reactivity of the complex. This gives the rate constant for the weakest nucleophile measured in a solvent.^[12] A smaller value of k_S indicates that the complex is more sensitive to the changes in the nucleophile. Ligands that are capable of forming dative π -bonding with the platinum(II) in the transition state have larger values of s (smaller k_S).^[12] This enables the addition of the electrons from the nucleophile to the

platinum(II) centre thereby making it easier for the entering group to take part in the transition state. The rate of reactions of such systems will exhibit a greater sensitivity towards the nucleophile.^[12]

Generally larger s values are found for complexes of platinum(II) with softer base ligands. However, few nucleophiles such as NO_2^- , $\text{SC}(\text{NH}_2)$ and SeCN^- do not obey the simple linear relationship between the $\log k_s$ against n_{Pt} (Equation 2.22, Figure 2.12). The reason for this is due to the π -accepting abilities of the ligands which would lower the energy of the transition state.^[2] This also depends up on the π -donor ability of the metal complex which makes some reagents more reactive towards some better π -donor metal complexes such as $[\text{PtCl}_4]^{2-}$ or less reactive to certain complexes such as $[\text{Pt}(\text{dien})\text{Br}]^+$ than the reference complex, $\text{trans-Pt}(\text{py})_2\text{Cl}_2$.^[12]

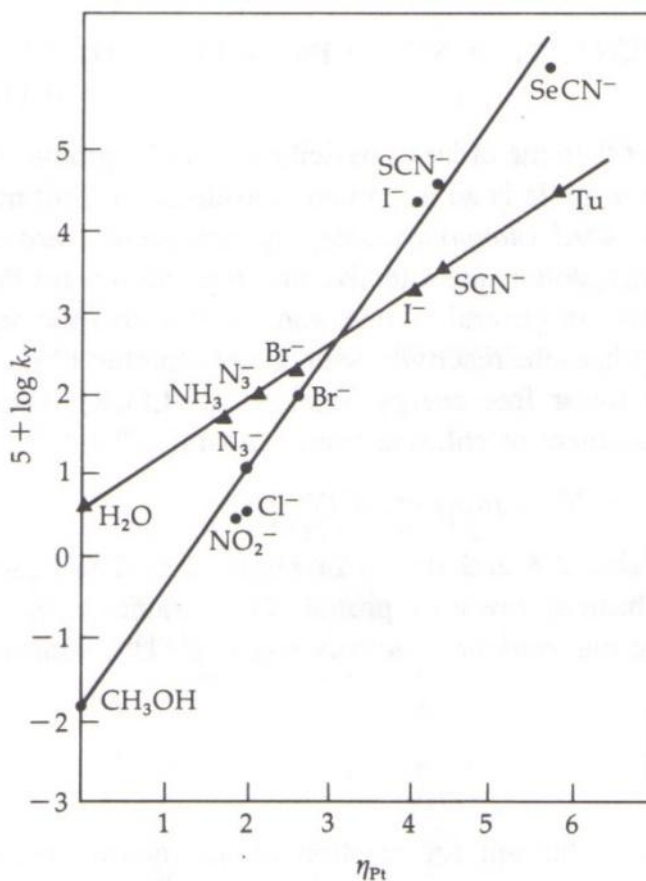


Figure 2.12 Correlation of the rates of reaction of platinum(II) complexes with the standard $\text{trans-Pt}(\text{py})_2\text{Cl}_2$ for different nucleophiles: •, $\text{trans-Pt}(\text{PEt}_3)_2\text{Cl}_2$ in methanol at 30 °C; ▲, $\text{Pt}(\text{en})\text{Cl}_2$ in water at 35 °C.^[12, 25, 32]

Furthermore, recent studies have shown that n_{Pt} scale is best applied to neutral nucleophiles and the charge plays a greater role in determining the reactivity^[37] while the effect of steric hindrance was found to play a minor role.^[50]

2.4.3. The *cis*-Effect

The reactivity of platinum(II) complexes are less sensitive to the electronic displacement properties of *cis* ligands than *trans* ligands. However, they are more sensitive to the steric hindrance in the *cis*-position.^[2] The *trans effect* is stronger by order of about 10^6 compared with the *cis*-effect.^[8] Since the effect of *cis*-ligand is smaller, it is more difficult to study the *cis* effect by varying the *cis* ligands.

Research has shown that good *trans* activating ligands have poor *cis*-directing effects.^[51, 52] The experimental results obtained for *cis*-Pt(PEt₃)₂LCl with pyridine (Equation 2.23) have shown the same trend for the corresponding *trans*-Pt(PEt₃)₂LCl with pyridine with the change of the *trans* ligand, L in the order of CH₃ > C₆H₅ > Cl⁻.^[53] The order of the reaction with the *cis* complex increased by a factor of three (Table 2.3)^[10] while the order was much higher for the *trans* complex.^[12]

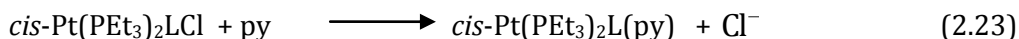


Table 2.3 The effect of *trans* ligand, L on the rate of reaction of *cis*-Pt(PEt₃)₂LCl with py.^[53]

| L | $k_1(10^2 \text{ s}^{-1})$ |
|--|----------------------------|
| Cl ⁻ | 1.7 |
| C ₆ H ₅ ⁻ | 3.8 |
| CH ₃ ⁻ | 6 |

For a square planar complex which undergoes an associative mechanism, an increase in the size of the incoming ligand would decrease the rate of substitution reaction. The orientation of the aromatic ring is perpendicular to the plane of the molecule and the nucleophile attacks either from above or below (Figure 2.3) of the plane and thus blocks the metal centre. This is further discussed in Section 2.4.4.

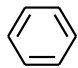
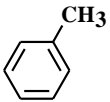
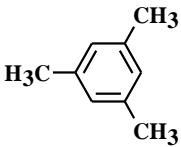
Experimental results have shown that for some platinum(II) complexes with weakly *trans* directing ligands, the *cis* neighbour has shown a greater influence on the kinetics than the *trans* neighbour.^[2]

2.4.4. The Steric Effect

An associative mode of mechanisms involves an increase in the steric hindrance in the transition state. As mentioned before even though the substitution reactions of square planar platinum(II) complexes are more sensitive to the changes in the *trans* ligand, the *cis*-effect also plays an important role when steric bulk is involved in the reaction centre (Section 2.4.3). The influence of the steric bulk to the rate of reaction could be either due to the steric bulk in the spectator ligand or in the incoming nucleophile.

The steric effect exerted in *cis* and *trans* isomers was studied by using complexes of *cis* and *trans*-Pt(PEt₃)₂LCl (L= phenyl, *o*-tolyl, mesityl). Table 2.4 illustrates the reaction rate constants obtained for the reaction of (PEt₃)₂LCl with pyridine with the changes in L.

Table 2.4 Steric effects on the rates of substitution of *cis*- and *trans*- Pt(PEt₃)₂LCl by pyridine.^[9, 10, 53]

| Ligand, L | <i>k</i> _{obs} , s ⁻¹ | |
|---|---|--|
| | <i>cis</i> -Pt(PEt ₃) ₂ LCl (0 °C) | <i>trans</i> -Pt(PEt ₃) ₂ LCl (25 °C) |
| L = phenyl  | 8.0x10 ⁻² | 1.2x10 ⁻⁴ |
| L = <i>o</i> -tolyl  | 2.0x10 ⁻⁴ | 1.7x10 ⁻⁵ |
| L = mesityl  | 1.0x10 ⁻⁶ (25 °C) | 3.4x10 ⁻⁶ |

The steric bulk reduces the reaction rate of *cis* complex as one moves from phenyl to the bulky mesityl to a greater extent even though the reaction with *cis*-mesityl was carried out at higher temperature. However, in the case of the *trans* complex the decrease in the rate is much smaller.^[10, 12] A larger decrease in the rates for the *cis* complexes were observed because in the trigonal bipyramidal transition state, the leaving group, Cl and the entering group are in equatorial positions.

For the *cis* isomer, the group **L** is in the axial position in the transition state, thus **L** interacts with the leaving group a 90° angle which causes more steric repulsion compared to the *trans* isomer where **L** occupies an equatorial position in the transition state, which interacts with the incoming group at an angle of 120° which is further apart.^[9] The decrease in the reaction is also contributed due to the aromatic ring being perpendicular to the plane of the complex and thus it blocks the attacking site of platinum (Figure 2.13).^[9] Also in the trigonal bipyramidal transition state the *cis* isomer offers more shielding than the *trans* isomer.

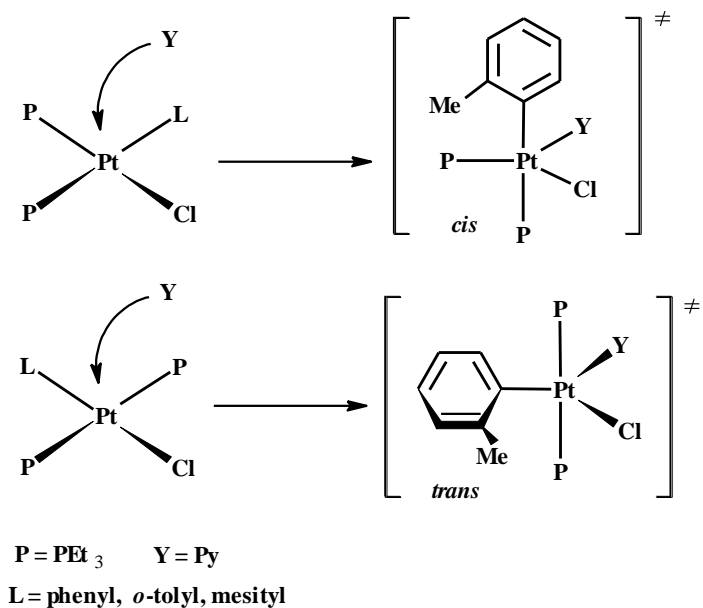
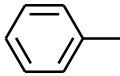
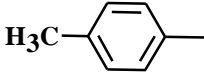
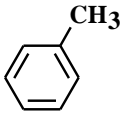
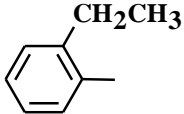
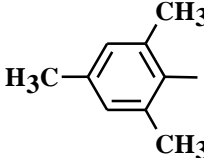
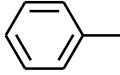
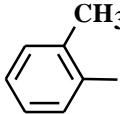
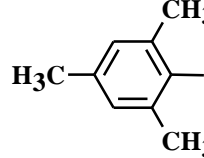


Figure 2.13 The steric effect of the aryl square planar complex showing the steric bulk for the *cis* isomer blocking the attacking site.^[9]

The increase in the bulk on the *cis* position to the leaving group further decreases the rate. The data obtained for the study of steric *cis* effect of *ortho*-methylation of aryl ligands (Equation 2.24 and Equation 2.25) are shown in Table 2.5.



Table 2.5 The rate constants for the reactions of steric *cis*-effect of *ortho*-methylation of an aryl ligand at 30 °C.^[54, 55]

| R | X | $10^3 k_1$ (s ⁻¹) | k_2 (dm ³ mol ⁻¹ s ⁻¹) |
|---|------------------|-------------------------------|--|
|  | <i>cis</i> -Br | 6000 | 21400 (X = Cl) |
|  | <i>cis</i> -Br | 4280 | |
|  | <i>cis</i> -Br | 54.4 | 2460 |
|  | <i>cis</i> -Br | 16.2 | |
|  | <i>cis</i> -Br | 0.19 | 0.312 |
|  | <i>trans</i> -Cl | 10 | 34.8 |
|  | <i>trans</i> -Cl | 2.29 | 0.9 |
|  | <i>trans</i> -Cl | 0.405 | 0.043 |

2.4.5. The Effect of Solvent

Sometimes the rate law for square planar reactions involve a reaction path which is attributed to the solvent attack. It was expected that the contribution of the solvent to the overall rate of reaction would be increased with the increasing in the coordination ability of the solvent.^[2, 12] Therefore, solvent effects play an important role in the substitution reactions of square planar complexes. The effect was shown by the experimental data (Table 2.6) obtained for the chloride exchange reaction for *trans*-Pt(py)₂Cl₂ (Equation 2.26).^[10]



Table 2.6 Effect of solvent on the chloride exchange reaction (Equation 2.26) at 25 °C.^[56]

| Coordinating | $k / (10^{-5} \text{ s}^{-1})$ | Weakly coordinating | $k / \text{M}^{-1} \text{ s}^{-1}$ |
|------------------|--------------------------------|-------------------------------|------------------------------------|
| DMSO | 380 | CCl ₄ | 10 ⁴ |
| H ₂ O | 3.5 | C ₆ H ₆ | 10 ² |
| EtOH | 1.4 | <i>i</i> -BuOH | 10 ⁻¹ |
| PrOH | 0.4 | Me ₂ C(O) | 10 ⁻² |
| | | DMF | 10 ⁻³ |

If the reaction is carried out in a coordinating solvent then the rate of reaction is found to be independent of the concentration of the chloride while the opposite is true for the weakly or non coordinating solvents. Furthermore with coordinating solvents such as DMSO, the rates of the reaction showed a direct dependence on the nucleophilicity of the solvent, ($k_S \gg k_{Cl}[\text{Cl}^-]$). For coordinating solvents the k_S value increases in the order:^[12]



It can be seen that the rate of exchange for DMSO is faster than that of water. This is because platinum(II) being a soft metal centre prefers to bond with larger S in DMSO than O in H₂O. If the role of the solvent is to solvate the leaving group, Cl⁻, then H₂O would be a better solvent for the reaction than DMSO.^[12] Therefore, in the transition state, Pt-solvent bond making plays an important role. For non-coordinating or poorly coordinating solvents, larger rates of reaction have been reported for non-polar solvents such as CCl₄ where the chloride acts as a nucleophile ($k_{Cl}[\text{Cl}^-] > k_S$).^[12] In such solvents a large k_S value is expected because the solvent can not coordinate to the metal.

2.4.6- The Effect of Leaving Group

The substitution reactions involve the replacement of different analogous groups from a substrate. Since square planar platinum(II) complexes mainly undergo associative mode of substitution reactions, the effect of the leaving group has a smaller influence to the rate of the substitution. However, certain reactions of platinum(II) square planar complexes have shown a dependence of the rate constant on the nature of the leaving group. Pt(dien)X⁺

systems (Equation 2.28) has been studied and kinetic data (Table 2.7)^[57, 58] has provided agreeable results on the leaving group effects.



Table 2.7 Effects of leaving group on the rates of reaction of Pt(dien) complexes in water at 25 °C.^[57, 58]

| Ligand, X | 10 ⁶ k _{obs} , s ⁻¹ |
|------------------------------|--|
| NO ₃ ⁻ | very fast |
| H ₂ O | 1900 |
| Cl ⁻ | 35 |
| Br ⁻ | 23 |
| I ⁻ | 10 |
| N ₃ ⁻ | 0.83 |
| SCN ⁻ | 0.3 |
| NO ₂ ⁻ | 0.05 |
| CN ⁻ | 0.017 |

The decrease in the rate of substitution for the changers X⁻ follows the order:



The magnitude of the difference of the rates of the substitution is approximately 10⁶ showing that the leaving groups have a considerable influence to the rates of the reaction (Table 2.7). This indicates that even for the associative mode of substitution, there is a substantial amount of Pt—X bond breaking in the transition state. This bond breaking is reaction specific and does not demand a dissociation process but simply requires that the Pt—X bond breaking make a comparable contribution to the Pt—py bond formation.^[12]

The experimental results also have shown that the order of the labilities of the complexes also depend on the order of their instabilities.^[2] The leaving groups which are high in the *trans effect* series are more difficult to replace. Strongly binding ligands such as CN⁻ dissociate more slowly. This is expected for the strong *trans* directing ligands since the *trans effect* depends on the strength of the π- and the σ-bonding capability and the Pt—X bond strength in the five coordinate transition state.^[2, 10] Since the leaving group, X, the entering group, Y are in the same plane in the transition state, the leaving group might play an important role in the energy of the transition state intermediate.^[2, 14]

2.5. Dissociative Mechanisms of Square Planar Complexes

Dissociative mechanisms of square planar reactions have seldom being noticed in the past. The main characteristics which favour the dissociative mechanism change over include:^[2]

- I. A sterically hindered metal centre (high electron density at the metal will destabilise the ground state by decreasing the electrophilicity of the metal centre and prevents the approach of nucleophile from axially position).^[24]
- II. A strong *trans* σ -donor ligand (strong *trans* σ -donor ligands will enhance the weakening of the metal- leaving group bond and will stabilise the 14-electron transition state).^[24]
- III. A weak nucleophile (solvolytic pathway dominates with weak nucleophiles if the solvent is strongly coordinative).

Certain platinum(II) complexes containing two strong *cis* σ -donor atoms such as carbon, sulfur or phosphorous are found to undergo dissociative type mechanism.^[21, 23, 24, 59] The strong σ -donor carbon atoms stabilise the 14-electron three coordinate intermediate. Complexes of the type *cis*-[Pt(Me)₂R₂] and *cis*-[Pt(Ph)₂R₂] (where R=DMSO or thioether), were found to undergo dissociative type mechanism. However, when one of the thioethers was replaced by a strong π -acceptor ligand (CO), the same compounds followed an associative type pathway.^[59] The stronger π -accepting CO ligand removes the electron density from the metal centre where by reducing the electronic repulsion between the axially incoming nucleophile and the metal centre and hence favours a five-coordinate transition state. Furthermore, the LUMO of the carbonyl substituted complex being perpendicular to the plane of the molecule allows a more favourable side for the attack by the nucleophile favouring an associative mechanism.^[59]

One of the significant effects of dissociative mechanism is its non-stereo selective substitution behaviour. In dissociative mechanisms, the T-shaped fourteen electrons, three coordinate intermediate lives long enough to undergo intermolecular rearrangements of '*cis*-like' configuration to a '*trans*-like' configuration. Addition of nucleophile results in isomerisation giving non-stereo specific products.^[2]

Dissociative mechanisms also have very low solvent effects.^[21] With very weak nucleophiles, solvolytic pathway predominates if the solvent is strongly coordinative.^[21] This is one of the shortcomings of this mechanism with weak nucleophiles.

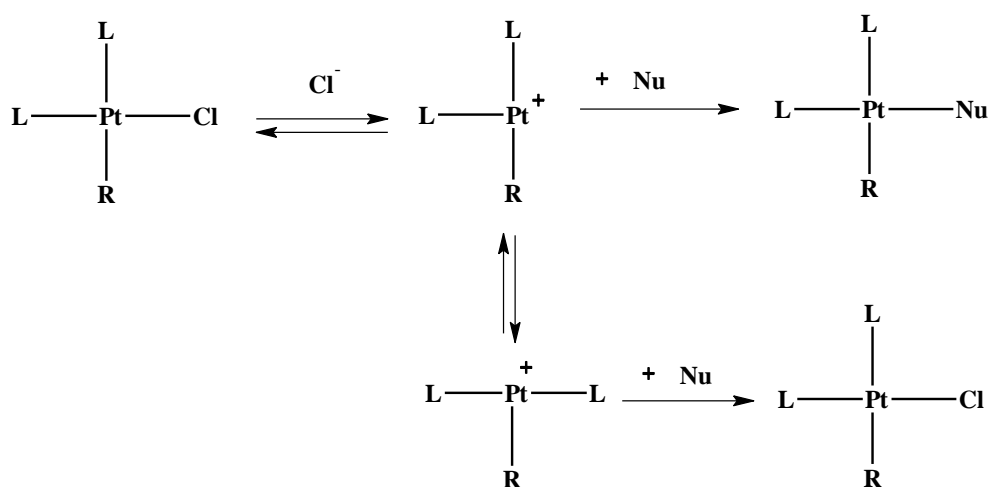


Figure 2.14 Representation of the non-stereospecific substitution of dissociation mechanism of a platinum(II) square planar complex due to the intermolecular rearrangements.^[13]

2.6. References

1. L. Arnaut, S. Formosinho and H. Burrows, *Chemical Kinetics From Molecular Structure to Chemical Reactivity*, Elsevier, New York, **2007**, p. 273-294.
2. M. L. Tobe and J. Burgess, *Inorganic Reaction Mechanisms*, Addison Wesley, London, **1999**, p. 30-39, 73-94, 103-106.
3. C. K. Ingold, *Structure and Mechanism in Organic Chemistry*, 2nd Ed., Cornell University Press, Ithaca, New York, **1969**, p. 241.
4. D. Benson, *Mechanisms of inorganic reactions in solution*, McGraw-Hill, London, **1968**, p. 19-31.
5. D. O. Cooke, *Inorganic Reaction Mechanisms*, The Chemical Society, London, **1979**, p. 1.
6. C. H. Langford and H. B. Gray, *Ligand Substitution Processes*, Benjamin, New York, **1965**, p.
7. G. L. Miessler and D. A. Tarr, *Inorganic Chemistry*, Pearson Education International, Singapore, **2004**, p. 415-426.
8. S. Ašperger, *Chemical Kinetics and Inorganic Reaction Mechanisms*, 2nd Ed., Kluwer Academic/Plenum Publisher, New York, **2003**, p. 38-39, 105-106, 140-153.
9. R. B. Jordan, *Reaction Mechanisms of Inorganic and Organometallic Systems*, Oxford University Press Inc, New York, **1991**, p. 23-30, 47-54, 58-60.
10. J. D. Atwood, *Inorganic and Organic Reaction Mechanisms*, 2nd Ed., Wiley-VCH Inc., New York, **1997**, p. 32-34, 43-61.
11. R. K. Murmann, R. T. M. Fraser and J. Bauman, *Mechanisms of Inorganic Reactions*, American Chemical Society, Washington, D. C., **1965**, p. 20-23, 81-97.
12. F. Basolo and R. G. Pearson, *Mechanisms of Inorganic Reactions*, 2nd Ed., Wiley, New York, **1967**, p. 193-195, 351-356, 369-400.
13. R. A. Henderson, *The Mechanisms of Reactions at Transition Metal Sites*, Oxford University Press, Oxford, **1993**, p. 1-22.
14. R. G. Wilkins, *Kinetics and Mechanisms of Reactions of Transition Metal Complexes*, 2nd Ed., VCH, Weinheim, **1991**, p. 199-201, 232-237.
15. D. Banerjea, F. Basolo and R. G. Pearson, *J. Am. Chem. Soc.*, **1957**, 79, 4055.
16. L. Cattalini, *Progr. Inorg. Chem.*, **1970**, 13, 263.
17. R. J. Cross, *Chem. Soc. Rev.*, **1985**, 14, 197.
18. R. J. Cross, *Adv. Inorg. Chem.*, **1989**, 34, 219.
19. A. Peloso, *Coord. Chem. Rev.*, **1973**, 10, 123.
20. L. Helm and A. E. Merbach, *Chem. Rev.*, **2005**, 105, 1923.

21. S. Lanza, D. Minniti, P. Moore, J. Sachinidis, R. Romeo and M. L. Tobe, *Inorg. Chem.*, **1984**, *23*, 4428.
22. R. Romeo, *Comment Inorg. Chem.*, **1990**, *11*, 21.
23. M. R. Plutino, L. M. Scolaro, R. Romeo and A. Grassi, *Inorg. Chem.*, **2000**, *39*, 2712.
24. R. Romeo, L. M. Scolaro, M. R. Plutino, F. F. De Biani, G. Bottari and A. Romeo, *Inorg. Chim. Acta*, **2003**, *350*, 143.
25. U. Belluco, L. Cattalini, F. Basolo, R. G. Pearson and A. Turco, *J. Am. Chem. Soc.*, **1965**, *87*, 241.
26. P. Haake, S. C. Chan and V. Jones, *Inorg. Chem.*, **1970**, *9*, 1925.
27. J. K. Beattie, *Inorg. Chim. Acta*, **1983**, *76*, L69.
28. C. F. Weber and R. van Eldik, *Eur. J. Inorg. Chem.*, **2005**, 4755.
29. A. Hofmann, D. Jaganyi, O. Q. Munro, G. Liehr and R. van Eldik, *Inorg. Chem.*, **2003**, *42*, 1688.
30. R. G. Pearson, *J. Amer. Chem. Soc.*, **1963**, *85*, 3533.
31. J. D. Page, *J. Chem. Educ.*, **1987**, *64*, 561.
32. U. Belluco, *Organometallic Coordination Chemistry of Platinum*, Academic Press, London, **1974**, p. 40-53, 138-160, 220-221.
33. I. I. Chernayev, *Ann. Inst. Platine U.S.S.R.*, **1928**, *6*, 55.
34. I. I. Chernayev, *Ann. Inst. Platine U.S.S.R.*, **1926**, *4*, 243, 246, 261.
35. Y. K. Syrkin, *Bull. Acad. Sci. U.S.S.R., Classe Sci. Chim.*, **1948**, 69.
36. L. Pauling, *The Nature of the Chemical Bond*, Ornell University Press, Ithaca, New York, **1960**, p. 332.
37. D. Banerjea, F. Basolo and R. G. Pearson, *J. Am. Chem. Soc.*, **1957**, *79*, 4055.
38. J. Chatt, L. A. Duncanson and L. M. Venanzi, *J. Chem. Soc.*, **1955**, 4456.
39. L. E. Orgel, *J. Inorg. Nucl. Chem.*, **1956**, *2*, 137.
40. H. R. Meerwein, *Sitzber. Ges. Beforder ges. Naturwe. Marburg.*, **1930**, *64*, 119.
41. A. A. Grinberg, *Acta Physiochim. USSR*, **1935**, *3*, 573.
42. C. Langford and H. B. Gray, *Ligand Substitution Processes*, W. A. Benjamin, New York, **1966**.
43. D. Jaganyi, A. Hofmann and R. van Eldik, *Angew. Chem. Int. Ed. Engl.*, **2001**, *40*, 1680.
44. H. B. Gray, *J. Am. Chem. Soc.*, **1962**, *84*, 1548.
45. R. G. Pearson, *J. Am. Chem. Soc.*, **1963**, *85*, 3533.
46. R. G. Pearson, *J. Chem. Educ.*, **1968**, *45*, 643.
47. R. G. Pearson, *J. Am. Chem. Soc.*, **1963**, *85*, 3533.
48. R. G. Pearson, H. Sobel and J. Songstad, *J. Am. Chem. Soc.*, **1968**, *90*, 319.
49. J. N. Bronsted, *J. Am. Chem. Soc.*, **1929**, *51*, 428.

50. H. Krüger and R. van Eldik, *J. Chem. Soc., Chem. Commun.*, **1990**, 330.
51. A. A. Grinberg, *J. Inorg. Chem. (USSR)*, **1959**, 4, 683.
52. I. B. Bersuker, *J. Struct. Chem.*, **1963**, 4, 419.
53. F. Basolo, J. Chatt, H. B. Gray, R. G. Pearson and B. L. Shaw, *J. Chem. Soc.*, **1961**, 2207.
54. R. Romeo, D. Minniti and M. Trozzi, *Inorg. Chem.*, **1976**, 15, 1134.
55. G. Faraone, V. Ricevuto, R. Romeo and M. Trozzi, *Dalton Trans.*, **1974**, 1377.
56. R. G. Pearson, H. B. Gray and F. Basolo, *J. Am. Chem. Soc.*, **1960**, 82, 787.
57. F. Basolo, H. B. Gray and R. G. Pearson, *J. Am. Chem. Soc.*, **1960**, 82, 4200.
58. H. B. Gray and R. J. Olcott, *Inorg. Chem.*, **1962**, 1, 481.
59. R. Romeo, A. Grassi and L. M. Scolaro, *Inorg. Chem.*, **1992**, 31, 4383.

Chapter 3

Kinetic Theory and Associated Techniques

3.1. Introduction

Chemical reactions occur at different rates. Some reactions occur at a very fast pace while others are so slow such that in practical terms they can be considered unoccurring.^[1] Chemical kinetics describes how fast a reaction occurs^[2] and is centred on the measurements of the rates of transformations.^[3-5] On the other hand, thermodynamics is concerned about how a chemical reaction occurs and it deals with the initial states of the reaction before the reaction occurs.^[3]

Kinetics of a chemical reaction was first studied by Ludwig Wilhelmy in 1850.^[3] He followed a reaction of hydrolysis of sucrose in acidic medium to give glucose and fructose at specific time intervals. Following Wilhelmy's observation, Marcellin Berthelot and Pean de St Gilles studied the ester hydrolysis of ethylacetate in aqueous ethanoic acid medium^[3] The results obtained for the reaction showed that the rate of the reaction was proportional to the concentration of both the ester and the acid.

The study of chemical kinetics is important for a number of reasons. Firstly, the data tells us the rate at which the reactants or products are consumed or formed. It describes the reaction pathways and the mechanisms involved in a chemical reaction and the factors which influence the formation of the products.^[5] Also, kinetic data helps to explain the relation between the structure of a chemical complex and its reactivity. The data is useful in predicting the stability or shelf-life^[6] of valuable chemical products, such as drugs.

Chemical reactions are often influenced by a number of factors.^[7] Therefore, to understand the kinetic behaviour of a chemical system, it is important to know the key factors which influence the rate of the reaction. These include:^[6]

- ✓ **Concentration:** The rate of reaction is dependent upon the concentration of the reactants. The higher the concentration, the more effective the collisions would be and thus the greater the rate.
- ✓ **Solvent properties:** Solvent properties such as polarity, donor atoms, added electrolyte, viscosity and the pH can influence the rate of the reaction.

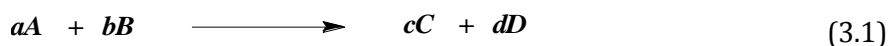
- ✓ **Physical conditions:** Physical conditions include factors such as pressure and temperature. For a given kinetic measurement normally such physical factors are normally kept constant.
- ✓ **Intensity of the absorbed radiation:** Depending on the nature of the reaction, light can be an influential factor for the rate of a reaction. However, the reaction should not be affected by the light intensity from the monochromator of the spectrophotometer.

Of the factors mentioned above, the central factor in chemical kinetics is the concentration of the reactants. Often the kinetics of the reacting system is studied by following the concentration of the reactants or products with respect to time. The concentration of the reactants and/or products can be determined by measurement of a physical property that is directly proportional to the concentration.

In this chapter a brief summary of the relevant rate laws and the pertinent experimental techniques commonly used in kinetic measurements will be given.

3.2. Rate Laws

The reaction rate can be expressed as the change in the rate of the reactant or the product per unit time.^[1, 8] Rates of the reaction expressed in this way are independent of the size of the sample under consideration. Consider the following chemical reaction:



where the capital letters represent the formulae of the chemical compounds in the reaction and the lower case letters represent the stoichiometry of the reaction. The units of rate are normally expressed in mol dm⁻³ s⁻¹.^[8, 9]

$$\text{Rate} = \frac{-d[\text{reactant}]}{dt} = \frac{d[\text{product}]}{dt} \quad (3.2)$$

where the negative sign indicates that the concentration of the reactant is decreased with time. Since the rate equation has the appropriate signs, the rate is always going to be a positive number. The rate law expresses the concentration of all the species that affect the rate.^[8] Therefore, the rate for *Equation 3.1* can be written as:

$$\text{Rate} = -\frac{1}{a} \cdot \frac{d[A]}{dt} = -\frac{1}{b} \cdot \frac{d[B]}{dt} = \frac{1}{c} \frac{d[C]}{dt} = \frac{1}{d} \frac{d[D]}{dt} \quad (3.3)$$

The rate law in general may be written as:

$$\text{Rate} = -k \prod_i [A_i]^{\alpha_i} [X_j]^{\beta_j} \quad (3.4)$$

where the A_i is the reactants, k is the rate constant, and X_j are other species such as catalysts that may affect the rate. α and β are the rate orders with respect to the reactants, A and B , respectively which are determined experimentally and is independent of the reaction stoichiometry.

The reaction order is then defined as:

$$\text{Reaction order} = \sum_i \alpha_i \quad (3.5)$$

The units of a rate of a reaction are $\text{mol dm}^{-3} \text{s}^{-1}$ and the units of k will depend on the reaction order.

3.3. Integrated Rate Expressions

3.3.1. Irreversible First-Order Reactions

Often most reactions are first-order or fit under first-order conditions. The first-order reaction,



gives a rate law,

$$\text{Rate} = -\frac{d[A]}{dt} = k_1[A]_t \quad (3.7)$$

which on rearrangement yields:

$$\frac{-d[A]}{[A]_t} = k_1 dt \quad (3.8)$$

Integrating from $t = 0$ to $t = t$ during which the concentration of reactants change from A_0 to A_t gives:

$$\int_{[A]_0}^{[A]_t} \frac{d[A]}{[A]} = -k_1 \int_0^t dt \quad (3.9)$$

$$\ln \frac{[A]_t}{[A]_0} = -k_1 t \quad (3.10)$$

$$\ln [A]_t = -k_1 t + \ln [A]_0 \quad (3.11)$$

where $[A]_0$ and $[A]_t$ are the concentrations of the reactant at time $t = 0$ and $t = t$.

Thus from Equation 3.11, a plot of $\ln[A]_t$ against time will be linear with a slope equal to $-k_1$.

Equation 3.11 can also be written as

$$[A]_t = [A]_0 e^{-k_1 t} \quad (3.12)$$

Thus the change in the concentration of the reactants or products follows an exponential decay or growth.

For a first-order reaction, any physical parameter that is proportional to the concentration such as absorbance, pressure, conductivity or volume can be used to follow the kinetics of the reaction.

3.3.2. Reversible First-Order Reactions

Certain reactions instead of going to completion attain equilibrium. For such reactions



the rate law for this reaction can be written as

$$\frac{d[B]}{dt} = \frac{-d[A]}{dt} = k_1[A]_t - k_{-1}[B]_t \quad (3.14)$$

At $t = 0$, $[B]_0 = 0$, and $[A]_t = [A]_0$

Thus

$$[B]_t = [A]_0 - [A]_t \quad (3.15)$$

Substituting *Equation 3.15* into *Equation 3.14* gives

$$-\frac{d[A]}{dt} = k_1[A]_t - k_{-1}([A]_0 - [A]_t) \quad (3.16)$$

At equilibrium the net reaction is zero, thus

$$-\frac{d[A]}{dt} = 0 \quad (3.17)$$

Applying *Equation 3.17* to *Equation 3.14* leads to

$$k_1[A]_{eq} = k_{-1}[B]_{eq} = k_{-1}([A]_0 - [A]_{eq}) \quad (3.18)$$

or

$$[A]_0 = \frac{k_1 + k_{-1}}{k_{-1}}[A]_{eq} \quad (3.19)$$

Substitution of *Equation 3.19* into *Equation 3.16* gives

$$-\frac{d[A]}{dt} = (k_1 + k_{-1})[A] - (k_1 + k_{-1})[A]_{eq} \quad (3.20)$$

Separation of variables leads to

$$\frac{d[A]}{([A]_t - [A]_{eq})} = -(k_1 + k_{-1})dt \quad (3.21)$$

Integration of *Equation 3.21*

$$\int_{[A]_0}^{[A]_t} \frac{d[A]}{([A]_t - [A]_{eq})} = -(k_1 + k_{-1}) \int_0^t dt \quad (3.22)$$

gives

$$\ln\left(\frac{[A]_0 - [A]_{eq}}{[A]_t - [A]_{eq}}\right) = (k_1 + k_{-1})t \quad (3.23)$$

by rearranging *Equation 3.23*

$$\ln([A]_t - [A]_{eq}) = -(k_1 + k_{-1})t + \ln([A]_0 - [A]_{eq}) \quad (3.24)$$

A plot of $\ln([A]_t - [A]_{eq})$ against time will produce a straight line of slope $-(k_1 + k_{-1})$. To obtain the individual rate orders, k_1 or k_{-1} one must also evaluate the equilibrium constant, K_{eq} .

$$K_{eq} = \frac{[B]_{eq}}{[A]_{eq}} = \frac{k_1}{k_{-1}} \quad (3.25)$$

Therefore the observed rate constant, k_{obs} becomes

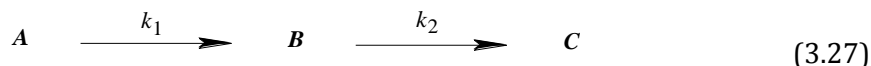
$$k_{obs} = (k_1 + k_{-1}) \quad (3.26)$$

The problem often encountered in measuring the first-order rate constant is the accurate measurement of $[A]_{eq}$.^[8, 10, 11]

3.3.3. Consecutive First-Order Reactions

Often ligand substitution reactions do not stop after one substitution but continue to give a more highly substituted complex where the product of the first reaction acts as a reactant for the subsequent reaction. These reactions are referred as consecutive reactions.^[6, 8, 12]

Consider the following consecutive irreversible reactions;



The rate law for the equations are as follows

$$\frac{-d[A]}{dt} = k_1[A] \quad (3.28)$$

$$\frac{d[B]}{dt} = k_1[A] - k_2[B] \quad (3.29)$$

$$\frac{d[C]}{dt} = k_2[B] \quad (3.30)$$

Assuming that at time $t = 0$, only the component A is present, *i.e.* $[B]_0$ and $[C]_0 = 0$, and at any time t ,

$$[A]_0 = [A]_t + [B]_t + [C]_t \quad (3.31)$$

Integration of Equation 3.28 gives

$$[A]_t = [A]_0 e^{-k_1 t} \quad (3.32)$$

By integrating Equation 3.29 using integrating factor method and substituting Equation 3.32 into Equation 3.29 yields

$$\frac{d[B]}{dt} = k_1[A]_0 e^{-k_1 t} - k_2[B]_t \quad (3.33)$$

Multiplying through by the integration factor, $e^{k_2 t}$ by both sides of Equation 3.33 followed by subsequent rearrangements lead to

$$\frac{d[B]e^{k_2 t}}{dt} = k_1[A]_0 e^{(k_2 - k_1)t} - k_2[B]_t e^{k_2 t} \quad (3.34)$$

Having the initial conditions, at time $t = 0$, $[B]_0 = 0$ and by applying product rule and integration of Equation 3.34 gives

$$\begin{aligned} \int_0^t \frac{d}{dt} ([B]_t e^{k_2 t}) &= k_1[A]_0 \int_0^t e^{(k_2 - k_1)t} dt \\ [B]_t &= k_1[A]_0 \frac{\int_0^t e^{(k_2 - k_1)t} dt}{e^{k_2 t}} \\ [B]_t &= \frac{[A]_0 k_1}{k_2 - k_1} [e^{-k_1 t} - e^{-k_2 t}] \end{aligned} \quad (3.35)$$

Applying mass law to Equation 3.31 to find the dependence of $[C]$ with time and by substituting Equation 3.32 and Equation 3.35 in to Equation 3.31 affords

$$[C]_t = [A]_0 \left(1 - \frac{k_2}{k_2 - k_1} e^{-k_1 t} + \frac{k_1}{k_2 - k_1} e^{-k_2 t} \right) \quad (3.36)$$

A simplified assumption called *steady state approximation* is often used for consecutive reactions. The assumption is that $[B]$ is small and does not change during the reaction hence $k_1 < k_2$.^[8]

Therefore, Equation 3.29 can be written as:

$$\frac{d[B]}{dt} = k_1[A]_t - k_2[B]_t \cong 0 \quad (3.37)$$

thus

$$[B]_t = \frac{k_1}{k_2} [A]_t \quad (3.38)$$

Substituting Equation 3.32 into Equation 3.38 yields

$$[B]_t = \frac{k_1}{k_2} [A]_0 e^{-k_1 t} \quad (3.39)$$

Rearranging Equation 3.31 to find the dependence the $[C]$ with time yields

$$[C]_t = [A]_0 - [A]_t - [B]_t \quad (3.40)$$

Substituting Equation 3.32 and Equation 3.39 into Equation 40 gives ^[8, 13]

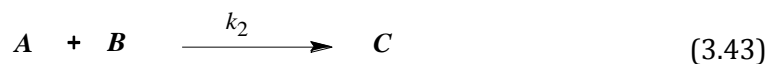
$$[C]_t = [A]_0 \left[1 - e^{-k_1 t} - \frac{k_1}{k_2} e^{-k_1 t} \right] \quad (3.41)$$

$$\cong [A]_0 [1 - e^{-k_1 t}] \quad (3.42)$$

3.3.4. Irreversible Second-Order Reactions

There are two types of second-order reactions. One is when the reaction is second-order with respect to only one of the reactant. The second type is when the reaction is first-order with respect to two different reactants which will be considered here.

For the given equation,



the rate law can be written as,

$$\text{Rate} = k[A][B] \quad (3.44)$$

$$\text{Rate} = \frac{d[C]}{dt} = -\frac{d[A]}{dt} = -\frac{d[B]}{dt} = k_2[A]_t[B]_t \quad (3.45)$$

If initially at $t = 0$, $[A] = [A]_0$ and $[B] = [B]_0$, and by letting 'x' be the amount of the reactants reacted in time t , then the concentration of $[A]$ at time t is $[A]_t = ([A]_0 - x)$ and $[B]_t = ([B]_0 - x)$

Therefore the rate after t seconds is,

$$-\frac{d[A]}{dt} = k_2([A]_0 - x)([B]_0 - x) \quad (3.46)$$

Since $\frac{dx}{dt} = -\frac{d[A]}{dt} = -\frac{d[B]}{dt}$ Equation 3.46 can be written as

$$\frac{dx}{dt} = k_2([A]_0 - x)([B]_0 - x) \quad (3.47)$$

Separating the variables lead to

$$\frac{dx}{([A]_0 - x)([B]_0 - x)} = k_2 dt \quad (3.48)$$

Integrating between the limits $x = 0$ to $x = x$ and $t = 0$ to $t = t$,

$$\int_0^x \frac{dx}{([A]_0 - x)([B]_0 - x)} = k_2 \int_0^t dt \quad (3.49)$$

leads to

$$\frac{1}{[A]_0 - [B]_0} \ln \frac{[B]_0([A]_0 - x)}{[A]_0([B]_0 - x)} = k_2 t \quad (3.50)$$

Since the initial concentration is much greater than the concentration of the reactants at time t , Equation 3.50 can be written as

$$\frac{1}{[A]_0 - [B]_0} \ln \frac{[B]_0[A]_t}{[A]_0[B]_t} = k_2 t \quad (3.51)$$

From the Equation 3.51, it can be seen that in order to determine the second-order rate constant, the $[A]_0$, $[B]_0$, $[A]_t$ and $[B]_t$ need to be known. In most kinetic experiments this is very time consuming and complicated.^[8, 10] Therefore, second-order reactions are usually studied under *pseudo* first-order conditions. This is achieved by providing one of the reagents in a large excess (at least 10-fold excess) such that its concentration remains constant during the reaction. For example if the $[B]_0 \gg [A]_0$ then the concentration of B remains relatively constant. Assuming that the reaction order with respect to A is one, then the rate law in Equation 3.45 becomes,

$$\begin{aligned}
 \frac{-d[A]}{dt} &= k_2[A]_t[B]_t \\
 &= (k_2[B]_0)[A]_t \\
 &= k_{\text{obs}}[A]_t
 \end{aligned}
 \tag{3.52}$$

where k_{obs} is the observed rate constant in s^{-1} .

Integration of Equation 3.52 and plotting the graph of $\ln[A]_t$ versus time t , would give the observed rate constant k_{obs} (s^{-1}) as the slope. To determine the second-order rate constant, k_2 , the experiment has to be repeated with different actual concentrations of B in large excess. This generates a number of k_{obs} values for $[B]_0$. Thus from Equation 3.52, k_{obs} can be written as:

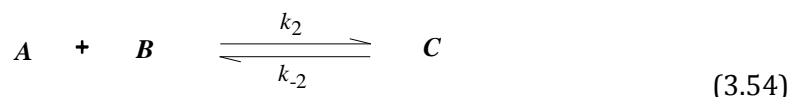
$$k_{\text{obs}} = k_2[B]_0 \tag{3.53}$$

A plot of k_{obs} versus $[B]_0$ will give the second-order rate constant, k_2 with the units $M^{-1} s^{-1}$.

In kinetic studies *pseudo* first-order reactions are often used to find the second-order rate constant when one of the reactant is very expensive or scarce. The component which is relatively cheap is used in excess when compared to the other reagent. In this way the second-order rate constant can be determined simply by dividing the first-order rate constant by the concentration of the excess component. The rate constant obtained in this way is independent of the concentration of the expensive or deficient reagent.^[10]

3.3.5. Reversible Second-Order Reactions

Some reactions do not always go to completion; instead they attain an equilibrium where the forward and the reverse reaction take place at the same time. An equilibrium reaction can be represented as follows



From Equation 3.54, it can be seen that the forward reaction is second-order and the reverse reaction is first-order. Thus it involves a mixed-order behaviour which is very complicated. Therefore to overcome the complexity, often *pseudo* first-order conditions is applied for

the forward reaction where $[B]_0 \gg [A]_0$. Thus such systems then become similar to reversible first-order reaction.

Treating *Equation 3.54* as a reversible first-order equation, the formation of C can be expressed as:

$$-\frac{d[A]}{dt} = -\frac{d[B]}{dt} = \frac{d[C]}{dt} = k_2[A]_t[B]_t - k_{-2}[C]_t \quad (3.55)$$

Assuming the stoichiometry of the reaction is 1:1:1 and the concentration of C at the beginning is zero, the mass balances at any time, t can be written as

$$\begin{aligned} [A]_t &= [A]_0 - [C]_t \\ [B]_t &= [B]_0 - [C]_t \end{aligned} \quad (3.56)$$

Therefore, at equilibrium the mass balance is:

$$\begin{aligned} [A]_{eq} &= [A]_0 - [C]_{eq} \\ [B]_{eq} &= [B]_0 - [C]_{eq} \end{aligned} \quad (3.57)$$

At equilibrium the forward and the reverse reaction takes place at the same rate. *i.e.*

$$-\frac{d[A]}{dt} = k_2[A]_{eq}[B]_{eq} - k_{-2}[C]_{eq} = 0 \quad (3.58)$$

thus

$$k_2[A]_{eq}[B]_{eq} = k_{-2}[C]_{eq} \quad (3.59)$$

By rearranging and substituting *Equation 3.57* and *Equation 3.58* into *Equation 3.59*, the following equation can be obtained

$$k_2[A]_{eq}[B]_{eq} = k_{-2}([A]_0 - [A]_{eq}) \quad (3.60)$$

Therefore,

$$k_{-2}[A]_0 = k_2[A]_{eq}[B]_{eq} + k_{-2}[A]_{eq} \quad (3.61)$$

Rearranging *Equation 3.56* for $[C]_t = [A]_0 - [A]_t$, and substituting into *Equation 3.55* gives:

$$\begin{aligned}
 -\frac{d[A]}{dt} &= k_2[A]_t[B]_t - k_{-2}([A]_0 - [A]_t) \\
 &= k_2[A]_t[B]_t - k_{-2}[A]_0 = k_{-2}[A]_t
 \end{aligned}
 \tag{3.62}$$

Combining Equations 3.61 and Equation 3.62 yields:

$$-\frac{d[A]}{dt} = k_2[A]_t[B]_t - k_2[A]_{eq}[B]_{eq} - k_{-2}[A]_{eq} + k_{-2}[A]_t
 \tag{3.63}$$

Applying *pseudo* first-order conditions where the $[B]_0 \gg [A]_0$, Equation 3.63 can be written as:

$$-\frac{d[A]}{dt} = k_2[A]_t[B]_0 - k_2[A]_{eq}[B]_0 - k_{-2}[A]_{eq} + k_{-2}[A]_t
 \tag{3.64}$$

By factorizing

$$-\frac{d[A]}{dt} = (k_2[B]_0 + k_{-2})([A]_t - [A]_{eq})
 \tag{3.65}$$

Separation of the variables followed by integration leads to

$$\begin{aligned}
 \int_{[A]_0}^{[A]_t} \frac{d[A]}{([A]_t - [A]_{eq})} &= -(k_2[B]_0 + k_{-2}) \int_0^t dt \\
 \ln \left(\frac{[A]_t - [A]_{eq}}{[A]_0 - [A]_{eq}} \right) &= -(k_2[B]_0 + k_{-2})t \\
 &= -k_{obs}t
 \end{aligned}
 \tag{3.66}$$

$$\text{where } k_{obs} = k_2[B]_0 + k_{-2}$$

A plot of k_{obs} versus $[B]_0$ gives a straight line of a slope of k_2 and an intercept of k_{-2} . The equilibrium constant, K can be obtained by the ratio, k_2/k_{-2} or can be measured thermodynamically.^[14] *Pseudo* first-order conditions are often used for the study of kinetic behaviour of square planar complexes.

3.4. Activation Parameters

The mechanism of a reaction is often determined based on the rate law. In addition, the activation parameters can also contribute additional and useful information to the study of reaction mechanisms. These relate to the different aspects of kinetics with thermodynamics. The activation parameters for a reaction can be obtained from the temperature dependence study of the rate constant.^[8, 10, 15] Activation parameters are often determined using either the Arrhenius equation^[8, 15] or by using absolute reaction rate theory (Transition State Theory).^[8]

3.4.1. The Arrhenius Equation

Arrhenius was the first to determine the quantitative relationship between the rate constant and the temperature.^[10] Arrhenius suggested the empirical relationship in the form^[16]

$$k = Ae^{(-E_a/RT)} \quad (3.67)$$

A = Arrhenius pre-exponential factor measured in $M^{-1} s^{-1}$

E_a = Arrhenius activation energy in $J mol^{-1}$

R = Gas constant equal to $8.314 J K^{-1} mol^{-1}$

T = temperature in Kelvin

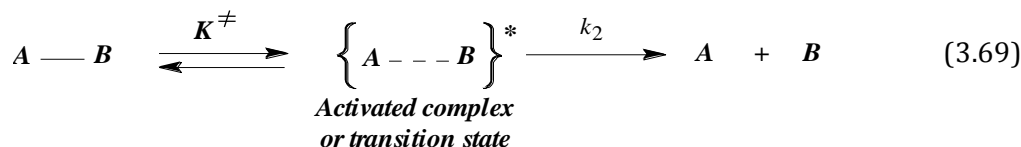
Equation 3.67 can be expressed in logarithmic form as follows

$$\ln k = \ln A - \frac{E_a}{R} \left(\frac{1}{T} \right) \quad (3.68)$$

The rate constant, k , is determined experimentally at different temperatures. A plot of $\ln k$ versus $\frac{1}{T}$ gives a slope of $-\frac{E_a}{R}$. The value of k is expected to increase with increase in temperature.^[8, 10] The Arrhenius equation is often used in kinetics where the measured rate constant is thought to be composite for specific rate constants.^[10]

3.4.2. The Transition-State Theory

The Transition-State Theory originally called “the absolute reaction rate theory” was developed for a gas phase dissociation process^[10] in 1935 by Henry Eyring and Michael Polanyi.^[10, 17, 18] This theory was based on an assumption that many reactions occur via a formation of a pre-equilibrium between the reactants and the activated transition state complex.^[10, 19] According to this theory a reaction can be described as follows^[10]



The rate equation for the reaction can be written as

$$\frac{d[A]}{dt} = k_2 \{A \cdots B\}^* \quad (3.70)$$

Thus the equilibrium constant is

$$K^\ddagger = \frac{\{A \cdots B\}^*}{[A - B]} \quad (3.71)$$

By rearranging *Equation 3.71* leads to

$$\{A \cdots B\}^* = K^\ddagger [A - B] \quad (3.72)$$

Substituting *Equation 3.72* into *Equation 3.70* gives,

$$\frac{d[A]}{dt} = k_2 K^\ddagger [A - B] \quad (3.73)$$

$$= \frac{k_b T}{h} K^\ddagger [A - B] \quad (3.74)$$

where k_b = Boltzmann constant ($1.38 \times 10^{-23} \text{ JK}^{-1}$)

h = the Planck constant ($6.626 \times 10^{-34} \text{ J s}^{-1}$)

By referring to *Equation 3.70*, the experimental second-order rate constant, k_{expt} can be written as

$$\frac{d[A]}{dt} = k_{\text{expt}}[A - B] \quad (3.75)$$

Comparing *Equation 3.74* and *Equation 3.75*, the experimental rate constant can now be expressed as

$$k_{\text{expt}} = \frac{k_b T}{h} K^\ddagger \quad (3.76)$$

Gibbs free energy of activation, ΔG^\ddagger , is expressed as

$$\Delta G^\ddagger = -RT \ln K^\ddagger \quad (3.77)$$

$$= \Delta H^\ddagger - T\Delta S^\ddagger \quad (3.78)$$

Substituting *Equation 3.77* and *Equation 3.78* into *Equation 3.76* affords

$$k_{\text{expt}} = \frac{k_b T}{h} e^{\left(\frac{-\Delta H^\ddagger}{RT}\right)} e^{\left(\frac{\Delta S^\ddagger}{R}\right)} \quad (3.79)$$

Rearranging and applying logarithm results

$$\ln\left(\frac{k_{\text{expt}}}{T}\right) = \frac{-\Delta H^\ddagger}{RT} + \left[\ln\left(\frac{k_b}{h} + \frac{\Delta S^\ddagger}{R}\right)\right] \quad (3.80)$$

and simplifying

$$\ln\left(\frac{k_{\text{expt}}}{T}\right) = \frac{-\Delta H^\ddagger}{R} \cdot \frac{1}{T} + \left[23.8 + \frac{\Delta S^\ddagger}{R}\right] \quad (3.81)$$

Thus activation parameters, enthalpy of activation, (ΔH^\ddagger) and entropy of activation, (ΔS^\ddagger) can be determined from a plot of $\ln\left(\frac{k_{\text{expt}}}{T}\right)$ versus $\frac{1}{T}$. ΔH^\ddagger can be determined from the slope of the graph and ΔS^\ddagger can be obtained from the y-intercept of the graph. This plot is known as Eyring plot.^[8, 19, 20] Since, ΔS^\ddagger is obtained by extrapolating the graph, the error associated with it is normally three times higher than that of ΔH^\ddagger .^[6]

3.5. Techniques Associated with the Study of Chemical Kinetics

Kinetic analysis often involves measuring physical properties such as pressure, conductivity, absorbance and density.^[4] Regardless of the physical quantity, the kinetic studies are related to the concentration of the product(s) or reactant(s) with respect to time. The choice of the experimental method depends on the nature and rapidity of the reaction.

To date a number of different techniques are available for kinetic studies. Most commonly used kinetic methods include nuclear magnetic resonance (NMR), UV/Visible spectrophotometry and pulse methods. Reactions which are too fast to study using conventional methods are often studied using special methods. Such reactions include reactions involving proton transfer, enzymes and non-covalent complex formation.^[20] The study of reactions occurring at “conventional” rates include, first mixing the reagents and then determining the decrease in the concentration of the reactant(s) or the increase in the concentration of the product(s) with respect to time.

Reaction rates that lie outside the time frame of the normal laboratory operations are studied using specialised techniques and instruments. This includes reactions which occur at very fast rates. Fast reactions are reaction systems whose reaction time varies from 1 minute to 10^{-14} seconds.^[6] One way of studying fast reactions is to bring their rates into the conventional time range by changing the conditions such as temperature, concentration or the solvent. However, this method is outdated^[6] and is reliable only if the reaction having half-life is greater than 1 hour.^[21]

A summary of the different reaction techniques employed in kinetic analysis is given in *Figure 3.1*.^[20] The different chemical and physical processes that can be investigated are shown in the upper region and the lower region shows the corresponding techniques that can be used to study the kinetic behaviour and the years in which they were investigated.

Conventional techniques are not applicable to very fast reactions because fast reactions take a very shorter period of time for the reaction to go to completion. Therefore, the time that it takes to mix the reagents and take the required measurements need to be short enough so that it does not interfere with the actual rate of the reaction. The two main methods often used to study fast reactions include flow methods and pulse methods.^[20] The two methods that are used in the current study are UV/Visible absorption spectrophotometry and the stopped-flow method. These two techniques will be discussed in more detail here.

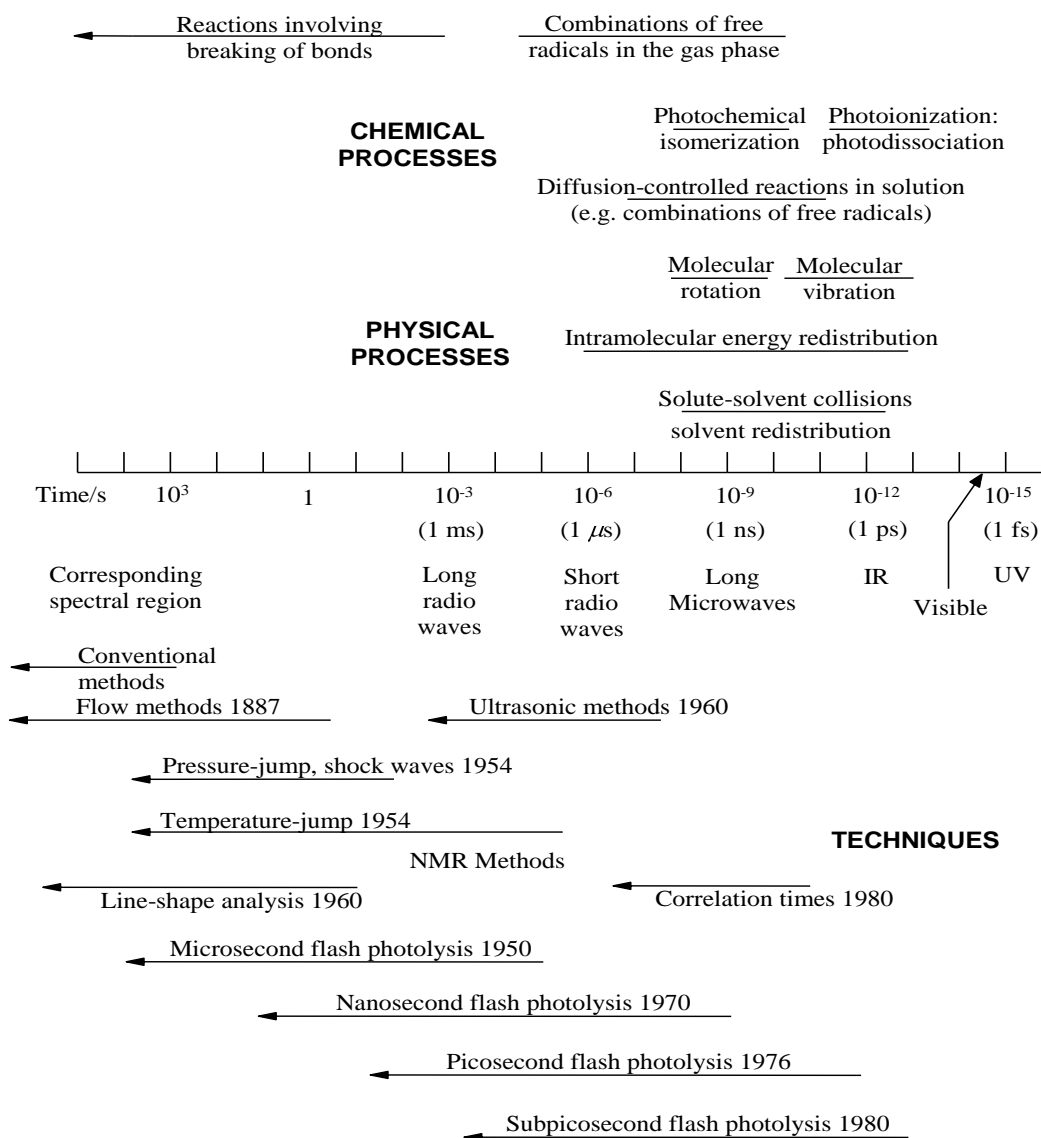


Figure 3.1 A summary of reaction techniques and their corresponding time scales.^[20]

3.5.1. UV/ Visible Spectrophotometry

UV/Visible spectrophotometry is one of the most powerful^[16] and commonly used techniques involved in the kinetic studies.^[8] It is a sensitive technique which can detect the sample concentrations ranging from 10^{-4} to 10^{-6} M.^[21] The key components of a spectrophotometer include the monochromator, light source, detector and the data processor. The photomultiplier tube is a commonly used detector in UV/Visible spectrophotometry. It consists of a cathode which emits electrons when struck by photon of radiation. The light source used is deuterium for UV and tungsten lamp for visible measurements. For UV/Visible region, normally glass prisms are used as

monochromators.^[22] Sample cells (cuvettes) are made up of quartz or fused silica and are transparent.

Radiation of more than one wavelength enters the monochromator and the grating prisms disperse the light into its component wavelengths and the monochromator allows a single wavelength to pass through. The beam then passes through the sample pathway. The photomultiplier detector then measures the transmitted radiation as photons. The photons hit the photoemittive cathode and electrons are kicked out from the cathode which is amplified at the dynodes where a cascade of electrons is produced before they are finally collected at the anode, resulting in a current that is amplified and measured. The UV/Visible spectrophotometer measures the absorbance ranging from 190 nm to 900 nm.

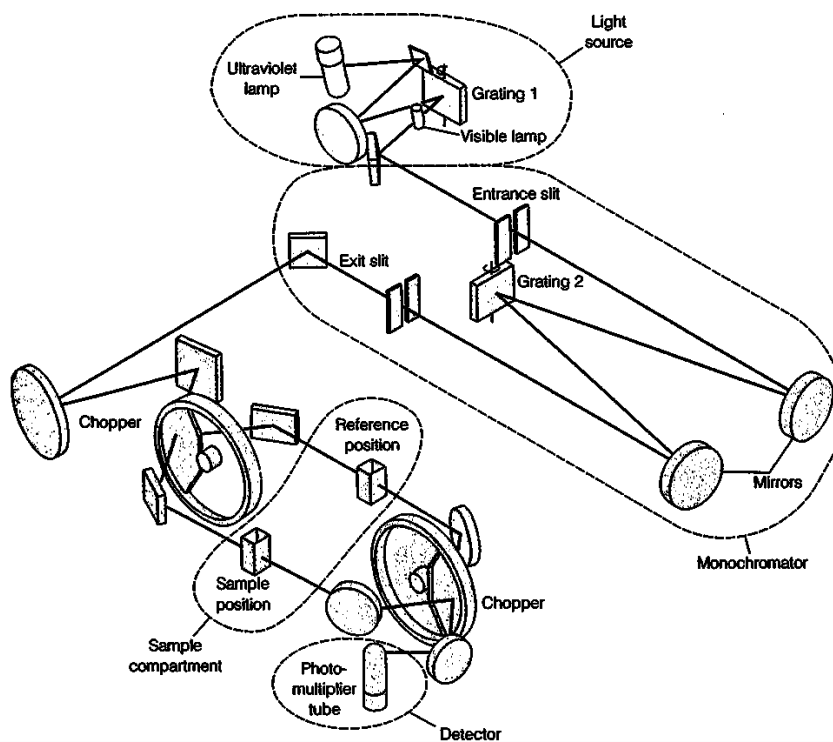


Figure 3.2 Schematic diagram of a UV/Visible spectrophotometry setup.^[23]

Modern spectrophotometers are based on a double-beam design where one beam passes through the reference solution while the second beam simultaneously passes through the sample.^[22] Outputs from the two are amplified, computed and displayed on the output device. The spectrophotometer measures the transmitted light from the sample. The transmitted light is converted into absorbance which is displayed on the screen.

The light transmitted from the sample can be represented as

$$T = \frac{I_0}{I} \quad (3.82)$$

Where I_0 = the intensity of the incident light

I = the intensity of the transmitted light

The absorbance can then be written as

$$A = -\log T \quad (3.83)$$

By applying Beer's law (Equation 3.84), the concentration of the sample can be determined from its absorbance. Beer's law states a linear relationship between the absorbance, concentration and the path length.^[22]

$$A = \varepsilon cl \quad (3.84)$$

Where A = absorbance

ε = molar absorptivity

c = concentration in mol dm⁻³

l = path length in cm

UV/Visible absorption spectra often involve broad absorptions that overlap with other species in the solution. Even though this makes the analysis of the product more difficult, kinetic analysis can be done on overlapping absorption spectra.^[19]

For a given first-order reaction,



At any time t , the absorption is given by

$$A_t = \varepsilon_X [X] + \varepsilon_Y [Y] \quad (3.86)$$

where A_t = the absorption at any time, t

$\varepsilon_X, \varepsilon_Y$ = molar absorptivity of X and Y respectively

When the reaction goes to completion, the absorbance is given by

$$A_{\infty} = \varepsilon_X [X]_0 + \varepsilon_Y [Y]_0 \quad (3.87)$$

where A_{∞} = absorbance at infinity

$[X]_0$ and $[Y]_0$ = initial concentration of X and Y respectively

For the kinetic analysis, the absorbance can be expressed as

$$\ln \frac{[X]_0}{[X]_t} = \ln \left(\frac{A_0 - A_{\infty}}{A_t - A_{\infty}} \right) = k_1 t \quad (3.88)$$

Figure 3.3 shows the reaction profile obtained for the substitution of $[\text{Pt}\{4'-(o\text{-tolyl})\text{-}2,2':6',2''\text{-terpyridine}\}\text{Cl}]\text{CF}_3\text{SO}_3$ with 1-methylimidazole (Structure given in Figure 5.1). The kinetics for the reaction was studied at 333 nm and the trace obtained for the reaction at 298.15 K is shown as an insert in Figure 3.3. The rate constant for the reaction was obtained by fitting first-order exponential decay function using Origin 5.0®.[24]

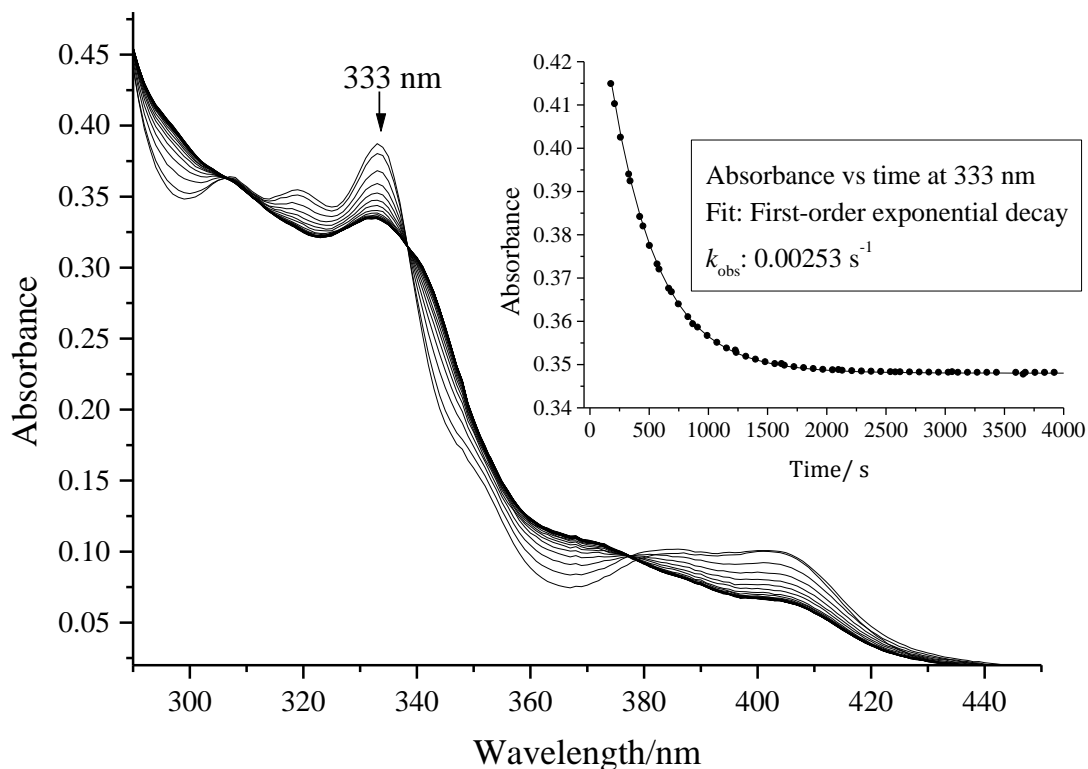


Figure 3.3 Spectrum obtained from Cary UV/Visible spectrophotometer for the substitution of Cl^- from $[\text{Pt}\{4'-(o\text{-tolyl})\text{-}2,2':6',2''\text{-terpyridine}\}\text{Cl}]\text{CF}_3\text{SO}_3$ ($2.50 \times 10^{-5} \text{ mol dm}^{-3}$) with 1-methylimidazole ($5.00 \times 10^{-4} \text{ mol dm}^{-3}$) in methanol solution ($I = 0.10 \text{ M}$ (0.09 M $\text{LiCF}_3\text{SO}_3 + 0.01 \text{ M NaCl}$)) at 333 nm and 298.15 K.

3.5.2. Flow Methods

Many chemical reactions occur too rapidly for conventional UV/Visible spectrophotometry. Such reactions require shorter sampling and mixing time. Often flow methods are used to overcome this problem. Flow methods involve flowing of two reactant solutions rapidly under pressure to a reaction mixing chamber and then to an observation chamber. Concentrations of the reactants or products are then measured at various positions of the tube at various time intervals. The time scale for mixing of flow methods varies approximately from 1 ms to 10 seconds. Reactions with half-lives of about 10^{-2} seconds are often studied using such methods.^[22] There are two common types of flow methods used namely, continuous flow method and stopped flow method.

Hartridge and Roughton^[25] pioneered continuous flow method by designing special mixing chambers to study the rapid reactions in solution.^[4] A schematic representation of continuous flow method is given in *Figure 3.4*. This method works on the principle where the two reacting solution are forced into the mixing chamber by the pistons. The resulting solution then flows through the observation tube, where spectroscopic detection takes place at specific distances downstream from the mixer. This method is normally used to study rapid solution reactions with half-lives of approximately 1 ms or greater.^[4] In this technique since a steady state is set up and the observation does not require being rapid. However, a longer observation time requires a larger amount of solutions. This problem can be solved by using stopped-flow technique.^[4]

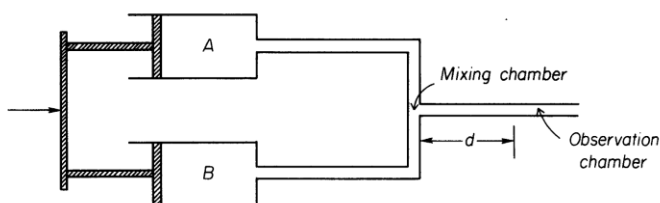


Figure 3.4 Diagrammatic representation of a continuous flow kinetic system. The letter *d* represents the distance from the mixture to the point of observation.^[11]

A schematic diagram of the stopped-flow technique is shown in *Figure 3.5*. This technique is designed to study the reaction of two substances where one of the reactant is placed in syringe **A** and the other in syringe **B**. The two syringes are kept at constant temperature of choice. In this method the two reacting solutions are rapidly forced into a mixing chamber by pressure. The mixing in stopped-flow takes approximately 0.001 seconds.^[22] From the mixing chamber the solution then goes into the reaction cuvette where the solutions

alternatively get mixed and then stops when the stopping syringe comes against its seating (Figure 3.5). The reaction is then flowed spectrophotometrically.

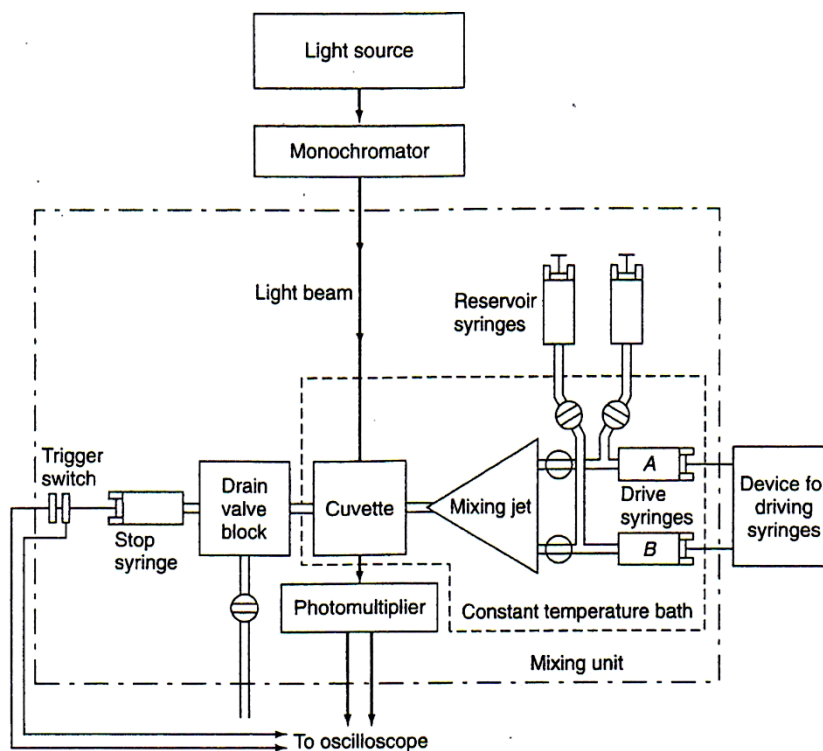


Figure 3.5 Diagrammatic representation of stopped-flow apparatus.^[20]

3.6. References

1. E. L. King, *How Chemical Reactions Occur: An Introduction to Chemical Kinetics and Reaction Mechanisms*, W. A. Benjamin, Inc, New York, **1964**, p. 1.
2. D. W. Ball, *Physical Chemistry*, Brooks/Cole, Pacific Grove, **2003**, p. 680-703.
3. M. Mortimer and P. Taylor, *Chemical Kinetics and Mechanism*, The Open University. Walton Hall, Milton Keys, MK76AA, London, **2002**, p. 11.
4. F. Wilkinson, *Chemical Kinetics and Reaction Mechanisms*, Van Nostrand Reinhold Company, New York, **1980**, p. 1-11, 66-99.
5. E. T. Denisov, O. M. Sarkisov and G. I. Likhtenshtein, *Chemical Kinetics: Fundermentals and New Development*, Elsevier Science & Technology Books, **2003**, p. 1-6.
6. J. H. Espenson, *Chemical Kinetic and Reaction Mechanisms*, 2nd Ed., McGraw-Hill, New York, **1995**, p. 1-80,155-159,161-162, 253-256.
7. M. F. C. Ladd and W. H. Lee, *Introduction to Physical Chemistry*, Cambridge University Press, New York, **1986**, p. 273-301.
8. J. D. Atwood, *Inorganic and Organic Reaction Mechanisms*, 2nd Ed., Wiley- VCH Inc., New York, **1997**, p. 1-32.
9. J. W. Moore and R. G. Pearson, *Kinetics and Mechanism*, 3rd Ed., John Wiley and Sons, New York, **1981**, p. 12-19.
10. R. B. Jordan, *Reaction mechanisms of Inorganic and Organometalic Systems*, Oxford University Press Inc, New York, **1991**, p. 1-17.
11. K. A. Connors, *Chemical Kinetics: The Study of Reaction Rates in Solution*, Wiley-VCH, New York, **1990**, p. 1-22, 176-180.
12. R. S. Logan, *Fundermentals of Chemical Kinetics*, Longman, **1996**, p. 1-27.
13. R. J. Silbey, R. A. Alberty and G. B. Mounji, *Physical Chemistry*, John Wiley and Sons, New York, **2005**, p. 642-654.
14. P. Atkins and J. de Paula, *Atkins' Physical Chemistry*, 8th Ed., Oxford University Press, **2006**, p. 479-815.
15. D. Benson, *Mechanisms of Inorganic Reactions in Solution*, McGraw-Hill, London, **1968**, p. 1-13.
16. R. G. Wilkins, *Kinetics and Mechanisms of Reactions of Transition Metal Complexes*, VCH, Weinheim, **1991**, p. 41-43.
17. H. Eyring, *J. Chem. Phys.*, **1935**, 3, 107.
18. M. G. Evans and M. Polanyi, *Trans. Faraday Soc.*, **1935**, 31, 875.
19. S. Ašperger, *Chemical Kinetics and Inorganic Reaction Mechanisms*, 2nd Ed., Kluwer Academic/ Plenum Publisher, New York, **2003**, p. 3, 7- 23.

20. K. J. Laidler, J. H. Meiser and B. C. Sanctuary, *Physical Chemistry*, 4th Ed., Houghton Mifflin Company, New York, **2003**, p. 374-379, 390-393.
21. D. Reddy, *PhD Thesis, Tuning the Reactivity of Platinum(II) Complexes*, University of Natal, Pietermaritzburg, South Africa, **2009**, pp. 88, 90.
22. D. A. Skoog, A. M. West, F. J. Holler and S. R. Crouch, *Fundamentals of Analytical Chemistry*, 8th Ed., Thomson Brooks/Cole, Canada, **2002**, p. 374-379, 720, 769-775.
23. D. C. Harris, *Quantitative Chemical Analysis*, 4th Ed., W. H. Freeman and Company, New York, **1995**, p. 480.
24. Microcal™ Origin™ Version 5.0. Microcal Software, Inc., One Roundhouse Plaza, Northampton, MA, 01060, USA, 1991-1997.
25. H. Hartridge and F. J. W. Roughton, *Proc. R. Soc.*, **1923**, A104, 376.

Chapter 4

Experimental: Synthesis and Kinetic Analysis of Platinum(II) Complexes

4.1. Materials and Methodology

Methyl-3-isoquinoline carboxylate (98%), *ortho*-tolualdehyde (98%), lithium trifluoromethanesulfonate (LiCF_3SO_3 , 96%), 2,2':6',2''-terpyridine (98%) and 1,5-cyclooctadiene (99%) were purchased from Aldrich and were used without further purification. The precursor *N*-{1-(2'-pyridyl)-1-oxo-2-ethyl}pyridinium iodide was kindly donated by D. Reddy^[1] (School of Chemistry, Pietermaritzburg).

The platinum salts, dichlorobis(benzonitrile)platinum(II), $[\text{Pt}(\text{Ph}(\text{CN})_2\text{Cl}_2]$, 99%) and potassium tetrachloroplatinate (K_2PtCl_4 , 99.99%) were purchased from Strem Chemicals and stored in a dessicator prior to use.

The neutral nucleophiles, imidazole (99.5%, Fluka) and from Aldrich, pyrazole (98%), 1-methylimidazole (99%), 1,2-dimethylimidazole (98%) and triazole (98%) were used as supplied. Silver hexafluoroantimonate (AgSbF_6 , 98%), and silver trifluoromethanesulfonate (AgCF_3SO_3 , 99+%) were purchased from Aldrich and stored under nitrogen prior to use. Ammonium acetate (NH_4OAc , 97%, Saarchem) was dried in a desiccator prior to use. Ethylacetate (99.8%, Sigma-Aldrich) was dried over potassium carbonate for several days prior to use.

Absolute ethanol (99.8%, Merck) was used as supplied. Methanol (Merck) was distilled over magnesium^[2] prior to use in kinetic analysis. Benzene[§] (BDA Chemicals) was dried using sodium[†] metal prior to use. Acetonitrile (BDH, $\geq 99.5\%$) was used without any further purification. All other chemicals were purchased from Aldrich and were used without further purification.

[§] Benzene is a suspected carcinogen and therefore necessary precautions must be taken when handling it.

[†] Sodium is highly flammable and must be handled with care.

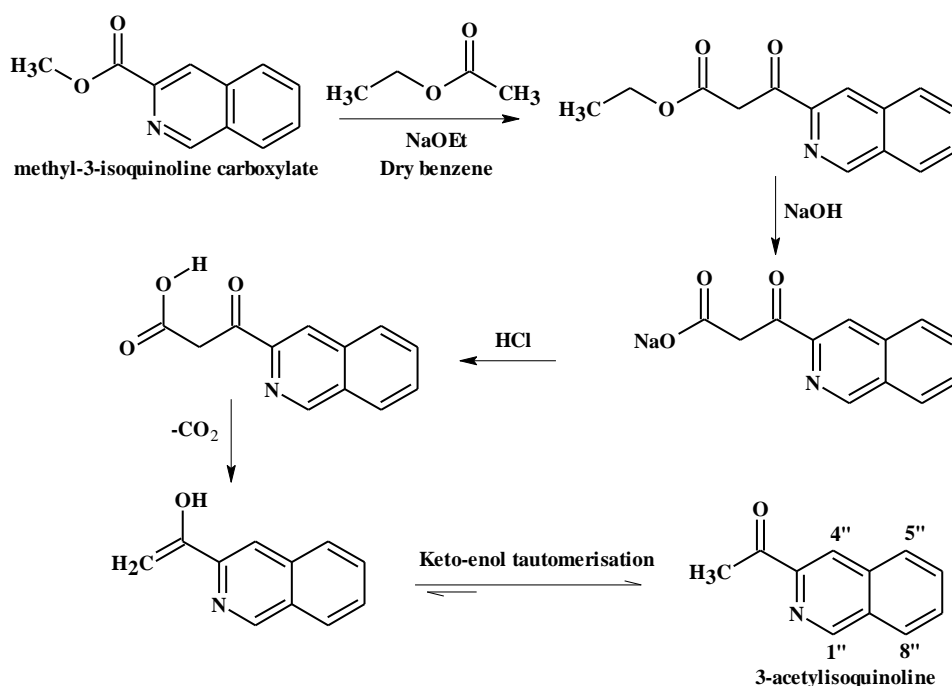
4.2. Synthesis

The platinum complex $[\text{Pt}\{4'-(o\text{-tolyl})-2,2':6',2''\text{-terpyridine}\}\text{Cl}]\text{CF}_3\text{SO}_3$ (**Pt3**) has been previously synthesised as reported in the literature^[3-5] and was donated by Summerton, Gertenbach and co-workers^[3] (Solid State Structure and Photophysical Properties of Polypyridyl Complexes). The platinum complex, $[\text{Pt}\{2-(2'\text{-pyridyl})-1,10\text{-phenanthroline}\}\text{Cl}]$, (**Pt2**) was donated by McMillin and co-workers^[6] (from the University of Purdue, West Lafayette, Indiana). The novel platinum complex, $[\text{Pt}\{4-(o\text{-tolyl})-6-(3''\text{-isoquinoyl})-2,2'\text{-bipyridine}\}\text{Cl}]\text{SbF}_6$ (**Pt4**) was synthesised and characterised. Reactions performed in the synthesis of (**Pt4**) were all carried out under nitrogen except the synthesis of 1-(3'-isoquinoyl)-3-(*o*-tolyl)-prop-2-en-1-one (Section 4.2.1.2).

4.2.1. Synthesis of the Ligand Precursors and the Polypyridyl Ligand

The precursor 3-acetylisquinoline was prepared according to literature.^[7] The precursor, 1-(3'-isoquinoyl)-3-(*o*-tolyl)-prop-2-en-1-one^[3] and the ligand, 4-(*o*-tolyl)-6-(3''-isoquinoyl)-2,2'-bipyridine were synthesised *via* a slight modification of the literature methods. ^[3, 4, 8, 9]

4.2.1.1. Synthesis of 3-acetylisquinoline

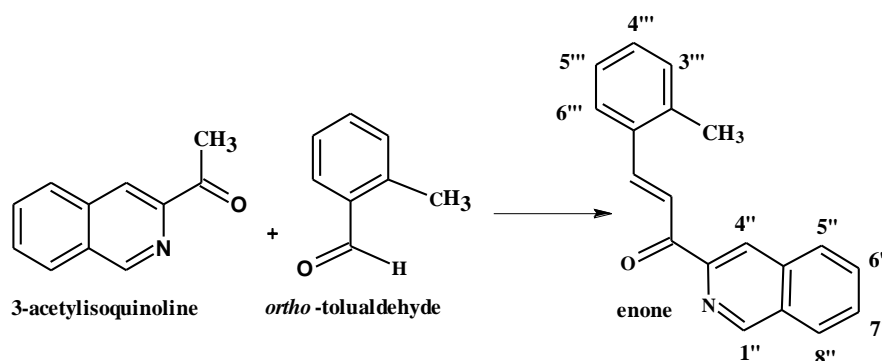


A mixture of methyl 3-isoquinolinecarboxylate (2.01 g, 10.7 mmol) and anhydrous ethylacetate (3.42 ml, 14.0 mmol) in benzene (35.0 ml) was added to sodium ethoxide (0.729 g, 10.7 mmol) in dry benzene (35 ml) with constant stirring. The resulting mixture was refluxed with stirring for 24 hours. The mixture was then cooled and poured into a solution of sodium hydroxide (0.429 g, 10.7 mmol) in water (15 ml). The light yellow solid formed was filtered off and water (40 ml) was added to the filtrate. After decantation of the phases, the benzene layer was washed with water and the combined aqueous layers were extracted with ether (3 x 30 ml). The combined organic layers were evaporated and combined with the light yellow solid. This was then refluxed in hydrochloric acid (32 ml, 4 M) for 2 hours. On cooling the mixture was made basic with sodium carbonate, the organic layer was extracted with ether (3 x 30 ml) and dried over sodium sulphate. Removal of solvent and drying gave 1.20 g of 3-acetylisquinoline.

3-acetylisquinoline

Yield: 1.20 g, 7.05 mmol (66%)
 IR (cm⁻¹): $\nu(\text{CO})$ 1689 cm⁻¹
¹H NMR[†]: 9.21 (1H, s, H^{1''}), 8.50 (1H, s, H^{4''}), 7.99-8.09 (1H, dd, H^{8''}, 6''), 7.73-7.80 (2H, m, H^{5'',7''}), 2.84 (3H, s, CH₃)
¹³C NMR(CDCl₃): 200.24 (1C, s, C=O) 151.94, 147.80, 130.97 (3C, s, quat.C), 130.97-120.33 (6C, s, phenyl CH), 26.65 (1C, s, CH₃)
 Melting point: 88.5 – 89.0 °C

4.2.1.2. Synthesis of 1-(3'-isoquinolyl)-3-(*o*-tolyl)-prop-2-en-1-one



Ortho-tolualdehyde (0.459 g, 3.79 mmol) and 3-acetylisquinoline (0.649 g, 3.79 mmol) were dissolved in absolute ethanol (15 ml) and cooled to 0 °C. Sodium hydroxide (4 ml, 1.0 M) was added dropwise and the reaction mixture stirred at 0 °C for 3 hours. The pale yellow product

[†] Measured in CDCl₃, δ ppm, s = singlet, dd = doublet of doublet, quat = quaternary, m = multiplet

was precipitated with ice. The precipitate was filtered, washed with 50% aqueous ethanol and dried *in vacuo*.

1-(3-isoquinoyl)-3-(*o*-tolyl)-prop-2-en-1-one:

Yield: 0.97 g, 3.55 mmol (94%)

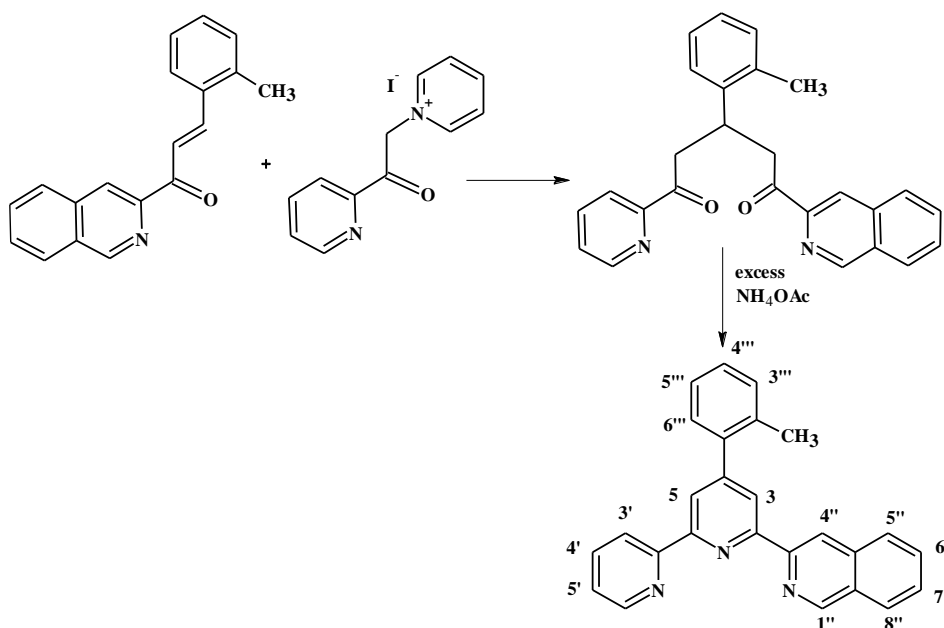
IR (cm⁻¹): $\nu(\text{CO}) = 1664 \text{ cm}^{-1}$, $\nu(\text{C}=\text{C}) = 1592, 1569 \text{ cm}^{-1}$

¹HNMR[†] (CDCl₃): 9.37 (1H, s, H^{1''}), 8.67 (1H, s, H^{4''}), 8.38 (1H, ³J_{HH} 15.78 Hz, CHCO), 8.34 (1H, ³J_{HH} 15.99 Hz, CHAr), 8.09 (2H, m, H^{8''}, 6'''), 7.91 (1H, d, H^{6''}), 7.80 (2H, m, H^{5''}, 7'''), 7.24-7.34 (3H, m, H^{3''}, 4'', 5'''), 2.56 (3H, s, CH₃)

LC/MS: [M + Na] = 296.1049 *m/z*

Melting point: 144.1 -144.8 °C

4.2.1.3. Synthesis of 4-(*o*-tolyl)-6-(3''-isoquinoyl)-2,2'-bipyridine



A mixture of 1-(3-isoquinoyl)-3-(*o*-tolyl)-prop-2-en-1-one (0.892 g, 3.26 mmol), *N*-{1-(2'-pyridyl)-1-oxo-2-ethyl}pyridinium iodide (PPI) (1.06 g, 3.26 mmol) and ammonium acetate (16.2 g, excess) was heated to reflux in absolute ethanol (10 ml) for 70 minutes. On cooling, the resultant precipitate was filtered and washed with 50% aqueous ethanol. The impure product was then carefully washed with ethanol (95%), leaving an off-white solid on

[†] Measured in CDCl₃, δ ppm, s = singlet, d = doublet, m = multiplet

the frit. The product was recrystallised from ethanol (95%) and dried *in vacuo*, the ligand formed as fine pale off-white needle like crystals.

4-(*o*-tolyl)-6-(3''-isoquinoyl)-2,2'-bipyridine

| | |
|---|---|
| Yield: | 0.410 g, 1.10 mmol (34%) |
| IR (KBr cm ⁻¹)‡: | 745(s), 760(vs), 795(vs), 893(vs), 946(m), 991(m), 1052(w), 1070(w), 1110(w), 1135(w), 1271(m), 1327(w), 1396(s), 1442(m), 1474(w), 1543(m), 1567(m), 1579(s), 1605(m), 1624(m) |
| ¹ H NMR (CDCl ₃)†: | 9.37 (1H, s, H ^{1''}), 9.07 (1H, s H ^{4''}), 8.77 (1H, d, H ³), 8.74 (1H, dd, H ⁵), 8.62 (1H, d, H ^{3'}), 8.49 (1H, d, H ^{6'}), 8.08 (2H, t, H ^{8'', 4'}), 7.95 (1H, m, H ^{6''}) 7.77 (1H, m, H ^{5''}), 7.66 (1H, m, H ^{7''}), 7.42 (1H, d, H ^{6'''}), 7.38 (1H, m, H ^{5'}), 7.33 (3H, m, H ^{3''', 4''', 5''}), 2.40 (3H, s, CH ₃) |
| ¹³ C NMR(CDCl ₃)†: | 156.4-155.1 (3C, s, quat. C's), 152.98 (1C, s, C ¹), 151.98 (1C, s, quat.C), 149.5 (1C, s, quat.C), 149.1 (1C, s, C ^{6'}), 139.8 (1C, s, quat.C), 136.9 (1C, s, C ^{4'}), 135.17-136.9.9 (2C, s, quat.C), 130.6 (1C, s, C ^{7''}), 130.40 (1C, s, phenyl CH), 129.39 (1C, s, C ^{6'''}), 128.8 (1C, s, quat.C), 128.13 (1C, s, phenyl CH), 127.75 (1C, s, C ^{8''}), 127.62 (1C, s, C ^{5''}), 127.64 (1C, s, C ^{5'''}), 127.53 (1C, s, C ^{6'''}), 125.9 (1C, s, phenyl CH), 123.81 (C, s, C ^{5'}), 122.0 (1C, s, C ³), 121.4 (1C, s, C ^{3'}), 121.2 (1C, s, C ^{5'}), 117.8 (1C, s, C ^{4''}), 20.8 (1C, s, CH ₃) |
| Melting point: | 150.2- 150.7 °C |
| LC/MS: | [M + Na] = 396.1476 <i>m/z</i> |
| UV/Vis (nm, MeCN): | 234, 253, 282, 292, 314 (π-π*) |
| <u>Elemental Analysis</u> | |
| Calculated: | % C, 83.6; % H, 5.1; % N, 11.3 |
| Found: | % C, 84.1; % H, 5.2; % N, 11.4 |

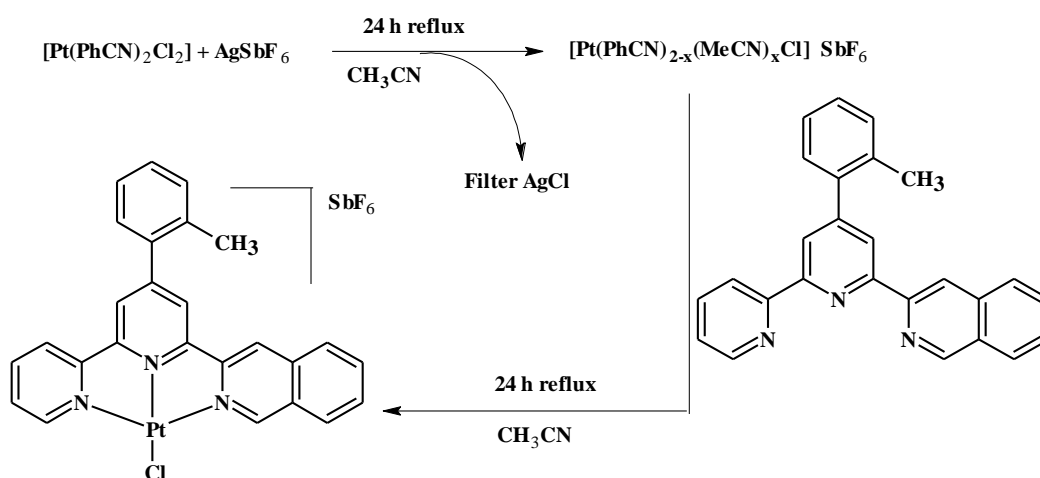
‡ vs = very strong, s = strong, m = medium, w = weak and b = broad.

† Measured in CDCl₃, δ ppm, s = singlet, quat = quaternary, m = multiplet, dd = doublet of doublet

4.2.2. Synthesis of Platinum(II) Complexes

The complex, $[\text{Pt}\{4-(o\text{-tolyl})-6-(3''\text{-isoquinoyl})-2,2'\text{-bipyridine}\}\text{Cl}]\text{SbF}_6$ (**Pt4**) was synthesised using a modification of the method used by Summerton.^[3] The precursor dichloro(1,5-cyclooctadiene)platinum(II)^[10] and the corresponding platinum(II) complex, $[\text{Pt}(\text{terpy})\text{Cl}]\text{Cl}\cdot 2\text{H}_2\text{O}$ (**Pt1**)^[11] (where terpy = 2,2':6',2''-terpyridine) were synthesised according to the literature procedures.

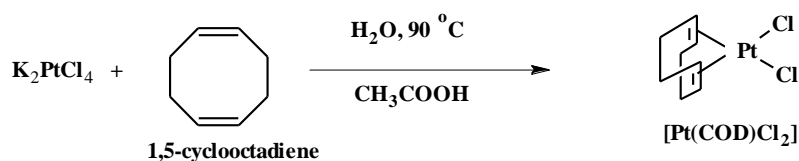
4.2.2.1. Synthesis of $[\text{Pt}\{4-(o\text{-tolyl})-6-(3''\text{-isoquinoyl})-2,2'\text{-bipyridine}\}\text{Cl}]\text{SbF}_6$



The silver salt AgSbF_6 (137 mg, 0.400 mmol) was dissolved in acetonitrile (5 ml) and added to a suspension of $[\text{Pt}(\text{PhCN})_2\text{Cl}_2]$ (198 mg, 0.400 mmol) in acetonitrile (12 ml). The mixture was refluxed overnight under an inert atmosphere and the resultant precipitate of AgCl was removed by filtration using 0.45 μm nylon filter membrane on millipore filtration unit. An equimolar amount of solid 4-(*o*-tolyl)-6-(3''-isoquinoyl)-2,2'-bipyridine (149 mg, 0.400 mmol) was added to the filtrate and the mixture was refluxed for an additional 24 hours. Once the reflux was complete, the mixture was filtered hot and the solvent partially removed under reduced pressure resulting in the precipitation of $[\text{Pt}\{4-(o\text{-tolyl})-6-(3''\text{-isoquinoyl})-2,2'\text{-bipyridine}\}\text{Cl}]\text{SbF}_6$. The product was washed on the frit with copious amounts of diethyl ether and then smaller amounts of cold acetonitrile. A scarlet red powder was obtained.

[Pt{4-(*o*-tolyl)-6-(3''-isoquinoyl)-2,2'-bipyridine}Cl]SbF₆

| | |
|---|--|
| Yield: | 0.32 g, 0.38 mmol (94%) |
| IR (cm ⁻¹) [§] : | $\nu(\text{isoqbipy})^{**} = 698(\text{w}), 727(\text{m}), 760(\text{vs}), 788(\text{s}), 885(\text{w}), 905(\text{w}), 976(\text{s}), 1037(\text{w}), 1161(\text{w}), 1244(\text{w}), 1285(\text{w}), 1388(\text{m}), 1418(\text{mw}), 1448(\text{w}), 1477(\text{mw}), 1556(\text{m}), 1610(\text{s})$ $\nu(\text{SbF}_6) = 656(\text{vs})$ |
| ¹ H NMR (DMSO) ^{††} : | 9.13 (1H, s, H ^{1''}), 9.06 (1H, s, H ^{4''}), 8.66, 8.64 (2H, dd, H ^{3',5'}), 8.48 (2H, m, H ^{3',6'}), 8.17 (2H, m, H ^{4',8''}), 7.93 (1H, dt, H ^{6''}), 7.80 (H, m, H ^{7''}), 8.80 (1H, m, H ^{5''}), 7.95-7.51 (5H, m, H ^{5',3'',4'',5'',6''}) 2.50 (3H, m, CH ₃) |
| ¹³ C NMR(DMSO) ^{**} : | 158.36, 155.39-150.94 (5C, s, quat.C's), 155.13 (1C, s, C ^{1''}), 150.68 (1C, s, C ^{3'}), 142.43 (1C, s, C ^{4'}), 137.68.1 (1C, s, quat.C), 136.10 (1C, s, C ^{6''}), 135.66-135.23 (2C, s, quat.C), 132.18 (1C, s, C ^{7''}), 131.52-127.00 (7C, s, C ^{8'',5'',5',3'',4'',5'',6''}), 125.89 (1C, s, C ^{6'}), 125.59 (1C, s, C ^{4''}), 124.89-124.58 (2C, s, C ^{3',5'}), 20.66 (1C, s, CH ₃) |
| ¹⁹⁵ Pt NMR (DMSO) | -2661.76 |
| LC/MS: | [M ⁺] = 603.0917 <i>m/z</i> |
| Melting point: | Decomposed above 290 °C |
| <u>Elemental Analysis</u> | |
| Calculated: | % C, 37.2; % H, 2.3; % N, 5.0 |
| Found: | % C, 37.4; % H, 2.3; % N, 5.2 |

4.2.2.2. Synthesis of Dichloro(1,5-cyclooctadiene) Platinum(II)^[10]

A filtered aqueous solution (35 ml) of K₂PtCl₄ (2.17 g, 5.23 mmol) was added to a solution of 1,5-cyclooctadiene (2.10 ml, 17 mmol) in glacial acetic acid (35 ml). The resulting mixture

[§] vs = very strong, s = strong, m = medium, mw = medium weak, w = weak and b = broad.

^{**} $\nu(\text{isoqbipy})$ refers to 4-(*o*-tolyl)-6-(3''-isoquinoyl)-2,2'-bipyridine ligand

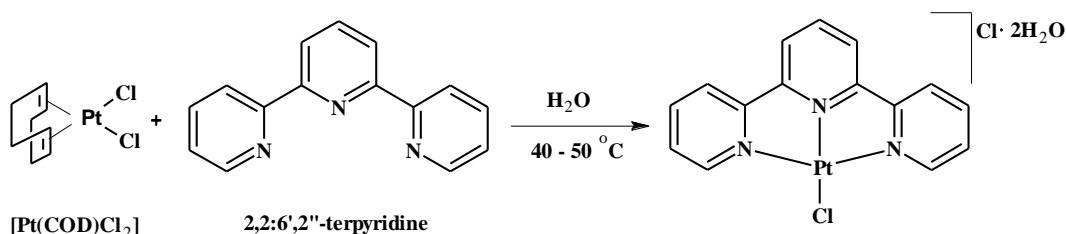
^{††} Measured in DMSO, δ ppm, s = singlet, quat = quaternary, m = multiplet, dt = doublets of triplets, dd = doublet of doublet

was stirred vigorously and heated to 90 °C for 30 minutes. A pale-yellow solution was formed. Pale-yellow crystals of dichloro(1,5-cyclooctadiene)platinum(II) precipitated before 30 minutes. After 30 minutes, the solution was cooled and solvent removed under reduced pressure to a final volume of approximately 10 ml. The crystals were filtered using 0.45 µm nylon filter membrane on millipore filtration unit, washed with copious amount of water, ethanol, and diethyl ether and dried in the oven at 100 °C for 1 hour.

Dichloro(1,5-cyclooctadiene)platinum(II)

Yield: 1.71 g, 4.57 mmol (87%)

4.2.2.3. Synthesis of 2,2':6',2''-terpyridine Platinum(II) (Pt1)^[11]



To a stirred solution of [Pt(COD)Cl₂] (500 mg, 1.34 mmol) in water (30 ml), 2,2':6',2''-terpyridine (313 mg, 1.34 mmol) was added. The mixture was stirred and warmed to between 45-50 °C for 15 minutes. The clear orange-red solution obtained was cooled to room temperature and filtered to remove any unreacted [Pt(COD)Cl₂]. Removal of solvent under reduced pressure gave an orange-red solid, [Pt(terpy)Cl]Cl·2H₂O, (**Pt1**). The product was collected, washed thoroughly with diethyl ether and air dried. Recrystallisation of the dried solid in a hot methanol/water mixture (50: 50) gave orange needle like crystals of the titled compound. The crystals were filtered using 0.45 µm nylon filter membrane on millipore filtration unit, washed with diethyl ether and air dried.

[Pt(terpy)Cl]Cl·2H₂O (Pt1):

Yield: 0.64 g, 1.19 mmol (89%)

IR (cm⁻¹)[§] ν(terpy) = 777(vs), 1030(w), 1118(w), 1246(w), 1316(w), 1399(m),
1451(s), 1475(s), 1605(vs), 3032(m), 3368(b)

Elemental Analysis:

Calculated: % C, 33.7; % H, 2.8; % N, 7.9

Found: % C, 33.9; % H, 2.8; % N, 7.8

[§] very strong, s= strong, m= medium, w= weak and b= broad.

4.2.2.4. Synthesis of [Pt{4'-(*o*-tolyl)terpy}MIm](CF₃SO₃)₂

The substituted complex of **Pt3** with imidazole was synthesised by a modification of the method employed by Pitteri and Bortoluzzi.^[12]

AgCF₃SO₃ (0.0246 g, 0.0959 mmol) was added under stirring in the dark, to a warm (40 °C) solution of **Pt3** (0.0674 g, 0.0959 mmol) in acetonitrile (5 ml). After 10 minutes the AgCl formed was removed by filtration using 0.45 µm nylon filter membrane on millipore filtration unit. To the resulting filtrate, 1-methylimidazole (0.0079 g, 0.0959 mmol) was added and stirred for 5 minutes at room temperature and diethyl ether (20 ml) was added to the solution. The precipitate was then filtered off and air dried. Yield: 0.0807 g, 0.0898 mmol, (95%). Crystals for X-ray determination were grown by dissolving the precipitate in nitromethane (1 ml) and passing diethyl ether vapour over it *via* vapour diffusion technique. Purple brown square shaped crystals suitable for X-ray determination were obtained after three days.

4.3. Single Crystal X-ray Diffraction Studies

The instrument used for the collection of the X-ray intensity data was an Oxford Diffraction Xcalibur 2 CCD 4-circle diffractometer linked to an Oxford Cryostat System. The room temperature data collection was done at 295 K. For the low temperature data collection at 100 K, the crystal was cooled under a nitrogen vapour stream. The data were collected using MoK α radiation (2.0 kW, 0.71073 Å), 0.75° frame widths, 20 s exposures at a crystal-to-detector distance of 50 mm, and omega 2-theta scans of -54.00 to 60.60° or -54.00 to 60.75° at $\theta = 30^\circ$. The data were reduced with the program CrysAlis RED^[13] (Version 170) using outlier rejection, scan speed scaling, as well as standard Lorentz and polarization correction factors. The structures were solved with SHELX-97^[14] using direct and Patterson methods with all non-hydrogen atoms refined anisotropically with SHELX-97^[14] (using WinGX^[15] as an interface). Hydrogen atoms were geometrically constrained (C—H = 1.05 Å) using the appropriate AFIX command and refined isotropically with U_{iso} fixed at 1.20 times the equivalent isotropic temperature factor for a parent sp² carbon atom, and 1.5 times for a parent sp³ carbon atom. Lattice constants, structure refinement details and final discrepancy indices for 4-(*o*-tolyl)-6-(3''-isoquinoly)-2,2'-bipyridine and [Pt{4'-(*o*-tolyl)-2,2':6',2''-terpyridine}MIm](CF₃SO₃)₂ (**Pt3-MIm**) (where MIm = 1-methylimidazole) are given in

Table 4.1. Plots were obtained with the program ORTEP-3 for Windows Version 2.02 (L. Farrugia, University of Glasgow, 2008).

Supplementary Data Available. The crystallographic data for both single crystal structure determinations are available in CIF format on the CD attached to the inside back cover of the thesis. Each CIF file has a partner CHECKCIF file that shows the results of the basic structural check applied by the PLATON^[16] program on the website of the International Union of Crystallography.^[17]

4.3.1. Crystal Structure of 4-(*o*-tolyl)-6-(3'-isoquinoyl)-2,2'-bipyridine Ligand

Crystals for X-ray determination were grown by slow evaporation of the ligand in 95% ethanol. Off-white needle-like crystals were isolated after four days. The crystal structure is given in *Figure 4.1*.

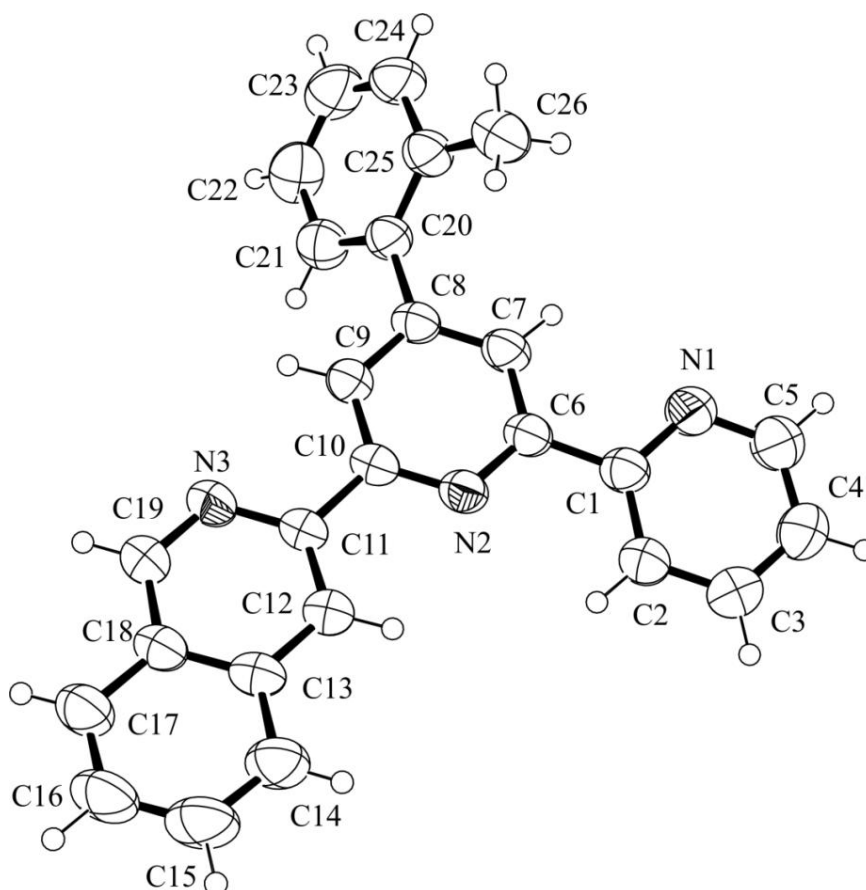


Figure 4.1 Perspective view showing the molecular geometry and atom numbering scheme for the 4-(*o*-tolyl)-6-(3'-isoquinoyl)-2,2'-bipyridine ligand. Non-H atoms are drawn as 50% thermal ellipsoids and the H atoms as spheres of arbitrary radius.

The terminal pyridine and isoquinoline ring systems adopt a *trans-trans* conformation about the interannular bonds C1—C6 and C10—C11 respectively. This conformation has been reported for the 2,2':6',2''-terpyridine^[18] and 4'-(phenyl)-2,2':6',2''-terpyridine^[19] ligands as well. The N2—C10—C11—N3 torsion angle is only 2.5° indicating that the isoquinoline moiety is essentially co-planar with the central pyridine ring. However, the N1—C1—C6—N2 torsion angle is quite large at 9.5° indicating some out-of-plane twisting of the outer pyridine ring. This is presumably due to crystal packing effects as on π -delocalisation grounds one would expect the entire bipyridyl-isoquinoyl moiety to be planar. Of particular interest is the C7—C8—C20—C25 torsion angle since this has been shown to be important in determining the crystal structures of platinum complexes of the 4'-(*o*-tolyl)terpy ligand.^[4] The value is 51.7°, showing a large twist of the *o*-tolyl group about the C8—C20 interannular bond *i.e.* the *o*-tolyl group twists out of the plane of the central pyridine ring by a large amount. This is to minimise steric repulsion between the methyl group and the hydrogen atom attached to C7. There is no reported crystal structure determination of the related 4'-(*o*-tolyl)terpy ligand. However, the out-of-plane twist of the *o*-tolyl group in the [Pt{4'-(*o*-tolyl)terpy}Cl]SbF₆ complex has been shown to be 64.4°^[4] In the next section we show that the angle of twist in the [Pt{4'-(*o*-tolyl)-2,2':6',2''-terpyridine}MIm](CF₃SO₃)₂ complex is 47.0° Clearly out-of-plane twisting is inevitable but the exact value of the torsion angle will depend on the crystal packing forces. Remaining bond lengths and angles are all normal.

4.3.2. Crystal Structure of [Pt{4'-(*o*-tolyl)terpy}MIm](CF₃SO₃)₂

The X-ray crystal structure obtained for the substituted complex is shown in *Figure 4.2*.

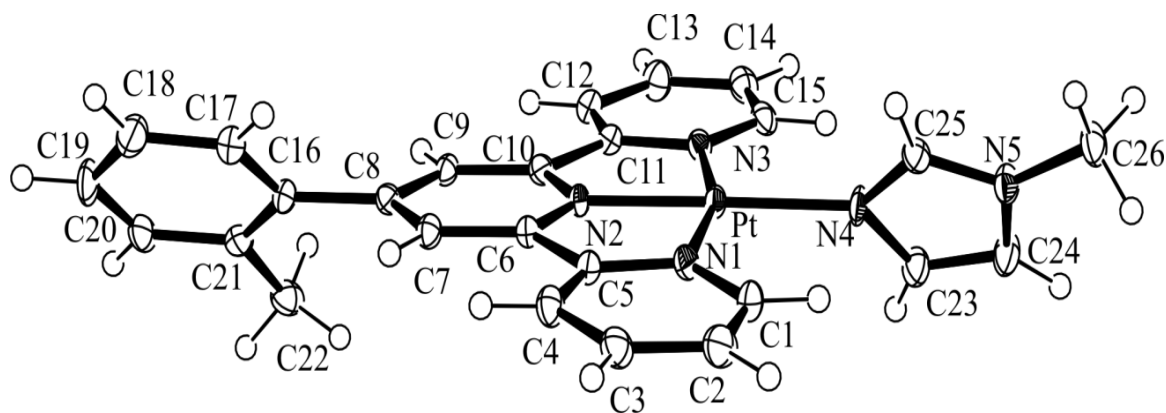


Figure 4.2 Perspective view of the dication in [Pt{4'-(*o*-tolyl)-2,2':6',2''-terpyridine}MIm](CF₃SO₃)₂ showing the molecular geometry and atom numbering scheme. Non-H atoms are drawn as 50% thermal ellipsoids and the H atoms as spheres of arbitrary radius.

Figure 4.2 gives a perspective view of the dication as well as the atom numbering scheme for the X-ray crystal structure of $[\text{Pt}\{4'-(o\text{-tolyl})\text{-}2,2':6',2''\text{-terpyridine}\}\text{MIm}](\text{CF}_3\text{SO}_3)_2$. Selected interatomic distances and angles are given in Table 4.2. The coordination geometry of the platinum centre deviates from square planar as is evident in the N1—Pt—N2 and N2—Pt—N3 bond angles of $80.9(1)^\circ$ and $81.1(1)$ respectively, as well as by a *trans* N1—Pt—N3 bite angle of $162.1(1)^\circ$, much smaller than the ideal value of 180° . This irregular square planar geometry is characteristic of terpyridyl platinum complexes and is imposed due to the geometric constraints of the tridentate ligand.^[4, 20-23] Also characteristic of such complexes is that the Pt—N2 (bridgehead N) bond length of $1.945(3)$ Å is significantly shorter than the Pt to the two outer nitrogen distances of $2.023(4)$ (Pt—N1) and $2.033(3)$ Å (Pt—N3) respectively.^[4, 20, 21] The terpyridyl moiety is essentially planar with similar bond lengths and angles to those reported for other related complexes.^[4]

As expected, the *o*-tolyl group is twisted about the C8—C16 interannular bond, as reflected in a C7—C8—C16—C21 torsion angle of 47° *i.e.*, the *o*-tolyl group twists out of the plane of the central pyridine ring. In the closely related complex, $[\text{Pt}\{4'-(o\text{-tolyl})\text{terpy}\}\text{Cl}]\text{SbF}_6$ the corresponding angle is 65.2 .^[4] This out of plane twist is due to the bulky nature of the methyl group causing a large rotation about the interannular bond in order to minimise steric repulsions between the hydrogens of the methyl group and the hydrogen attached to C7 (Figure 4.2).

Of particular relevance to this work is that the crystal structure determination confirms that the methylimidazole ligand (the nucleophile in the kinetic studies) is bonded to the platinum centre in its fourth coordination site. As expected, coordination is through the lone pair on the imine nitrogen: the Pt—N4 distance of $2.031(3)$ Å is very similar to the Pt—N1 and Pt—N3 (outer N) distances of the terpy ligand and fits within the range of Pt—N distances reported for platinum(II) complexes of the methylimidazole ligand, in particular $[\text{Pt}(\text{terpy})\text{MIm}]^+$.^[21] Notable here is the large twist of the imidazole ring out of the plane of the terpy moiety; this twist is measured by a N1—Pt—N4—C23 torsion angle of 60° . Unlike the *4'*-*o*-tolyl group, there is no *ortho* substituent on the imidazole ring. However, there would be steric repulsions between the hydrogens (H1 and H15) attached to C1 and C15 and the hydrogens attached to C23 and C25 (H23 and H25) were the imidazole group to be coplanar with the terpy moiety: see Figure 4.2 and note that the $\text{H1}\cdots\text{H23}$ and $\text{H15}\cdots\text{H25}$ non-bonded contact distances of ~ 2.7 Å are close to the sum of the van der Waals radii for two hydrogen atoms of 2.4 Å.^[24] We conclude the discussion of the structure of the dication with the following interesting observation. The *direction* of the out of plane twists of the *o*-tolyl and imidazole groups is the same, as reflected in a dihedral angle between the planes

defined by the phenyl group and the imidazole group of only 10°. Presumably this is due to crystal packing effects, since consideration of the isolated dication would not necessarily lead to the same result. Finally, note that the dication is chiral: though there is no chiral centre as such, the out of plane twists of the *o*-tolyl and imidazole groups ensure its chirality. In fact, the chloride ion precursor, [Pt{4'-(*o*-tolyl)terpy}Cl]⁺, must also be chiral because of the out of plane twist of the *o*-tolyl moiety.^[4] This could have implications for the reactivity of the complex, in particular with respect to substitution by chiral nucleophiles.

Table 4.1 Crystal structure, data collection and refinement details for 4-(*o*-tolyl)-6-(3''-isoquinolyl)-2,2'-bipyridine (ligand) and [Pt{4'-(*o*-tolyl) terpy}MIm](CF₃SO₃)₂ (complex)

| Compound | ligand | complex |
|--|--|---|
| Empirical formula | C ₂₆ H ₁₉ N ₃ | C ₂₈ H ₂₃ F ₆ N ₅ O ₆ PtS ₂ |
| <i>M_r</i> | 373.46 | 898.72 |
| Crystal size/ mm | 0.05 × 0.20 × 0.40 | 0.20 × 0.20 × 0.25 |
| <i>T</i> / K | 293 | 100 |
| λ/ Å | 0.71073 | 0.71073 |
| Crystal system | monoclinic | triclinic |
| Space group | <i>P</i> 2 ₁ / <i>n</i> | <i>P</i> -1 |
| <i>a</i> / Å | 15.183(6) | 10.318(4) |
| <i>b</i> / Å | 8.530(4) | 12.100(5) |
| <i>c</i> / Å | 15.976(6) | 12.915(6) |
| α/ ° | 90 | 105.648(6) |
| β/ ° | 107.281(5) | 98.516(5) |
| γ/ ° | 90 | 92.891(4) |
| <i>V</i> / Å ³ | 1976(2) | 1529(1) |
| <i>Z</i> | 4 | 2 |
| <i>D_c</i> /g cm ⁻³ | 1.256 | 1.953 |
| μ/ mm ⁻¹ | 0.075 | 4.815 |
| <i>F</i> (000) | 784 | 876 |
| θ Range/ ° | 2-32 | 2-32 |
| Reflections collected (independent) | 14057 (3900) | 15971 (9498) |
| observed [<i>I</i> > 2σ(<i>I</i>)] | 2311 | 8024 |
| <i>R</i> _{int} | 0.0329 | 0.0409 |
| No. refined parameters (restraints) | 263 (0) | 435 (0) |
| Final <i>R</i> ₁ [<i>I</i> > 2σ(<i>I</i>)] | 0.0489 | 0.0391 |
| Final <i>wR</i> ₂ (all data) | 0.1438 | 0.0987 |
| Max, Min Δρ/ e Å ⁻³ | 0.15, -0.19 | 1.78, -3.06 |

Table 4.2 Selected bond lengths and angles for [Pt{4'-(*o*-tolyl)terpy}MIm](CF₃SO₃)₂

| Distances (Å) | | Angles (°) | |
|---------------|----------|------------|----------|
| Pt—N1 | 2.023(4) | N1—Pt—N2 | 80.9(1) |
| Pt—N2 | 1.945(3) | N1—Pt—N3 | 162.1(1) |
| Pt—N3 | 2.033(4) | N1—Pt—N4 | 98.7(1) |
| Pt—N4 | 2.031(4) | N2—Pt—N3 | 81.1(1) |
| N4—C23 | 1.390(7) | N2—Pt—N4 | 179.1(2) |
| N4—C25 | 1.340(6) | N3—Pt—N4 | 99.2(2) |
| N5—C24 | 1.365(8) | Pt—N4—C23 | 126.8(4) |
| N5—C25 | 1.330(7) | Pt—N4—C25 | 126.5(5) |
| C23—C24 | 1.361(9) | | |

4.4. Instrumentation and Physical Measurements

4.4.1. Characterisation

¹H NMR and ¹³C NMR were recorded on either a Bruker Avanced 400 or 500 MHz spectrometer, at 298.15 K using Si(CH₃)₄ as the reference for the chemical shifts. ¹⁹⁵Pt NMR were done on a 500 MHz spectrometer (¹⁹⁵Pt, 107.5 MHz) chemical shifts externally referenced to K₂[PtCl₆]. Kinetic analyses were studied either on Varian Cary 100 Bio UV/Visible spectrophotometer with an attached Varian Peltier temperature-controller in it with an online kinetic applications or an Applier Photophysics SX.18MV (v 4.33) stopped-flow reaction analyser coupled with an online data acquisition system. Infrared (IR) spectra were determined using KBr discs on a Perkin Elmer Spectrum One FTIR spectrophotometer. Mass spectra were obtained on a Hewlett Packard HP5988A GC-MS using electron impact (IE) negative ionisation mode. Elemental analyses were performed at the Institute for Inorganic Chemistry, University of Erlangen-Nürnberg, Egerlandstr. 1, Erlangen, Germany. Melting points were done on a Stuart melting point apparatus SMP3 with a slope of 1 °C/min. Quartz cuvettes (2 x 4, 37 mm light path) were used in all kinetic investigations done on the UV/Visible absorption spectrophotometer.

4.4.2. Computational Modelling

Computational modelling for the complexes **(Pt1)**, **(Pt2)**, **(Pt3)**, and **(Pt4)** were done as cations for the chloro complexes and as dications for the azole substituted complexes using the software package Spartan® '04 for Windows®.^[25, 26] using the B3LYP^[27], density functional method (DFT)^[28, 29] and the LACVP+** (Los Alamos Core Valence Potentials)^[30] pseudo potential basis set. B3LYP relates to the hybrid functional Becke's three parameter formulation^[27] which has been proven to be better to traditional functional. The LACVP basis set employs effective core potentials for K-Cu, Pb-Ag, Cs-La and Hf-Au, whereas Pople's 6-31G** basis set describes second and third rows s- and p-block elements.^[31, 32]

4.5. Kinetic Analyses

All kinetic measurements were performed under *pseudo*-first-order conditions using at least 10-fold excess of the nucleophile. The wavelengths chosen for the kinetic investigations were pre-determined using UV/Visible absorption spectra obtained from Varian Cary 100 Bio UV/Visible spectrophotometer. Substitution reactions which took less than sixteen minutes to go to completion were studied on an Applied Photophysics SX.18MV (v4.33) stopped-flow system coupled with an online data acquisition system, otherwise UV/Visible spectrophotometer was used. All measurements were carried out in a thermostated environment to within ± 0.1 °C. All data were graphically analysed using a graphical analysis software package, Origin 5.0®.^[33]

The electrolyte for the nucleophiles and the platinum complexes were prepared by dissolving a known amount of lithium trifluoromethanesulfonate (LiCF_3SO_3 , 7.02 g, 0.045 mol) and NaCl (0.29 g, 0.005 mol) in freshly distilled methanol or HPLC grade methanol (500 ml) to afford a solution of concentration 0.10 M (0.09 M LiCF_3SO_3 and 0.01 M NaCl). Lithium trifluoromethanesulfonate was used as the anion since the triflate anion does not coordinate to platinum complexes.^[34] Sodium chloride was used to prevent spontaneous solvolysis.

4.5.1. Preparation of Platinum Complexes for Kinetic Analyses

Solutions of the metal complexes were prepared by dissolving a known amount of the platinum complex in methanol solution of constant ionic strength of 0.10 M ($I = 0.1$ M, $\text{LiCF}_3\text{SO}_3 + \text{NaCl}$). Solution of **(Pt3)** was prepared by dissolving a known amount of platinum complex in methanol solution to give a platinum concentration of 5.00×10^{-5} M for **Pz**, **Im**, **MIm**, **DMIm** and **Tz** before mixing. The concentration of **(Pt4)** was 5.00×10^{-5} M for the reactions of **Pz**, **MIm**, **DMIm** and **Tz** and 4.95×10^{-5} for the reactions of **Im** before mixing. The concentrations of **Pt1** and **Pt2** solutions for the substitution reactions were 3.01×10^{-5} M before mixing.

4.5.2. Preparation of Nucleophile Solutions for Kinetic Analysis

The solutions of nucleophiles, *viz.* **Pz**, **Im**, **MIm**, **DMIm** and **Tz** were prepared by dissolving a known amount of the required nucleophile in 100 ml methanol solution of fixed ionic strength ($I = 0.1$ M, (0.09 M $\text{LiCF}_3\text{SO}_3 + 0.01$ M NaCl)) to afford a concentration of *ca.* 50 times greater than that of the metal complex. The other nucleophile solutions were prepared by subsequent dilutions of the same stock solution to afford a series of standards of 10, 20, 30 and 40 times that of the platinum complex.

4.5.3. Preliminary Kinetic Investigations

The reaction time and the wavelength for the kinetic studies was determined using UV/Visible spectroscopy. The instrument lamps, *i.e.* UV (D_2) lamp and a visible lamp (tungsten halogen) were allowed to warm up for an hour prior to use. The two compartments of tandem quartz cuvettes were filled with equal volumes of nucleophile and platinum complex solutions with caution taken to prevent premature mixing of the solutions. The solutions were allowed to equilibrate at 298.15 K for about ten minutes. After an initial scanning over a range of 200-800 nm, the solutions were mixed thoroughly and the second spectrum was obtained at subsequent scans recorded at three minute intervals for the first 20 minutes followed by every five minutes until no further change in absorption was observed in the spectral range. Kinetic investigations were done using the information from

the UV scanning. The wavelength at which the greatest absorbance change with no steep tangent was used for the subsequent kinetic analyses. Reactions which take less than sixteen minutes to complete were studied using stopped-flow technique. Reactions of **Pt2** with **MIm** were done on stopped-flow except at 288.15 K and both 10 and 20 fold at 293.15 K and 298.15 K. All the reactions of **Pt1**, **Pt3** and **Pt4** were studied on the UV/Visible spectrophotometer.

4.5.4. Kinetic Measurements

All reactions were done under *pseudo* first-order conditions with at least 10 fold excess of nucleophiles. As mentioned before, the lamps of the UV/Visible spectrophotometer were first warmed up and allowed to stabilise at the required temperature prior to kinetic measurements. The instrument was then zeroed at the required wavelength using the methanol solution ($I = 0.1$ M, $\text{LiCF}_3\text{SO}_3 + \text{NaCl}$). The tandem cuvettes were filled with the respective solutions of the platinum complex and the nucleophile and equilibrated at the required temperature for ten minutes. After an initial absorbance measurement the two solutions were quickly mixed and the substitution reaction was analysed by measuring the change in absorbance over time until no change in absorbance was observed. All kinetic substitutions investigated on UV/Visible spectrophotometry were done in duplicate.

The reactions which took less than sixteen minutes to go to completion were studied using stopped-flow technique (substitution reactions of **Pt2** with **MIm**). The Xenon Arc Lamp (150 W) of the instrument was first allowed to warmed up for about an hour prior to use. The reaction chamber of the instrument was thoroughly rinsed with ultra pure water and then with methanol solution ($I = 0.1$ M, $\text{LiCF}_3\text{SO}_3 + \text{NaCl}$). After rinsing, the instrument was equilibrated at 298.15 K for 10 minutes and then zeroed using the methanol solution at the selected wavelength for the kinetic analysis. The sample syringes were then rinsed with a small amount of the relevant solutions (either the platinum complex solution or the nucleophile solution) and filled with the respective solutions of either the metal complex or the nucleophile. The solutions were then equilibrated to the required temperature for about ten minutes. Equal volumes of the two solutions were then injected into the reaction chamber under nitrogen pressure of 800 kPa. The change in absorbance for the nucleophile substitution reaction was then monitored spectroscopically. After determining the reaction time, the consecutive measurements were then carried out automatically. Each k_{obs} value

obtained from the stopped-flow represent an average of seven to eight values (k_{obs} values given in *Appendix B*).

All the kinetic substitution reactions (studied both on UV/Visible spectrophotometry and stopped-flow technique) were fitted to first-order exponential decay function to generate the observed *pseudo*-first-order rate constants, (k_{obs}), using *Equation 4.1*^[35] at all concentrations and the temperatures.

$$A_t = A_0 + (A_0 - A_\infty) \text{expt}(-k_{\text{obs}}t) \quad (4.1)$$

where A_0 , A_t and A_∞ represent the absorbance of the reaction mixture initially, at the time, t and at the end of the reaction respectively.

The observed rate constant, k_{obs} , for the nucleophiles of different concentrations were determined by the same manner. The observed rate constants are given in the *Appendix B* (*Table B.2- Table B.9*). The second-order rate constant, k_2 and k_{-2} for the reactions of the platinum complexes with the nucleophiles were obtained from the slopes and the intercepts of the graphs of k_{obs} versus the concentration of the nucleophile (*Equation 3.66*)^[35] drawn by using the graphical analysis software package, Origin 5.0[®].^[33]

$$k_{\text{obs}} = k_2[\text{Nu}]_0 + k_{-2} \quad (3.66)$$

The temperature dependent studies were conducted in a similar manner with all the concentrations of the nucleophiles. The temperature dependent studies were done at five different temperatures within the range 15 - 40 °C in 5 °C intervals since the concentration dependence studies showed a back reaction except for **Pt1**, **Pt3** and **Pt4** with **DMIm**, and **Pz** and **Tz** with **Pt1** which gave linear fits with no meaningful intercepts for the plots of k_{obs} versus $[\text{Nu}]$ at 298.15 K. Graphs of $\ln(k_2/T)$ versus $1/T$ were then drawn using Origin 5.0[®].^[33] Activation parameters, entropy of activation (ΔS^\ddagger) and enthalpy of activation (ΔH^\ddagger) were then obtained by applying the slopes and the y-intercepts to the Eyring equation (*Equation 3.81*).

$$\ln\left(\frac{k_2}{T}\right) = \frac{-\Delta H^\ddagger}{R} \cdot \frac{1}{T} + \left(23.8 + \frac{\Delta S^\ddagger}{R}\right) \quad (3.81)$$

4.6. References

1. D. Reddy, *PhD Thesis, Tuning the Reactivity of Platinum(II) Complexes*, University of Natal, Pietermaritzburg, South Africa, **2009**, pp. 104, 138-139.
2. D. D. Perrin, W. L. F. Armarego and D. R. Perrin, *Purification of Laboratory Chemicals*, Pergamon, Oxford, **1980**.
3. G. C. Summerton, *PhD Thesis, Solid State Structures and Photophysical Properties of Polypyridyl Complexes of platinum(II)*, University of Natal, Pietermaritzburg, South Africa, **1997**, pp. 23-25,32-33,70-75,153-154.
4. J. S. Field, R. J. Haines, D. R. McMillin and G. C. Summerton, *J. Chem. Soc., Dalton Trans.*, **2002**, 1369.
5. J. S. Field, J. A. Gertenbach, R. J. Haines, L. P. Ledwaba, N. T. Mashapa, D. R. McMillin, O. Q. Munro and G. C. Summerton, *Dalton Trans.*, **2003**, 1176.
6. J. J. Moore, J. J. Nash, P. E. Fanwick and D. R. McMillin, *Inorg. Chem.*, **2002**, *41*, 6387.
7. C. O. Dietrich-Buchecker, P. A. Marnot and J. P. Sauvage, *Tetrahedron Lett.*, **1982**, *23*, 5291.
8. R. Büchner, C. T. Cunningham, J. S. field, R. J. Haines, D. R. McMillin and G. C. Summerton, *J. Chem. Soc., Dalton Trans.*, **1999**, 711.
9. F. Michalec, S. A. Bejune, D. G. Cuttall, G. C. Summerton, J. A. Gertenbach, J. S. Field, R. J. Haines and D. R. McMillin, *Inorg. Chem.*, **2001**, *40*, 2193.
10. J. X. McDermott, J. F. White and G. M. Whitesides, *J. Am. Chem. Soc.*, **1976**, *98*, 6521.
11. G. Annibale, M. Brandolisio and B. Pitteri, *Polyhedron*, **1995**, *14*, 451.
12. Oxford Diffraction Ltd., Abingdon, Oxford OX14 1RL, UK, **2003**.
13. G. M. Sheldrick, SHELXS97 and SHELXL-97/2, programs for crystal structure determination and refinement University of Göttingen, Germany, **1997**.
14. L. J. Farrugia, *J. Appl. Cryst.*, **1999**, *32*, 837.
15. A. L. Spek, PLATON, A multipurpose crystallographic tool; Utrecht University, Utrecht, The Netherlands, **2001**.
16. International Union of Crystallography website: www.iucr.org.
17. C. A. Bessel, R. F. See, D. I. Jameson, M. R. Churchill and K. J. Takeuch, *J. Chem. Soc., Dalton Trans.*, **1992**, 3223.
18. E. C. Constable, A. M. W. Cargill, N. T. Armarodi, V. Balzani and M. Maistric, *Polyhedron*, **1992**, *11*, 2707.
19. B. Pitteri and M. Bortoluzzi, *Polyhedron*, **2006**, *25*, 2698.

20. R. Buchner, C. T. Cunningham, J. S. Field, R. J. Haines, D. R. McMillin and G. C. Summerton, *J. Chem. Soc., Dalton Trans.*, **1999**, 711.
21. J. Müller, E. Freisinger, P. Lax, D. A. Megger and F. Polonius, -A., *Inorg. Chim. Acta*, **2007**, *360*, 255.
22. A. Sengul, *Turk. J. Chem.*, **2004**, *28*, 667.
23. P. Ledwaba, O. Q. Munro and K. Stewart, *Acta Cryst.*, **2009**, *E65*, 0376.
24. F. A. Momany, L. M. Carruthers, R. F. McGuire and H. Scheraga, *J. Phys. Chem.*, **1974**, *78*, 1595.
25. Sparttan '04, Ink., 18401 Von Karman Avenue, Suite 370, Irvine, CA, 92612, USA; Q-Chem, Inc., The Design Centre, Suite 690, 5001 Baum Blvd., Pittsburgh, PA, 15213, USA. **2004**. <http://wavefunction.com/>
26. J. Kong, C. A. White, A. I. Krylov, C. D. Sherrill, R. D. Adamson, T. R. Furlani, M. S. Lee, A. M. Lee, S. R. Gwaltney, T. R. Adams, C. Ochsenfeld, A. T. B. Gilbert, G. S. Kedziora, V. A. Rassolov, D. R. Maurice, N. Nair, Y. Shao, N. A. Besley, P. E. Maslen, J. P. Dombroski, H. Daschel, W. Zhang, P. P. Korambath, J. Baker, E. F. C. Byrd, T. Van Voorhuis, M. Oumi, S. Hirata, C.-P. Hsu, N. Ishikawa, J. Florian, A. Warshel, B. G. Johnson, P. M. W. Gill, M. a. Head-Gordon and J. A. Pople, *J. Computational Chem.*, **2000**, *21*, 1532.
27. A. G. Becke, *J. Chem. Phys.*, **1993**, *98*, 5648.
28. R. A. Friesner, *Chem. Phys. Lett.*, **1985**, *116*, 39.
29. R. A. Friesner, *Ann. Rev. Phys. Chem.*, **1991**, *42*, 341.
30. P. J. Hay and W. R. Wadt, *J. Chem. Phys.*, **1985**, *82*, 299.
31. V. A. Rassolov, J. A. Pople, M. A. a. Ratner and T. L. Windus, *J. Chem. Phys.*, **1998**, *109*, 1223.
32. M. M. Francl, W. J. Pietro, W. J. Hehre, J. S. Binkley, M. S. Gordon, D. J. a. DeFrees and J. A. Pople, *J. Chem. Phys.*, **1982**, *77*, 3654.
33. Microcal™, Origin™ Vresion 5.0, Microcal Software, Inc., One Roundhouse Plaza, Northampton, MA, 01060, USA, **1991-1997**.
34. A. Hofmann, L. Dahlenburg and R. van Eldik, *Inorg. Chem.*, **2003**, *42*, 6528.
35. J. D. Atwood, *Inorganic and Organometallic Reaction Mechanisms*, 2nd Ed., Wiley-VCH Inc, New York, **1997**, p. 43-61.

Chapter 5

Results and Discussion

5.1. Synthesis and Characterisation of the Complexes

The platinum(II) complex, [Pt(terpy)Cl]Cl·2H₂O (where terpy = 2,2':6',2''-terpyridine) (**Pt1**) was synthesized according to literature procedure.^[1] The compound was characterized by using Infrared (IR) and elemental analysis. The characteristic data obtained for the platinum(II) complex is in good agreement with the structural formula and the literature data available.^[2]

The novel platinum(II) complex, [Pt{4-(*o*-tolyl)-6-(3'-isoquinoyl)-2,2'-bipyridine}Cl]SbF₆ (**Pt4**) was synthesised and characterised (*Chapter 4.2*). All the characteristic data obtained are in good agreement with the structural formulae of the intermediates and the final complex. The compound was synthesised by using a slightly modified method of the Kröhnke synthesis.^[3] This was achieved by replacing the 2-acetylpyridine in the first stage of Kröhnke synthesis with 3-acetylisquinoline.

Since 3-acetylisquinoline was not commercially available, the first challenge in this synthesis was to prepare the isoquinoline precursor. The chosen method for the synthesis of this precursor was a method used by Sauvage *et al.*^[4] which made use of 3-acetylisquinoline as an intermediate to synthesise cyclo- and non-cyclometalated ruthenium(II) complexes. This part of the synthesis was carried out under inert conditions.

The first step of this reaction involves a Claisen condensation of the methyl-3-isoquinole carboxylate with sodium ethoxide to produce a β -ketoester. The product was precipitated with sodium hydroxide, followed by acid work-up and subsequent rearrangement. Subsequent removal of carbon dioxide favoured the formation of the desired enol product in a moderately good yield (66%). The characterisations were done using Nuclear Magnetic Resonance (NMR) ¹H NMR, ¹³C NMR and IR. A strong peak, at 1689 cm⁻¹, for the ν (C=O) bond was observed from the IR spectrum of this precursor. The ¹H NMR and ¹³C NMR spectra were recorded in deuterated chloroform and the data are in good agreement with the structural formula of the molecule.

In following with Kröhnke methodology, the 3-acetylisquinoline was reacted with *ortho*-tolualdehyde by Aldol condensation to give the desired 1-(3-isoquinoyl)-3-(*o*-tolyl)-prop-2-en-1-one (Chapter 4.2.1.2). The IR spectrum of the enone exhibits a prominent peak at 1664 cm⁻¹, indicating the presence of the ketone carbonyl (C=O) bond and also, distinctive peaks in the range 1621-1400 cm⁻¹ corresponding to the aromatic alkene (C=C) and (C=N) were also observed. Successful synthesis of the enone was confirmed by the ¹H NMR data which showed a characteristic vicinal coupling constant, J_{HH} 13.49 Hz, for the *trans* alkene.^[5]

The ligand was synthesised in a comparably low yield (34%) and was characterised using ¹H NMR, ¹³C NMR, IR, Liquid Chromatography-Mass Spectroscopy (LC-MS), elemental analysis and X-ray crystallography. The ¹H NMR and ¹³C NMR spectra were recorded in deuterated chloroform. To aid the spectral assignments for the ligand, absolute value COrrrelation Spectroscopy (COSY), Heteronuclear Single Quantum Correlation (HSQC) and Heteronuclear Multiple-Bond Correlation (HMBC) NMR experiments were used. The spectral data obtained is in good agreement with the structural formula of the ligand. Furthermore, the X-ray crystal structure obtained for the ligand indicates that the synthesis of the ligand was successful.

The synthesis of **Pt4** was successful as the characteristic data are in good agreement with the structural formula. From the IR spectrum, a small shift to lower wavenumber (ca. < 15 cm⁻¹) of $\nu(\text{C}=\text{C})$ (aromatic) and $\nu(\text{C}=\text{N})$ bands for the metal complex compared to that of the free ligand indicates the coordination *via* the nitrogen atoms of the ligand. The ¹H NMR and ¹³C NMR for **Pt4** was recorded in deuterated DMSO. The spectral assignments for the metal complex were made with the aid of COSY, HSQC, Nuclear Overhauser Enhancement Spectroscopy (NOESY) or Nuclear Overhauser Effect (NOE) ¹⁵N HMBC.

NOE irradiation at CH₃ produced responses at 7.6 ppm and 8.66 ppm which are due to H³/H⁵ and H^{3''}. In the NOESY spectrum H³ (δ_{H} 8.7 ppm) showed a spatial correlation with H^{4''} (δ_{H} 9.06 ppm, singlet) and a doublet due to H^{3'} and H^{6''} (δ_{H} 8.48 ppm and 7.9 ppm). The NOE effect of H^{4''} gave responses at 8.66 ppm due to H³/H⁵ and 7.80 ppm due to H^{5''}. The NOE effect of H^{1''} gave a response at 8.17 ppm due to H^{8''}. Since selective COSY at 8.5 ppm shows no response at 7.9 ppm, the ¹H NMR signal at 7.9 ppm is not part of the same spin system as bulk protons at 8.5 ppm. Multiplicity at 8.5 suggests two overlapping doublets corresponding to H^{3'}/H^{6'} and H^{5'}.

In the ¹⁵N HMBC spectrum, the nitrogen atoms N1, N2 and N3 (See Figure 5.1) were correlated with the protons around the nitrogen centre. The signals due to H³ and H⁵ were confirmed from ¹⁵N HMBC which showed a signal at 208 ppm (N2). Also from the ¹⁵N HMBC

spectrum the signal at 193 ppm (N1) is connected to the signals at 9.1 ppm and 9.13 ppm due to H^{1'} and H^{4'} respectively. Furthermore, by the signal at 200 ppm (N3) in the ¹⁵N HMBC spectrum confirms the protons, H^{3'}, H^{5'} and H^{6'} which corresponds to 8.47 ppm and 7.6 ppm. The signals due to H^{7''} and H^{6''} are confirmed by 2D-COSY experiments and the signal due to H^{4'} is assigned from 2D COSY and ¹⁵N HMBC. Elimination of the processed protons leave the signals due to H^{4''}, ^{5''}, ^{6''}. The coordination of platinum was confirmed by the presence of a ¹⁹⁵Pt peak at -2661.76 ppm which is in agreement with the chemical shift observed for NMR ¹⁹⁵Pt.^[6]

The four platinum(II) complexes and the nucleophiles studied in this investigation are shown in *Figure 5.1*. The crystal structure for **Pt3** has been published before.^[7, 8] To ensure that the anticipated substitution reactions have taken place, crystals were grown for the substituted complex of **Pt3** with 1-methylimidazole (**MIm**) as the nucleophile. The procedure followed for crystal growth of the substituted complex was a slight modification of the method employed by Pitteri and Bortoluzzi^[9]. X-ray crystal structure and the data are given in *Section 4.3.2*.

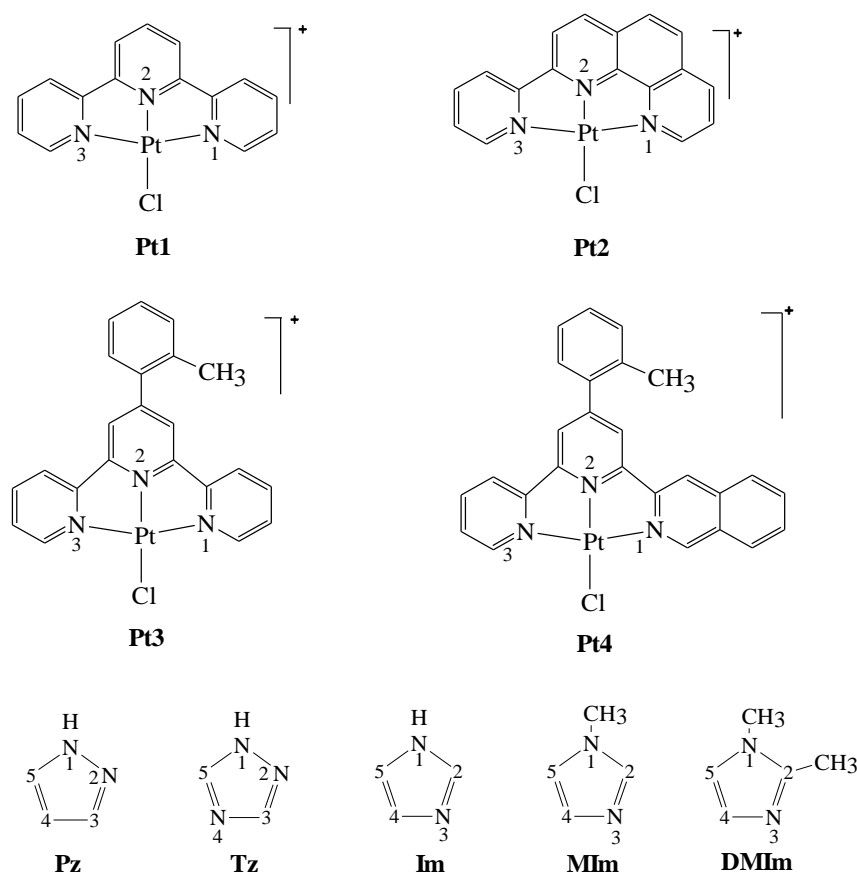
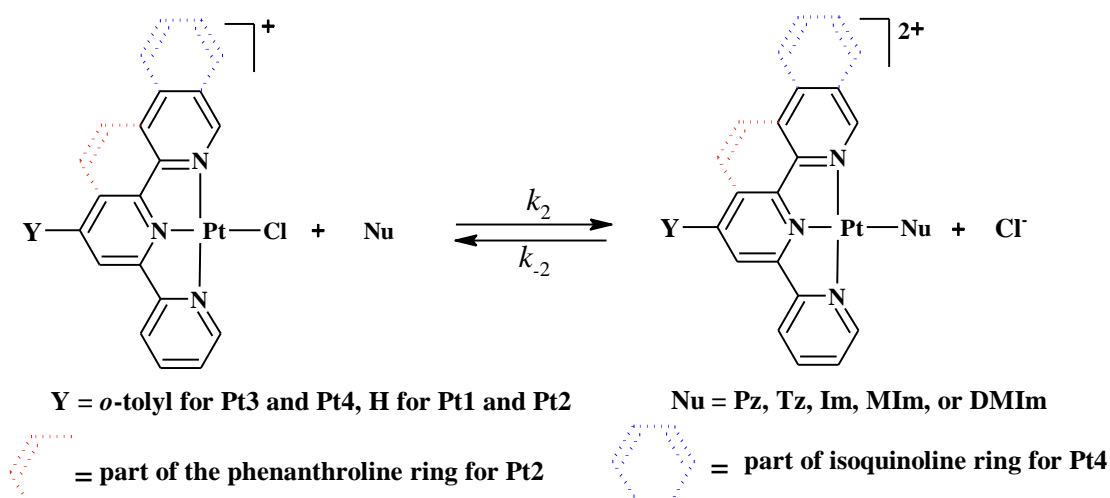


Figure 5.1 Structures of platinum(II) complexes and the nucleophiles used in kinetic investigations. Anions are omitted for simplicity.

5.2. Kinetic Results

Substitution reactions of chloride displacement in square planar platinum(II) complexes (*Reaction 1*) were studied using a series of neutral nitrogen donor nucleophiles (Nu), *i.e.*, pyrazole (**Pz**), triazole (**Tz**), Imidazole (**Im**), 1-methylimidazole (**MIm**) and 1,2-dimethylimidazole (**DMIm**) (*Figure 5.1*) under *pseudo* first-order conditions using UV/Visible spectrophotometry and conventional stopped-flow techniques.

Reaction 1



As already mentioned, a suitable wavelength for the kinetic studies were predetermined using UV/Visible spectrophotometry. A typical spectrum obtained from the UV/Visible spectrophotometry is shown in *Figure 5.2*.

The presence of clear isobestic points in the spectrum indicates that the reactants are being changed to the product(s) at constant ratio.^[10] The observed spectral changes from the UV/Visible spectra indicate presence of a single chemical change and therefore the substitution reactions studied are the replacement of the coordinated chloride by the N-donor nucleophiles.^[9, 11] For each kinetic investigation the wavelength which has the greatest change in absorbance was used in the kinetic analysis.

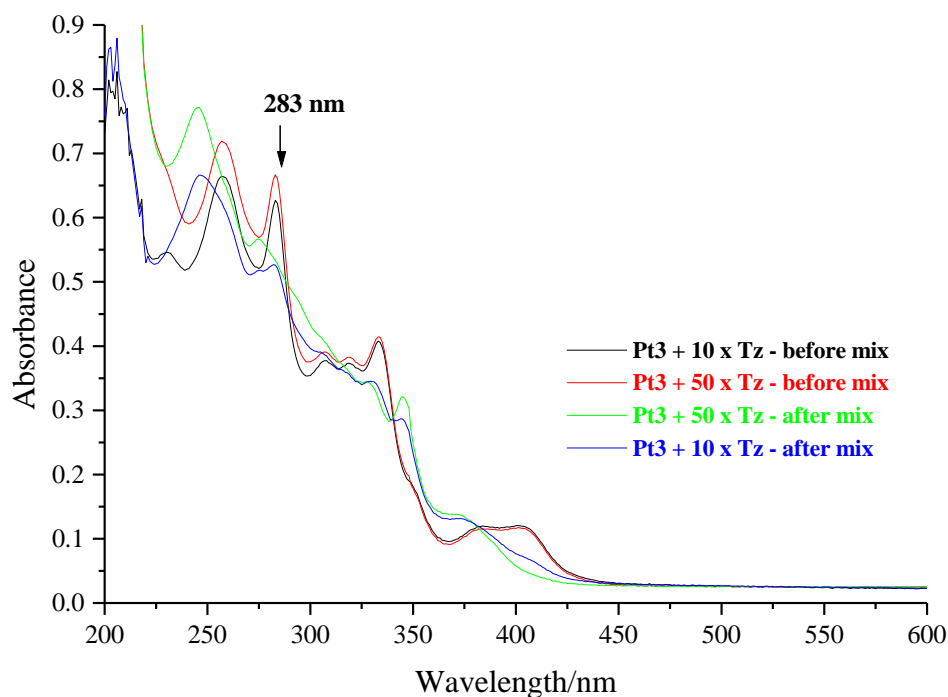


Figure 5.2 Absorbance change for the reactions of Pt3 (2.50×10^{-5} M) with triazole $10 \times 2.50 \times 10^{-5}$ M and $50 \times 2.50 \times 10^{-5}$ M in methanol solution ($I = 0.1$ M, (0.09 M $\text{LiCF}_3\text{SO}_3 + 0.01$ M NaCl)) at 298.15 K.

A typical kinetic trace obtained from the UV/Visible spectrophotometry for the reaction of Pt3 (2.50×10^{-5} M) with triazole (1.25×10^{-3} M) in a solution of ionic strength of 0.1 M (0.09 M $\text{LiCF}_3\text{SO}_3 + 0.01$ M NaCl) at 308.15 K is shown in Figure 5.3.

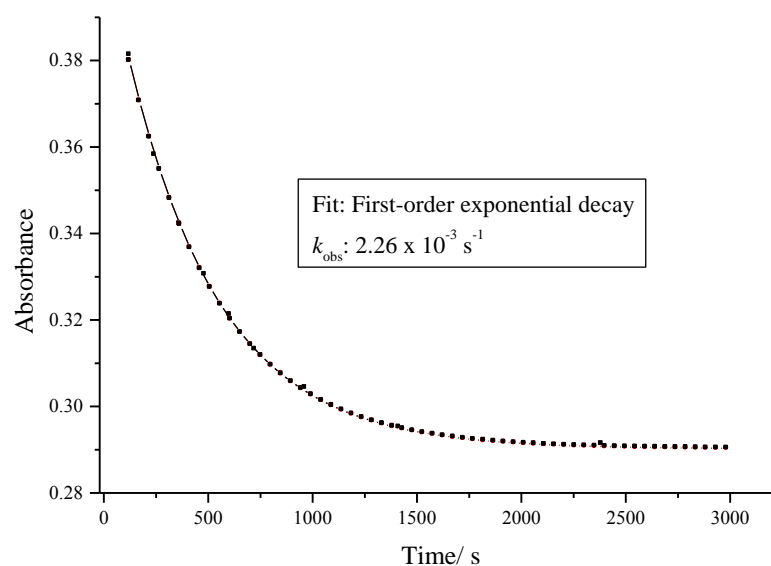


Figure 5.3 Spectrum obtained from Cary UV/Visible spectrophotometer for the reaction of Pt3 (2.50×10^{-5} M) with triazole (1.25×10^{-3} M) in methanol solution ($I = 0.10$ M (0.09 M $\text{LiCF}_3\text{SO}_3 + 0.01$ M NaCl)) at 333 nm at 308.15 K.

The substitution reactions which took less than sixteen minutes to go to completion were studied by using conventional stopped-flow. A typical stopped-flow kinetic trace recorded for the reaction of **Pt2** with 1-methylimidazole is shown in *Figure 5.4*.

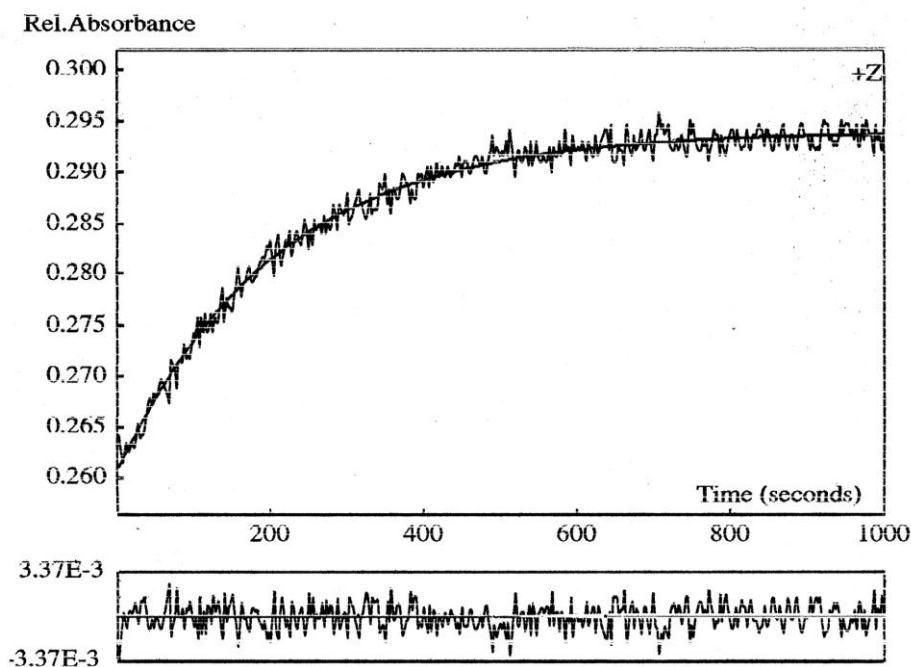


Figure 5.4 First-order exponential fit and residuals (lower part) for the reaction of **Pt2** (1.53×10^{-5} M) with 1-methylimidazole (4.59×10^{-4} M) in methanol solution ($I = 0.10$ M (0.09 M $\text{LiCF}_3\text{SO}_3 + 0.01$ M NaCl)) at 311 nm and 298.15 K.

The *pseudo* first-order rate constants, k_{obs} obtained from the kinetic traces were then plotted against the concentration of the nucleophiles to generate the second-order rate constants. Representative plots obtained for **Pt1** are shown in *Figures 5.5*.

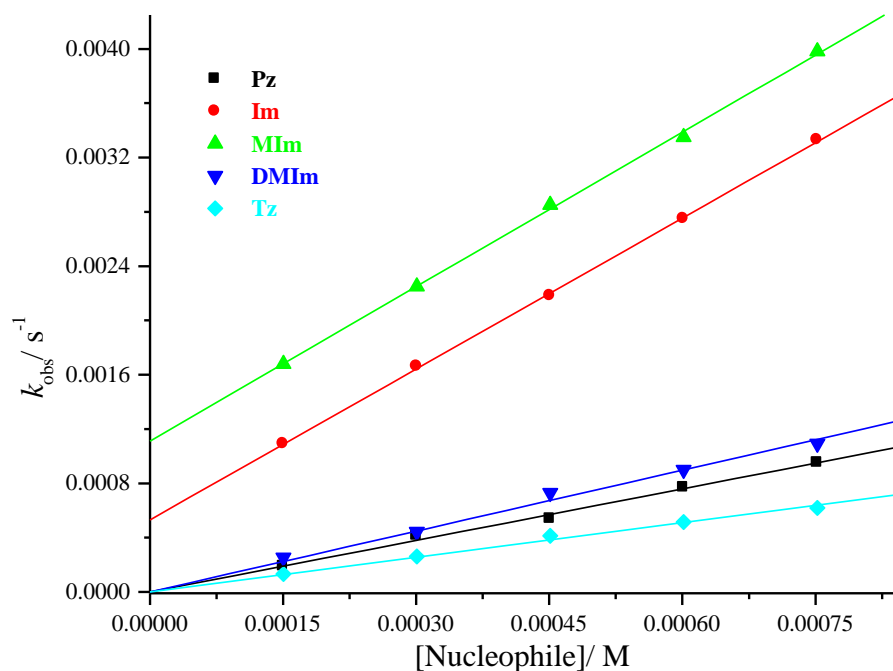


Figure 5.5 Dependence of the *pseudo* first-order rate constants (k_{obs}) on the concentrations of the nucleophiles for the chloride substitution from Pt1 in methanol solution ($I = 0.10$ M (0.09 M $LiCF_3SO_3 + 0.01$ M NaCl)) at 298.15 K.

Straight lines with non-zero intercepts were obtained for all the concentration dependent kinetic reactions except for Pt3, Pt4 and Pt1 with DMIm and Pt1 with Pz and Tz, which gave no meaningful intercepts. Since sodium chloride was used to prevent spontaneous solvolysis reaction, the observed non-zero intercept is an indication of the back reaction, thus the reactions observed can be represented by Equation 5.1.

$$k_{obs} = k_2[Nu] + k_{-2} \quad (5.1)$$

where k_2 and k_{-2} are the second-order rate constant for the forward and the reverse reaction respectively.

The second-order rate constants, k_2 and k_{-2} obtained from the slopes and the intercepts of the plots at 298.15 K are summarised in Table 5.1. Data for the substitution reactions of Pt1 with Pz and Im from the literature^[9] are included for comparison.

Table 5.1 Summary of second-order rate constants and their standard deviations for the displacement of the chloride from the platinum(II) complexes by **Pz**, **Tz**, **Im**, **MIm** and **DMIm** in methanol, ($I = 0.10 \text{ M}$ ($0.09 \text{ M LiCF}_3\text{SO}_3 + 0.01 \text{ M NaCl}$)) at 298.15.

| Nu | Parameter | k_2 and k_{-2} in $\text{M}^{-1} \text{s}^{-1}$ respectively, for the forward and the reverse reactions of the complexes studied | | | | |
|-------------|-----------|--|----------------------------------|----------------------------------|----------------------------------|-----------------------|
| | | Pt1 | Pt2 | Pt3 | Pt4 | *(Pt1) ^[9] |
| Pz | k_2 | 1.26 ± 0.02 | 3.20 ± 0.16 | 0.942 ± 0.18 | 0.36 ± 0.01 | 0.48 ± 0.01 |
| | k_{-2} | N/A | $(8.85 \pm 0.81) \times 10^{-4}$ | $(2.35 \pm 0.15) \times 10^{-4}$ | $(2.20 \pm 0.07) \times 10^{-4}$ | 39.0 ± 1.00 |
| Tz | k_2 | 0.85 ± 0.02 | 1.50 ± 0.05 | 0.79 ± 0.03 | 0.29 ± 0.02 | |
| | k_{-2} | N/A | $(1.63 \pm 0.23) \times 10^{-4}$ | $(6.37 \pm 2.64) \times 10^{-5}$ | $(2.00 \pm 1.27) \times 10^{-5}$ | |
| Im | k_2 | 3.70 ± 0.04 | 5.91 ± 0.18 | 3.03 ± 0.03 | 0.85 ± 0.06 | 6.70 ± 0.10 |
| | k_{-2} | $(5.31 \pm 0.19) \times 10^{-4}$ | $(8.88 \pm 0.90) \times 10^{-4}$ | $(5.77 \pm 0.25) \times 10^{-4}$ | $(2.08 \pm 0.52) \times 10^{-4}$ | 0.059 ± 0.01 |
| MIm | k_2 | 3.79 ± 0.07 | 7.93 ± 0.62 | 3.16 ± 0.08 | 1.05 ± 0.04 | |
| | k_{-2} | $(1.11 \pm 0.03) \times 10^{-3}$ | $(1.10 \pm 0.31) \times 10^{-3}$ | $(9.49 \pm 0.62) \times 10^{-4}$ | $(2.20 \pm 0.52) \times 10^{-4}$ | |
| DMIm | k_2 | 1.49 ± 0.03 | 2.04 ± 0.02 | 1.31 ± 0.02 | 0.36 ± 0.01 | |
| | k_{-2} | N/A | $(1.80 \pm 0.10) \times 10^{-4}$ | N/A | N/A | |

* k_2 and k_{-2} obtained for the substitution reactions of **Pt1** with **Pz** and **Im** in methanol at 25 °C.

A comparison of the reactivity of the complexes studied is given in *Table 5.2* and *Table 5.3*. **Pt1** and **Im** are used as the bases, respectively in *Table 5.2* and *Table 5.3* for the comparison of the observed reaction rates.

Table 5.2 Relative rates of the complexes based on k_2 ; **Pt1**, **Pt2**, **Pt3** and **Pt4** with **Pz**, **Tz**, **Im**, **MIm** and **DMIm** with **Pt1** taken as the basis.

| Complex | Pz | Tz | Im | MIm | DMIm |
|------------|------|------|------|------|------|
| Pt1 | 1 | 1 | 1 | 1 | 1 |
| Pt2 | 2.56 | 1.83 | 1.59 | 2.09 | 1.44 |
| Pt3 | 0.75 | 0.97 | 0.81 | 0.83 | 0.93 |
| Pt4 | 0.29 | 0.35 | 0.23 | 0.28 | 0.26 |

Table 5.3 Relative rates based on k_2 of the complexes; **Pt1**, **Pt2**, **Pt3** and **Pt4** with **Pz**, **Tz**, **Im**, **MIm** and **DMIm** with **Im** taken as the basis.

| Complex | Pz | Tz | Im | MIm | DMIm |
|------------|------|------|----|------|------|
| Pt1 | 0.34 | 0.22 | 1 | 1.02 | 0.38 |
| Pt2 | 0.54 | 0.25 | 1 | 1.34 | 0.35 |
| Pt3 | 0.31 | 0.26 | 1 | 1.04 | 0.43 |
| Pt4 | 0.43 | 0.34 | 1 | 1.24 | 0.43 |

The temperature dependence of the rate constants were studied over a range of either 15-35 °C or 20-40 °C depending on the reactivity behaviour of the complexes with the nucleophiles. The corresponding activation parameters, entropy of activation (ΔS^\ddagger) and enthalpy of activation (ΔH^\ddagger) are obtained by using the Eyring equation (*Equation 3.81*)^[12] and are summarised in *Table 5.4*. The plots obtained for **Pt2** for the forward reactions using the Eyring equation are shown in *Figure 5.6*. Given in *Figure 5.7* is a typical Eyring plot obtained for the reverse reaction of **Pt3** with the nucleophiles. Eyring plots for the forward reactions of **Pt1**, **Pt3** and **Pt4** and reverse reactions of **Pt1**, **Pt2** and **Pt4** are given in *Appendix B*.

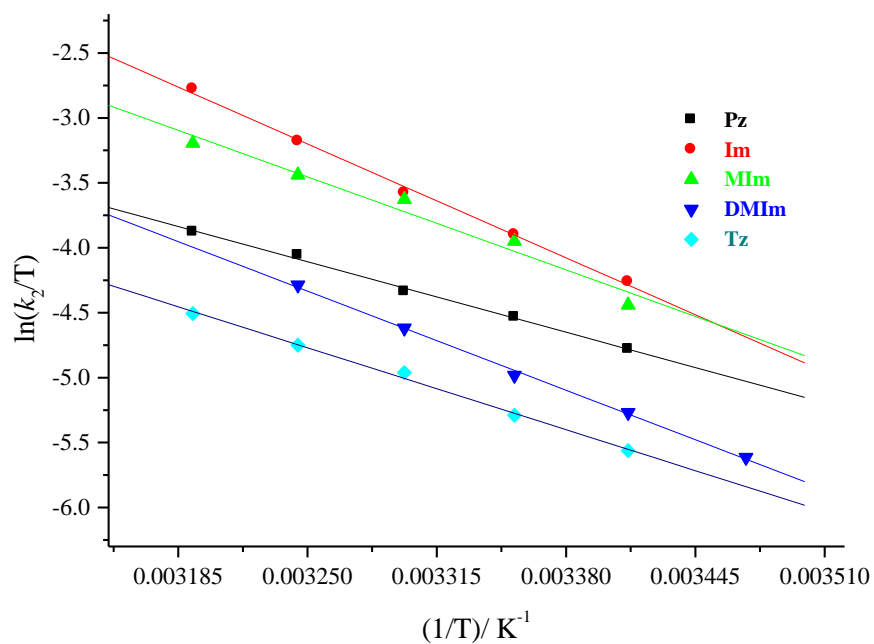


Figure 5.6 Plots of $\ln(k_2/T)$ against $1/T$ for the reactions of Pt2 with the nucleophiles at various temperatures in the range 15-40 °C.

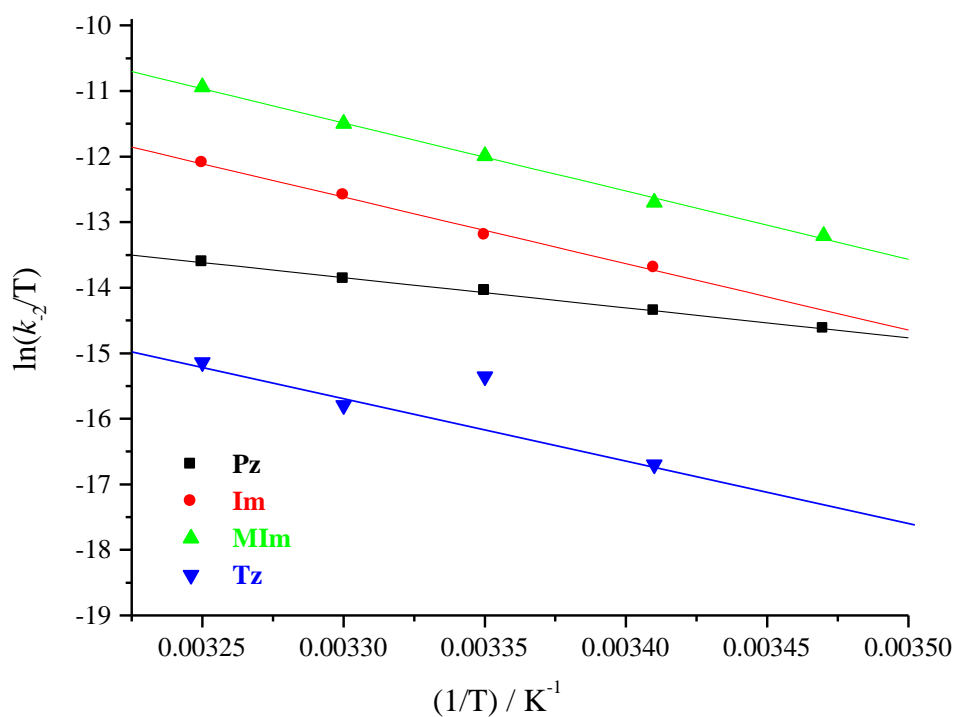


Figure 5.7 Plots of $\ln(k_2/T)$ against $1/T$ for the reactions of Pt3 with the nucleophiles at various temperatures in the range 15-40 °C.

Table 5.4 Summary of activation parameters for the forward and the reverse reactions[§] with their corresponding standard deviations for the chloride substitution reactions of the platinum(II) complexes studied with Pz, Im, MIm, DMIm and Tz in methanol ($I = 0.10$ M (0.09 M LiCF₃SO₃ + 0.01 M NaCl)).

| Nu | Activation Parameter | ΔH^\ddagger in kJ mol ⁻¹ and ΔS^\ddagger in J K ⁻¹ mol ⁻¹ for the Complexes | | | |
|-------------|-----------------------|--|-------------|-------------|---------------|
| | | Pt1 | Pt2 | Pt3 | Pt4 |
| Pz | ΔH_f^\ddagger | 44.0 ± 1.3 | 34.7 ± 1.2 | 48.9 ± 0.7 | 56.5 ± 4.4 |
| | ΔS_f^\ddagger | -96 ± 4 | -119 ± 4 | -82 ± 2 | -63 ± 15 |
| | ΔH_r^\ddagger | N/A | 33.5 ± 5.9 | 37.4 ± 1.4 | 25.2 ± 5.4 |
| | ΔS_r^\ddagger | N/A | -191 ± 20 | -190 ± 5 | -164 ± 18 |
| Tz | ΔH_f^\ddagger | 39.7 ± 3.0 | 40.2 ± 1.7 | 54.8 ± 2.6 | 65.6 ± 2.6 |
| | ΔS_f^\ddagger | -114 ± 10 | -106 ± 6 | -63 ± 9 | -36 ± 9 |
| | ΔH_r^\ddagger | N/A | 69.6 ± 15.2 | 70.0 ± 38.1 | 9.1 ± 13.7 |
| | ΔS_r^\ddagger | N/A | -92 ± 50 | -81 ± 12 | -309.2 ± 44.8 |
| Im | ΔH_f^\ddagger | 50.9 ± 1.1 | 56.0 ± 1.7 | 48.9 ± 0.7 | 49.3 ± 3.0 |
| | ΔS_f^\ddagger | -67 ± 3 | -43 ± 6 | -72 ± 2 | -81 ± 10 |
| | ΔH_r^\ddagger | 61.0 ± 9.9 | 56.5 ± 6.2 | 83.6 ± 4.5 | 94.2 ± 13.3 |
| | ΔS_r^\ddagger | -110 ± 33 | -115 ± 21 | -27 ± 15 | -3 ± 44 |
| MIm | ΔH_f^\ddagger | 45.6 ± 1.2 | 44.6 ± 4.2 | 43.2 ± 1.9 | 58.7 ± 4.7 |
| | ΔS_f^\ddagger | -84 ± 4 | -79 ± 14 | -91 ± 6 | -73 ± 16 |
| | ΔH_r^\ddagger | 93.1 ± 6.1 | 75.4 ± 37 | 87.1 ± 3.6 | 79.8 ± 4.7 |
| | ΔS_r^\ddagger | 5 ± 20 | 112 ± 11 | -11 ± 12 | -47 ± 16 |
| DMIm | ΔH_f^\ddagger | 56.4 ± 8.5 | 48.7 ± 1.8 | 51.3 ± 1.5 | 61.7 ± 0.8 |
| | ΔS_f^\ddagger | -53 ± 28 | -76 ± 6 | -71 ± 5 | -47 ± 3 |
| | ΔH_r^\ddagger | N/A | 61.4 ± 5.3 | N/A | N/A |
| | ΔS_r^\ddagger | N/A | -111 ± 18 | N/A | N/A |

[§] the letters _f and _r represents the forward and the reverse reactions respectively.

5.3. Computational Analysis

Preliminary computational modelling of the platinum(II) complexes were done in order to help to explain the kinetic trends observed and to determine the influence of the molecular structure on the observed reactivity of the platinum(II) complexes. As mentioned earlier computational modelling for the platinum(II) complexes were done as cations for the chloro complexes and as dications for the azole substituted complexes.

The RMS fit of the DFT-calculated and the X-ray structure^[8] of an analogous complex of **Pt3**, [Pt{4'-(*o*-tolyl)terpy}Cl]SbF₆, when gauged using HyperChem Pro 6.03^[13] showed that the RMS difference between the X-ray structure from the Cambridge Structural Database^[14] and the DFT-calculated structure was only 0.0523 Å.^[15] Thus DFT-calculated structures are acceptable due to the similarity between the X-ray and the DFT-calculated complexes.^[15]

The geometry optimized structures and the electron density distribution functions obtained for **Pt1**, **Pt2**, **Pt3** and **Pt4** from the computational analysis are shown in *Table 5.5*. A summary of respective bond lengths and the bond angles obtained from the modelled structures of the platinum complexes are given in *Table 5.6* and *Table 5.7* respectively. The bond angles and the bond lengths were further analysed using the crystallographic data available in literature. The numbering employed for the respective atoms are shown in *Figure 5.8*.

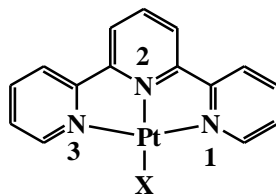


Figure 5.8 Numbering scheme employed for the atoms around the platinum centre for the platinum(II) complexes investigated. X represents Cl in the forward reactions and N4 (from azole) in the reverse reactions. The bond angles, bond lengths and atomic charges are referred according to the numbering scheme shown.

Table 5.5 Geometry-optimised structures of the platinum complexes investigated and distribution of the electron density on the platinum complexes. The blue area indicates the most electropositive areas and the red region indicates the most electronegative areas. Included in this *Figure* is a nucleophile substituted complex for the product of the kinetic reaction of Pt3 with MIm, ([Pt{4'-(*o*-tolyl)terpy}MIm](CF₃SO₃)₂) (Pt3-MIm).

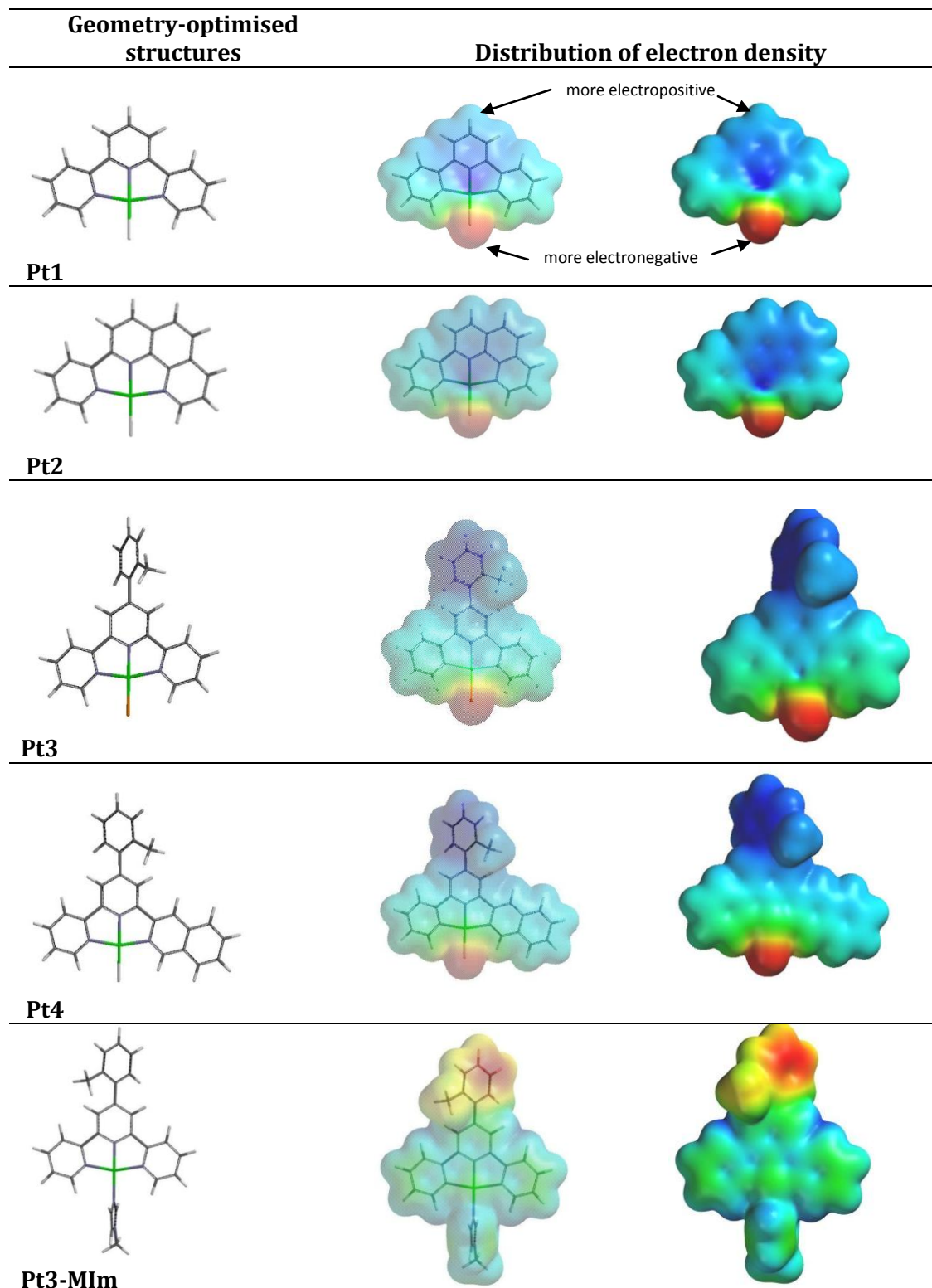


Table 5.6 Selected bond lengths (Å) for the platinum complexes Pt1, Pt2, Pt3, Pt4 and Pt3-MIm obtained from the computational studies, literature and the X-ray crystal structure.

| Complex | Pt—N1 (<i>cis</i>) | Pt—N2 (<i>trans</i>) | Pt—N3 (<i>cis</i>) | Pt—X [†] |
|-----------|-------------------------------|-------------------------------|-------------------------------|-------------------------------|
| Pt1* | 2.052 (2.002) ^[16] | 1.966 (1.940) ^[16] | 2.052 (2.004) ^[16] | 2.347 (2.296) ^[16] |
| Pt2 | 2.074 | 1.965 | 2.061 | 2.344 |
| Pt3* | 2.053 (2.019) ^[7] | 1.964 (1.924) ^[7] | 2.054 (2.027) ^[7] | 2.351 (2.296) ^[7] |
| Pt4 | 2.050 | 1.967 | 2.053 | 2.355 |
| Pt3-MIm** | 2.067 (2.023) | 1.969 (1.945) | 2.076 (2.033) | 2.082 (2.031) |

* the values in brackets in green were obtained for the X-ray crystal structure from the literature.

**the values in brackets in blue were obtained from the X-ray crystal structure (Figure 4. 2, this work).

Table 5.7 Summary of selected Bond Angles(°) for Pt1, Pt2, Pt3, Pt4, Pt3-MIm obtained from DFT-calculations, X-ray crystal structure and from literature.^[7, 16]

| Complex | †X-Pt-N1 | †X-Pt-N2 | †X-Pt-N3 | N1-Pt-N2 | N1-Pt-N3 | N2-Pt-N3 |
|-----------|----------------------------------|-----------------------------------|---------------------------------|---------------------------------|-----------------------------------|---------------------------------|
| Pt1* | 99.18 (100.1) ^[16] | 179.93 (178.7) ^[16] | 99.25 (99.0) ^[16] | 80.79 (79.9) ^[16] | 161.58 (160.8) ^[16] | 80.79 (81.0) ^[16] |
| Pt2 | 98.64 | 179.89 | 101.03 | 81.28 | 160.33 | 79.05 |
| Pt3* | 99.44 (99.2) ^[7] | 179.90 (176.) ^[7] | 99.33 (99.0) ^[7] | 80.63 (81.2) ^[7] | 161.23 (161.7) ^[7] | 80.63 (80.6) ^[7] |
| Pt4 | 99.01 | 179.98 | 99.45 | 80.97 | 161.54 | 88.57 |
| Pt3-MIm** | 99.53 (98.7) | 179.88 (179.1) | 99.69 (99.2) | 80.37 (80.9) | 160.78 (162.1) | 80.41 (81.1) |

* the values in brackets in green were obtained for the X-ray crystal structure from the literature.

** the values in brackets in blue were obtained from the X-ray crystal structure (Figure 4. 2, this work).

Table 5.5 includes a modelled structure, Pt3-MIm obtained for the substituted complex of Pt3 with 1-methylimidazole. The structure of the Pt-MIm cation obtained from the crystal structure analysis of [Pt{4'-(*o*-tolyl)-2,2':6',2''-terpyridine}MIm](CF₃SO₃)₂ given in Figure 4.2. The data obtained from the computational modelling and the crystal structure clearly shows that the *o*-tolyl on the terpy ring and the 1-methylimidazole ring attached on the platinum centre are not co-planar with the terpy ligand backbone. The *o*-tolyl group on the terpy ring is twisted in order to accommodate the steric strain due to the interactions between the *o*-tolyl group and the hydrogens attached on the central pyridine on the terpy ligand^[17]. A

[†] X = N for Pt3-MIm, otherwise X = Cl

similar twist is observed in the molecular structure obtained for the ligand, 4-(*o*-tolyl)-6-(3'-isoquinoyl)-2,2'-bipyridine (*Figure 4.1*), which is caused due to the interactions between the hydrogens on the central pyridine ring and the *o*-tolyl group (H7 and H9, See *Figure 4.1*). Furthermore, the methylimidazole ring has twisted from the Pt—N bond in order to reduce the steric strain between the 1-methylimidazole ring and the protons on the two arms of the pyridine rings (H1 and H15, See *Figure 4.2*) on the terpy ligand frame.

Since the frontier orbital energy is an important tool to understand the substitution mechanism of inorganic reactions, the energy for the Highest Occupied Molecular Orbital (HOMO) and the Lowest Unoccupied Molecular Orbital (LUMO) were obtained from the computational modelling and are shown in *Table 5.8* and *Table 5.9*. Studies have shown that electron donating groups attached to the terpy moiety increases the HOMO-LUMO gap while electron withdrawing groups decrease the HOMO-LUMO gap.^[18-20] The calculated HOMO-LUMO energies and the HOMO-LUMO energy gap for the platinum(II) complexes are given in *Table 5.9*. The decrease in the orbital energy gap from **Pt4** < **Pt3** < **Pt2** is expected. In the case of **Pt3** and **Pt4** the *o*-tolyl group at the central pyridine ring of the chelate backbone functions as an electron donating group. One would therefore expect the substitution reactions of **Pt3** and **Pt4** to be slower than that of **Pt2** and **Pt1**. The increase in the conjugation within the terpy system would decrease the HOMO-LUMO energy gap. This is true when comparing the HOMO-LUMO energy gap of **Pt2** where **Pt2** has extended π -conjugation in the *cis/trans* position through the phenanthroline (phen) subgroup. However, **Pt4**, in spite of having extended π -conjugation in comparison to **Pt3**, shows a higher HOMO-LUMO energy gap. This observation indicates that two opposing processes are taking place. The increased π -conjugation in **Pt4** does not function as such but rather appear that the isoquinoline ring is a weaker π -acceptor but a stronger σ -donor than pyridine.

In the case of **Pt2**, π -back-bonding is stronger than the σ -donation through the nitrogens, where the opposite is true for N1 of **Pt4**. The NBO charges on the donor nitrogen atoms as shown in *Table 5.10* suggest that the platinum metal is surrounded by a ring of negative charge. The magnitude of the charge on N1 of **Pt4** has an opposite effect to that of the N1 of **Pt2**. The results support the thinking that the net effect of the isoquinoline ring in **Pt4** is electron donating through σ -effect while the phenanthroline ring in **Pt2** it is electron withdrawing through the π -back-bonding effect.

Table 5.8 DFT-calculated (B3LYP/LACVP+**) molecular orbitals, *i.e.* HOMO's and LUMO's for the platinum complexes investigated.

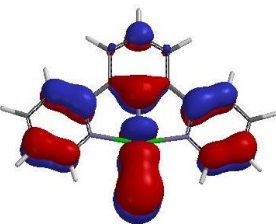
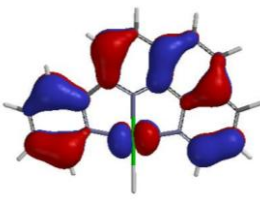
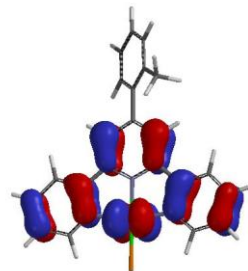
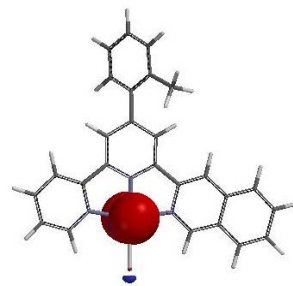
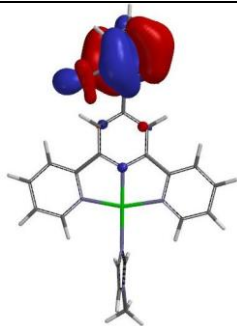
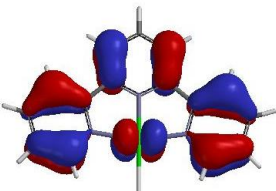
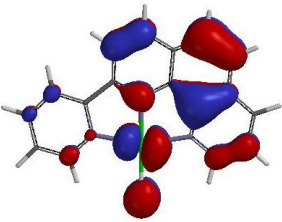
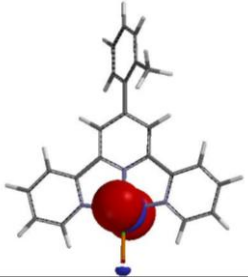
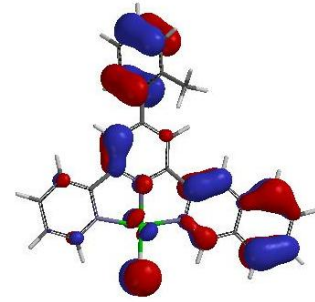
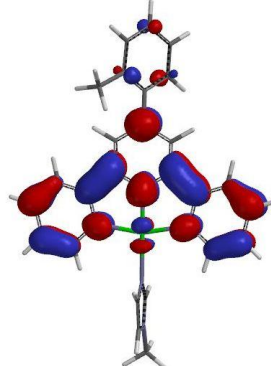
| Complex | Pt1 | Pt2 | Pt3 | Pt4 | Pt3-MIm |
|---------|---|---|--|--|--|
| HOMO |  |  |  |  |  |
| LUMO |  |  |  |  |  |

Table 5.9 Energies of HOMO-LUMO obtained for the platinum(II) complexes studied. Geometry optimised studies done using the B3LYP/LACVP+** level of theory.

| Complex | HOMO/eV | LUMO/eV | ΔE /eV |
|---------|---------|---------|----------------|
| Pt1 | -9.45 | -6.16 | 3.29 |
| Pt2 | -9.37 | -6.24 | 3.13 |
| Pt3 | -9.14 | -5.92 | 3.21 |
| Pt4 | -8.95 | -5.62 | 3.33 |

Figure 5.9 shows a graphical representation of the HOMO-LUMO energies of the platinum(II) complexes investigated. Based on the HOMO-LUMO energy gap values, the order of reactivity should be **Pt2 > Pt3 > Pt1 > Pt4** as against the observed order of **Pt2 > Pt1 > Pt3 > Pt4**. The observed higher reactivity of **Pt1** over **Pt3** is explained later in the dissertation.

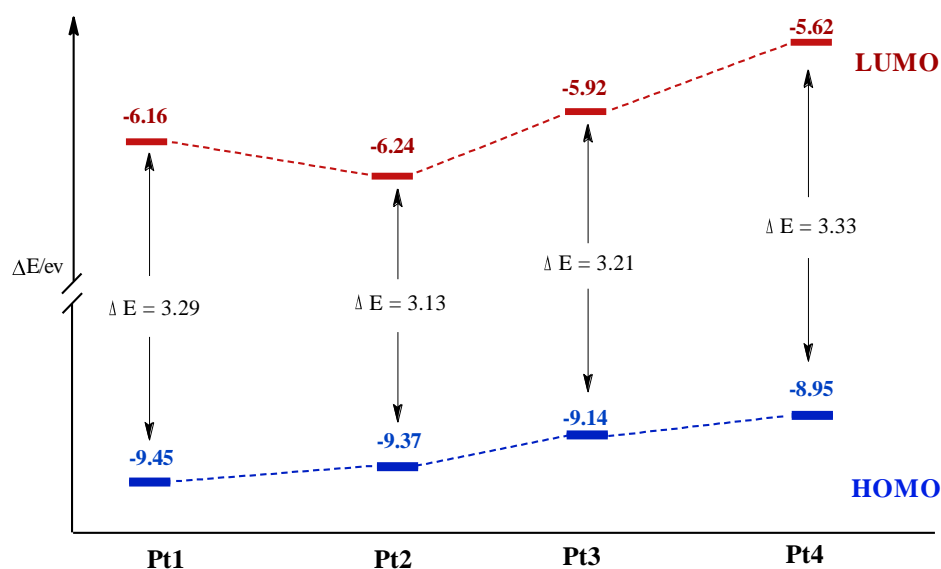


Figure 5.9 HOMO and LUMO energy gap for the platinum(II) complexes investigated.

Table 5.10 The DFT-calculated NBO charges on the central Pt, the donor nitrogen atoms and the leaving group, Cl.

| Complex | Pt | N1 | N2 | N3 | Cl |
|---------|-------|--------|--------|--------|--------|
| Pt1 | 1.227 | -0.599 | -0.565 | -0.599 | -0.637 |
| Pt2 | 1.225 | -0.592 | -0.556 | -0.596 | -0.638 |
| Pt3 | 1.222 | -0.599 | -0.572 | -0.599 | -0.645 |
| Pt4 | 1.218 | -0.609 | -0.575 | -0.596 | -0.653 |

The computational work also included the calculation of the bond lengths (*Table 5.11*) and the NBO charges (*Table 5.12*) for the N-donor substituted complexes. One notices the general increase in the Pt—N4 (N4 from azole, See *Figure 5.8*) bond lengths. The energies of the

HOMO-LUMO for the substituted platinum complexes are tabulated in *Table 5.13* and is shown graphically in *Figure 5.10*. Comparing the trend with that shown in *Figure 5.10* there is not much difference, apart from the fact that final energy level is much lower. This indicates that the substituted complexes are energetically much more stable.^[21]

Table 5. 11 Selected bond lengths (Å) for the N-donor substituted platinum(II) complexes Pt1, Pt2, Pt3 and Pt4 obtained from the computational studies.

| Nu | Bond length | Complex | | | |
|-------|------------------------|---------|--------|-------|-------|
| | | Pt1 | Pt2 | Pt3 | Pt4 |
| Pz | Pt—N1 (<i>cis</i>) | 2.068 | 2.095 | 2.067 | 2.061 |
| | Pt—N2 (<i>trans</i>) | 1.968 | 1.965 | 1.961 | 1.962 |
| | Pt—N3 (<i>cis</i>) | 2.067 | 2.077 | 2.067 | 2.069 |
| | Pt—N4 (<i>azole</i>) | 2.075 | 2.076 | 2.082 | 2.083 |
| Tz | Pt—N1 (<i>cis</i>) | 2.068 | 2.096 | 2.071 | 2.064 |
| | Pt—N2 (<i>trans</i>) | 1.967 | 1.965 | 1.963 | 1.963 |
| | Pt—N3 (<i>cis</i>) | 2.071 | 2.078 | 2.069 | 2.071 |
| | Pt—N4 (<i>azole</i>) | 2.087 | 2.085 | 2.090 | 2.091 |
| Im | Pt—N1 (<i>cis</i>) | 2.067 | 2.093 | 2.068 | 2.063 |
| | Pt—N2 (<i>trans</i>) | 1.971 | 1.968 | 1.964 | 1.965 |
| | Pt—N3 (<i>cis</i>) | 2.068 | 2.078 | 2.067 | 2.069 |
| | Pt—N4 (<i>azole</i>) | 2.077 | 2.076 | 2.084 | 2.084 |
| MIm | Pt—N1 (<i>cis</i>) | 2.068 | 2.094 | 2.067 | 2.061 |
| | Pt—N2 (<i>trans</i>) | 1.972 | 1.969 | 1.969 | 1.967 |
| | Pt—N3 (<i>cis</i>) | 2.067 | 2.076 | 2.076 | 2.069 |
| | Pt—N4 (<i>azole</i>) | 2.074 | 2.074 | 2.082 | 2.078 |
| DMIIm | Pt—N1 (<i>cis</i>) | 2.067 | 2.094 | 2.067 | 2.061 |
| | Pt—N2 (<i>trans</i>) | 1.974 | 1.971 | 1.965 | 1.968 |
| | Pt—N3 (<i>cis</i>) | 2.067 | 2.076 | 2.066 | 2.069 |
| | Pt—N4 (<i>azole</i>) | 2.074 | 2.0763 | 2.081 | 2.082 |

Table 5.12 The DFT-calculated NBO charges on the central Pt, the donor nitrogen atoms and the leaving group, (N-donor azole). Geometry optimised studies done using the B3LYP/LACVP+** level of theory.

| Nu | Atom | Complex | | | |
|-------------|------------------|---------|--------|--------|--------|
| | | Pt1 | Pt2 | Pt3 | Pt4 |
| Pz | Pt | 1.277 | 1.273 | 1.270 | 1.267 |
| | N1 | -0.606 | -0.600 | -0.607 | -0.618 |
| | N2 | -0.576 | -0.567 | -0.592 | -0.595 |
| | N3 | -0.606 | -0.603 | -0.607 | -0.607 |
| | N4(azole) | -0.606 | -0.532 | -0.530 | -0.526 |
| Tz | Pt | 1.275 | 1.275 | 1.271 | 1.267 |
| | N1 | -0.607 | -0.600 | -0.606 | -0.617 |
| | N2 | -0.576 | -0.565 | -0.590 | -0.593 |
| | N3 | -0.606 | -0.602 | -0.606 | -0.606 |
| | N4(azole) | -0.547 | -0.739 | -0.738 | -0.734 |
| Im | Pt | 1.281 | 1.278 | 1.275 | 1.271 |
| | N1 | -0.304 | -0.598 | -0.605 | -0.616 |
| | N2 | -0.574 | -0.565 | -0.598 | -0.593 |
| | N3 | -0.604 | -0.601 | -0.605 | -0.605 |
| | N4(azole) | -0.717 | -0.716 | -0.715 | -0.712 |
| MIm | Pt | 1.283 | 1.280 | 1.276 | 1.273 |
| | N1 | -0.603 | -0.598 | -0.604 | -0.615 |
| | N2 | -0.574 | -0.565 | -0.589 | -0.593 |
| | N3 | -0.603 | -0.600 | -0.605 | -0.605 |
| | N4(azole) | -0.721 | -0.721 | -0.720 | -0.717 |
| DMIm | Pt | 1.284 | 1.281 | 1.277 | 1.274 |
| | N1 | -0.603 | -0.597 | -0.604 | -0.614 |
| | N2 | -0.574 | -0.566 | -0.589 | -0.591 |
| | N3 | -0.603 | -0.600 | -0.604 | -0.604 |
| | N4(azole) | -0.721 | -0.720 | -0.720 | -0.717 |

Table 5.13 Energies of HOMO-LUMO obtained for the substituted platinum(II) complexes. Geometry optimised studies done using the B3LYP/LACVP+** level of theory.

| Nu | Fontal orbital energy | Complex | | | |
|-------|-----------------------|---------|--------|--------|--------|
| | | Pt1 | Pt2 | Pt3 | Pt4 |
| Pz | HOMO | -13.18 | -12.77 | -11.33 | -11.14 |
| | LUMO | -9.01 | -9.02 | -8.59 | -8.21 |
| | ΔE | 4.17 | 3.75 | 2.74 | 2.93 |
| Tz | HOMO | -13.33 | -12.81 | -11.34 | -11.15 |
| | LUMO | -9.17 | -9.05 | -8.62 | -8.23 |
| | ΔE | 4.16 | 3.76 | 2.72 | 2.92 |
| Im | HOMO | -12.98 | -12.65 | -11.24 | -11.05 |
| | LUMO | -8.87 | -8.88 | -8.40 | -8.08 |
| | ΔE | 4.11 | 3.77 | 2.84 | 2.97 |
| MIm | HOMO | -12.76 | -12.58 | -11.19 | -11.02 |
| | LUMO | -8.79 | -8.81 | -8.40 | -8.02 |
| | ΔE | 3.79 | 3.77 | 2.79 | 3.00 |
| DMIIm | HOMO | -12.35 | -12.27 | -11.20 | -10.92 |
| | LUMO | -8.76 | -8.77 | -8.39 | -8.02 |
| | ΔE | 3.59 | 3.50 | 2.81 | 2.90 |

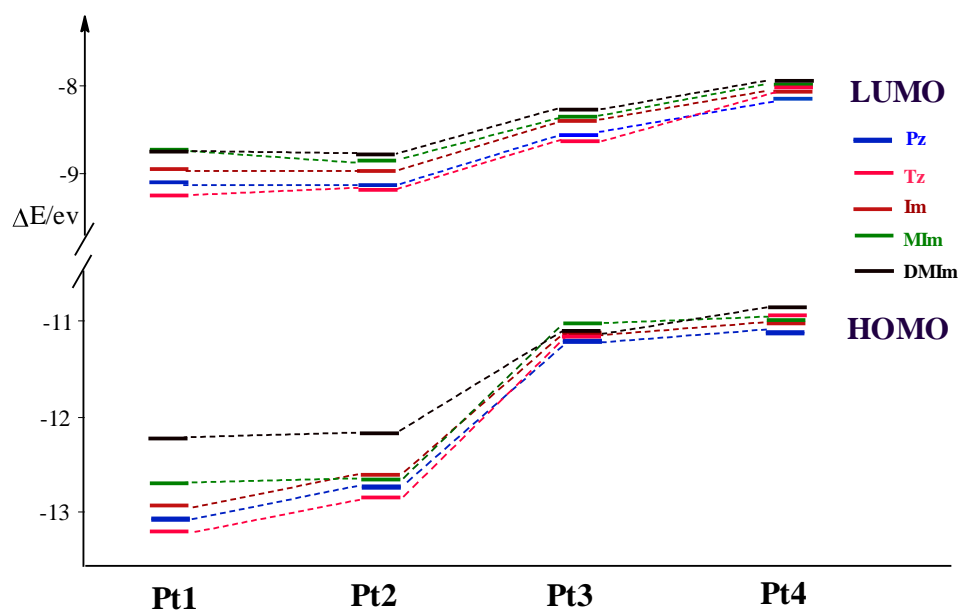


Figure 5.10 The HOMO and LUMO energy gap for the N-donor substituted platinum(II) complexes.

5.4. Discussion

As mentioned earlier in this thesis, the current study is focused on the effect of increasing π -conjugation in the *cis* and *cis/trans* positions of the terpy moiety, on the rate of substitution of the chloride ligand. The platinum(II) complexes studied followed a two term rate law with the general associative mode of activation which is characteristic of square planar platinum(II) complexes. The relatively low enthalpies of activation, (ΔH^\ddagger) and large negative entropies of activation, (ΔS^\ddagger) obtained for the forward reactions further support the associative mode of activation.

5.4.1 Kinetic Study of the Displacement of Chloride by Nitrogen Donors

In comparing the reactivity of the chloride complexes, the data in *Table 5.1* clearly shows a higher reactivity for **Pt2** compared to the other platinum(II) complexes investigated. Using **Pt1** as a basis for comparison, it can be seen that the reactivity of **Pt2** is 2.6 times faster than **Pt1**, 3.4 times faster than **Pt3** and 9 times faster than **Pt4**. Therefore, the observed trend for the reactivity of the complexes is **Pt2** > **Pt1** > **Pt3** > **Pt4**. This order of reactivity is true for all the nucleophiles investigated as illustrated in *Table 5.2*. The difference in the reactivity can be explained in terms of the extended π -conjugation and the presence of the *o*-tolyl group on

the terpy moiety. The increase in the π -conjugation in the terpy moiety is expected to increase the reactivity of the complex through an increase in π -back-bonding which would make the platinum atom more electrophilic than that of **Pt1** and hence more reactive. However, the *o*-tolyl group on the terpy fragment is expected to decrease the reactivity by inductively donating electrons to the metal centre making the platinum atom less electrophilic than that of **Pt1** and therefore less reactive.^[15] To analyse this, computational data and crystallographic data are used to compare the respective bond lengths, the bond angles and the atomic charges.

The structural formulae of the platinum complexes, **Pt1**, **Pt2**, **Pt3** and **Pt4** show similarity in the geometry and the planarity of the complexes. When considered the geometry of the platinum centres, all the complexes have distorted square planar geometry with the bite angle of 160-161°, deviating from linearity. This deviation is caused due to the geometric constraints which deviates the N—Pt—N bond angles (*Table 5.7*) from 90° to approximately 81°^[15, 22-24] (Also see *Figure 4.2*). In **Pt3** and **Pt4**, the *o*-tolyl group lies out-of-plane with respect to the central polypyridyl ligand in order to reduce the non-bonded repulsions between the methyl protons and the protons on the C7 and C9 position of the central pyridine ring (See *Figure 4.1* and *Figure 4.2*).^[17] This deviation of the *o*-tolyl from planarity prevents any π -electronic communication or any π -back-bonding between the *o*-tolyl ring and the terpy moiety.^[25] If there was this π -electronic communication, then the energy gap between the HOMO and LUMO orbitals would be more distinct^[15] (*Table 5.8*, *Table 5.9* and *Figure 5.9*). Furthermore, any steric retardation of this methyl group to the entering nucleophile is minimal as it is not in a close proximity to the reactive platinum centre.^[25]

The DFT-calculated bond lengths for the complexes show an increase in the ground state Pt—Cl bond length from **Pt4** > **Pt3** > **Pt1** > **Pt2** respectively (*Table 5.6*). This trend in the Pt—Cl bond length is due to the ground state π -accepting ability of the terpy moiety of the complexes. The observed reactivity trend is however reversed, **Pt2** > **Pt1** > **Pt3** > **Pt4**. As the extended π -conjugation increases in the *cis/trans* position, the π -acceptor ability of the ligand increases. This lowers the energy of π^* ligand orbitals. In **Pt2**, the extended π -conjugation in the *cis/trans* position allows a better electronic communication with the phenanthroline moiety hence **Pt2** is a better π -accepter compared to the other three complexes. Thus results a smaller frontier orbital energy gap. Consequently, the Pt—Cl bond lengthens in the transition state which results in a weaker Pt—Cl bond and hence greater reactivity towards the entering nucleophile. Hence the observed reactivity trend is reversed from the trend obtained for the DFT-calculated Pt—Cl bond lengths.

As can be seen from the previous work,^[15, 25, 26] the extent of π -back-bonding in similar systems can be controlled by substituents in the ancillary positions of the chelate backbone which subsequently influences the reactivity of the platinum complexes. From this investigation, it is clear that the reactivity of **Pt3** is slower compared to the reactivity of **Pt1**. The observed difference can be explained in terms of the inductive effect of the *o*-tolyl group which donates electrons to the platinum centre. As a result the π -acceptor ability of the chelate backbone is reduced which renders the metal centre in **Pt3** less electrophilic than that of **Pt1**.

As can be seen from *Table 5.6*, the consequences of the replacement of the para hydrogen on the central pyridine ring of **Pt1** by an electron donating *o*-tolyl group as in **Pt3** causes an increase in the Pt—Cl bond length in the ground state due to the increase in the electron density at the metal centre along the *trans* axis. This stabilises the ground state and destabilises the transition state complex.^[15, 25, 26] As a result the energy of the π -anti-bonding orbitals increase, thus the reactivity of the platinum complex decreases. This explanation is consistent with the conclusions drawn by both Jaganyi *et al.*^[25, 26] and Lowe *et al.*^[27] for the substitution reaction of similar analogues of platinum complexes.

The effect of extended π -conjugation within the chelate framework on the lability of the metal centre is clearly evident from the reaction rates shown for **Pt1** and **Pt2** (*Table 5.2*). The observed rate constants for the substitution reactions of **Pt2** are higher than **Pt1** by a factor of 2 on average. The difference in reactivity can be accounted for in terms of the amplified aromaticity on the chelate backbone of **Pt2** compared to the terpy moiety in **Pt1**. This increased π -conjugation enhances the π -back-bonding ability of the chelate ligand by decreasing the energy of the ligand π^* orbitals^[28] which in turn increases the rates of the substitution reactions.

The effect of the extended π -conjugation can also be explained in terms of electronic communication within the π -acceptor ligands. In **Pt2**, the extended π -conjugation on the chelate backbone increases the π -acceptor ability of the ligand which effectively increases the π -back-bonding from the metal centre to the anti-bonding π -orbitals of the ligand system, resulting in a better electronic communication between the phenanthroline and the pyridine sub unit. This consequently increases the electrophilicity of the metal centre^[25] and hence the reactivity.

The main interaction responsible for the increase in the reactivity is between the empty p_z orbitals of the metal and the π -acceptor orbitals on the ligand.^[18, 25] Since the empty p_z orbitals get filled in the transition state, it stabilizes the five coordinate intermediate

compared to the ground state [18, 29, 30] via π -back-bonding. This decreases the activation energy or the energy separation of the frontier molecular orbitals (HOMO and LUMO) of the complex and promotes the approach of the nucleophile to the reactive metal centre.[25, 30] This is characteristic of an associative mode of reaction mechanism where the reactivity is mainly enhanced by the π -acceptor property of the ligand.[31] From the DFT-calculated frontier orbital diagrams (Table 5.8), it can be seen that in **Pt2**, most of the HOMO electron density is located on the aromatic ligand system making the metal centre more positive. Hence, as expected, the observed reactivity of **Pt2** is higher than that of **Pt1**.

From the four complexes investigated, the smallest energy separation of frontier orbital ($\Delta E = E_{\text{HOMO}} - E_{\text{LUMO}}$) is observed for **Pt2** (Table 5.9, Figure 5.9). This clearly shows the stronger π -back-bonding ability of **Pt2** compared to the other platinum(II) complexes investigated. On the contrary, the DFT-calculated energy gap for **Pt1** is higher than that of the energy gap observed for **Pt3**. This agrees with the findings of Jaganyi *et al.*[15] The observed increase in the rate of substitution with the increase of the π -conjugation of **Pt2** compared to **Pt1** is expectable. Earlier studies by Hofmann *et al.*[18] showed an increase in the rate by a factor of approximately 2.2-3.5 with the increase in the π -conjugation from Pt-dien to Pt-aminomethyl-pyridine.

The effect of the extended π -conjugation at one of the *cis* positions of the chelate framework is evident from the reactivity of **Pt4**. By looking at the structures of **Pt3** and **Pt4**, the extended π -conjugation of the isoquinoline ring in the *cis* position of **Pt4** was expected to increase the substitution reactions by increasing the π -back-bonding effect of the chelate framework. However, when compared the reactivity of **Pt3** and **Pt4**, results obtained show that the reactivity of **Pt3** is nearly three times higher than that of **Pt4** for the nucleophiles studied (Table 5.2). The observed difference in the rate constants can be explained by using the bond lengths [25] and the NBO charges on the central platinum and the nitrogen atoms around the reactive metal centre using DFT-calculations in Table 5.6 and Table 5.10.

In **Pt3**, the Pt—N1 bond (2.053 Å) and the equivalent Pt—N3 bond length (2.054 Å) are similar whilst in **Pt4**, the Pt—N1 bond (2.050 Å) is slightly shorter than the Pt—N3 bond (2.053 Å). This slight decrease in bond length in **Pt4** can be attributed to the fact that the isoquinoline ring is a better σ -electron donor than pyridine. The comparisons of the NBO charges on the atoms (Table 5.10) show a slightly more negative charge for the central platinum atom in **Pt4** (1.218) than that of **Pt3** (1.222). Thus σ -donor character of *cis* isoquinoline ring is more prominent compared to its π -acceptor ability. This makes the metal

centre slightly less electrophilic in **Pt4** than in **Pt3** which becomes evident in their reactivities.

When comparing the energy separation of the frontier orbitals ($\Delta E = E_{\text{HOMO}} - E_{\text{LUMO}}$) of the two complexes (Table 5.8 and Table 5.9), a larger ΔE obtained for **Pt4** indicates a smaller metal-to-ligand charge transfer (MLCT). Noteworthy here is the difference in the DFT-calculated ground state HOMO of **Pt3** and **Pt4**. The latter has its HOMO electron density significantly concentrated on the platinum centre, which decreases the electrophilicity of the metal centre (Table 5.8). This clearly indicates that the isoquinoline ring acts as a better σ -donor. Hence, the observed difference in the HOMO electron density distribution between the **Pt3** and **Pt4** is attributed due to the presence of the isoquinoline ring in **Pt4**. Therefore, computational data supports the observed experimental trend for the two complexes.

To understand the observed kinetics of **Pt4** further, in particular why the kinetics is so different to that of **Pt3**, the UV/Visible absorption spectrum of **Pt4** is compared with that of **Pt3** in Figure 5.11; also shown in the Figure is the absorption spectrum of the free 4-(*o*-tolyl)-6-(3''-isoquinoyl)-2,2'-bipyridine ligand. The relatively intense higher energy bands in the 250-350 nm region are due to π - π^* absorptions localized on the conjugated ligand system.^[32] Of more relevance to the discussion are the MLCT bands, because these involve a transition from the Pt 5d HOMO to a π^* -LUMO on the ligand; these occur at wavelengths longer than 350 nm, as has been shown by other workers.^[7, 8, 33-37]

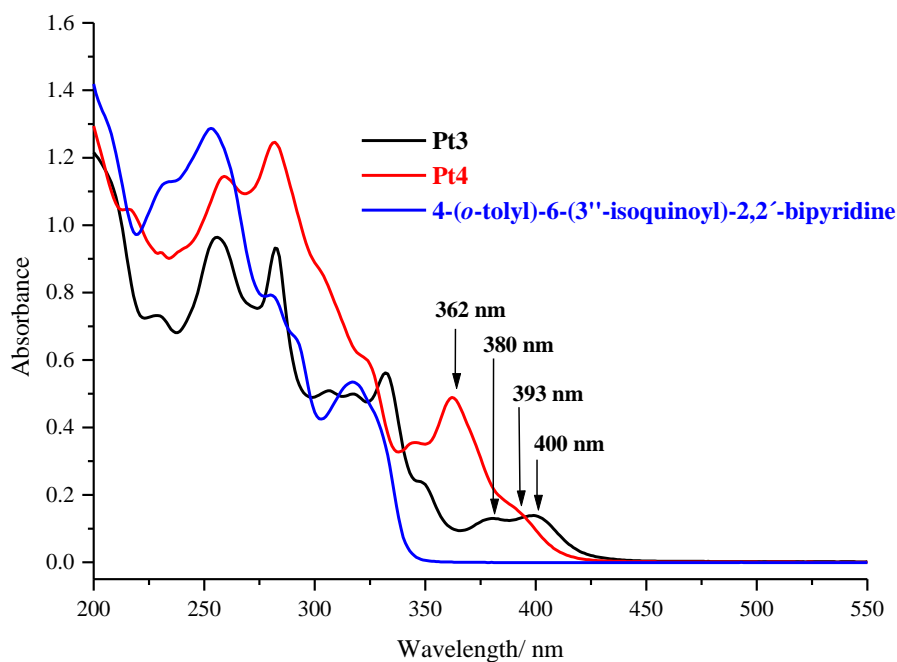


Figure 5.11 Absorption spectrum of **Pt3**, **Pt4** and the ligand of **Pt4**, (4-(*o*-tolyl)-6-(3''-isoquinoyl)-2,2'-bipyridine) in acetonitrile solution.

As can be seen by inspection of *Figure 5.11*, the MLCT bands for **Pt4** are shifted to shorter wavelengths as compared to those for **Pt3**: specifically from 380 and 400 nm for **Pt3** to 362 and 393 (a shoulder) for **Pt4**. Thus, there is a shift to higher energies for the MLCT transitions in **Pt4** as compared to **Pt3** *i.e.* there must be a widening of the energy gap between the *d*-orbital HOMO and the ligand-based π^* -LUMO in **Pt4**. Of course, the absorption spectra in themselves cannot explain the increase in the HOMO-LUMO energy gap. However, the DFT-calculations described in *Section 5.3* are helpful in this regard. As shown in *Figure 5.9* there is indeed an increase in the HOMO-LUMO energy gap for **Pt4** (3.33 eV) as compared to **Pt3** (3.21 eV) predicted by the DFT-calculations. Of relevance to the kinetics of **Pt4** is the question of exactly why the HOMO-LUMO gap widens for **Pt4**. As shown in *Figure 5.11* the energy of the HOMO actually increases when a pyridine is replaced with an isoquinolyl moiety. However, the increase is small, whereas the energy of the LUMO rises from -5.92 eV for **Pt3** to -5.62 eV for **Pt4**, a substantial increase of 0.3 eV that more than compensates for the slight increase in the energy of the HOMO— hence the net widening of the HOMO-LUMO energy gap for **Pt4**. The dramatically higher energy for the π^* -LUMO localized on the ligand of **Pt4** (See *Table 5.8*) has as a result that the 4-(*o*-tolyl)-6-(3'-isoquinoyl)-2,2'-bipyridine ligand must be a weak π -acceptor ligand, certainly weaker than the terpy ligand. At first this seems counter-intuitive, since the extension of a pyridine to an isoquinolyl moiety is expected to increase the π -conjugation of the ligand, and hence its π -acceptor abilities. That this is not the case is shown by the DFT-calculations, and is probably due to the fact that the introduction of an isoquinolyl moiety breaks the C_2 -symmetry of the parent terpy ligand.

The increase in the π -conjugation in the *cis* position by a σ -donor group in fact decreases the π -back-bonding ability of the ligand in **Pt4**. This decreases the electrophilicity of the metal centre and hence hinders the approach of the incoming nucleophile resulting in a slower rate of ligand substitution.

However, from the DFT-calculated LUMO orbital diagram for **Pt3** (*Table 5.8*) it is arguable that the π^* anti-bonding orbitals of the ligand in **Pt3** is weaker than the ligand in **Pt4**. However, the DFT-calculated orbital diagram is similar to what Jaganyi *et al.*^[15] had previously reported. The HOMO-LUMO energy gap for **Pt3** agrees with the observed kinetic trend.

The second-order rate constants obtained for the forward reactions depend on both the steric and electronic factors of the entering nucleophiles which is typical of square planar

platinum(II) complexes.^[9, 21, 38, 39] In terms of the dependence of the steric hindrance of the nucleophiles on the substitution reactions, evidence can be derived when the most sterically hindered **DMIm** is considered. The most sterically hindered **DMIm** showed a much slower reactivity compared to **MIm** and **Im** for all the platinum complexes. However, the less sterically hindered nucleophile, **Im** showed a slower reactivity than the more hindered **MIm**. On this basis, the reactivity of the nucleophiles followed the trend **MIm** > **Im** > **DMIm** > **Pz** > **Tz** for the studied platinum(II) complexes.

Since the rate of the associative mode of substitution reactions of square planar d^8 systems are strongly dependent on the nucleophilicity of the entering nucleophile,^[38-40] the observed trend can be explained by means of basicity usually measured by the pK_a of the N-donor heterocyclic nucleophiles.^[9, 38, 41, 42] In order to investigate the relationship between the basicity of the nucleophiles and the observed reactivity trend, a Linear Free Energy Relationship (LFER) was determined according to Equation 5.2.^[9]

$$\log k_2 = \alpha(pK_a) + b \quad 5.2$$

where α and b account for the electronic and steric effects.

A plot of $\log k_2$ against pK_a of the nucleophiles is given in Figure 5.12 using the data in Table 5.14.

Table 5.14 The logarithm of second-order rate constants, k_2 for the forward reactions of the platinum complexes studied and the pK_a of the nucleophiles studied.

| Nu | $*pK_a^{[43-45]}$ | $\log k_2$ | | | |
|-------------|-------------------|------------|-------|--------|--------|
| | | Pt1 | Pt2 | Pt3 | Pt4 |
| Pz | 2.52 | 0.100 | 0.506 | -0.026 | -0.441 |
| Tz | 2.19 | -0.071 | 0.175 | -0.102 | -0.543 |
| Im | 7.00 | 0.569 | 0.771 | 0.482 | -0.072 |
| MIm | 7.33 | 0.579 | 0.900 | 0.500 | 0.021 |
| DMIm | 8.00 | 0.174 | 0.310 | 0.118 | -0.440 |

* pK_a values from: ^[43-45]

As can be seen in Figure 5.12, except for the sterically hindered nucleophile, **DMIm**, the pK_a of the entering nucleophiles linearly fit to the LFER described in Equation 5.2. The linear trends observed for the four complexes with all the nucleophiles have slopes of (0.117±0.014), (0.134±0.015), (0.116±0.004) and (0.098±0.010) for **Pt1**, **Pt2**, **Pt3** and **Pt4**, respectively. The slope of the graph indicates the electrophilicity of the metal centre which is the ability of the platinum(II) centre to discriminate the incoming ligands of different basicity.^[38, 39] The positive slopes indicate the increase of the electron density around the reactive metal centre

which is typical of associative mode of substitution behaviour. Since the observed slopes are less than one, it signifies the π -acceptor ability of the added azole ligands and the mixing of the orbitals from the azole ligand and the π -orbitals of the metal.^[46]

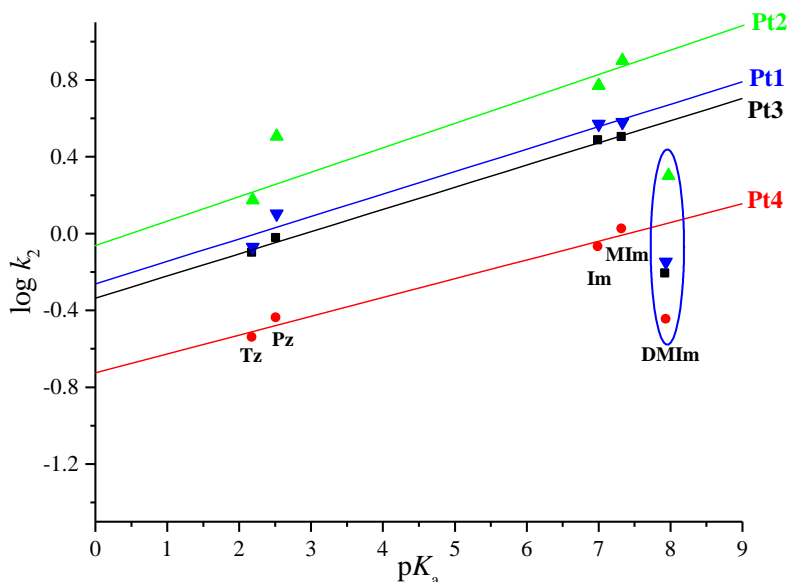


Figure 5.12 Plot of variation of $\log k_2$ obtained for the substitution reactions against the pK_a values of the nucleophiles studied.

The ability of the substrate to discriminate among the entering azoles followed the order **Pt2** > **Pt1** > **Pt3** > **Pt4**. This trend can be rationalised on the basis of the electronic features of the tridentate chelate ligands where the increased π -back-bonding ability of the chelate backbone is observable. The significance of this trend indicates the order of the energy requirements for moving the systems from the ground state to the transition state.^[39] In the case of **Pt2**, this energy barrier is minimum as observed from the computational analysis of HOMO and LUMO energy (*Table 5.9, Figure 5.9*).

The observed linearity is in agreement with the previously studied substitution reactions^[39] of $[\text{Pd}(\text{terpy})\text{C I}]^+$ and $[\text{Pt}(\text{terpy})\text{C I}]^+$ with pyridines^[11, 41] and $[\text{Pt}(\text{terpy})\text{C I}]^+$ with five-membered N-donor heterocycles.^[9] However, deviation of **DMIm** from the observed reactivity trend can be explained by means of steric effect since the LFER works well for sterically less hindered nucleophiles.^[11, 21]

Presence of an α -methyl group to the N-donor atom creates steric retardation to the entry of the heterocyclic nitrogen ligand.^[9, 38] The magnitude of the steric repulsion generated is

related to the free rotation of the ligand around the Pt—N(azole) bond.^[9, 42] In the observed associative reaction mechanism, the transition state contains a well formed Pt—N bond and a weak Pt—Cl bond. In the trigonal bipyramidal intermediate, the two outer pyridine rings of the terpy moiety lie in the axial positions and the steric interactions between the α -methyl protons of the nucleophile and the protons on the terpy ring can interfere with the free rotation of the newly formed Pt—N bond^[9, 42] which slows down the substitution reaction (Figure 5.13). The steric bulk affects the energy of the ground state as well as the transition state complex.^[38] Therefore, the entry of a bulky nucleophile is kinetically less favoured in the observed associative mode of reactions because the formation of the trigonal bipyramidal intermediate involves a higher energy.^[10]

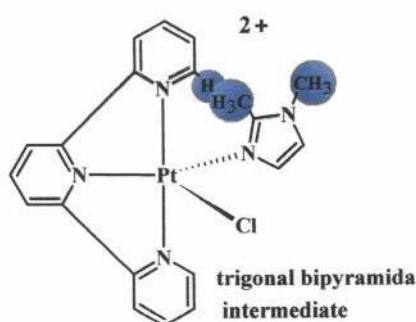


Figure 5.13 Putative representation of the interaction of the α -methyl group on the DMIm with the pyridine hydrogen of $[\text{PtCl}]^+$ showing the steric congestion in the trigonal bipyramidal intermediate. Diagram modified from Ref.^[9]

The slower reactivity of α -substituted methylimidazole is further explained by Catalán and Elguero^[47] in terms of charge dispersion through hydrogen bonding with the solvent (water) which decreases the basicity of the α -substituted heterocyclic ligand in solution. The steric retardation due to the interaction of the α -substituted methyl with solvent was also observed for the kinetic studies done by Bellicini *et al.*^[38] on platinum(II) complexes in methanol. The observed effect was thought to be due to a relatively weak bond formation with the solvent and the incoming ligand. This solvent effect decreases the nucleophilicity of the ligand and thus the reactivity in solution.^[47] In the case of **DMIm**, the steric interactions and charge dispersion *via* hydrogen bonding might be reasonable for lowering the basicity of the nucleophile in the reaction medium (in this case methanol), thus resulting in the observed reactivity being slower than the rest of the nucleophiles.

From the four platinum(II) complexes investigated, the experimental results in Table 5.1 show that the substitution reactions of **Pt2** are least sensitive to the steric hindrance of the

entering nucleophiles (in this case **DMIm**) while the least reactive **Pt4** is the most sensitive to the steric effect of entering nucleophile.

On the other hand, the higher reactivity of the **MIm** can be explained to be due to the inductive effect of the methyl group attached to N1 position of the methyl ring. This inductive donation of the electrons from the methyl group in **MIm** makes the N3 more basic. Since this methyl group is further away from the pyridine rings on the terpy moiety, the steric congestion in the transition state is minimised. In the case of **DMIm**, the steric effect dominates over the inductive effect of the methyl groups. Therefore, the observed trend is expectable for the five membered N-donor heterocycles since the methyl group in the α -position with respect to the N-donor atom in heterocyclic nucleophiles lead to steric congestion in the transition state.^[9, 48]

The reactivity of **Pz**, **Im** and **Tz** followed the listed pK_a trend of the nucleophiles. The nucleophiles with the higher pK_a value react faster with the metal complexes. The smaller pK_a value of **Pz** compared to **Im** is due to the poor delocalization of the charge in **Pz** conjugate acid compared to the conjugate acid of **Im**.^[44] The poor delocalization usually occurs when **Pz** is protonated and leads to more destabilization of the π -bonding in **Pz**.^[49] This destabilization is more prominent for **Pz** than **Im**. In the case of **Pz**, due to the presence of a vicinal nitrogen, **Pz** has a slightly lower binding energy (0.309 a.u) than **Im** (0.335 a.u).^[49] The smallest pK_a value and the slowest reactivity of **Tz** can be accounted for due to the stronger inductive effect of N1 and N2 which pull the electron cloud from the vicinal nitrogen. This makes the N4 more electron rich since it experiences a smaller inductive pull compared to N1 and N2. The smallest pK_a value of **Tz** is also thought to be due to the increase in the number of nitrogen atoms in the five membered ring.^[49] Apart from the lower pK_a , the lower reactivity of both **Pz** and **Tz** is also due to their relatively higher stability compared to the other azoles.^[49]

Since the nucleophiles, **Pz**, **Im**, **MIm**, **DMIm** and **Tz** are ambidentate ligands, it is important to identify their binding site to the Platinum(II) centre. Analogues of **Pz** and **Im** are π -excessive N-heteroaromatic systems and their π -electrons are largely delocalised over the aromatic ring while the non-bonded electrons lie on the pyridine type nitrogens (N2 for pyrazole and N3 for imidazole and its analogues, N3 and N4 for triazole (See *Figure 5.14*).

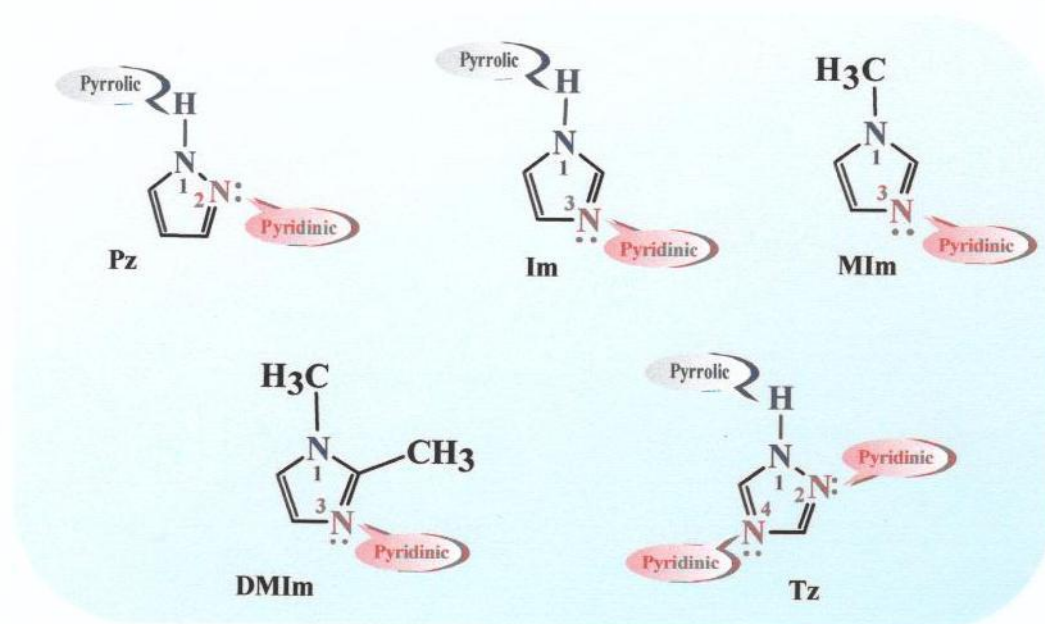


Figure 5.14 Structure of the nucleophiles investigated indicating the different nitrogen atoms.

Past studies support the binding of pyrazole and imidazole analogues with metal centres *via* the pyridine type basic N.^[50-52] Therefore, bonding to the platinum centre is more likely *via* the pyridinic N. To investigate this further, DFT-calculated NBO charges and the geometry optimised structures of the nucleophiles along with their potential energies are used (Figure 5.15).

The calculated NBO charges for **Pz** and **Im** show higher negative charges for N1 than N2 and N3, respectively. According to a DFT study done by Matulis *et al.*^[53] the NBO charge is a measure of π -electron delocalisation and shows the degree of the aromaticity of the atom in the five membered aromatic heterocyclic ring. Since pyrrolic N1 contributes two electrons to the 6π -electronic system and the other four electrons are contributed by the other four atoms, the extent of the participation of the p_z orbitals in aromaticity from the pyrrolic N1 is higher than that of the pyridinic nitrogen. Furthermore, N1 being sp^3 hybridised, the lone pair of electrons on this nitrogen is sterically more hindered by the hydrogen atom. In addition, the lone pair electrons on N1 is not available for bonding as it is incorporated in the aromatic ring system while the lone pair electrons on N2 is less hindered and more available for bonding with the platinum.

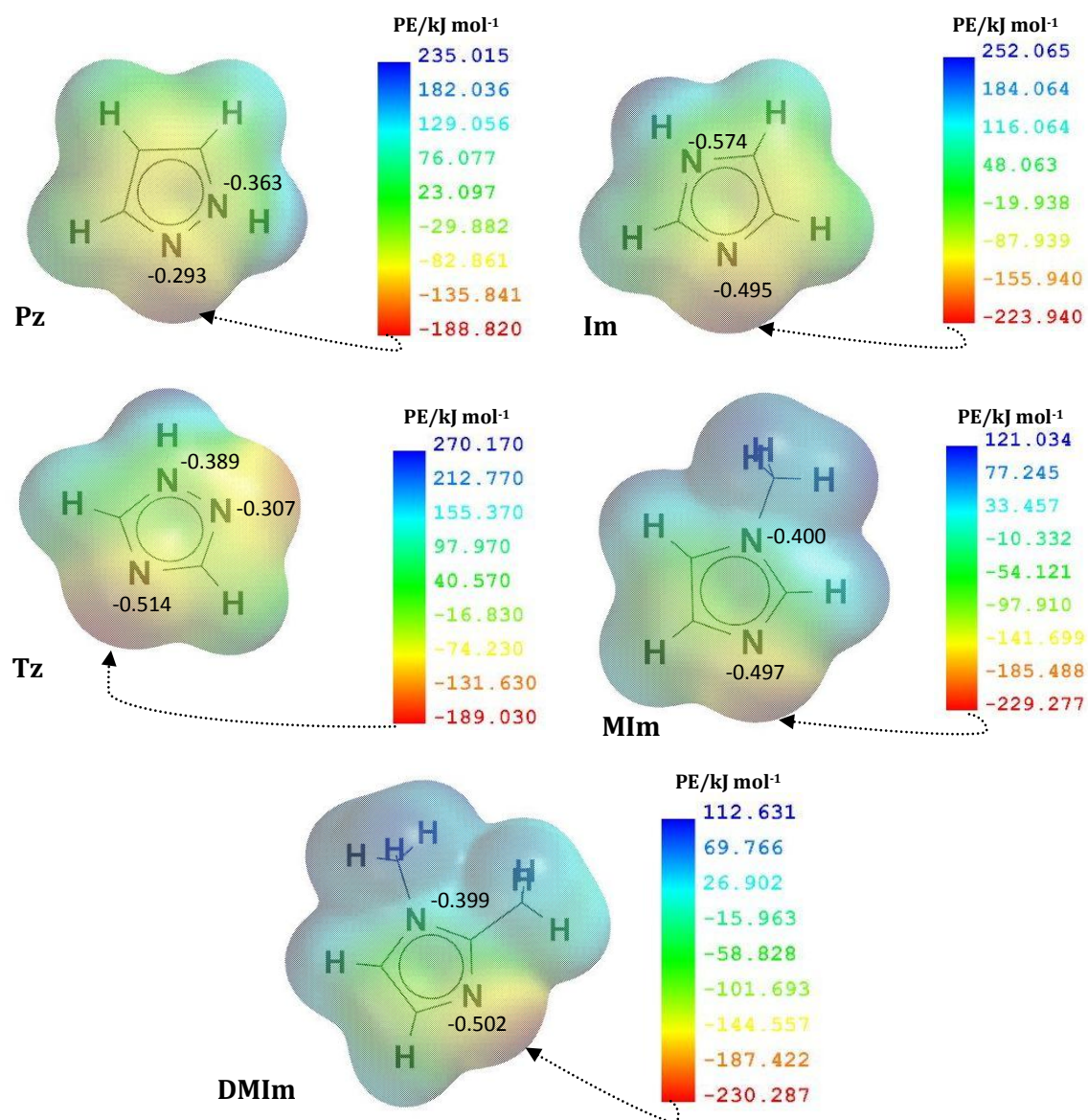
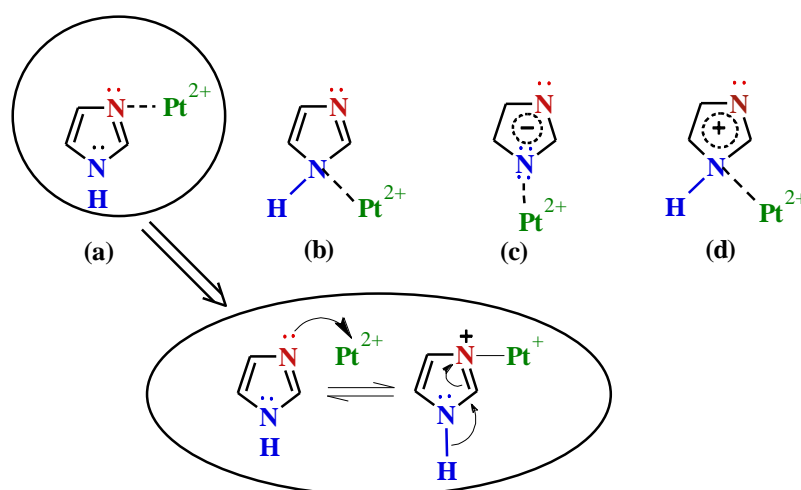


Figure 5. 15 Geometry-optimised structures of the nucleophiles investigated and distribution of the electrons on the nucleophiles. The blue area indicates the most electropositive areas and the red region indicates the most electronegative areas. Given on the diagram are the NBO charges for the nitrogen atoms and the potential energy of the electron density with respect to the electron distribution.

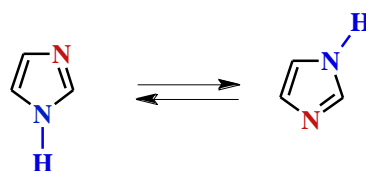
As can be seen from the optimised geometry structures of the azoles in *Figure 5.15*, the overall electron densities of **Pz** and **Im** predominantly lie on the pyridinic nitrogens (N2 and N3, respectively). Thus, in the case of **Pz**, the bonding to the platinum centre is most likely *via* N2. In solution **Pz** undergoes tautomerisation and bonding through the acidic nitrogen is also possible depending on the pH of the medium. However, experimental evidence supports the binding capabilities of 1H-pyrazole to metals *via* its basic N2.^[49, 54, 55] Furthermore, the crystal

structures obtained by Gillham^[56] for the platinum complexes, **Pt1** and **Pt3** with **Pz** further support the binding of the **Pz** ligand *via* its basic N2.

In the case of **Im**, electrophilic attack on the imidazole nitrogens result in four possible transition state structures as shown in *Scheme 5.1*. Therefore, for a neutral imidazole ligand, the binding with any of the nitrogens is possible. However, the binding with the pyrrolic nitrogen would involve the use of two electrons from the 6π -electron system which disrupts the aromaticity of the ring. This is not energetically favourable. Because of this energy barrier, the structure **(a)** (*Scheme 5.1*) is energetically favoured over the other transition-state structures.^[49] However, the acidic proton can be removed in the presence of a suitable base. A large body of experimental evidence supports the favourable coordination of **Im** to platinum *via* its basic N3.^[49-51, 55] The observed similarity between the charge densities on N1 and N3 may be due to the symmetric nature of imidazole and the attainment of tautomeric equilibrium in solution shown in *Scheme 5.2*.



Scheme 5.1 The possible resonance structures for the electrophilic attack and the possible resonance structures for the formation of energetically most favourable complex.^[49]



Scheme 5.2 Tautomeric resonance structures of imidazole.

For the *N*-methyl substituted imidazole, the lone pair of electrons on the pyrrolic nitrogen can interact with the C—H and C—C σ^* bonding of the methyl substituent.^[55] These interactions reduce the contribution from the pyrrolic nitrogen lone pair to the π -delocalised

aromatic system.^[55] The observed DFT-calculated NBO charges on N1 and N3 of 1-methylimidazole further support this explanation. Hence, in **MIm**, the charge on the pyrrolic N1 is smaller than that of pyridinic N3. When considering the binding of **MIm**, both the DFT-calculations and the experimental evidence support the potential binding of platinum to both N3 and C4^[6] (where the DFT-calculated NBO charge for N3 and C4 are equal). However, this ambiguity is ruled out in this study since the molecular structure (*Figure 4.2*) obtained for **Pt3-MIm** clearly shows the binding of N3 to the platinum centre. As expected for the sterically more hindered **DMIm**, the DFT-calculated NBO charges show a higher charge density for the N3 centre. The pyridinic nitrogen has an α -methyl group which further enhances the electron density on the N3 centre. So the metal-ligand binding is most likely to be *via* its N3 lone pair electrons. In addition, the crystal structures obtained by Gillham^[56] for **Pt1** with **MIm** and **DMIm** support the binding of the azole ligands *via* their pyridinic N3 position.

In the case of **Tz**, both N1 and N2 inductively pull their electron cloud greater than N4. The electron loss from the ring due to N2 and N4 is compensated by the mesomeric electron donation by N1. Since N1 and N2 are in the vicinal positions, the inductive pull of the electron cloud by either of them results in a smaller net negative charge on both N1 and N2 compared to N4. Both DFT-calculations and the literature findings support the binding of the ligand to the metal *via* N4 as it is the most basic centre.^[44, 46]

Catlán *et al.*^[57] have used gas phase DFT-calculated ΔG° values as a measure to demonstrate the effect of benzannulation effect on azole systems to measure their acidity or basicity in terms of their polarisability. Assuming that gas phase DFT-calculated ΔG° and potential energy (PE) have no significant difference, the PE of the azoles at the pyridinic nitrogens (See *Figure 5.15*) can be used to show the basicity of the azoles at the nitrogen centres. The lower the PE, the more stable the electron density is and the higher the nucleophilicity of the atomic centre. On this basis, a plot of DFT-calculated PE incorporated in *Figure 5.15*, against the pK_a of the azoles gave a linear fit (*Figure 5.16*). The linearity of the graph is a measure of the polarisability of the azoles.^[57]

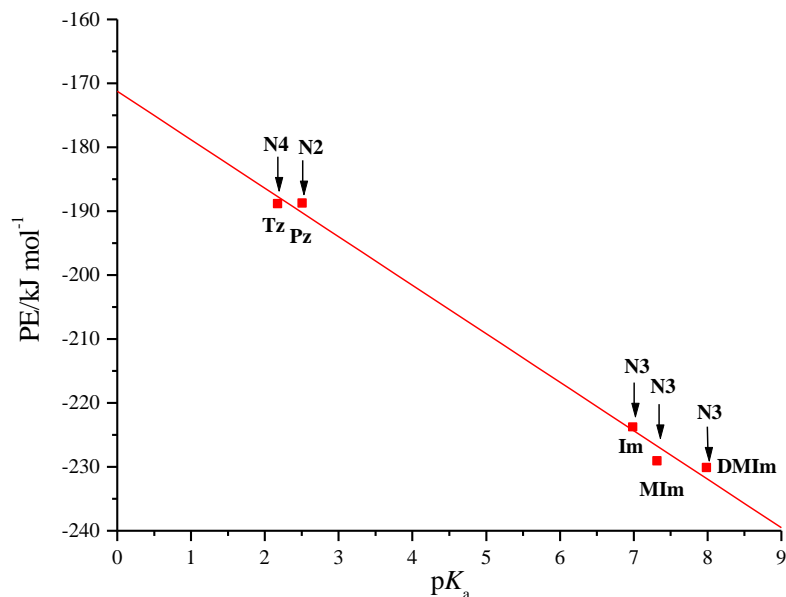


Figure 5.16 Plot of DFT-calculated potential energy at the pyridinic nitrogen centres (shown as in *Figure 5.15*) against the pK_a of the azoles.

In this case the order of the polarisability of the azoles is **DMIm** > **MIm** > **Im** > **Tz** ≈ **Pz**. The difference in PE values obtained for the pyridinic nitrogens in **DMIm** and **MIm** are very small with a difference of 1.01 kJ mol⁻¹. This value is approximately 5 times smaller for **Tz** and **Pz** with a difference of 0.21 kJ mol⁻¹. Therefore, the PE obtained for N4 and N3 respectively, for **Tz** and **Pz** are assumed to be approximately equal. This is somewhat the same as the order of the basicity (nucleophilicity) of the azoles. Except for **DMIm**, this trend agrees with the reactivity trend observed for the forward reactions with **Pz** having a slightly higher reactivity than **Tz**. However, **DMIm** does not agree with the trend even though it has the strongest polarisability or nucleophilicity. The reason is due to its high steric hindrance.

Therefore, based on the experimental evidence and the literature findings, it can be concluded that the heterocyclic N-donor nucleophiles investigated bind to the platinum centre through their basic pyridinic nitrogen *i.e.* N2, N3, N3, N3 and N4, in **Pz**, **Im**, **MIm**, **DmIm** and **Tz** respectively.

From the activation parameters in *Table 5.4*, it is evident that for the forward reactions, the substitution reactions support an associative mode of activation. The relatively large and negative entropies of activations indicate more ordered transition state complexes than either the reactants or the products. The relatively low enthalpies of activation indicate the ease of the Pt—N(azole) bond formation due to the electrophilicity of the metal centre. This associative mode of activation for the chloride substitution reactions are in agreement with

the results previously shown for the substitution reactions of square planar platinum(II) terpy complexes.^[15, 18, 26, 40, 58, 59]

5.4.2 Accounting for the Reverse Reactions

In the reverse substitution reactions, the N-donor heterocyclic ligands are replaced by the chloride ion. Except in the reactions of **Pz** and **Im** with **Pt1** and the more sterically hindered nucleophile **DMIm** with **Pt3**, **Pt4** and **Pt1**, all the other reactions followed a two term rate law, where k_{-2} represents the reverse reaction. From the k_{-2} values given in *Table 5.1*, it can be seen that the lability of the N-donor ligands in the reverse reactions are significantly lower than those of the forward reactions. The reason for the observed smaller rate of reverse reactions is because in the N-donor substituted platinum(II) complexes, the newly formed Pt—N bond is reinforced by the π -back-bonding with the platinum centre.^[9] This π -back-bonding arises due to the interactions between the π^* orbitals of the aromatic five membered ligand and the filled d orbitals of the platinum(II).^[9, 60]

The replacement of the N-donor ligands by Cl^- depends on both the basicity and the steric effect. When comparing the basicity of the leaving groups with the reactivity of the reverse step, the observed rates of reaction do not follow the expected trend observed by Ray *et al.*^[10] and Pitteri *et al.*^[39] for square planar platinum(II) complexes where the second order rate constant decreases with the increase in the basicity of the leaving group. This is because the stronger the heterocyclic base, the stronger it donates π -electrons from the ligand orbitals to the metal d -orbitals. However, it is arguable that the increase in the basicity of the leaving group would always decrease the reactivity. To explain this further, one needs to consider the steric effects of the leaving azoles, Pt—N(azole) bond lengths and the charge on the platinum(II) centre for the azole substituted complexes.

The lack of reversibility with the reactions of the platinum complexes with the sterically hindered **DMIm** may have been due to the steric congestion at the platinum centre in the transition state which disfavours the formation of the Pt—Cl bond. However, the observed reverse reaction of **DMIm** with **Pt2** might be due to the higher electrophilicity of the metal centre which pulls in the incoming nucleophile (Cl ligand) allowing the formation of the five membered trigonal bipyramidal intermediate. The NBO charges (*Table 5.12*) for the N-donor substituted complexes illustrate a higher positive charge at the platinum(II) for **Pt2**. The stronger *cis/trans* π -acceptor ligand in **Pt2** stabilizes the increased electron density in the five membered trigonal bipyramidal transition state during associative mode of ligand

substitution. Because of the *cis/trans* effect as a result of the extended π -conjugation of the phenonthriline-pyridne ring system, the electrophilicity at the metal centre was increased. This was further enhanced by the presence of a fairly less hindered and more basic ligand, **MIm**. Thus the incoming chloride ligand is strongly attracted by the platinum centre leading to the enhanced displacement of the N-donor ligands.

The DFT-calculated NBO charges for the N-donor substituted **Pt1** complexes have relatively higher electropositive platinum centres in all cases. When considered the reactivity of **Pt1**, **Pt2**, **Pt4** and **Pt3**, the observed experimental trend is in agreement with the DFT-calculated NBO charges at the platinum(II) centre. The lack of reversibility in **Pt1** might be due to the higher frontal orbital energy gap for the N-donor substituted **Pt1** complexes compared to that of **Pt2**, **Pt3** and **Pt4** (Figure 5.10). However, the HOMO-LUMO energy gaps shown in Figure 5.10 illustrate that both **Pt3** and **Pt4** have more effective π -overlapping between the π -accepting orbitals of the metal and π -donating orbitals of the ligands resulting in a smaller frontal orbital energy gap compared to that of **Pt2** and **Pt1**. The observed HOMO-LUMO energy gaps for **Pt2** from the DFT-calculations however do not follow the order of the observed experimental rates *i.e.* **Pt2** > **Pt3** > **Pt4**. The reason may be due to the ground state stabilization attained through π -back-donation from the filled metal *d* orbitals to the empty anti-bonding orbitals of the azole ligands. The stronger π -back-bonding resulted in shorter Pt—N bonds compared to that of Pt—Cl.

By using Equation 5.2, one can therefore correlate the variation of the DFT-calculated ground state Pt—N(azole) bond lengths to the pK_a of the leaving azoles in order to establish the extent of π -back-bonding between platinum(II) and the azoles. A linear relationship was obtained for the plots of $r_{\text{Pt-N}}$ against the pK_a of the respective azoles (Figure 5.17). This relationship normally describes the energetic contributions to the formation and breaking of bonds and to the free-energy of activation, and is characteristic of square planar d^8 metal centres such as gold(III).^[21] Since gold(III) and platinum(II) form low-spin d^8 complexes, the same relationship can be applied for platinum(II) as well.

[†] r is the Pt—N bond lengths (N = N2, N4, N3, N3 and N3 for **Pz**, **Tz**, **Im**, **MIm** and **DMIm** respectively).

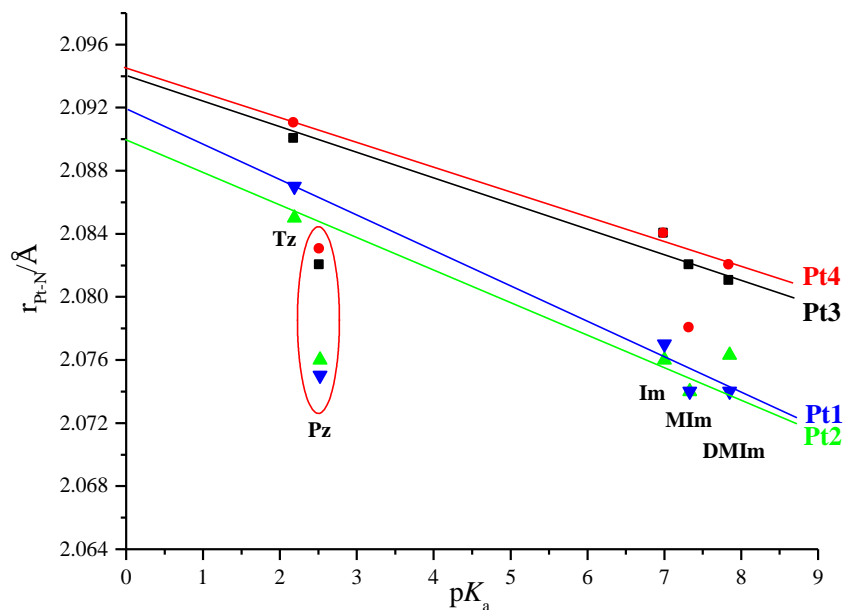


Figure 5.17 Plots for the DFT-calculated $r_{\text{Pt-N}}$ bond lengths against the $\text{p}K_{\text{a}}$ of the leaving groups for the replacement of azole by chloride.

The observed linearity is comparable to those obtained for other N-donor five membered substituted d^8 low spin metal complexes of gold(III).^[21] The slope of this linear fit is a measure of the metal centre to discriminate the nucleophiles.^[21] In other words it is a measure of electrophilicity of the metal centre. The plots of $r_{\text{Pt-N}}$ against the $\text{p}K_{\text{a}}$ gave expected linear fits for the replacement of azole ligands by chloride from **Pt1**, **Pt2**, **Pt3** and **Pt4**, and the free-energy relationships derived were $r_{\text{Pt-N}} = ((-2.29 \pm 0.25) \times 10^{-3})\text{p}K_{\text{a}} + 2.092 \pm 1.60 \times 10^{-3}$, $r_{\text{Pt-N}} = ((-2.02 \pm 0.23) \times 10^{-3})\text{p}K_{\text{a}} + 2.089 \pm 1.39 \times 10^{-3}$, $r_{\text{Pt-N}} = ((-1.55 \pm 0.06) \times 10^{-3})\text{p}K_{\text{a}} + 2.093 \pm 4.02 \times 10^{-5}$ and $r_{\text{Pt-N}} = ((-1.52 \pm 0.08) \times 10^{-3})\text{p}K_{\text{a}} + 2.094 \pm 4.91 \times 10^{-5}$ respectively. As can be seen from the slopes, the increase of electron density on the platinum(II) centre in **Pt3** is slightly higher than that of **Pt4**. It is also evident that **Pt2** and **Pt1** have greater electrophilicity as shown by the higher value of the slope of LFER. From the graph, the observed trend for the increase in the electrophilicity of the N-donor substituted metal centres is **Pt1** > **Pt2** > **Pt3** > **Pt4** and agrees with the trend obtained for the NBO charges given in *Table 5.12* for the N-donor substituted complexes. The observed experimental trend for the reverse reactivity fairly agrees with this trend for **Pt2** > **Pt3** > **Pt4**.

The increased electron density at the metal centre is due to the σ -donation from the azole ligands to the metal centre and may directly or indirectly influence the Pt—N bond length. Once coordinated with the azole ligand, inductive σ -donation affects the charge on the metal centre. The positive platinum centre pulls the ligand electron cloud towards the metal centre

and reduces the electron density on the pyrrolic nitrogen. This σ inductive effect drops-off with the increasing distance from the ionisable proton of the azole to the metal centre.^[46] Based on this concept, one would therefore expect the σ -donation to be more pronounced for platinum complexes with **Pz** compared to the other azole ligands studied. Thus the DFT-calculated Pt—N bond lengths for **Pz** substituted complexes are significantly shorter as seen in *Figure 5.17*.

The observed reverse reactivity is governed by not only the basicity of the leaving group but also the nature of the leaving group. The rate of replacement of the azole ligands by the chloride from the *N*-substituted complexes depends on the ground state Pt—N(azole) bond strength which is governed by the interactions between the ground state π^* orbitals of the azole ligands and the $5d$ orbitals of the platinum centre.^[21] These interactions stabilise the ground state *N*-donor substituted platinum complexes by π -back-donation from the filled $5d_{xz}$ and $5d_{yz}$ orbitals of the platinum centre to the anti-bonding orbitals of the azole ligand.^[21] The consequences of this π -back-donation result in the enforcement of Pt—N(azole) bond^[9] leading to a slower reactivity. In addition, since pyrazoles and imidazoles are π -excessive systems, LMCT interactions (including π -donations from the azole to the metal) can influence the strength of Pt—N(azole) bond. However, the Pt—N(azole) bond strengthening depends on the basicity of the azole. For this particular type of aromatic nucleophiles, the lower the pK_a , the smaller the σ -donation from the azole to the platinum centre, and the greater the π -acceptor property of the azole ligand (*Figure 5.18*). Hence, a stronger Pt—N bond results with an accompanying slower replacement of the azole ligand by the chloride. This explains the observed slower reverse rates of reaction for **Tz** and the observed fastest reverse reactivity of **MIm** followed by **Im** or **Pz** with the platinum complexes.

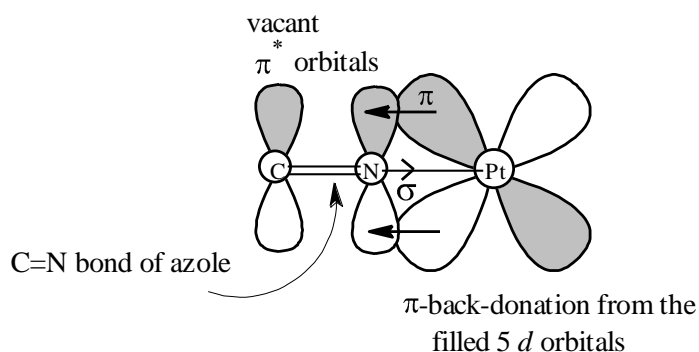


Figure 5.18 Movement of electrons from the filled $5d$ orbitals of platinum to the antibonding orbitals of the azole ligand and the π , σ -donation from azole to the platinum centre in the ground state.

Therefore, in the rate determining transition state the Pt—N bond is only partially weakened while the Pt—Cl bond is formed to a greater extent. As a result, we can conclude that the observed reverse reactivities are controlled by the extent of π -back-bonding between the $5d_{xz}$ and $5d_{yz}$ orbitals of the platinum centre and the π -accepting anti-bonding orbitals of the azole in the ground state.

The observed activation parameters for the reverse reactions support an associative mode of mechanism. The positive entropies of activation for **Pt2** and **Pt1** are due to the intrinsic error associated with the determination of the values.^[61]

5.5. References

1. G. Annibale, M. Brandolisio and B. Pitteri, *Polyhedron*, **1995**, *14*, 451.
2. D. Reddy *PhD Thesis, Tuning Reactivity of Platinum(II) Complexes, University of Natal, Pietermaritzburg, RSA*, **2009**, pp. 104, 138-139.
3. F. Kröhnke, *Synthesis*, **1976**, 1-24.
4. C. O. Dietrich-Buchecker, P. A. Marnot and J. P. Sauvage, *Tetrahedron Lett.*, **1982**, *23*, 5291.
5. P. Y. Bruice, *Organic Chemistry*, 4th Ed., Pearson Prentice Hall, California, **2004**, p. 551-558.
6. J. Müller, E. Freisinger, P. Lax, D. A. Megger and F. Polonius, -A., *Inorg. Chim. Acta.*, **2007**, *360*, 255.
7. J. S. Field, R. J. Haines, D. R. McMillin and G. C. Summerton, *J. Chem. Soc., Dalton Trans.*, **2002**, 1369-1376.
8. J. S. Field, J. A. Gertenbach, R. J. Haines, L. P. Ledwaba, N. T. Mashapa, D. R. McMillin, O. Q. Munro and G. C. Summerton, *Dalton Trans.*, **2003**, 1176.
9. B. Pitteri and M. Bortoluzzi, *Polyhedron*, **2006**, *25*, 2698.
10. M. Ray, S. Bhattacharya and P. Banerjee, *Polyhedron*, **1999**, *18*, 1569.
11. B. Pitteri, G. Marangoni, F. V. Visentin, L. Cattalini and T. Bobbo, *Polyhedron*, **1997**, *17*, 475.
12. J. D. Atwood, *Inorganic and Organic Reaction Mechanisms*, 2nd Ed., Wiley- VCH Inc., New York, **1997**, p. 43-46.
13. *Hyper Chem Pro 6.03*, Hypercube, Inc., Gainesville, FL, **2000**.
14. *Conquest version 1.9*, Cambridge Crystallographic Data Centre, Cambridge, UK, **2006**.
15. D. Jaganyi, K. L. de Boer, J. Gertenbach and J. Perils, *Int. J. Chem. Kinet.*, **2008**, *40*, 809.
16. J. J. Moore, J. J. Nash, P. E. Fanwick and D. R. McMillin, *Inorg. Chem.*, **2002**, *41*, 6387.
17. G. C. Summerton, *PhD Thesis, Solid State Structures and Photophysical Properties of Polypyridyl Complexes of platinum(II), University of Natal, Pietermaritzburg, RSA*, **1997**, pp. 23-25, 70-75, 153-154.
18. A. Hofmann, D. Jaganyi, O. Q. Munro, G. Liehr and R. van Eldik, *Inorg. Chem.*, **2003**, *42*, 1688.
19. D. Jaganyi, A. Hofmann and R. van Eldik, *Angew. Chem. Int. Ed. Engl.*, **2001**, *40*, 1680-1683.
20. R. Romeo, Plutino.M.R, L. M. Scolaro, S. Stoccoro and G. Minghetti, *Inorg. Chem.*, **2000**, *39*, 4749-4755.
21. B. Pitteri and M. Bortoluzzi, *Eur. J. Inorg. Chem.*, **2007**, *28*, 4456.

22. T. K. Aldridge, E. M. Stacy and D. R. McMillin, *Inorg. Chem.*, **1994**, *33*, 722.
23. C. R. Hecker, P. E. Fanwick and D. R. McMillin, *Inorg. Chem.*, **1991**, *30*, 659.
24. Y. Hu, M. H. Wilson, R. Zong, C. Bonnefous, D. R. McMillin and R. P. Thummel, *Dalton Trans.*, **2005**, 354-358.
25. D. Jaganyi, D. Reddy, J. A. Gertenbach, A. Hofmann and R. van Eldik, *Dalton Trans.*, **2004**, 299.
26. D. Reddy and D. Jaganyi, *Dalton Trans.*, **2008**, 6724.
27. C. A. Carr, J. M. Richards, S. A. Ross and G. Lowe, *J. Chem. Research (S)*, **2000**, *12*, 566.
28. C.-Y. Hung, T.-L. Wang, Y. Jang, W. Y. Kim, R. H. Schmehl and R. P. Thummel, *Inorg. Chem.*, **1996**, *35*, 5953.
29. S. Otto and L. I. Elding, *J. Chem. Soc., Dalton Trans.*, **2002**, 2354.
30. C. J. Jones and J. R. Thornback, *Medicinal Applications of Coordination Chemistry*, Royal Society of Chemistry, Cambridge, **2007**, p. 92-95.
31. A. Hofmann, L. Dahlenburg and R. van Eldik, *Inorg. Chem.*, **2003**, *42*, 6528.
32. D. R. McMillin and J. J. Moore, *Coord. Chem. Rev.*, **2002**, *229*, 113.
33. J. S. Field, J. Gertenbach, R. J. Haines, O. Q. Munro and D. R. McMillin, *Zeitschrift für Naturforschung*, **2007**, *62b*, 447.
34. R. Buchner, C. T. Cunningham, J. S. field, R. J. Haines, D. R. McMillin and G. C. Summerton, *J. Chem. Soc., Dalton Trans.*, **1999**, 711.
35. J. F. Michalec, S. A. Bejune, D. G. Cuttell, G. C. Summerton, J. A. Gertenbach, J. S. Field, R. J. Haines and D. R. McMillin, *Inorg. Chem.*, **2001**, *40*, 2193.
36. S. E. Hobert, J. T. Carney and S. D. Cummings, *Inorg. Chem. Acta*, **2001**, *318*, 89.
37. M. H. Wilson, L. P. Ledwaba, J. S. Field and D. R. McMillin, *J. Chem. Soc., Dalton Trans.*, **2005**, 2754.
38. M. Bellicini, L. Cattalini, G. Marangoni and B. Pitteri, *J. Chem. Soc. Dalton Trans.*, **1994**, 1805.
39. B. Pitteri, G. Marangoni, L. Cattalini, F. Visentin, V. Bertolasi and P. Gilli, *Polyhedron*, **2001**, *20*, 869.
40. C. F. Weber and R. van Eldik, *Eur. J. Inorg. Chem.*, **2005**, *23*, 4755
41. Z. D. Bugarcic, B. Petrovic and E. Zangrando, *Inorg. Chim. Acta*, **2004**, *357*, 2650.
42. B. Pitteri, G. Marangoni and L. Cattalini, *J. Chem. Soc. Dalton Trans.*, **1994**, 3539.
43. A. Ohno, M. Ogawa, Y. Mikata and M. Goto, *Bull. Chem. Soc. Jpn.*, **1990**, *63*, 813.
44. T. Eicher and S. Hauptmann, *The Chemistry of Heterocycles*, Wiley-VCH Verlag GmbH & Co. KGaA, Weinheim, **2003**, p. 165-173, 179-184, 208-212.
45. S. L. Newmyer and P. R. O. de Montellano, *J. Biol. Chem.*, **1996**, *271*, 14891.
46. C. R. Johnson, W. W. Henderson and R. E. Shepherd, *Inorg. Chem.*, **1984**, *23*, 2754.

47. J. Catalán and J. Elguero, *J. Chem. Soc. Parkin Trans.II.*, **1983**, 1869.
48. P. Bruno and M. Bortoluzzi, *Polyhedron*, **25**, 2698.
49. A. R. Katritzky and C. W. Rees, *Comprehensive Heterocyclic Chemistry: The Structure, Reactions, Synthesis and uses of Heterocyclic Compounds*, (Ed. K. T. Potts), Pergamon Press, New York, **1984**, pp. 168-189, 217-230, 345-358, 362- 394, 734-790.
50. S. D. Cummings, *Coord. Chem. Rev.*, **2009**, *253*, 1495.
51. E. M. A. Ratilla, H. M. Brothers II and N. M. Kostic, *J. Am. Chem. Soc.*, **1987**, *109*, 4592.
52. A. W. RoszaK, O. Clement and E. Buncel, *Acta Cryst.*, **1996**, *C52*, 1645.
53. V. E. Matulis, Y. S. Halauko, O. A. Ivashkevich and P. N. Gaponik, *J. Mol. Struct.*, **2009**, *909*, 19.
54. M. A. Halcrow, *Dalton Trans.*, **2009**, 2059.
55. G. Albertin, S. Antoniutti, J. Castro, S. Garcia-Fontán and E. Gurabardhi, *J. Organomet. Chem.*, **2006**, *691*, 1012.
56. K. J. Gillham, *MSc Thesis, (Unpublished Results), A Detailed Kinetic and Mechanistic Investigation into the Rate of Chloride Substitution from Chloro Terpyridine Platinum(II) and Analogous Complexes by a Series of Azole Nucleophiles, University of Natal, Pietermaritzburg, RSA*, **2010**.
57. J. Catalán, J. Palomar and J. L. G. de Paz, *Int. J. Mass Spectrom. Ion Processes.*, **1998**, *175*, 51.
58. D. Jaganyi and F. Tiba, *Trans. Met. Chem.*, **2003**, *28*, 803.
59. R. van Eldik, T. Asano and W. J. Le Noble, *Chem. Rev.*, **1989**, *89*, 549.
60. A. Cornia, A. C. Febretti, M. Bonivento and L. Cattalini, *Inorg. Chim. Acta*, **1997**, *225*, 405.
61. A. Hofmann and R. van Eldik, *Dalton Trans.*, **2003**, 2979.

Chapter 6

Conclusions and Future Work

6.1 Conclusion

In the present study we have investigated the effect of increasing the extended π -conjugation in the *cis* and the *cis/trans* position of the terpy moiety on the rate of chloride substitution from a series of platinum(II) complexes. As expected the increase in the extent of π -back-bonding chelate through ancillary substitution in **Pt3** in comparison to **Pt1** decreased the reactivity of the metal centre by decreasing the π -acceptor ability of the ligand.^[1, 2]

The rate of chloride substitution has increased in **Pt2** with the increase in the π -conjugation of the chelate backbone within the *cis/trans* position. This increase in the π -back-bonding ability of the chelate backbone makes the platinum centre more electrophilic. Thus the rate of ligand substitutions was accelerated.

However, when compared the reactivity of **Pt3** and **Pt4**, the present results reveal that the increase in the π -conjugation in one of the *cis* positions of the chelate backbone in **Pt4** decreases the π -acceptor ability of the chelate backbone. The stronger *cis* σ -effect^[3] of the isoquinoline ring in **Pt4** dominates over the π -acceptor ability of the ligand and reduces the electrophilicity of the metal centre leading to a slower reactivity.

The observed reactivity trend for the forward reaction was **Pt2** > **Pt1** > **Pt3** > **Pt4**. The observed trend was further supported by the computational analysis done for the complexes. From the DFT-calculations, it was clear that a considerable amount of HOMO electrons of **Pt2** are located on the chelate backbone while the HOMO electrons of **Pt4** are entirely concentrated on the platinum centre.

The rate of substitution is also influenced by the basicity of the entering N-donor heterocyclic nucleophiles giving rise to a LFER for the less hindered nucleophiles which is expected of associative mechanisms.^[4, 5] The reactivity of the N-donor heterocycles was increased with the increase in the basicity for the sterically less hindered azoles. The observed reactivity trend for the chloride substitution by the azoles studied followed the trend, **MIm** > **Im** > **DMIIm** > **Pz** > **Tz**. The observed activation parameters further support the associative mode of the reaction mechanisms observed.

In the reverse reactions, the rate or the replacement of the azoles by the chloride ligand is controlled by the extent of π -back-bonding between the $5d_{xz}$ and $5d_{yz}$ orbitals of the platinum centre and the antibonding orbitals of the azoles. The observed smaller rate constants for the reverse reactions were due to the relative stability and stronger Pt—N(azole) bond resulted from the π -back-bonding between the metal centre and the π^* orbitals of the azoles.

6.2 Future Work

In the current study, the effect of increasing the π -conjugation in the *cis* and *cis/trans* position to the substitution of the chloride ligands was studied. However, there is still much more that need be done to understand the mechanistic and kinetic behaviour of these complexes in biological systems.

Firstly, the complexes can be studied over a pH range, especially around the physiological pH and temperature. This would help to understand the kinetic behaviour of the complexes in biological environments.

Secondly, since platinum(II) terpy,^[6-13] polypyridyl and 1,10-phenanthroline^[7, 14] complexes are biologically active, the kinetic behaviour and the selective binding of the complexes to DNA can be studied in order to understand the pharmaceutical importance of the complexes. Since the kinetics of platinum(II) complexes with biologically active ligands are of research interest,^[15] the substitution reactions of the platinum(II) complexes can also be studied using biologically active nucleophiles such as histidine at physiological pH and temperature. The kinetic and the mechanistic information obtained from such studies may contribute to the design and development of effective platinum(II) antitumor drugs.

Furthermore, increased water solubility of platinum(II) anticancer drugs has been one of the key research interests in the pharmaceutical industry. Since the chloride platinum(II) complexes are less water soluble than the aqua complexes,^[16] a lot of ongoing research is focused on the kinetics of hydrolysis^[17] and aqua ligand substitution of the platinum(II) systems.^[18] Therefore, the kinetics of the aqua platinum(II) complexes with nucleophiles would give an important insight to elucidate the anticancer activity of the platinum(II) complexes investigated.^[19, 20] Since, a considerable kinetic research is focused on the basicity of the incoming nucleophiles,^[4, 18, 21-23] the study of kinetic behaviour of the platinum(II) complexes and nucleophiles in an aqueous medium would become increasingly significant.

6.3 Supporting Information

Supporting Information is available in the compact CD attached to the inside back cover of this dissertation. This includes the data for X-ray single crystal structure determination as CIF files and the fid files of the NMR spectra.

6.4 References

1. D. Jaganyi, D. Reddy, J. A. Gertenbach, A. Hofmann and R. van Eldik, *Dalton Trans.*, **2004**, 299.
2. D. Jaganyi, K. L. de Boer, J. Gertenbach and J. Perils, *Int. J. Chem. Kinet.*, **2008**, *40*, 809.
3. A. Hofmann, L. Dahlenburg and R. van Eldik, *Inorg. Chem.*, **2003**, *42*, 6528.
4. B. Pitteri and M. Bortoluzzi, *Polyhedron*, **2006**, *25*, 2698.
5. B. Pitteri and M. Bortoluzzi, *Eur. J. Inorg. Chem.*, **2007**, *28*, 4456.
6. S. C. Cummings, *Coord. Chem. Rev.*, **2009**, *253*, 1495.
7. D.-L. Ma, C.-M. Che and S.-C. Yan, *J. Am. Chem. Soc.*, **2009**, *131*, 1835.
8. G. Lowe, A. S. Droz, T. Vilaivan, G. W. Weaver, L. Tweedale, J. M. Pratt, P. Rock, V. Yardley and S. L. Croft, *J. Med. Chem.*, **1999**, *42*, 999.
9. G. Lowe, J. A. McCloskey, J. Ni and T. Vilaivan, *Bioorg. Med. Chem.*, **1996**, *4*, 1007.
10. C. S. Peyratout, T. K. Aldridge, D. K. Crites and D. R. McMillin, *Inorg. Chem.* **1995**, *34*, 4484.
11. S. Bonse, J. M. Richards, S. A. Ross, G. Lowe and R. L. Krauth-Siegel, *J. Med. Chem.*, **2000**, *43*, 4812.
12. A. McCoubrey, H. C. Latham, P. R. Cook, A. Rodger and G. Lowe, *FEBS Lett.*, **1996**, *380*, 73.
13. W. D. McFadyen, L. P. G. Wakelin, I. A. G. Roos and B. L. Hillcoat, *J. Biochem.*, **1987**, *242*, 177.
14. N. J. Wheate, R. I. Talen, A. M. Krause-Heuer, R. L. Cook, S. Wang, V. J. Higgins and J. R. Aldrich-Wright, *Dalton Trans.*, **2007**, 5055.
15. P. S. Sengupta, R. Sinha and G. S. De, *Transition Met. Chem.*, **2001**, *26*, 638.
16. E. Wong and C. M. Giandomenico, *Chem. Rev.*, **1999**, *99*, 2451.
17. L. A. S. Costa, W. R. Rocha, W. B. De Almeida and H. F. Dos Santos, *Chem. Phys. Lett.*, **2004**, *387*, 182.
18. Z. D. Bugarcic, S. T. Nandibewoor, M. S. A. Hamza, F. Heinemann and R. van Eldik, *Dalton Trans.*, **2006**, 2984.
19. P. S. Sengupta, S. Ghosh and G. S. De, *Transition Met. Chem.*, **2000**, 25.
20. P. S. Sengupta, R. Sinha and G. S. De, *Ind. J. Chem. Sect. A*, **2001**, *40A*, 509.
21. B. Pitteri, G. Marangoni, L. Cattalini, F. Visentin, V. Bertolasi and P. Gilli, *Polyhedron*, **2001**, *20*, 869.
22. B. Pitteri, G. Marangoni and L. Cattalini, *J. Chem. Soc. Dalton Trans.*, **1994**, 3539.
23. M. Bellicini, L. Cattalini, G. Marangoni and B. Pitteri, *J. Chem. Soc. Dalton Trans.*, **1994**, 1805.

Appendix A- Selected Spectra for the Platinum(II) Complexes Synthesised

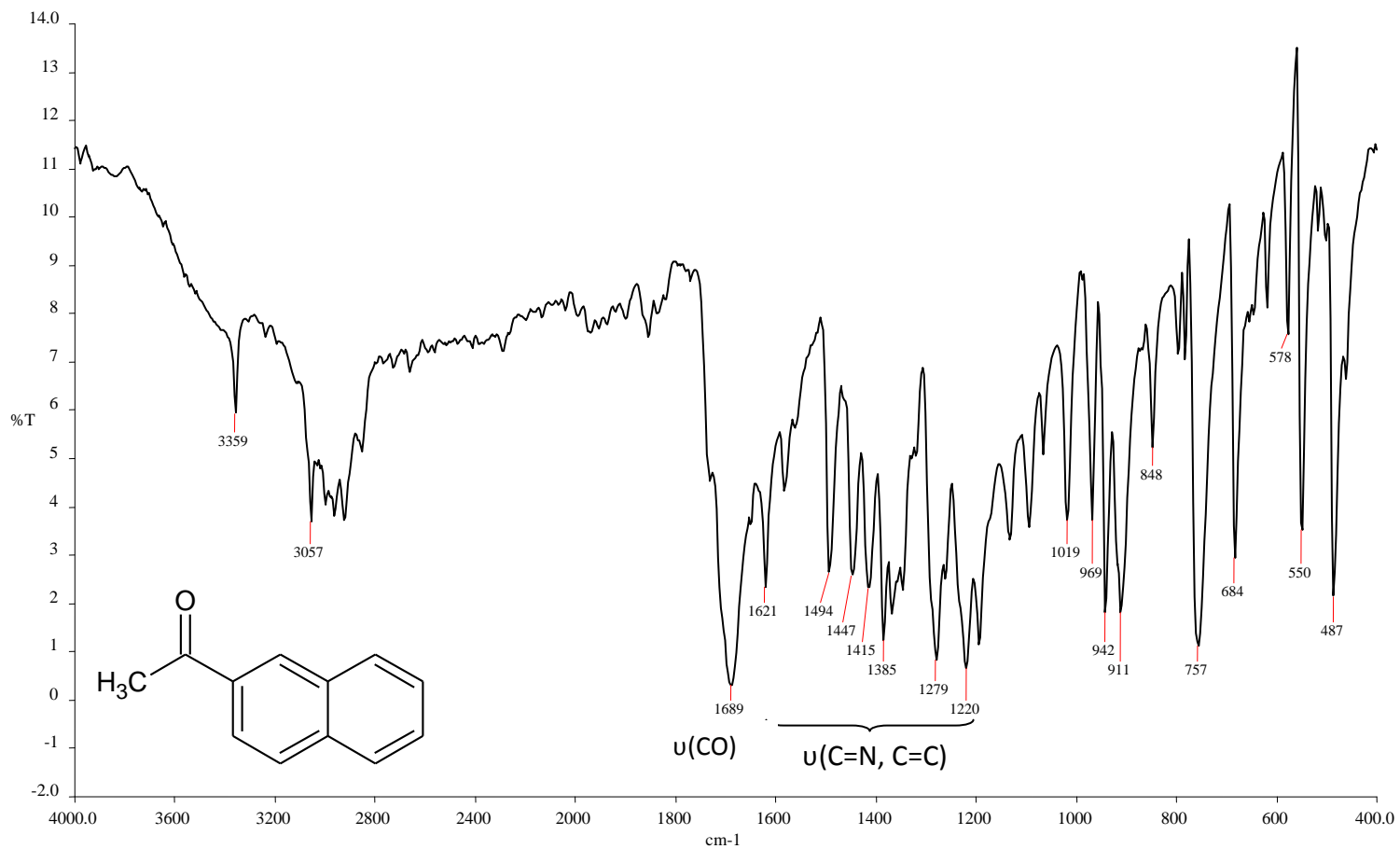


Figure A 1 IR Spectrum of 3-acetyloquinoline recorded as a KBr disc.

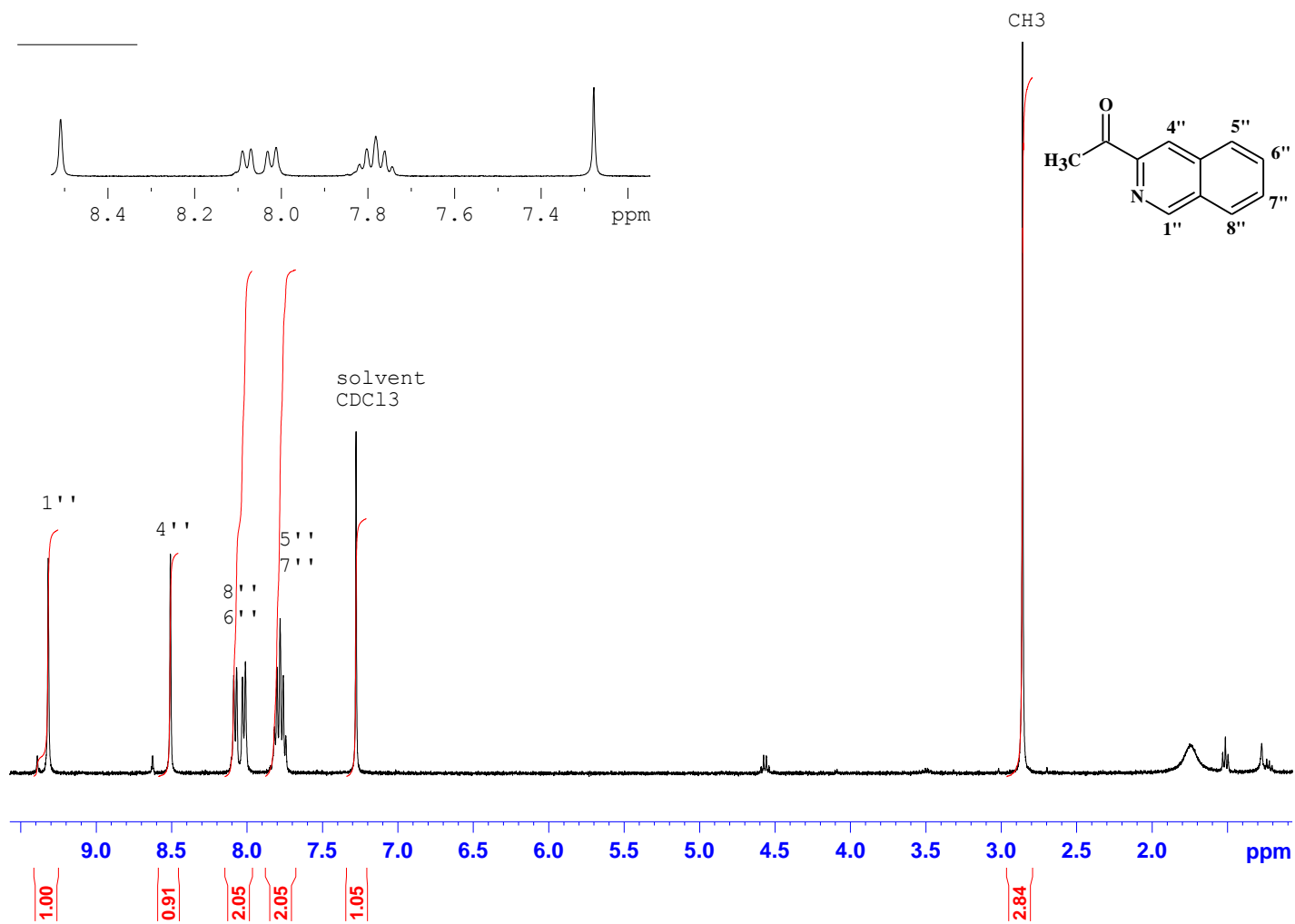


Figure A 2 ^1H NMR spectrum of 3-acetylisoquinoline in deuterated chloroform.

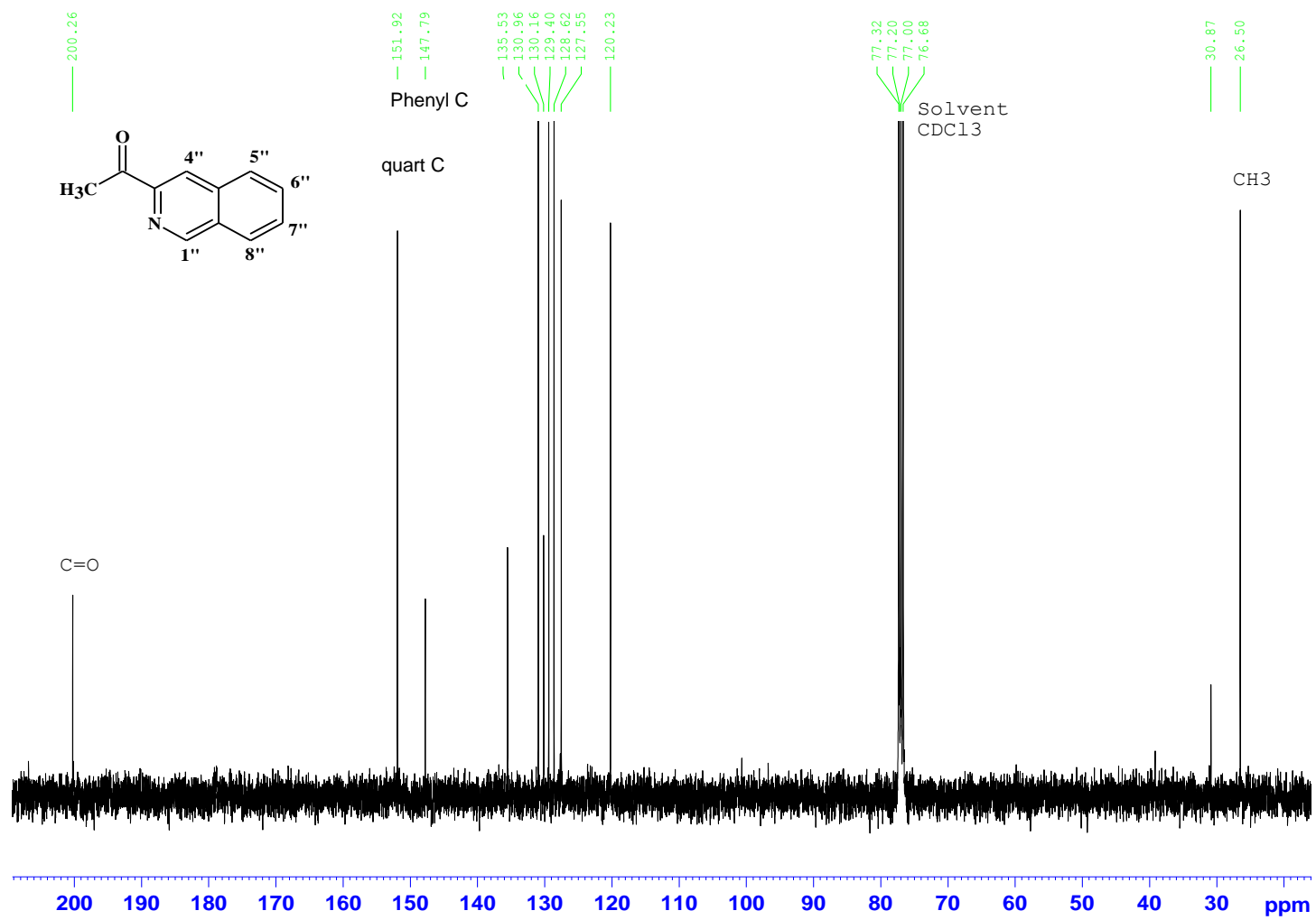


Figure A 3 ^{13}C NMR spectrum of 3-acetyloquinoline in deuterated chloroform.

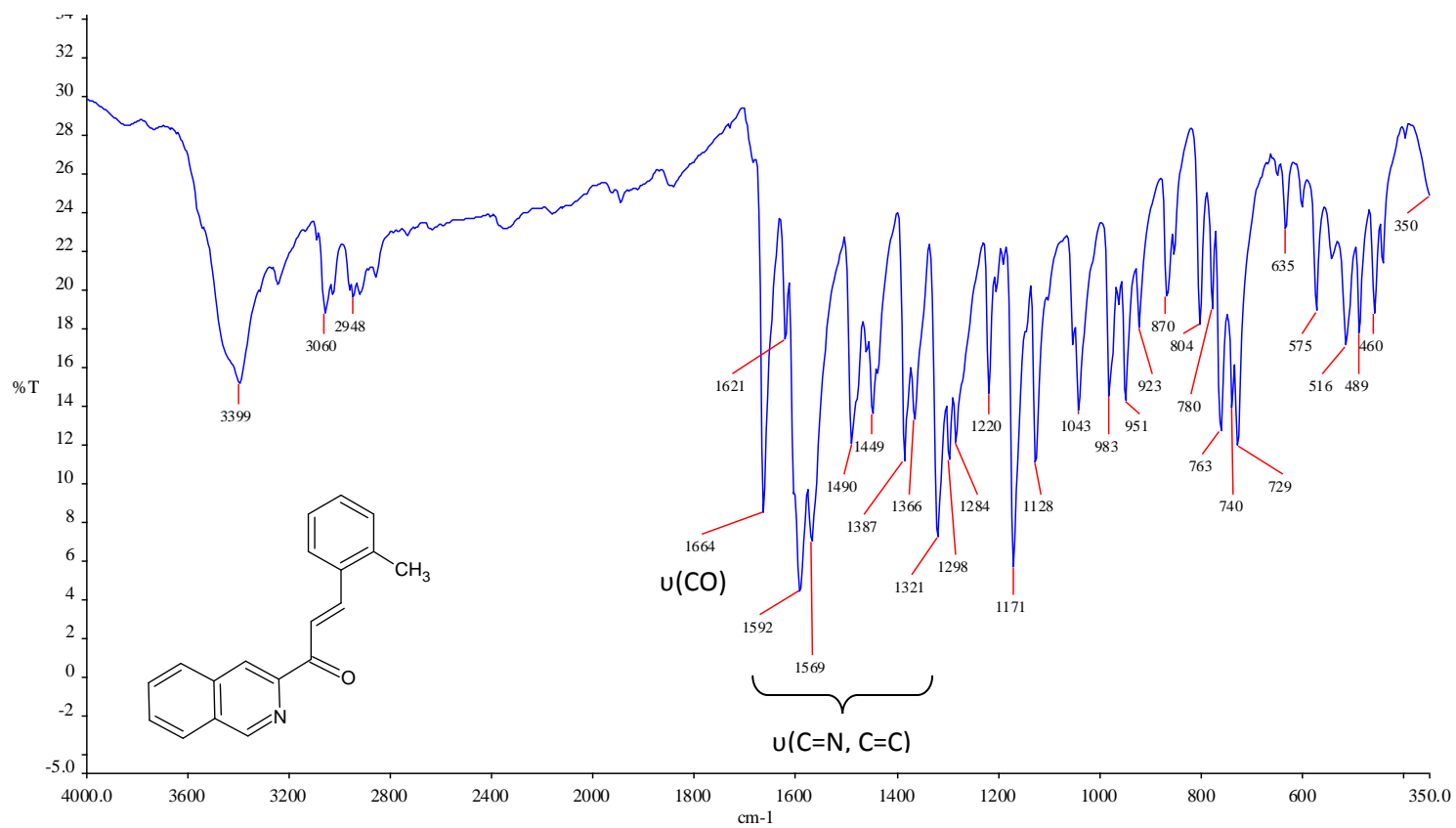


Figure A 4 IR Spectrum of 1-(3'-isoquinoyl)-3-(o-tolyl)-prop-2-en-1-one recorded as a KBr disc.

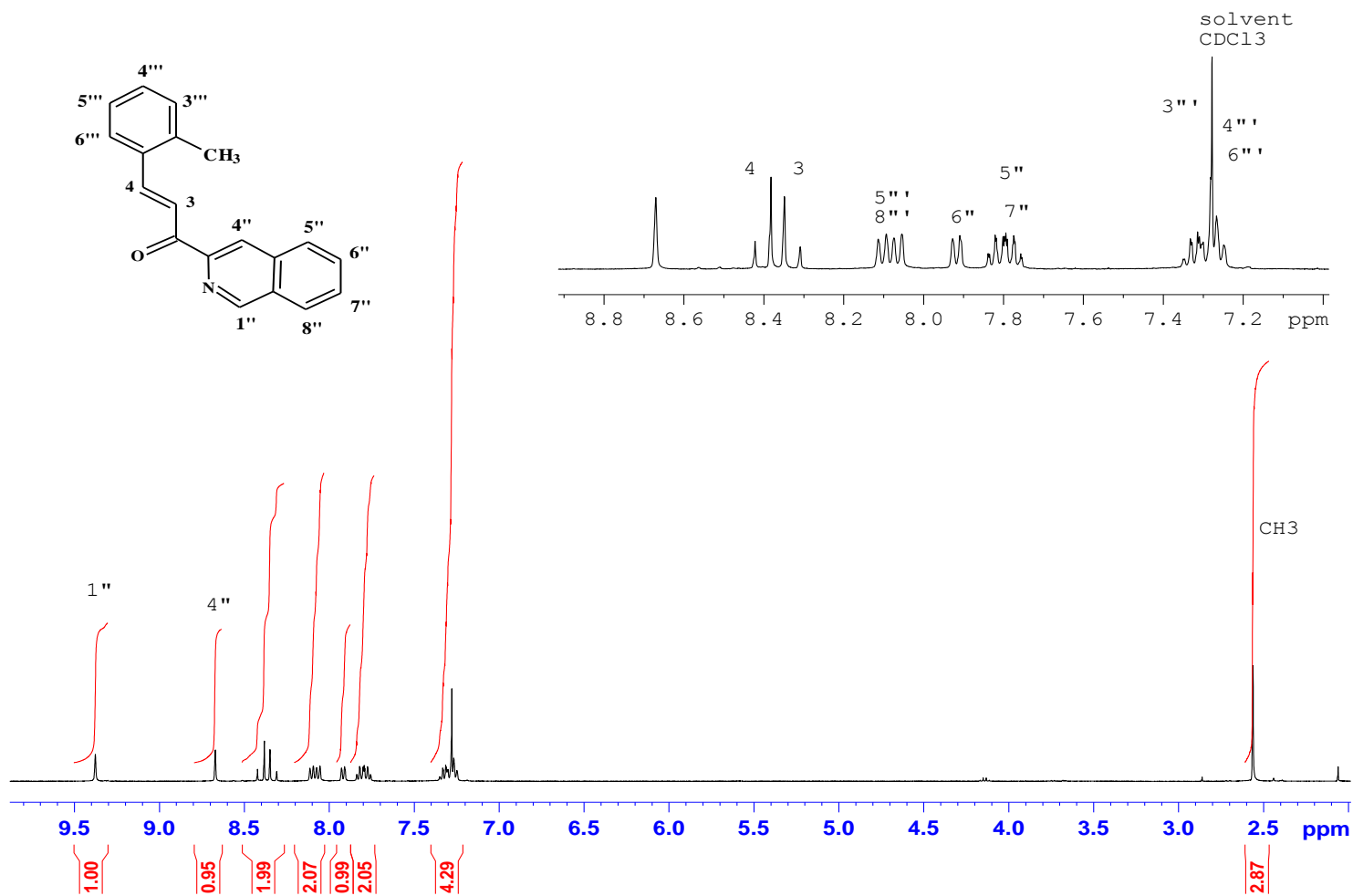


Figure A 5 ¹H NMR spectrum of 1-(3'-isoquinoly)-3-(o-tolyl)-prop-2-en-1-one.

Elemental Composition Report

Page 1

Single Mass Analysis

Tolerance = 5.0 PPM / DBE: min = -1.5, max = 50.0

Element prediction: Off

Number of isotope peaks used for i-FIT = 3

Monoisotopic Mass, Even Electron Ions

10 formula(e) evaluated with 1 results within limits (all results (up to 1000) for each mass)

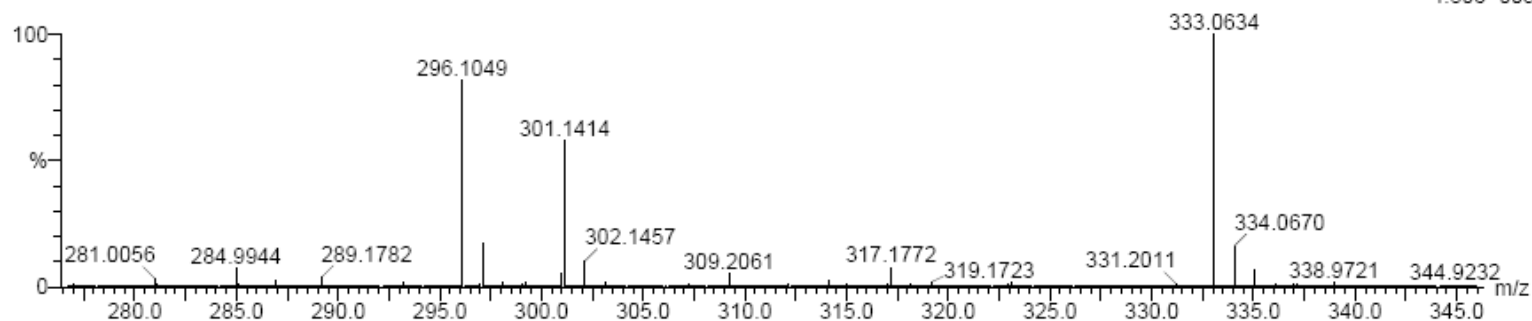
Elements Used:

C: 15-20 H: 10-20 N: 0-2 O: 0-2 Na: 0-1

Aishath Shaira

QR201 21 (0.341) Cm (1:60)

TOF MS ES+
4.80e+005



Minimum: -1.5
Maximum: 5.0 5.0 50.0

| Mass | Calc. Mass | mDa | PPM | DBE | i-FIT | i-FIT (Norm) | Formula |
|----------|------------|------|------|------|-------|--------------|----------------|
| 296.1049 | 296.1051 | -0.2 | -0.7 | 12.5 | 616.5 | 0.0 | C19 H15 N O Na |

Figure A 6 Mass spectrum of 1-(3'-isoquinolyl)-3-(o-tolyl)-prop-2-en-1-one.

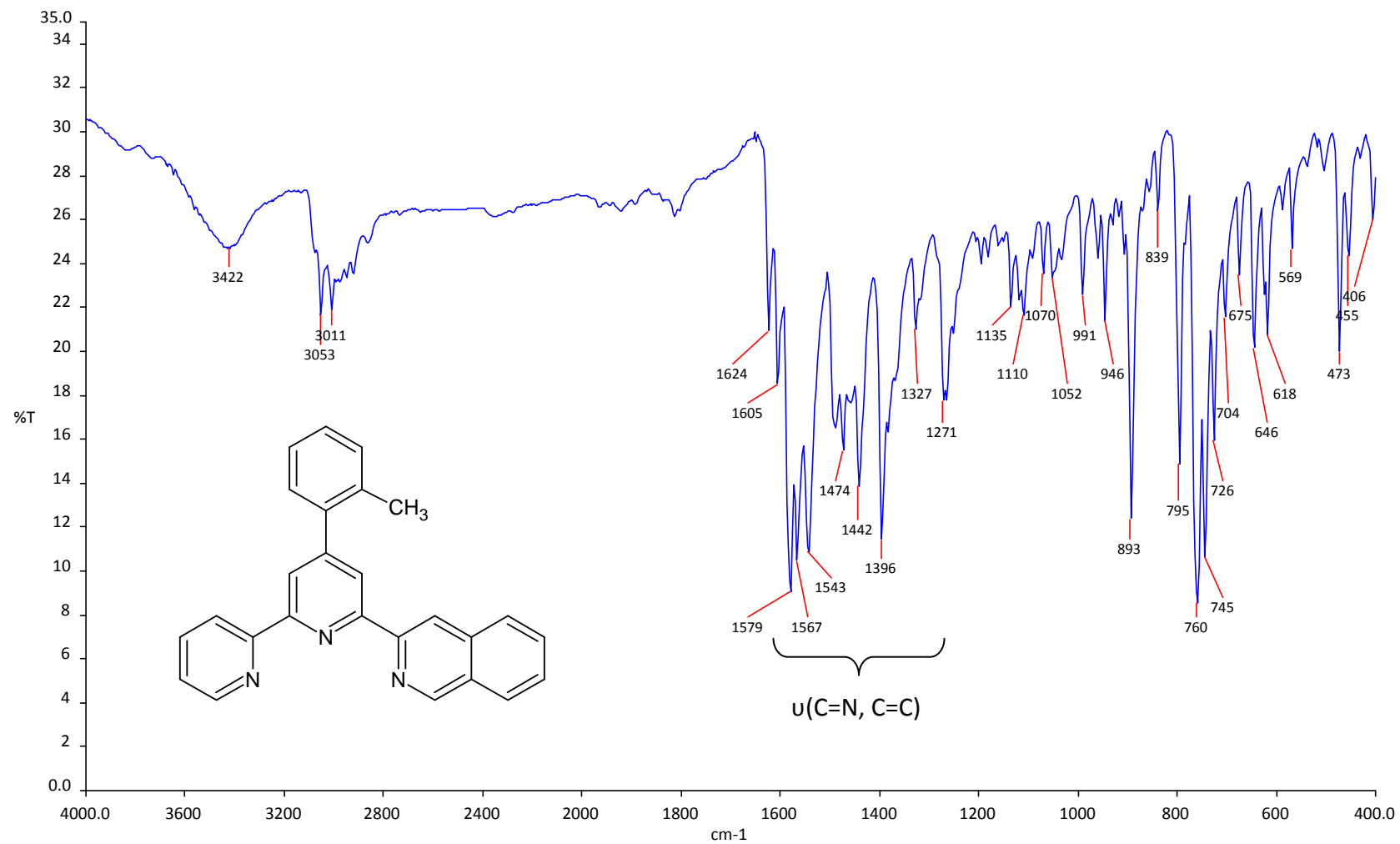


Figure A 7 IR Spectrum of 4-(o-tolyl)-6-(3'-isoquinoyl)-2,2'-bipyridine recorded as a KBr disc.

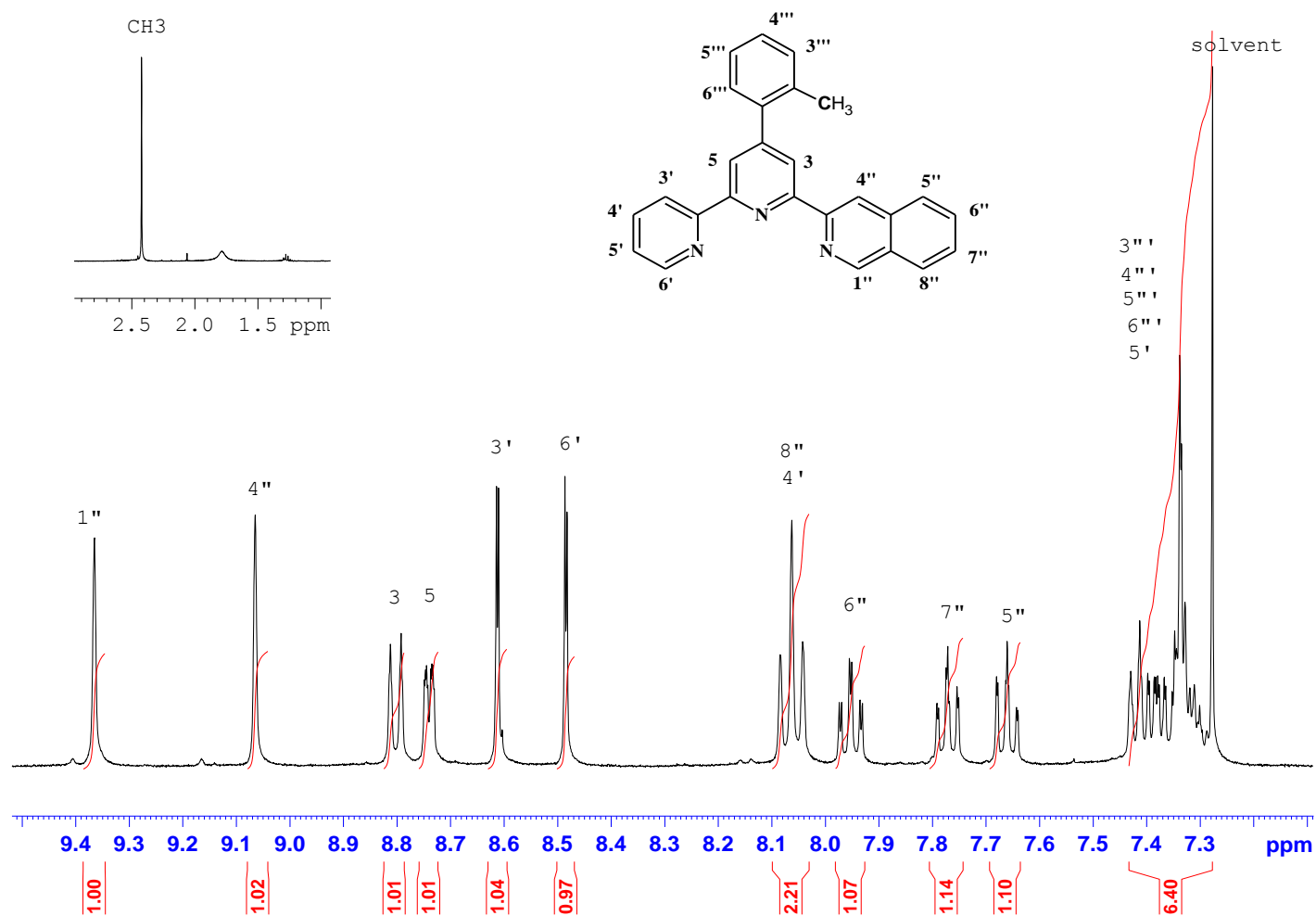


Figure A 8 ¹H NMR spectrum of 4-(*o*-tolyl)-6-(3'-isoquinoyl)-2,2'-bipyridine in deuterated chloroform.

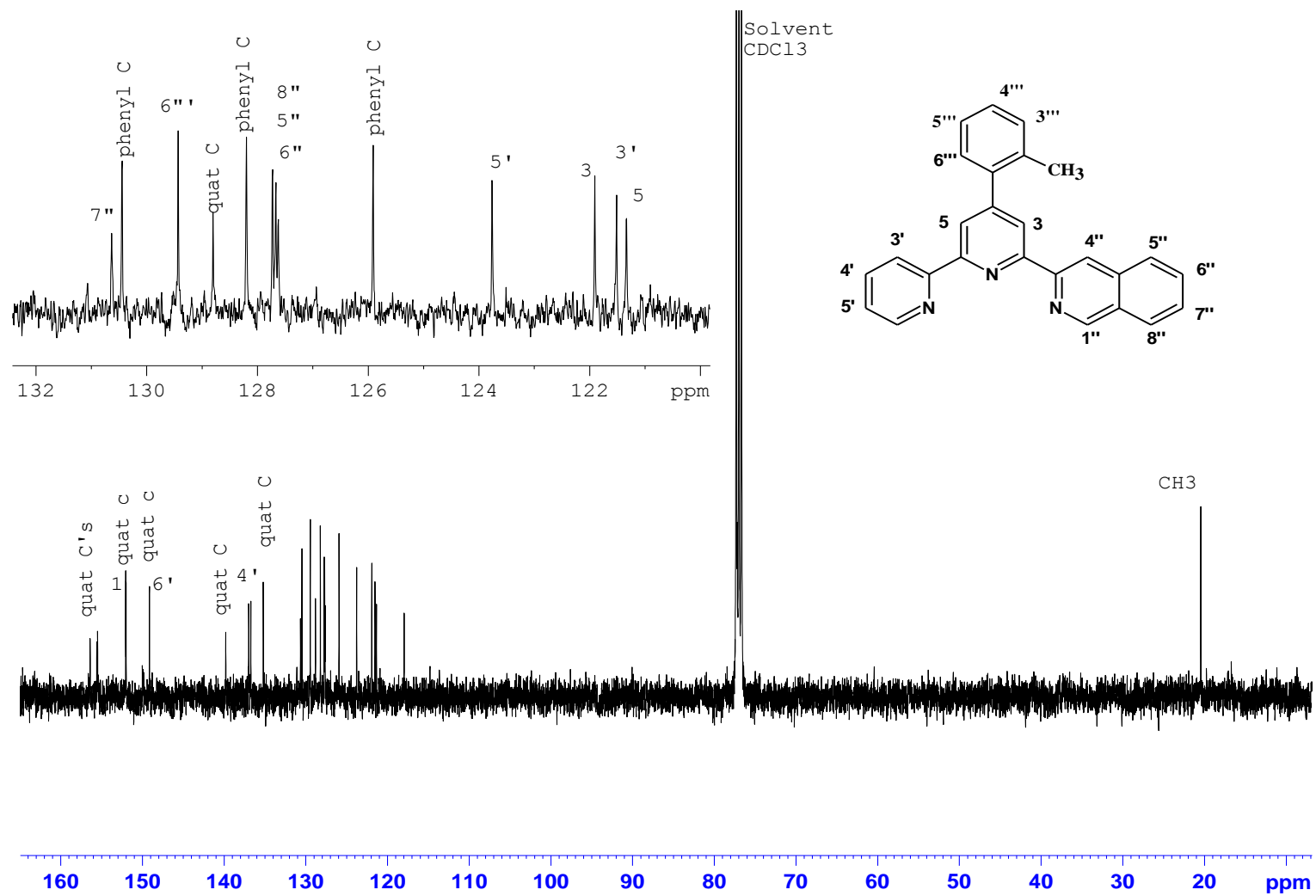


Figure A 9 ^{13}C NMR spectrum of 4-(*o*-tolyl)-6-(3'-isoquinoyl)-2,2'-bipyridine in deuterated chloroform.

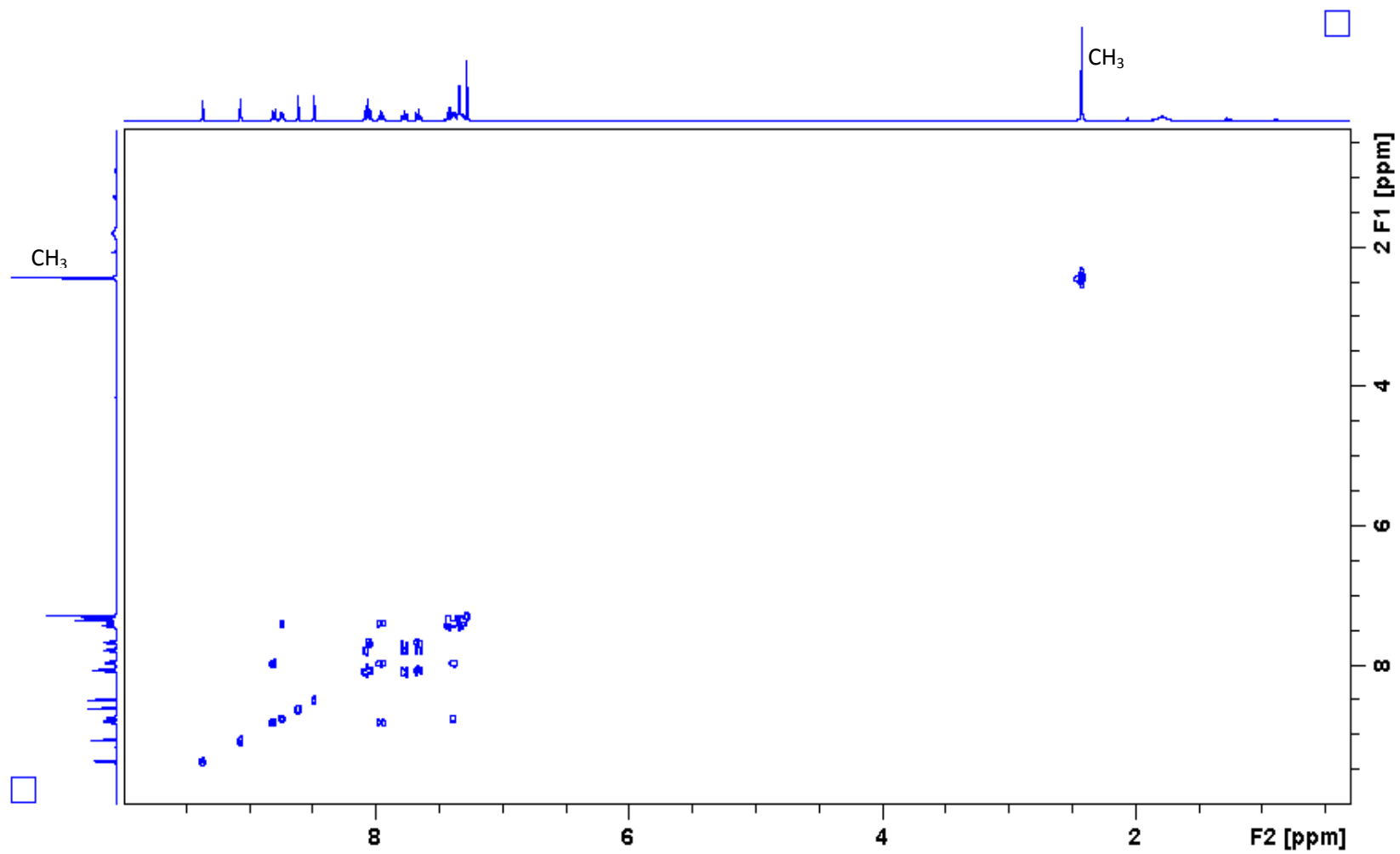


Figure A 10 COSY NMR spectrum of 4-(*o*-tolyl)-6-(3'-isoquinoyl)-2,2'-bipyridine in deuterated chloroform.

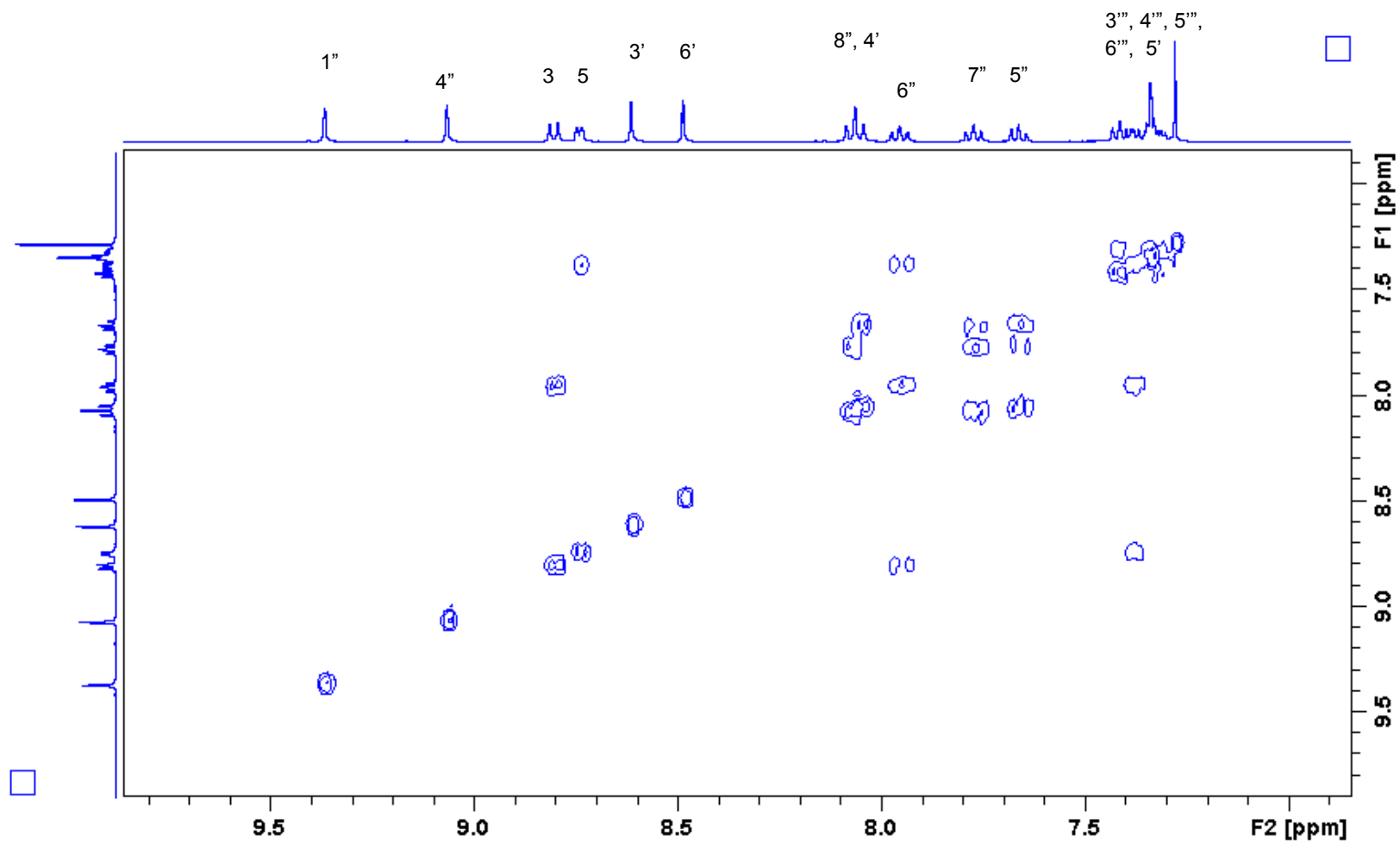


Figure A 11 COSY NMR spectrum of 4-(*o*-tolyl)-6-(3'-isoquinoyl)-2,2'-bipyridine in deuterated chloroform. Spectrum zoomed in to show the signals due to the protons on aromatic rings.

Elemental Composition Report

Page 1

Single Mass Analysis

Tolerance = 5.0 PPM / DBE: min = -1.5, max = 50.0

Element prediction: Off

Number of isotope peaks used for i-FIT = 3

Monoisotopic Mass, Even Electron Ions

10 formula(e) evaluated with 1 results within limits (all results (up to 1000) for each mass)

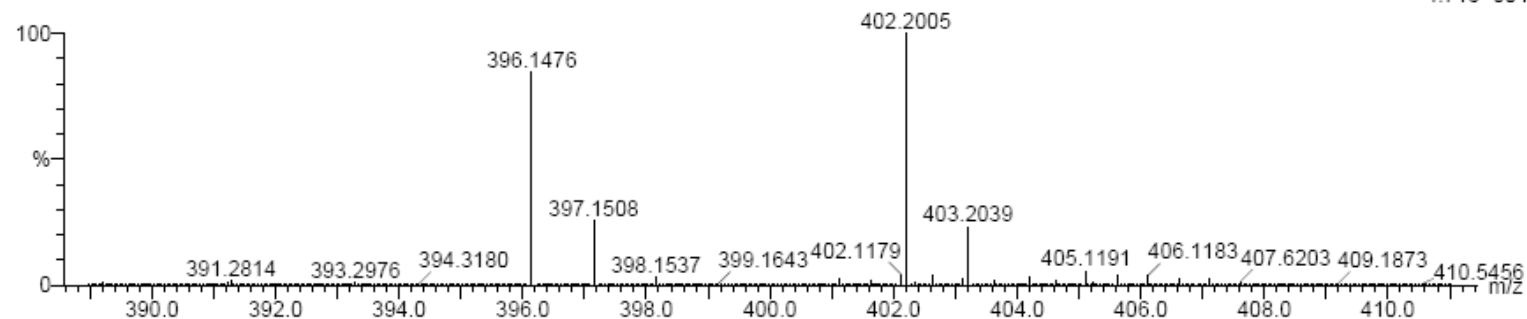
Elements Used:

C: 20-30 H: 15-25 N: 0-5 Na: 0-1

Aishath Shaira

L01 19 (0.307) Cm (1:60)

TOF MS ES+
4.71e+004



Minimum: -1.5
Maximum: 5.0 5.0 50.0

| Mass | Calc. Mass | mDa | PPM | DBE | i-FIT | i-FIT (Norm) | Formula |
|----------|------------|------|------|------|-------|--------------|---------------|
| 396.1476 | 396.1477 | -0.1 | -0.3 | 18.5 | 449.3 | 0.0 | C26 H19 N3 Na |

Figure A 12 Mass spectrum of 4-(*o*-tolyl)-6-(3'-isoquinoyl)-2,2'-bipyridine.

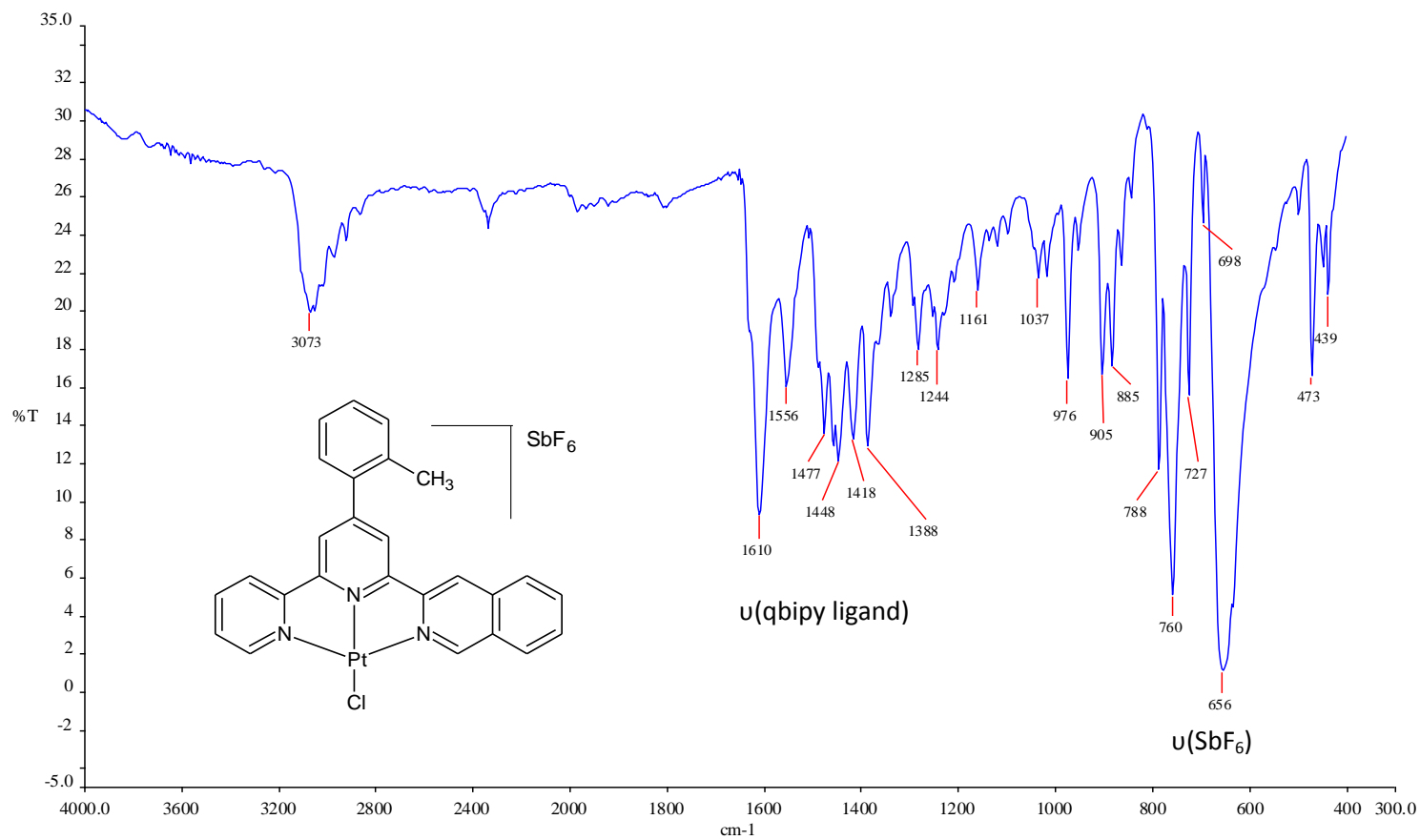


Figure A 13 IR spectrum of [Pt{4-(*o*-tolyl)-6-(3'-isoquinoyl)-2,2'-bipyridine}Cl]SbF₆ recorded as a KBr disc.

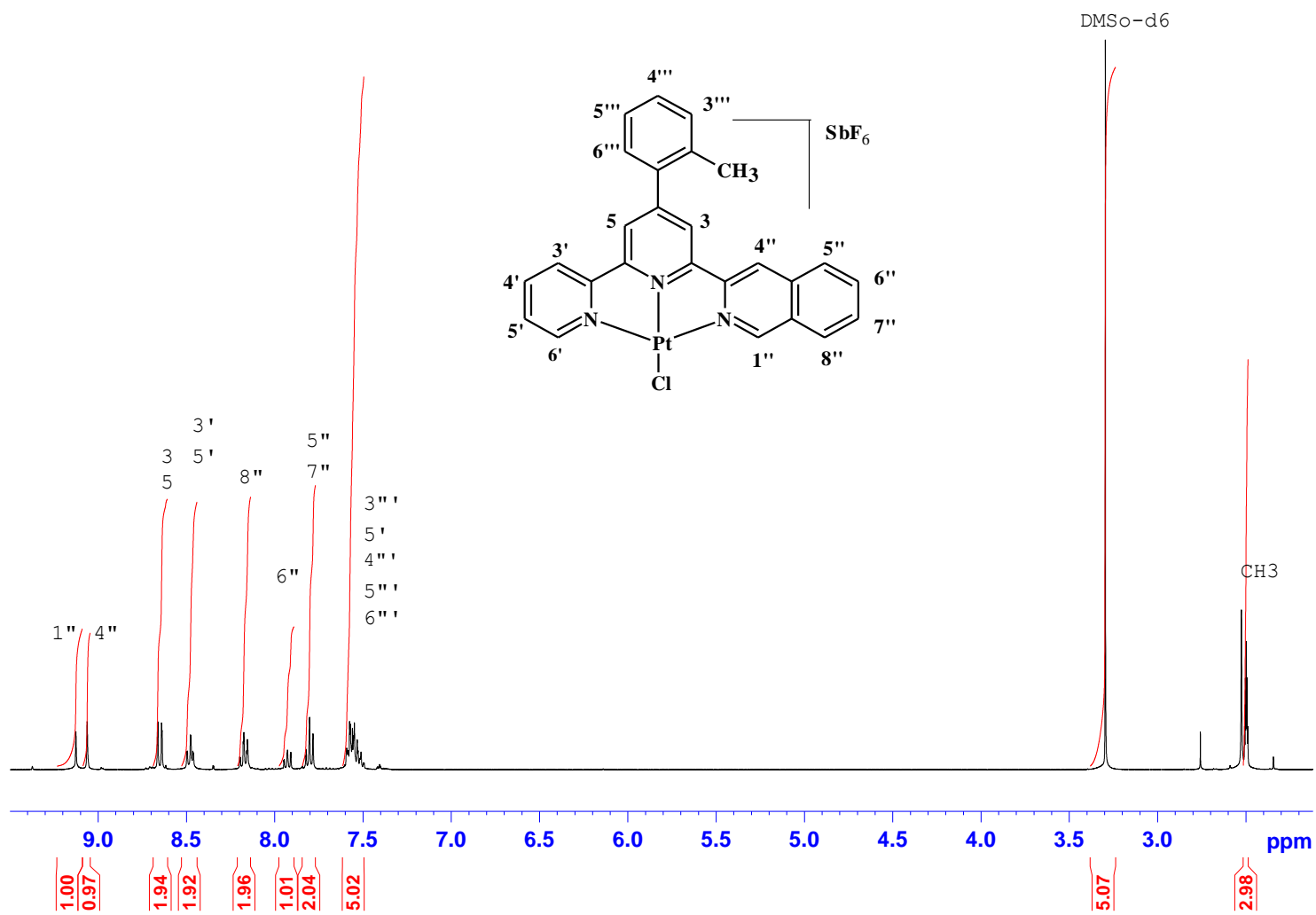


Figure A 14 ^1H NMR spectrum of $[\text{Pt}\{4\text{-(}o\text{-tolyl)}\text{-6-(3''-isoquinoyl)-2,2'\text{-bipyridine}}\text{Cl}]\text{SbF}_6$ in DMSO-d_6 .

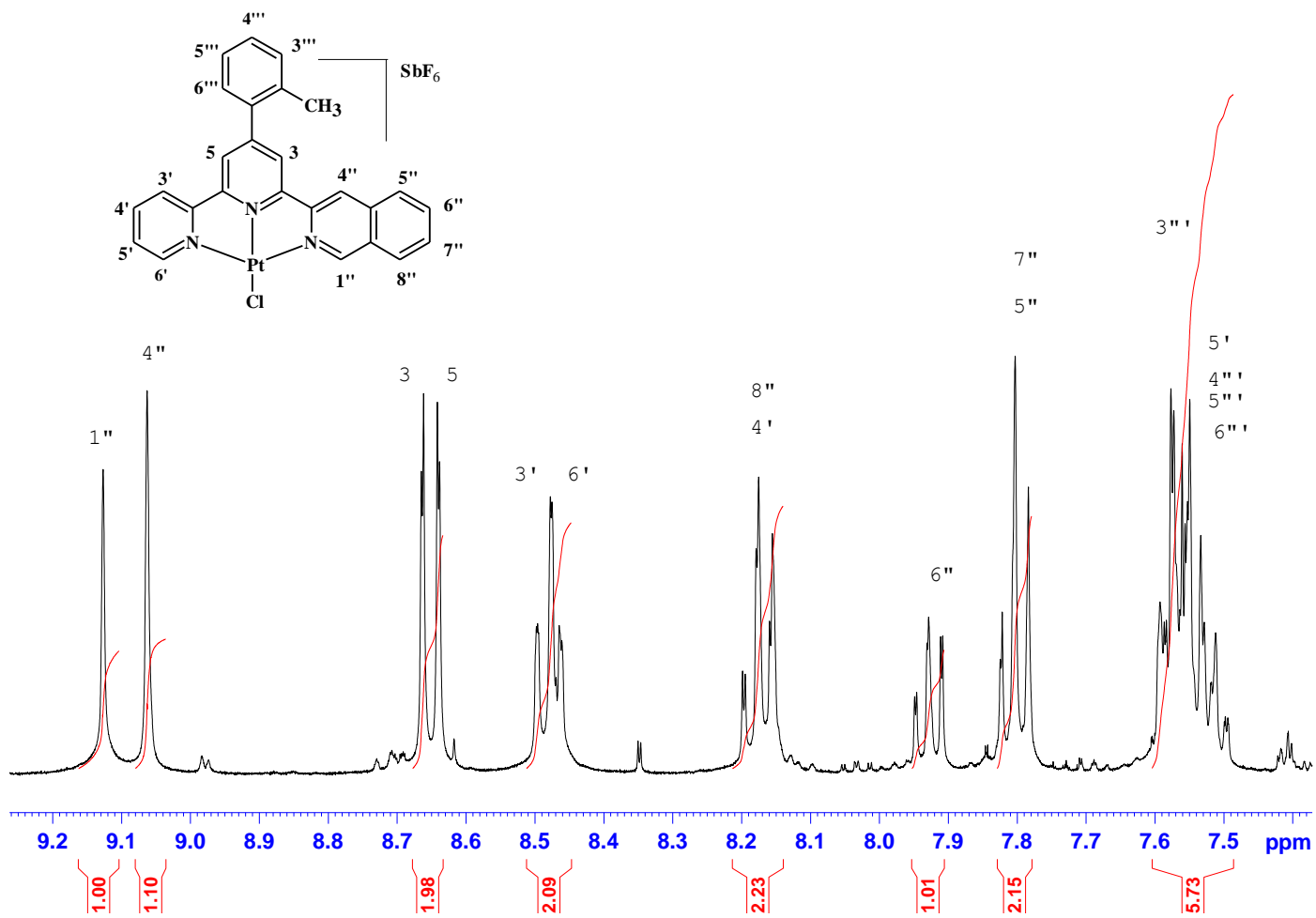


Figure A 15 ¹H NMR spectrum of [Pt{4-(o-tolyl)-6-(3'-isoquinoyl)-2,2'-bipyridine}Cl]SbF₆ in DMSO-d₆. Spectrum zoomed in to show the signals due to the protons on the aromatic rings.

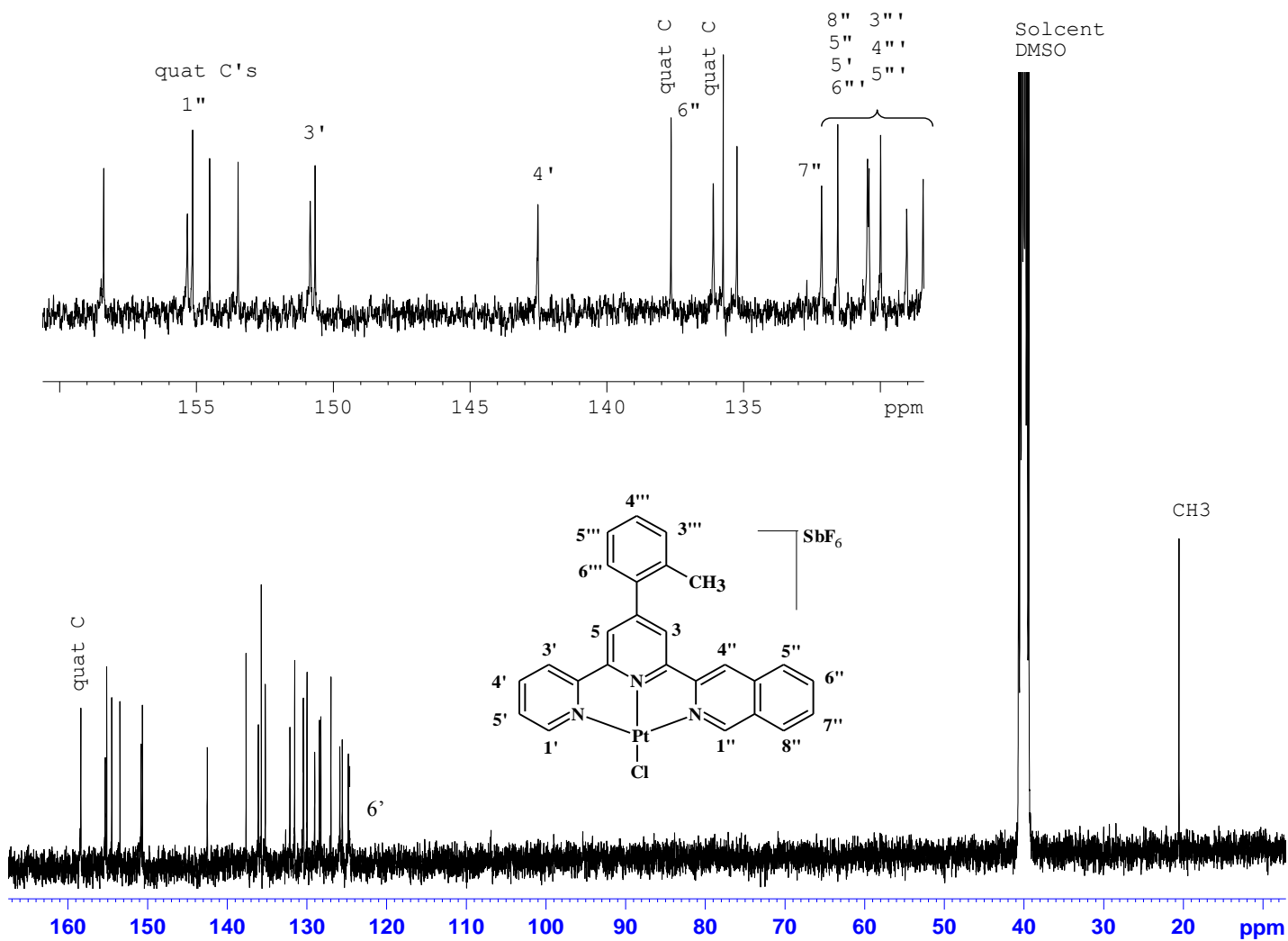


Figure A 16 ^{13}C NMR spectrum of $[\text{Pt}\{4\text{-}(o\text{-tolyl})\text{-}6\text{-}(3'\text{-isoquinoyl})\text{-}2,2'\text{-bipyridine}\}\text{Cl}]\text{SbF}_6$ in DMSO-d_6 .

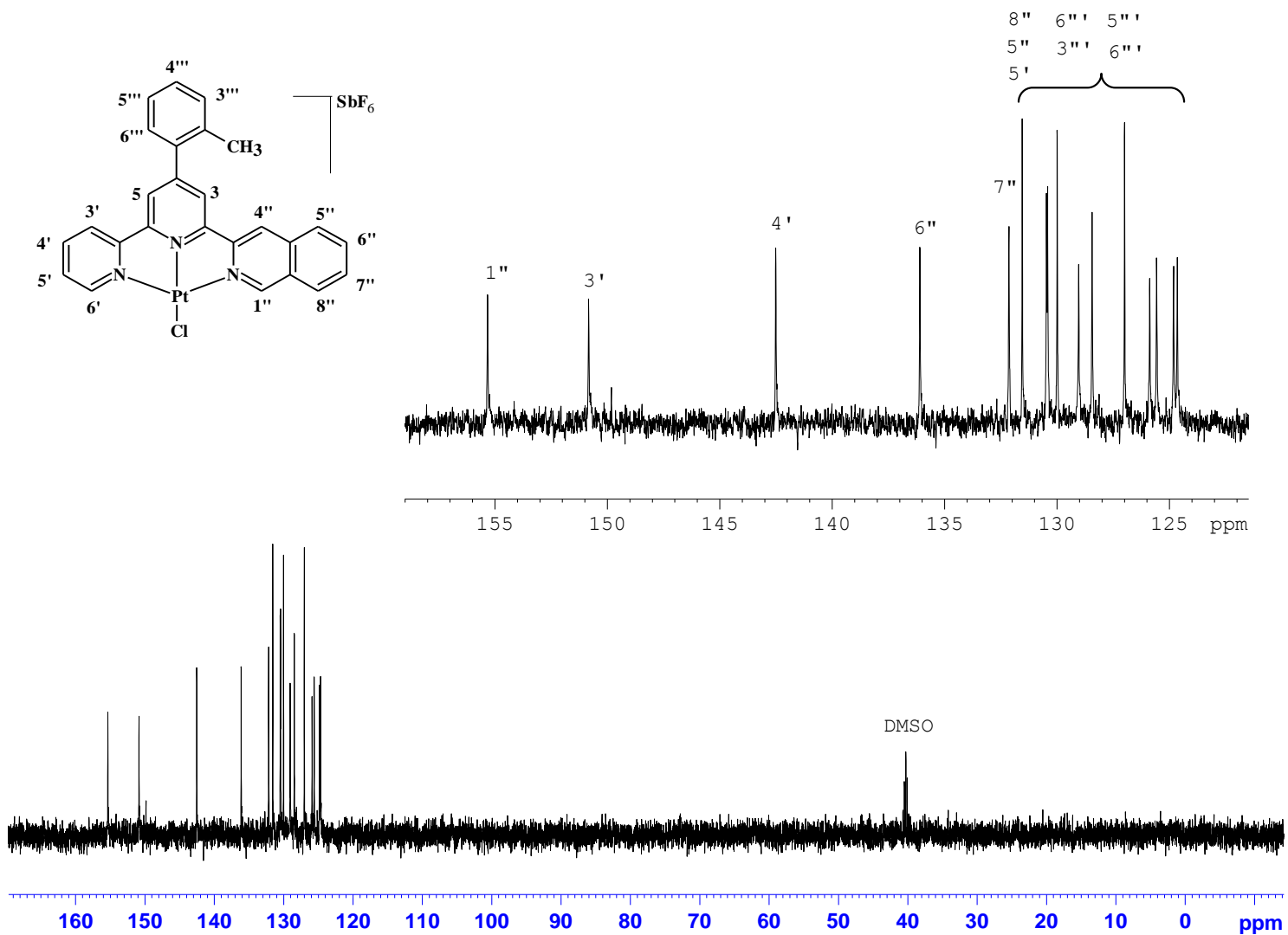


Figure A 17 DEPT 90 NMR spectrum of $[Pt(4-(o\text{-tolyl})-6-(3'\text{-isoquinoyl})-2,2'\text{-bipyridine})Cl]SbF_6$ in DMSO-d₆.

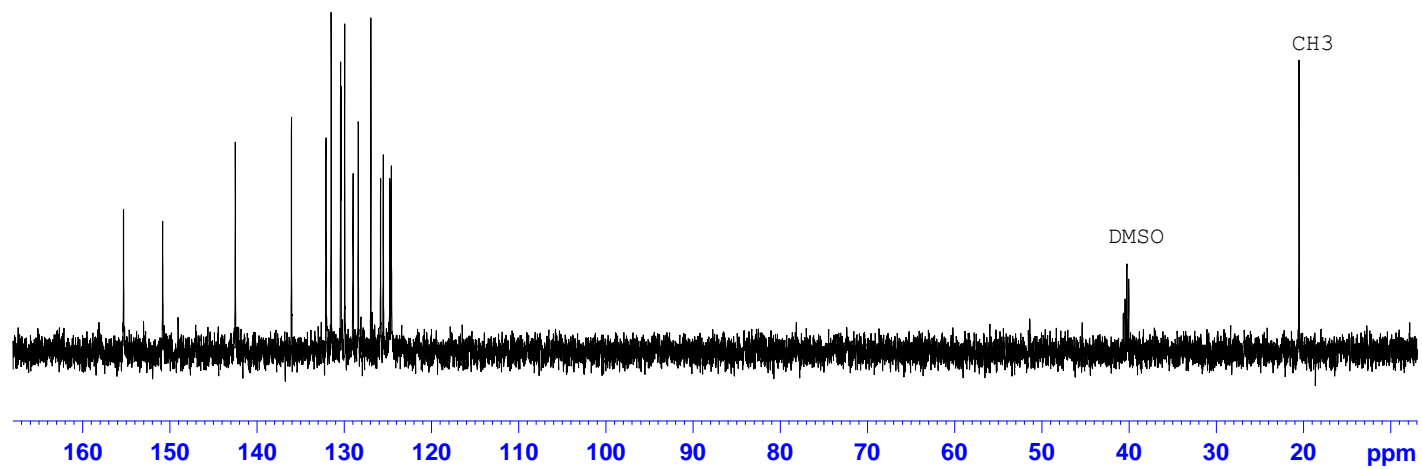
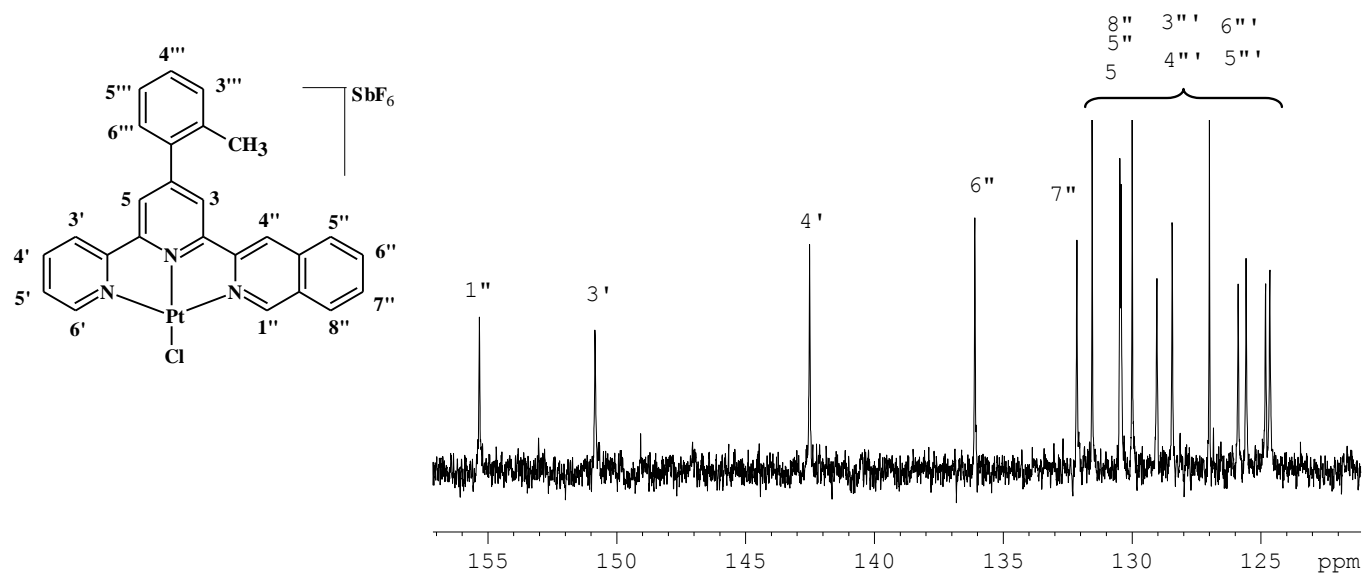


Figure A 18 DEPT 135 NMR spectrum of $[Pt\{4-(o\text{-tolyl})-6-(3''\text{-isoquinoyl})-2,2'\text{-bipyridine}\}Cl]SbF_6$ in DMSO-d₆.

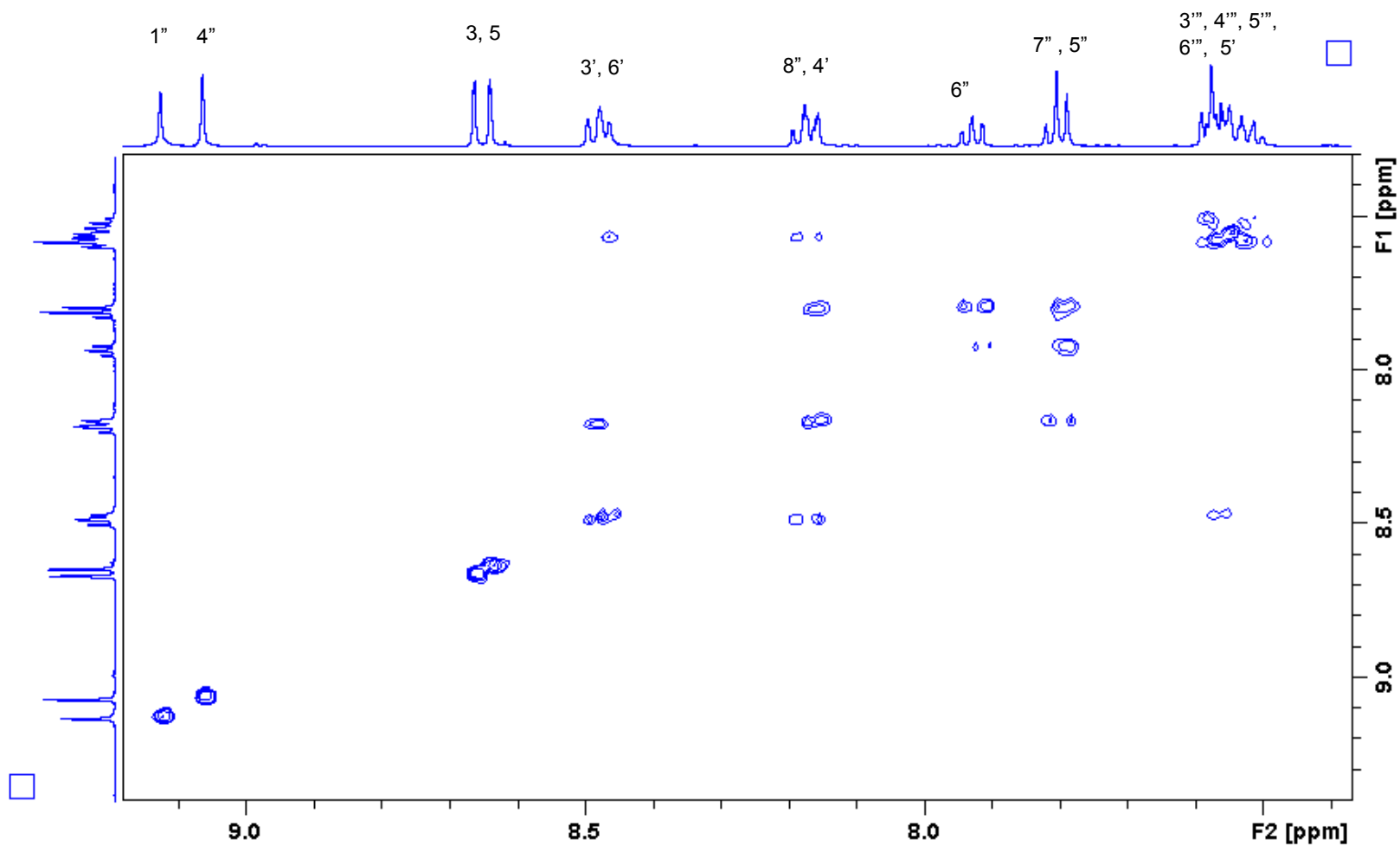


Figure A 19 COSY NMR spectrum of $[\text{Pt}\{4\text{-}(o\text{-tolyl})\text{-}6\text{-}(3''\text{-isoquinoyl})\text{-}2,2'\text{-bipyridine}\}\text{Cl}]\text{SbF}_6$ in DMSO-d_6 . Spectrum zoomed in to show the signals due to the protons on the aromatic rings.

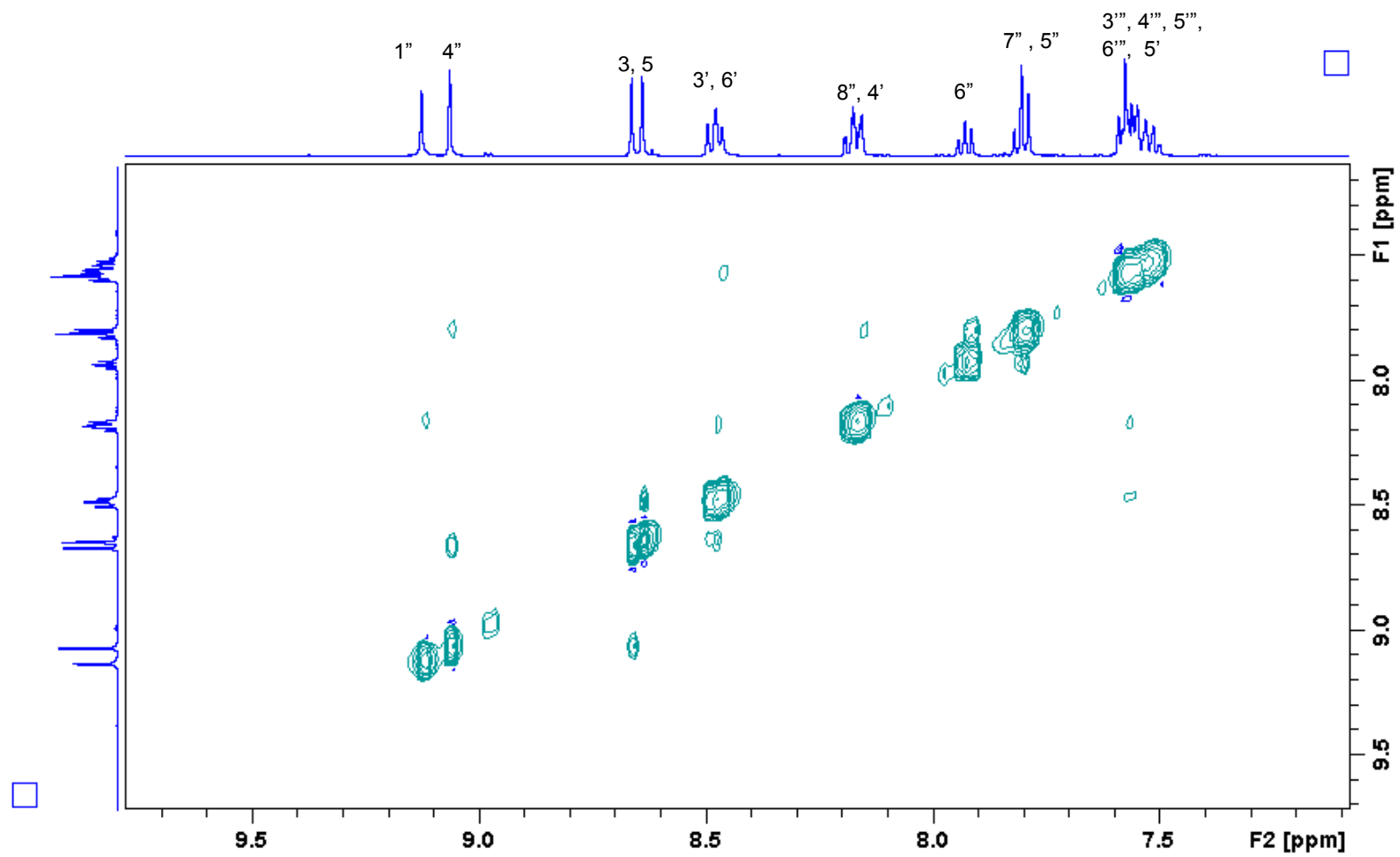


Figure A 20 NOESY NMR spectrum of [Pt{4-(*o*-tolyl)-6-(3'-isoquinoyl)-2,2'-bipyridine}Cl]SbF₆ in DMSO-d₆. Spectrum zoomed in to show the signals due to the protons on the aromatic rings.

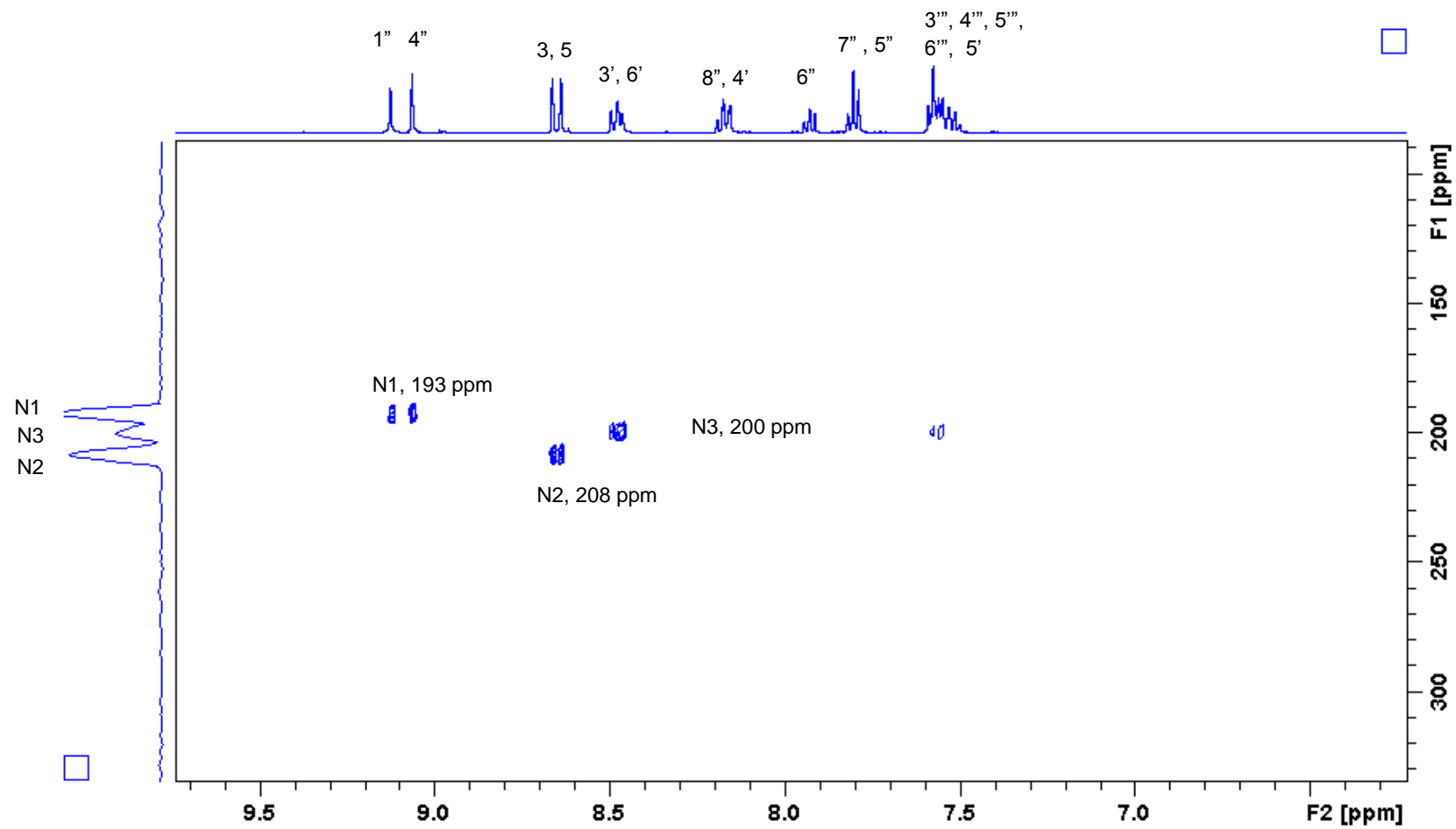


Figure A 21 ¹⁵N HMBC NMR spectrum of [Pt{4-(*o*-tolyl)-6-(3'-isoquinoyl)-2,2'-bipyridine}Cl]SbF₆ in DMSO-d₆.

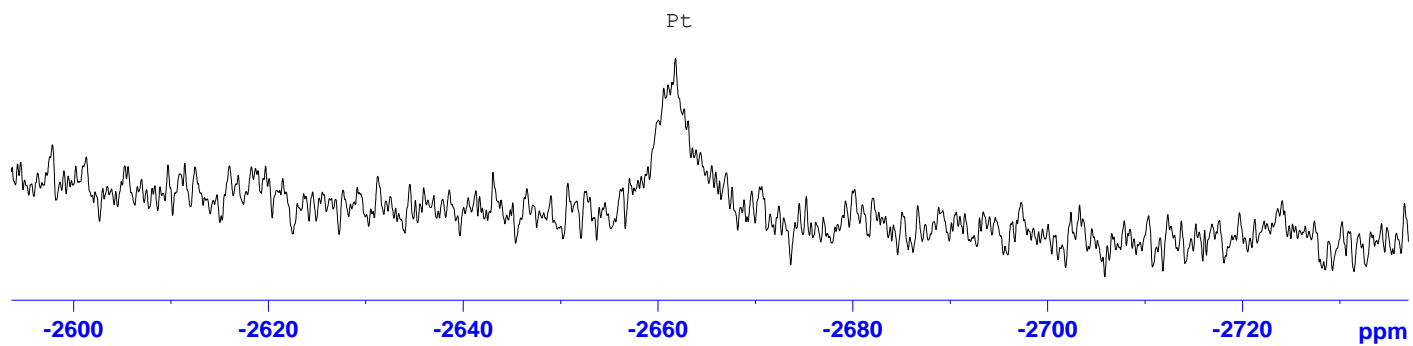
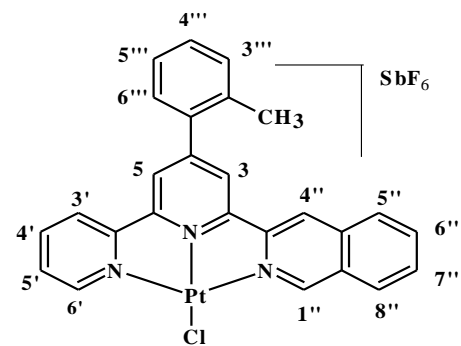


Figure A 22 ^{195}Pt NMR spectrum of $[\text{Pt}\{4\text{-}(o\text{-tolyl})\text{-}6\text{-}(3'\text{-isoquinoyl})\text{-}2,2'\text{-bipyridine}\}\text{Cl}]\text{SbF}_6$ in DMSO-d_6 .

Elemental Composition Report

Page 1

Single Mass Analysis

Tolerance = 5.0 PPM / DBE: min = -1.5, max = 50.0

Element prediction: Off

Number of isotope peaks used for i-FIT = 3

Monoisotopic Mass, Even Electron Ions

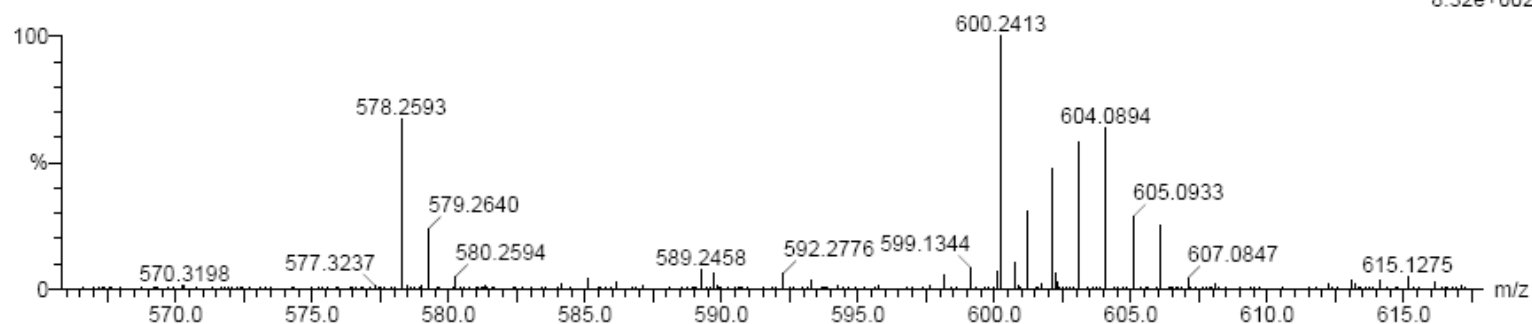
20 formula(e) evaluated with 1 results within limits (all results (up to 1000) for each mass)

Elements Used:

C: 25-30 H: 10-20 N: 0-3 Cl: 0-2 Pt: 0-1

Aishath Shaira
Pt01 14 (0.222)

TOF MS ES+
8.32e+002



Minimum: -1.5
Maximum: 5.0 5.0 50.0

| Mass | Calc. Mass | mDa | PPM | DBE | i-FIT | i-FIT (Norm) | Formula |
|----------|------------|-----|-----|------|-------|--------------|------------------|
| 603.0917 | 603.0915 | 0.2 | 0.3 | 19.5 | 80.9 | 0.0 | C26 H19 N3 Cl Pt |

Figure A 23 Mass spectrum of [Pt{4-(*o*-tolyl)-6-(3'-isoquinoyl)-2,2'-bipyridine}Cl]SbF₆.

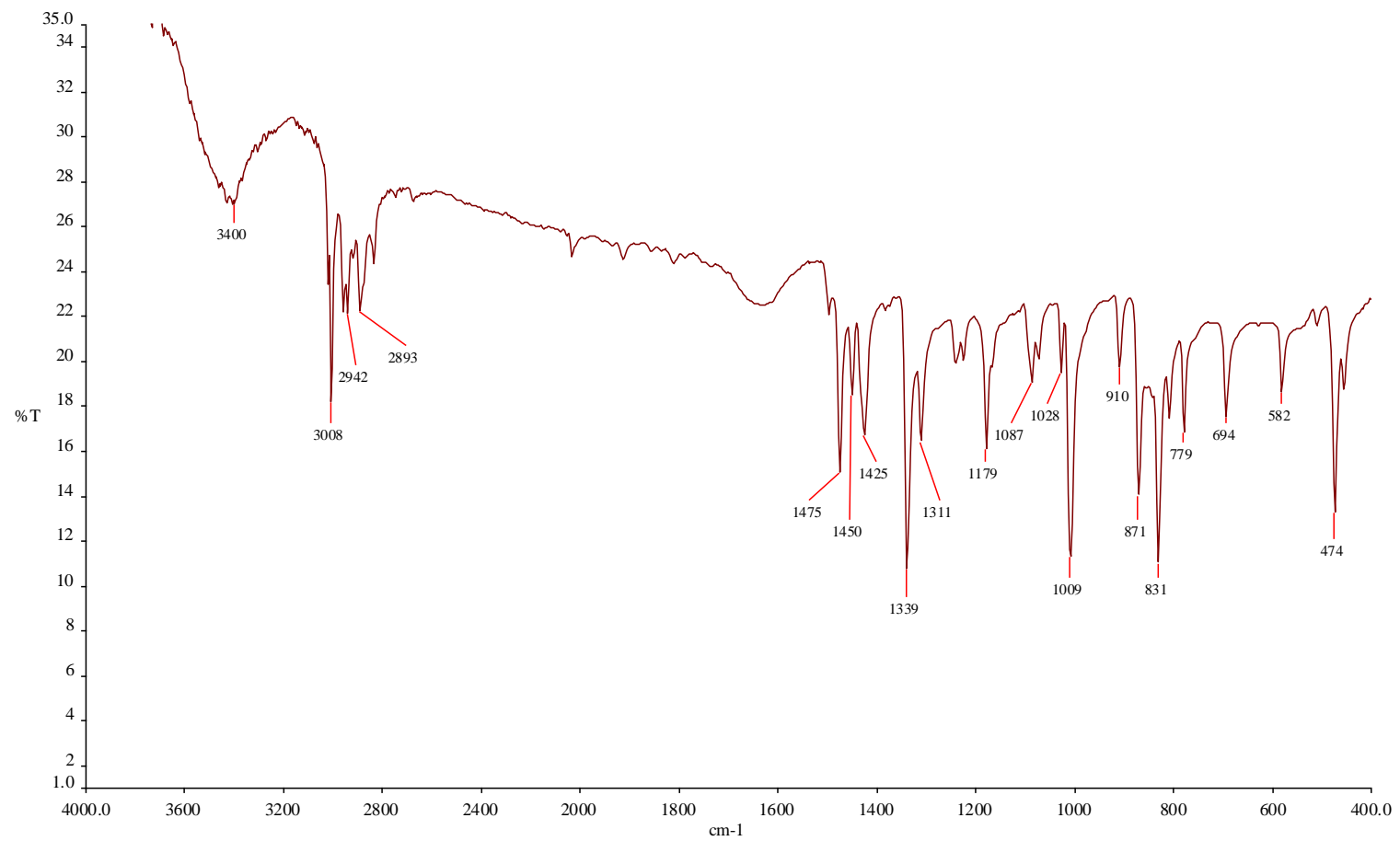


Figure A 24 IR Spectrum of Dichloro(1,5-cyclooctadiene)platinum(II) obtained as a KBr disc.

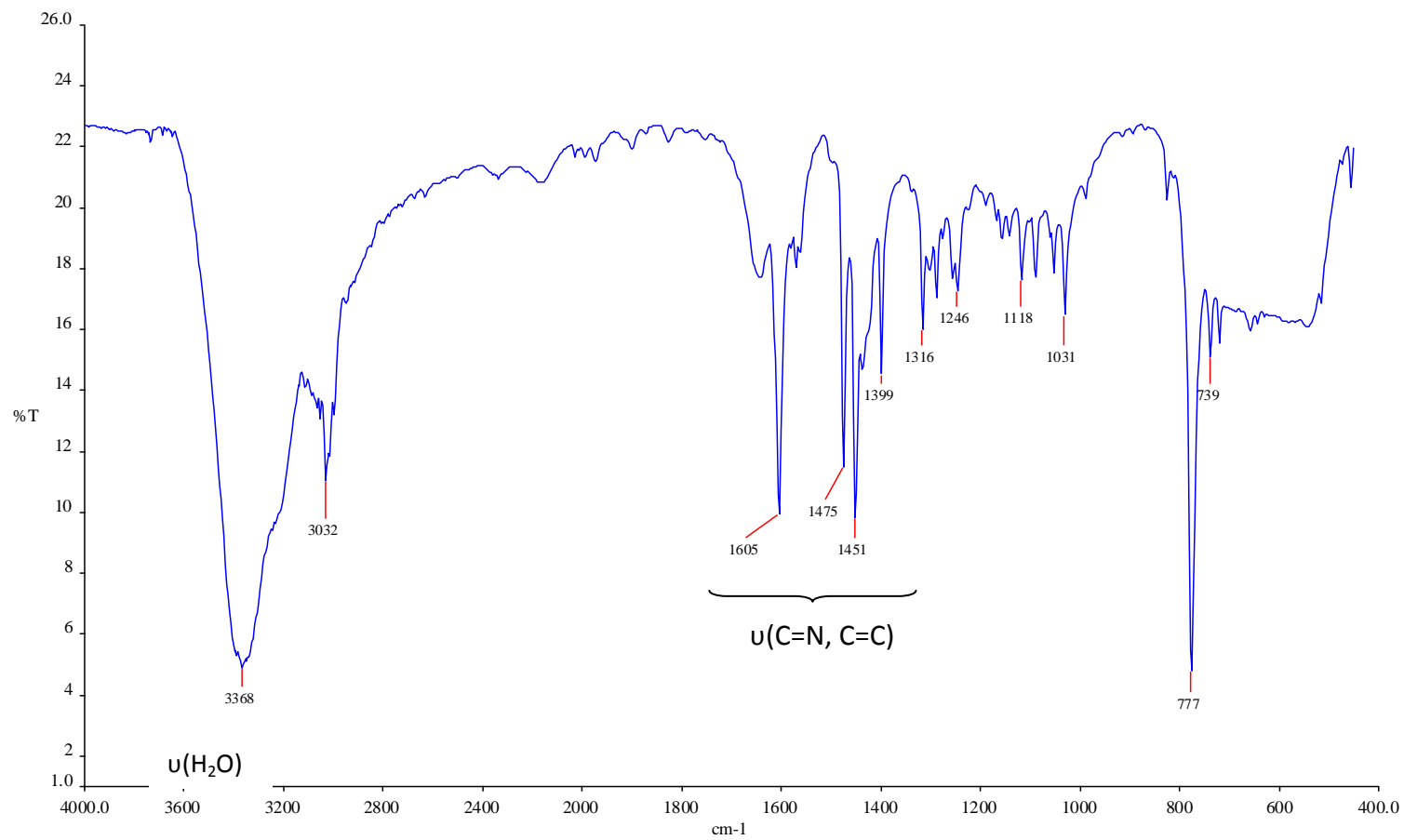


Figure A 25 IR spectrum of [Pt(2,2':6',2''-terpyridine)Cl]Cl·2H₂O recorded as a KBr disc.

Elemental Composition Report

Page 1

Single Mass Analysis

Tolerance = 5.0 PPM / DBE: min = -1.5, max = 50.0

Element prediction: Off

Number of isotope peaks used for i-FIT = 3

Monoisotopic Mass, Odd and Even Electron Ions

34 formula(e) evaluated with 1 results within limits (all results (up to 1000) for each mass)

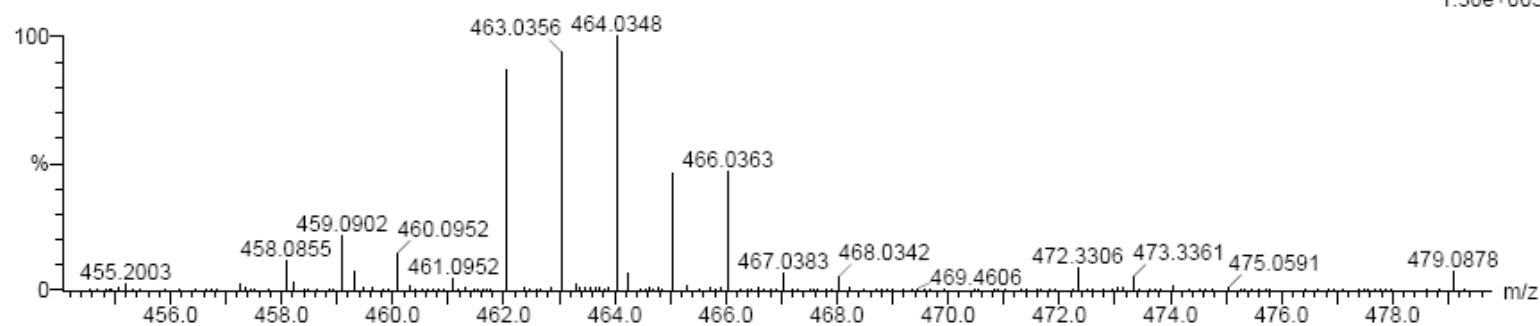
Elements Used:

C: 0-20 H: 0-20 N: 0-5 Cl: 1-2 Pt: 0-1

Aishath Shaira

Pt4 2 2 (0.017)

TOF MS ES+
1.30e+003



Minimum: -1.5
Maximum: 5.0 5.0 50.0

| Mass | Calc. Mass | mDa | PPM | DBE | i-FIT | i-FIT (Norm) | Formula |
|----------|------------|------|------|------|-------|--------------|------------------|
| 464.0348 | 464.0368 | -2.0 | -4.3 | 12.0 | 122.7 | 0.0 | C15 H12 N3 Cl Pt |

Figure A 26 Mass spectrum of [Pt(2,2':6',2''-terpyridine)Cl]Cl·2H₂O.

Appendix B- Kinetic Investigation: Data and Selected Spectra

Table B 1 Summary of selected wavelengths (nm) for the kinetic investigations.

| Complex | Nucleophile | | | | |
|---------|-------------|-----|-----|------|-----|
| | Pz | Im | MIm | DMIm | Tz |
| Pt1 | 281 | 332 | 342 | 342 | 344 |
| Pt2 | 313 | 311 | 313 | 311 | 312 |
| Pt3 | 333 | 333 | 333 | 402 | 333 |
| Pt4 | 363 | 363 | 352 | 363 | 385 |

Table B 2 Average observed rate constants, k_{obs}^a at 298.15 K for the reaction of Pt1 (1.51×10^{-5} M) with the nucleophiles at various concentrations.

| [Pz]/mM | k_{obs}/s^{-1} | [Im]/mM | k_{obs}/s^{-1} | [MIm]/mM | k_{obs}/s^{-1} | [DMIm]/mM | k_{obs}/s^{-1} | [Tz]/mM | k_{obs}/s^{-1} |
|---------|------------------|---------|------------------|----------|------------------|-----------|------------------|---------|------------------|
| 0.151 | 0.0001884 | 0.151 | 0.0010856 | 0.151 | 0.0016843 | 0.151 | 0.0002523 | 0.151 | 0.0001309 |
| 0.301 | 0.000413 | 0.301 | 0.0016581 | 0.301 | 0.0022468 | 0.301 | 0.0004408 | 0.301 | 0.0002601 |
| 0.451 | 0.0005387 | 0.451 | 0.002182 | 0.451 | 0.0028518 | 0.451 | 0.0007285 | 0.451 | 0.0004141 |
| 0.602 | 0.0007697 | 0.602 | 0.0027498 | 0.602 | 0.0033492 | 0.602 | 0.0008976 | 0.602 | 0.0005146 |
| 0.752 | 0.0009506 | 0.752 | 0.0033294 | 0.752 | 0.0039837 | 0.752 | 0.0010913 | 0.752 | 0.0006186 |

^a k_{obs} values obtained from at least two kinetic runs.

Table B 3 Average observed rate constants, k_{obs}^a at 298.15 K for the reaction of Pt2 (1.51×10^{-5} M) with the nucleophiles at various concentrations.

| [Pz]/mM | $k_{\text{obs}}/ \text{s}^{-1}$ | [Im]/mM | $k_{\text{obs}}/ \text{s}^{-1}$ | [MIm]/mM ^b | $k_{\text{obs}}/ \text{s}^{-1}$ | [DMIm]/mM | $k_{\text{obs}}/ \text{s}^{-1}$ | [Tz]/mM | $k_{\text{obs}}/ \text{s}^{-1}$ |
|---------|---------------------------------|---------|---------------------------------|-----------------------|---------------------------------|-----------|---------------------------------|---------|---------------------------------|
| 0.151 | 0.001324 | 0.151 | 0.0017293 | 0.151 | 0.0023379 | 0.151 | 0.0004911 | 0.151 | 0.0004112 |
| 0.301 | 0.0018341 | 0.301 | 0.0026562 | 0.301 | 0.0031658 | 0.301 | 0.0007861 | 0.301 | 0.0005921 |
| 0.451 | 0.0024013 | 0.451 | 0.003682 | <i>0.451</i> | 0.0049686 | 0.451 | 0.0011089 | 0.451 | 0.0008292 |
| 0.602 | 0.0028742 | 0.602 | 0.0043965 | <i>0.602</i> | 0.0060475 | 0.602 | 0.0013959 | 0.602 | 0.0010546 |
| 0.752 | 0.0032104 | 0.752 | 0.0052996 | <i>0.752</i> | 0.0068633 | 0.752 | 0.0017156 | 0.752 | 0.0013057 |

^a k_{obs} values obtained from at least two kinetic runs.

^b k_{obs} values in italics are obtained from stopped-flow techniques by an average of at least five to eight runs.

Table B 4 Average observed rate constants, k_{obs}^a at 298.15 K for the reaction of Pt3 (2.50×10^{-5} M) with the nucleophiles at various concentrations.

| [Pz]/mM | $k_{\text{obs}}/ \text{s}^{-1}$ | [Im]/mM | $k_{\text{obs}}/ \text{s}^{-1}$ | [MIm]/mM | $k_{\text{obs}}/ \text{s}^{-1}$ | [DMIm]/mM | $k_{\text{obs}}/ \text{s}^{-1}$ | [Tz]/mM | $k_{\text{obs}}/ \text{s}^{-1}$ |
|---------|---------------------------------|---------|---------------------------------|----------|---------------------------------|-----------|---------------------------------|---------|---------------------------------|
| 0.250 | 0.000472 | 0.250 | 0.001322 | 0.250 | 0.00177 | 0.250 | 0.0003737 | 0.250 | 0.0002696 |
| 0.500 | 0.000718 | 0.500 | 0.002089 | 0.500 | 0.00253 | 0.500 | 0.0006772 | 0.500 | 0.0004343 |
| 0.750 | 0.000932 | 0.750 | 0.002887 | 0.750 | 0.00329 | 0.750 | 0.0010419 | 0.750 | 0.0006617 |
| 1.00 | 0.00117 | 1.00 | 0.003602 | 1.00 | 0.00404 | 1.00 | 0.0012893 | 1.00 | 0.0008832 |
| 1.25 | 0.00142 | 1.25 | 0.004355 | 1.25 | 0.00496 | 1.25 | 0.0016073 | 1.25 | 0.0010329 |

^a k_{obs} values obtained from at least two kinetic runs.

Table B 5 Average observed rate constants, k_{obs}^a at 298.15 K for the reaction of Pt4 (2.50×10^{-5} M) with the nucleophiles at various concentrations.

| [Pz]/mM | k_{obs}/s^{-1} | [Im]/mM | k_{obs}/s^{-1} | [MIm]/mM | k_{obs}/s^{-1} | [DMIm]/mM | k_{obs}/s^{-1} | [Tz]/mM | k_{obs}/s^{-1} |
|---------|------------------|---------|------------------|----------|------------------|-----------|-----------------------|---------|-----------------------|
| 0.250 | 0.0003182 | 0.248 | 0.0003890 | 0.250 | 0.0004581 | 0.250 | 9.62×10^{-5} | 0.250 | 8.89×10^{-5} |
| 0.500 | 0.0003936 | 0.495 | 0.0006845 | 0.500 | 0.0007705 | 0.500 | 0.0001841 | 0.500 | 0.0001603 |
| 0.750 | 0.0004888 | 0.740 | 0.0007877 | 0.750 | 0.0010318 | 0.750 | 0.0002831 | 0.750 | 0.0002365 |
| 1.00 | 0.0005850 | 0.990 | 0.0010746 | 1.00 | 0.001244 | 1.00 | 0.0003818 | 1.00 | 0.0003228 |
| 1.25 | 0.0006756 | 1.24 | 0.0012393 | 1.25 | 0.0015333 | 1.25 | 0.0004676 | 1.25 | 0.0003657 |

^a k_{obs} values obtained from at least two kinetic runs.

Table B 6 Average rate constants, k_{obs} obtained from for the reactions of Pt1 (1.51×10^{-5} M) with the different concentrations of the nucleophiles at different temperatures.

| Nucleophile | Conc/mM | $k_{\text{obs}}/ \text{s}^{-1}$ obtained at different temperatures in Kelvin | | | | | |
|-------------|---------|--|-----------------------|-----------------------|-----------------------|-----------------------|-----------------------|
| | | 288.15 | 293.15 | 298.15 | 303.15 | 308.15 | 313.15 |
| Pz | 0.451 | | 4.64×10^{-4} | 5.39×10^{-4} | 7.80×10^{-4} | 0.00115 | 0.00157 |
| Im | 0.151 | 4.29×10^{-4} | 6.54×10^{-4} | 0.00109 | 0.00143 | 0.00211 | |
| | 0.301 | 7.45×10^{-4} | 0.00101 | 0.00166 | 0.00219 | 0.00285 | |
| | 0.451 | 0.00101 | 0.0015 | 0.00218 | 0.00308 | 0.00415 | |
| | 0.602 | 0.00127 | 0.0019 | 0.00275 | 0.00395 | 0.00562 | |
| | 0.752 | 0.00155 | 0.00231 | 0.00333 | 0.00458 | 0.00651 | |
| MIm | 0.151 | 4.58×10^{-4} | 0.00102 | 0.00168 | 0.00285 | 0.00443 | |
| | 0.301 | 8.23×10^{-4} | 0.00134 | 0.00225 | 0.0036 | 0.00568 | |
| | 0.451 | 0.00113 | 0.00178 | 0.00285 | 0.00425 | 0.00666 | |
| | 0.602 | 0.00142 | 0.00219 | 0.00335 | 0.00496 | 0.00778 | |
| | 0.752 | 0.00165 | 0.00265 | 0.00398 | 0.00591 | 0.00877 | |
| DMIm | 0.451 | | 3.72×10^{-4} | 7.28×10^{-4} | 8.22×10^{-4} | 0.00135 | 0.00215 |
| Tz | 0.451 | | 2.67×10^{-4} | 4.14×10^{-4} | 5.55×10^{-4} | 7.10×10^{-4} | 8.48×10^{-4} |

Table B 7 Average rate constants, k_{obs} obtained from for the reactions of Pt2 (1.51×10^{-5} M) with the different concentrations of the nucleophiles at different temperatures.

| Nucleophile | Conc/mM | $k_{\text{obs}}/ \text{s}^{-1}$ obtained at different temperatures in Kelvin | | | | | |
|------------------------|---------|--|-----------------------|-----------------------|-----------------------|-----------------------|-----------------------|
| | | 288.15 | 293.15 | 298.15 | 303.15 | 308.15 | 313.15 |
| Pz | 0.151 | | 0.00122 | 0.00132 | 0.00164 | 0.00247 | 0.00293 |
| | 0.301 | | 0.00154 | 0.00183 | 0.00222 | 0.00335 | 0.00364 |
| | 0.451 | | 0.00188 | 0.0024 | 0.0029 | 0.00408 | 0.00481 |
| | 0.602 | | 0.00228 | 0.00287 | 0.00342 | 0.00496 | 0.00583 |
| | 0.752 | | 0.0027 | 0.00321 | 0.00402 | 0.00568 | 0.00671 |
| Im | 0.151 | | 0.0011 | 0.00173 | 0.00282 | 0.00378 | 0.00881 |
| | 0.301 | | 0.00179 | 0.00266 | 0.0038 | 0.00524 | 0.01176 |
| | 0.451 | | 0.00245 | 0.00368 | 0.00484 | 0.00795 | |
| | 0.602 | | 0.00293 | 0.0044 | 0.00642 | 0.00928 | 0.01826 |
| | 0.752 | | 0.00359 | 0.0053 | 0.00777 | 0.01128 | 0.01998 |
| ^bMIm | 0.151 | 8.93×10^{-4} | 0.00132 | 0.00234 | <i>0.00489</i> | <i>0.0081</i> | |
| | 0.301 | 0.00124 | 0.00197 | 0.00317 | <i>0.00586</i> | <i>0.00912</i> | |
| | 0.451 | 0.00178 | <i>0.00316</i> | <i>0.00497</i> | <i>0.00766</i> | <i>0.01197</i> | |
| | 0.602 | 0.00249 | <i>0.00412</i> | <i>0.00605</i> | <i>0.00878</i> | <i>0.01301</i> | |
| | 0.752 | 0.00282 | <i>0.00451</i> | <i>0.00686</i> | <i>0.01074</i> | <i>0.01565</i> | |
| DMIm | 0.151 | 1.76×10^{-4} | 2.41×10^{-4} | 4.91×10^{-4} | 6.97×10^{-4} | 9.96×10^{-4} | |
| | 0.301 | 3.23×10^{-4} | 4.62×10^{-4} | 7.86×10^{-4} | 0.00117 | 0.00167 | |
| | 0.451 | 4.82×10^{-4} | 6.82×10^{-4} | 0.00111 | 0.00156 | 0.00237 | |
| | 0.602 | 6.43×10^{-4} | 9.56×10^{-4} | 0.00140 | 0.00196 | 0.00303 | |
| | 0.752 | 8.04×10^{-4} | 0.00113 | 0.00172 | 0.00254 | 0.0035 | |
| Tz | 0.151 | | 1.99×10^{-4} | 4.11×10^{-4} | 4.52×10^{-4} | 5.23×10^{-4} | 6.94×10^{-4} |
| | 0.301 | | 3.78×10^{-4} | 5.92×10^{-4} | 7.80×10^{-4} | 0.0011 | 0.00124 |
| | 0.451 | | 5.27×10^{-4} | 8.29×10^{-4} | 0.00106 | 0.00141 | 0.00185 |
| | 0.602 | | 7.34×10^{-4} | 0.00105 | 0.00138 | 0.00175 | 0.00223 |
| | 0.752 | | 8.69×10^{-4} | 0.00131 | 0.00175 | 0.00221 | 0.0028 |

^b k_{obs} values in italics are obtained from stopped-flow techniques by an average of at least seven runs

Table B 8 Average rate constants, k_{obs} obtained from for the reactions of Pt3 (2.50×10^{-5} M) with the different concentrations of the nucleophiles at different temperatures.

| Nucleophile | Conc/mM | $k_{\text{obs}}/ \text{s}^{-1}$ obtained at different temperatures in Kelvin | | | | | |
|--------------------------|---------|--|----------|----------|----------|----------|----------|
| | | 288.15 | 293.15 | 298.15 | 303.15 | 308.15 | 313.15 |
| Pz | 0.250 | 0.000218 | 0.000328 | 0.000472 | 0.000614 | 0.000874 | |
| | 0.500 | 0.000371 | 0.000489 | 0.000718 | 0.000907 | 0.001258 | |
| | 0.750 | 0.000512 | 0.000705 | 0.000932 | 0.001324 | 0.001679 | |
| | 1.00 | 0.000582 | 0.000872 | 0.00117 | 0.001632 | 0.002124 | |
| | 1.25 | 0.000689 | 0.000978 | 0.001423 | 0.001901 | 0.002695 | |
| Im | 0.250 | 0.000436 | 0.000838 | 0.001322 | 0.001930 | 0.002967 | |
| | 0.500 | 0.000946 | 0.001412 | 0.002089 | 0.003251 | 0.004697 | |
| | 0.750 | 0.001208 | 0.001912 | 0.002887 | 0.004325 | 0.006184 | |
| | 1.00 | 0.001584 | 0.002491 | 0.003601 | 0.005124 | 0.007441 | |
| | 1.25 | 0.001957 | 0.002949 | 0.004355 | 0.006242 | 0.008891 | |
| MIm | 0.250 | | 0.001159 | 0.001773 | 0.002867 | 0.004416 | 0.007554 |
| | 0.500 | | 0.0017 | 0.002530 | 0.003955 | 0.006061 | 0.00917 |
| | 0.750 | | 0.002191 | 0.003289 | 0.005004 | 0.00749 | 0.011484 |
| | 1.00 | | 0.002897 | 0.004044 | 0.005917 | 0.009103 | 0.012801 |
| | 1.25 | | 0.003466 | 0.004962 | 0.006988 | 0.010396 | 0.015241 |
| ^bDMIIm | 0.750 | 0.000483 | 0.000669 | 0.001042 | 0.001453 | 0.002023 | |
| Tz | 0.250 | 8.62E-05 | 0.000162 | 0.00027 | 0.000333 | 0.000528 | |
| | 0.500 | 0.000946 | 0.000534 | 0.000434 | 0.000631 | 0.001733 | |
| | 0.750 | 0.000387 | 0.000448 | 0.000662 | 0.000979 | 0.00131 | |
| | 1.00 | 0.000597 | 0.000587 | 0.000883 | 0.00127 | 0.001759 | |
| | 1.25 | 0.000702 | 0.000694 | 0.001033 | 0.001524 | 0.00215 | |

^b k_{obs} obtained for 30 fold nucleophile concentration, 0.750 mM, at different temperatures

Table B 9 Average rate constants, k_{obs} obtained from for the reactions of Pt4 (2.50×10^{-5} M)* with the different concentrations of the nucleophiles at different temperatures.

| Nucleophile | Conc/mM | $k_{\text{obs}}/ \text{s}^{-1}$ obtained at different temperatures in Kelvin | | | | | |
|-------------------------|---------|--|----------------------|-----------------------|-----------------------|-----------------------|-----------------------|
| | | 288.15 | 293.15 | 298.15 | 303.15 | 308.15 | 313.15 |
| Pz | 0.250 | | 0.000263 | 0.000318 | 0.000384 | 0.000601 | 0.000532 |
| | 0.500 | | 0.000296 | 0.000394 | 0.000595 | 0.000766 | 0.000856 |
| | 0.750 | | 0.000351 | 0.000489 | 0.000622 | 0.000894 | 0.001109 |
| | 1.00 | | 0.000407 | 0.000585 | 0.000754 | 0.001173 | 0.001432 |
| | 1.25 | | 0.000503 | 0.000676 | 0.000901 | 0.00138 | 0.001651 |
| Im | 0.248 | | 0.000226 | 0.000389 | 0.000584 | 0.0009 | 0.001371 |
| | 0.495 | | 0.000391 | 0.000685 | 0.000929 | 0.001423 | 0.002141 |
| | 0.740 | | 0.000537 | 0.000788 | 0.001199 | 0.001808 | 0.002662 |
| | 0.990 | | 0.000688 | 0.001075 | 0.001539 | 0.002239 | 0.003335 |
| | 1.24 | | 0.000903 | 0.001239 | 0.001903 | 0.002673 | 0.003941 |
| MIm | 0.250 | | 0.000285 | 0.000458 | 0.000801 | 0.000983 | 0.001918 |
| | 0.500 | | 0.000442 | 0.00077 | 0.001179 | 0.001752 | 0.002704 |
| | 0.750 | | 0.000618 | 0.001032 | 0.001516 | 0.002338 | 0.003419 |
| | 1.00 | | 0.000781 | 0.001244 | 0.001852 | 0.003019 | 0.004141 |
| | 1.25 | | 0.000895 | 0.001533 | 0.002253 | 0.003474 | 0.004975 |
| ^bDMIm | 0.750 | 0.000114 | 0.000172 | 0.000283 | 0.000427 | 0.000638 | |
| Tz | 0.250 | | 8.4×10^{-5} | 8.89×10^{-4} | 1.47×10^{-4} | 1.77×10^{-4} | 2.75×10^{-4} |
| | 0.500 | | 0.000121 | 0.00016 | 2.61×10^{-4} | 3.49×10^{-4} | 5.05×10^{-4} |
| | 0.750 | | 0.000171 | 0.000237 | 3.32×10^{-4} | 5.70×10^{-4} | 7.80×10^{-4} |
| | 1.00 | | 0.000223 | 0.000323 | 4.23×10^{-4} | 7.51×10^{-4} | 0.00104 |
| | 1.25 | | 0.000243 | 0.000366 | 5.69×10^{-4} | 8.58×10^{-4} | 0.00127 |

^b k_{obs} obtained for 30 fold nucleophile concentration, 0.750 mM, at different temperatures

* Concentration of Pt4 is 2.48×10^{-5} M for the reactions of imidazole

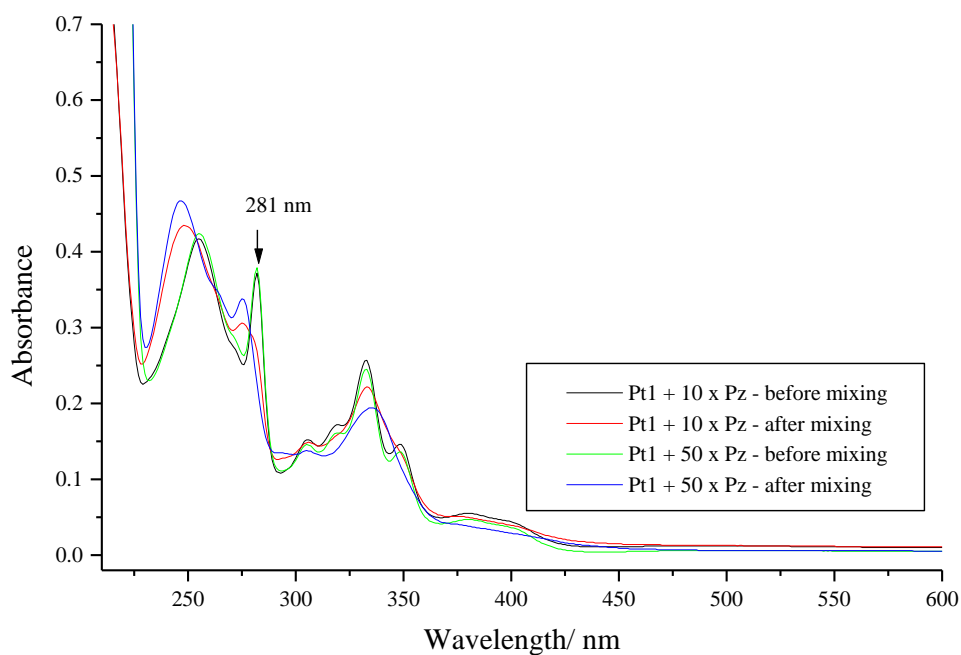


Figure B 1 Change in absorbance for the reaction of Pt1 (1.51×10^{-5} M) with pyrazole (1.51×10^{-4} M (10 fold) and 7.52×10^{-4} M (50 fold)) in methanol ($I = 0.1$ M, $\text{LiCF}_3\text{SO}_3 + \text{NaCl}$) at 298.15 K.

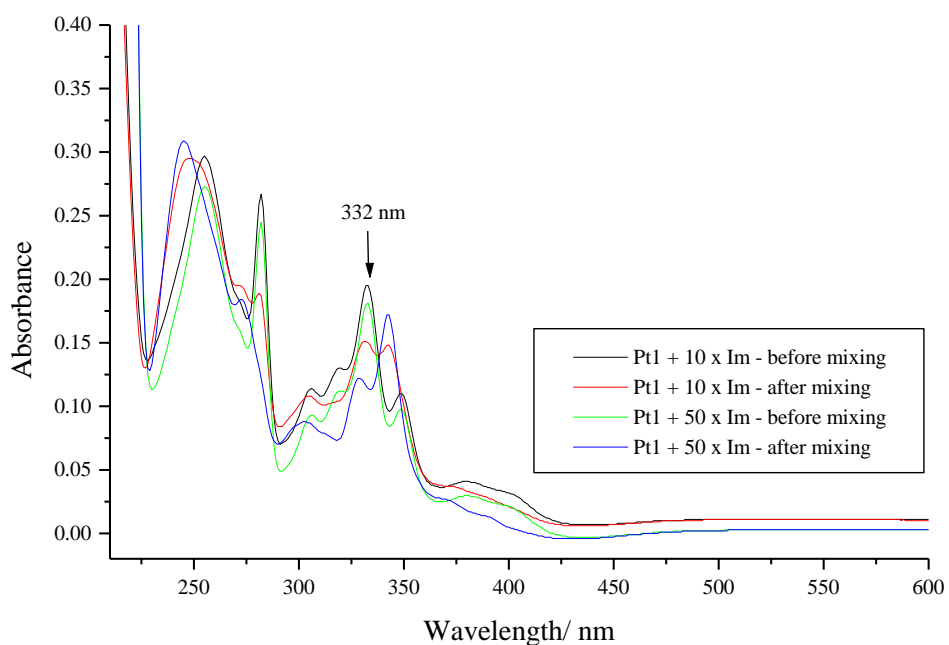


Figure B 2 Change in absorbance for the reaction of Pt1 (1.51×10^{-5} M) with imidazole (1.51×10^{-4} M (10 fold) and 7.52×10^{-4} M (50 fold)) in methanol ($I = 0.1$ M, $\text{LiCF}_3\text{SO}_3 + \text{NaCl}$) at 298.15 K.

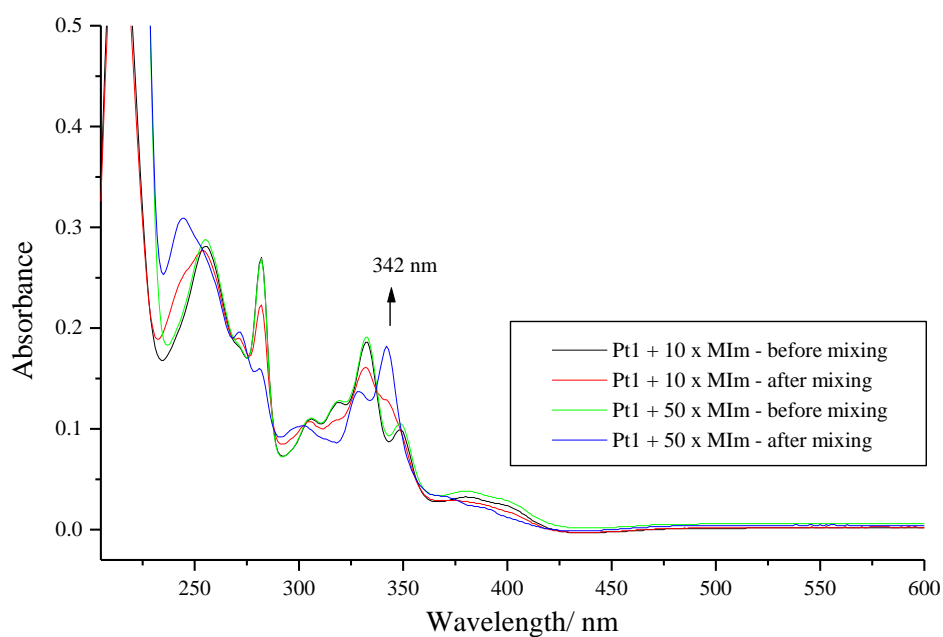


Figure B 3 Change in absorbance for the reaction of Pt1 (1.51×10^{-5} M) with 1-methylimidazole (1.51×10^{-4} M (10 fold) and 7.52×10^{-4} M (50 fold)) in methanol ($I = 0.1$ M, $\text{LiCF}_3\text{SO}_3 + \text{NaCl}$) at 298.15 K.

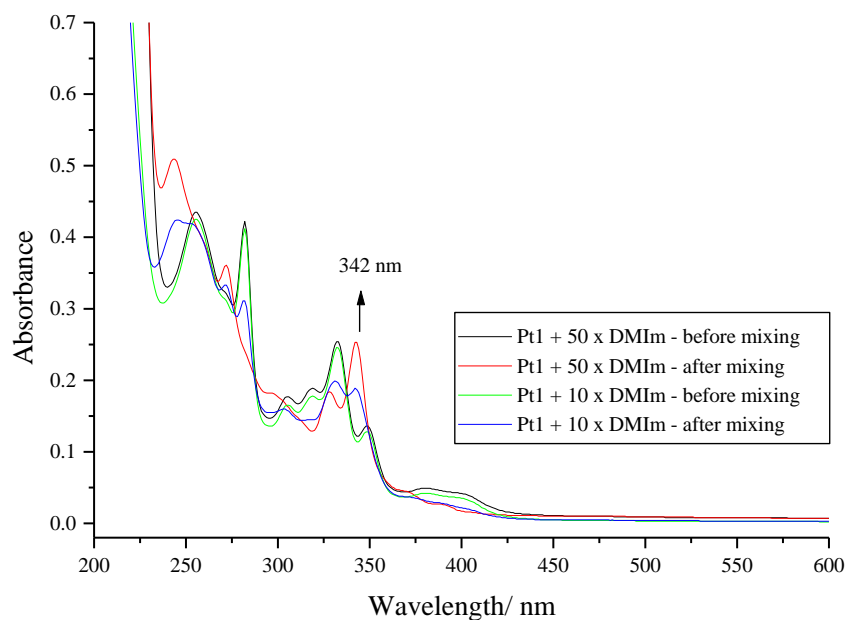


Figure B 4 Change in absorbance for the reaction of Pt1 (1.51×10^{-5} M) with 1,2-dimethylimidazole (1.51×10^{-4} M (10 fold) and 7.52×10^{-4} M (50 fold)) in methanol ($I = 0.1$ M, $\text{LiCF}_3\text{SO}_3 + \text{NaCl}$) at 298.15 K.

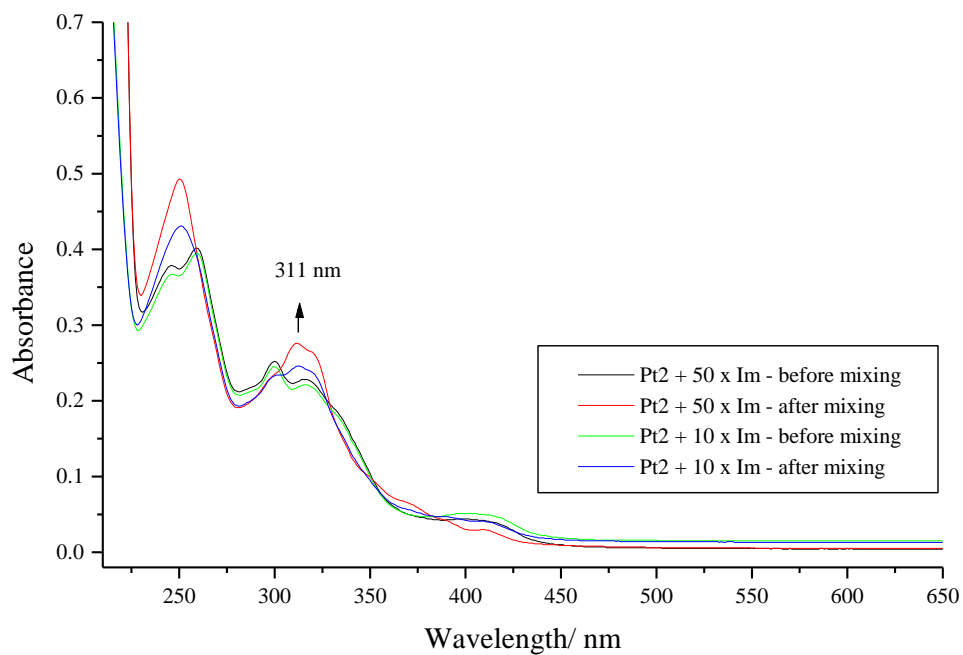


Figure B 5 Change in absorbance for the reaction of Pt2 (1.51×10^{-5} M) with imidazole (1.51×10^{-4} M (10 fold) and 7.52×10^{-4} M (50 fold)) in methanol ($I = 0.1$ M, $\text{LiCF}_3\text{SO}_3 + \text{NaCl}$) at 298.15 K.

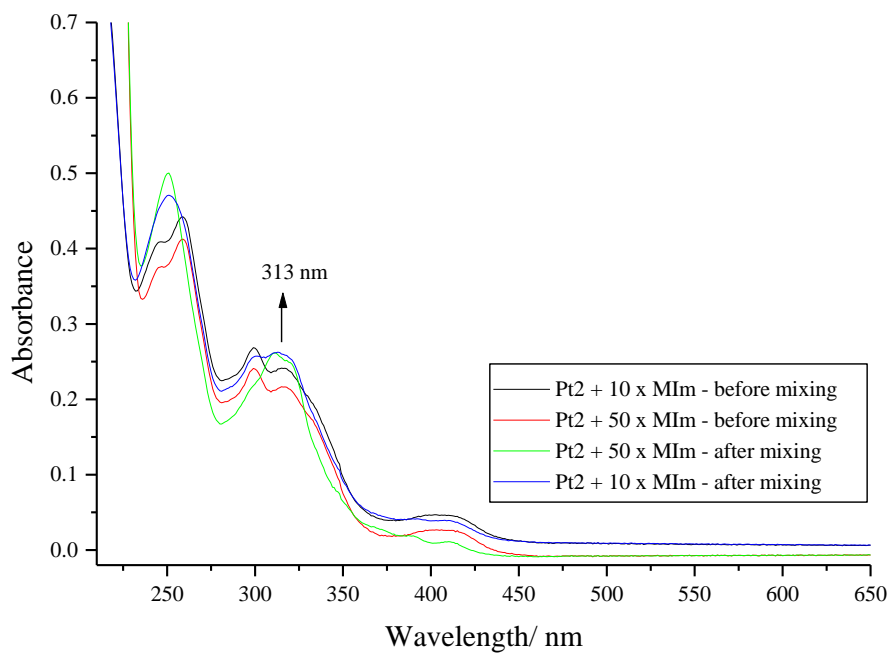


Figure B 6 Change in absorbance for the reaction of Pt2 (1.51×10^{-5} M) with 1-methylimidazole (1.51×10^{-4} M (10 fold) and 7.52×10^{-4} M (50 fold)) in methanol ($I = 0.1$ M, $\text{LiCF}_3\text{SO}_3 + \text{NaCl}$) at 298.15 K.

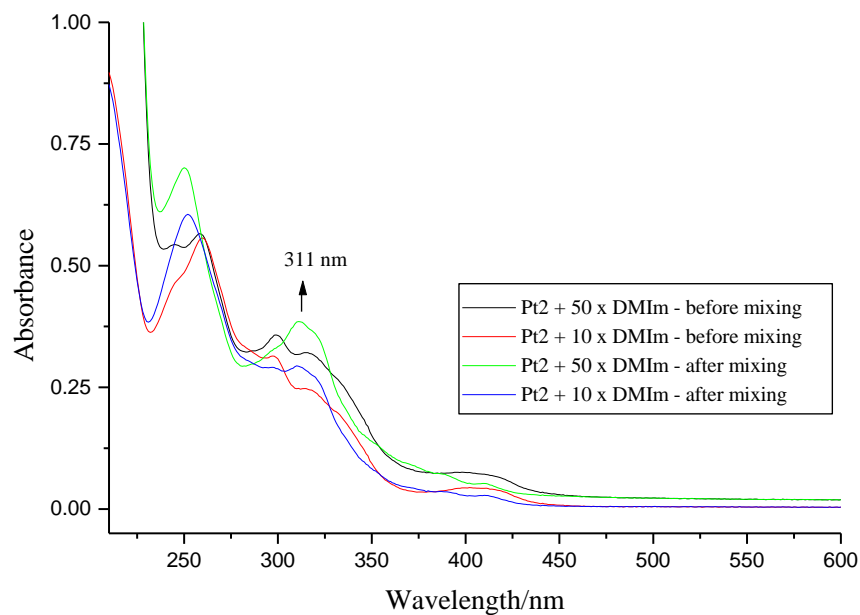


Figure B 7 Change in absorbance for the reaction of Pt2 (1.51×10^{-5} M) with 1,2-dimethylimidazole (1.51×10^{-4} M (10 fold) and 7.52×10^{-4} M (50 fold)) in methanol ($I = 0.1$ M, $\text{LiCF}_3\text{SO}_3 + \text{NaCl}$) at 298.15 K.

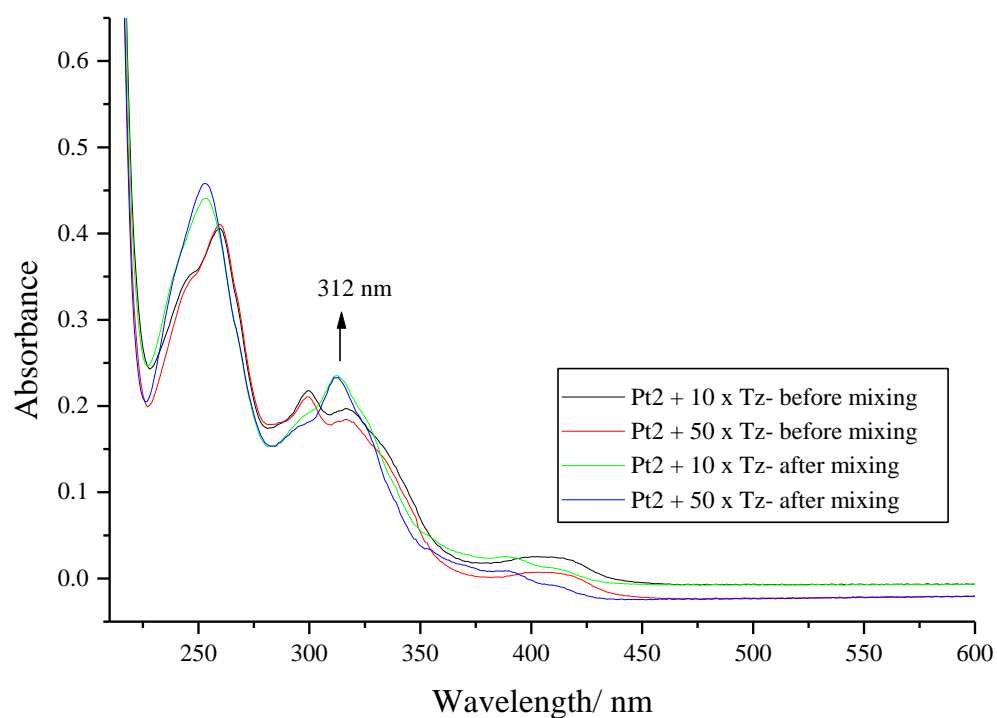


Figure B 8 Change in absorbance for the reaction of Pt2 (1.51×10^{-5} M) with triazole (1.51×10^{-4} M (10 fold) and 7.52×10^{-4} M (50 fold)) in methanol ($I = 0.1$ M, $\text{LiCF}_3\text{SO}_3 + \text{NaCl}$) at 298.15 K.

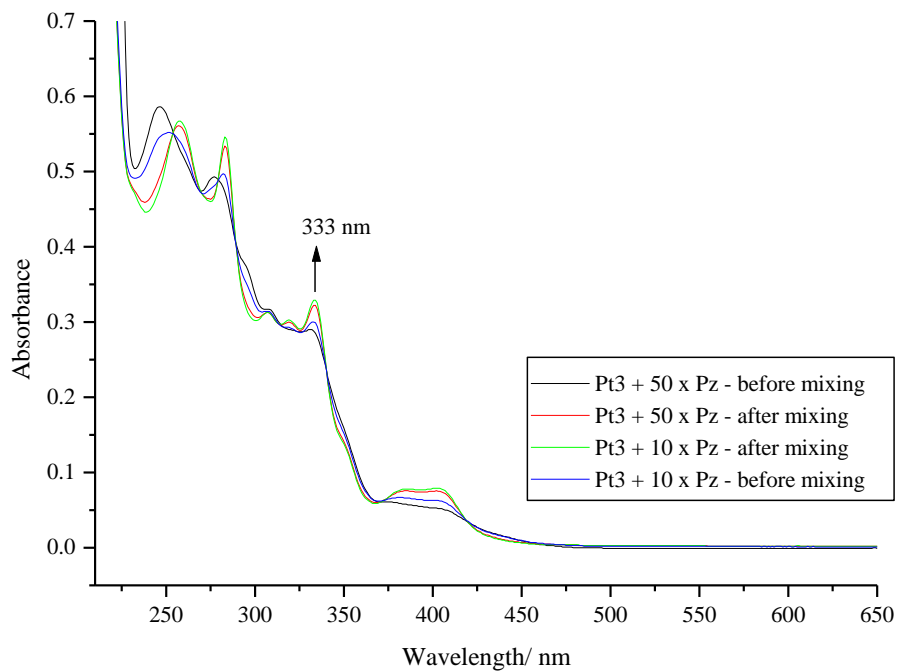


Figure B 9 Change in absorbance for the reaction of Pt3 (2.50×10^{-5} M) with pyrazole (2.5×10^{-4} M (10 fold) and 1.25×10^{-3} M (50 fold)) in methanol ($I = 0.1$ M, $\text{LiCF}_3\text{SO}_3 + \text{NaCl}$) at 298.15 K.

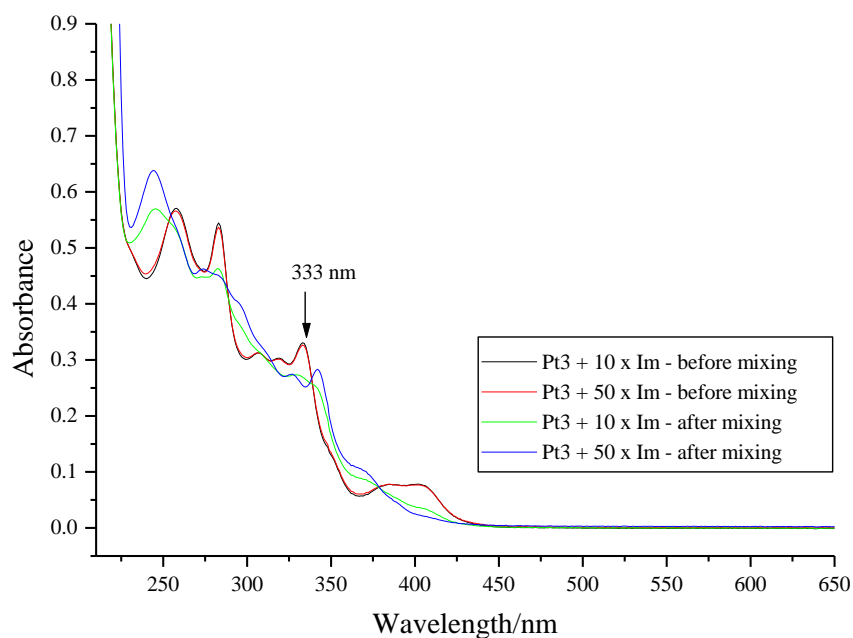


Figure B 10 Change in absorbance for the reaction of Pt3 (2.50×10^{-5} M) with imidazole (2.5×10^{-4} M (10 fold) and 1.25×10^{-3} M (50 fold)) in methanol ($I = 0.1$ M, $\text{LiCF}_3\text{SO}_3 + \text{NaCl}$) at 298.15 K.

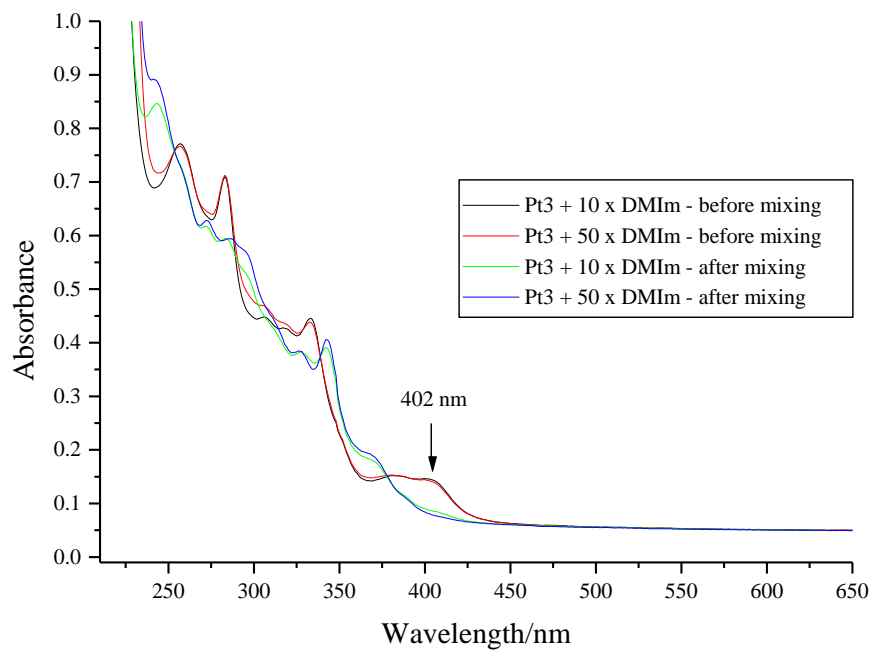


Figure B 11 Change in absorbance for the reaction of Pt3 (2.50×10^{-5} M) with 1,2-dimethylimidazole (2.50×10^{-4} M (10 fold) and 1.25×10^{-3} M (50 fold)) in methanol ($I = 0.1$ M, $\text{LiCF}_3\text{SO}_3 + \text{NaCl}$) at 298.15 K.

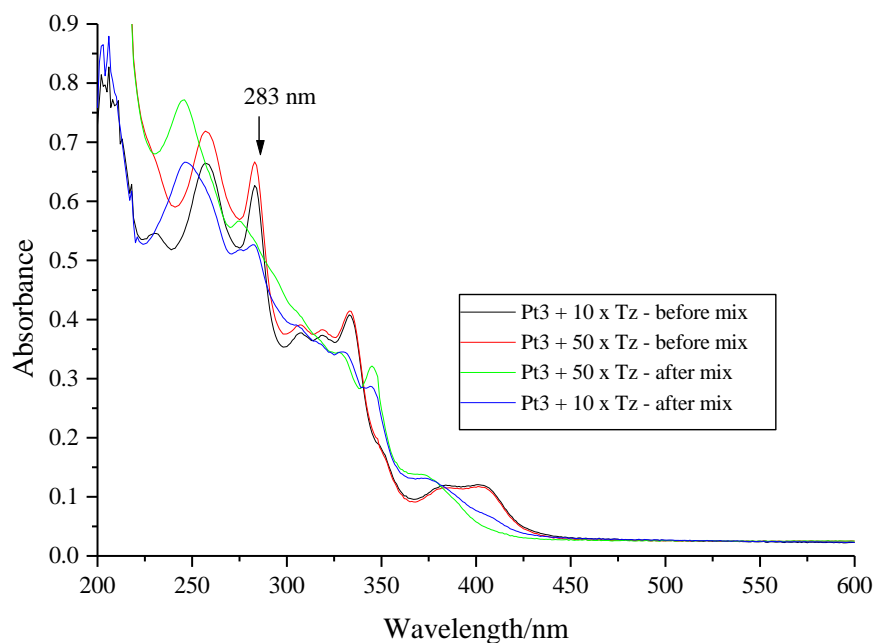


Figure B 12 Change in absorbance for the reaction of Pt3 (2.50×10^{-5} M) with triazole (2.50×10^{-4} M (10 fold) and 1.25×10^{-3} M (50 fold)) in methanol ($I = 0.1$ M, $\text{LiCF}_3\text{SO}_3 + \text{NaCl}$) at 298.15 K.

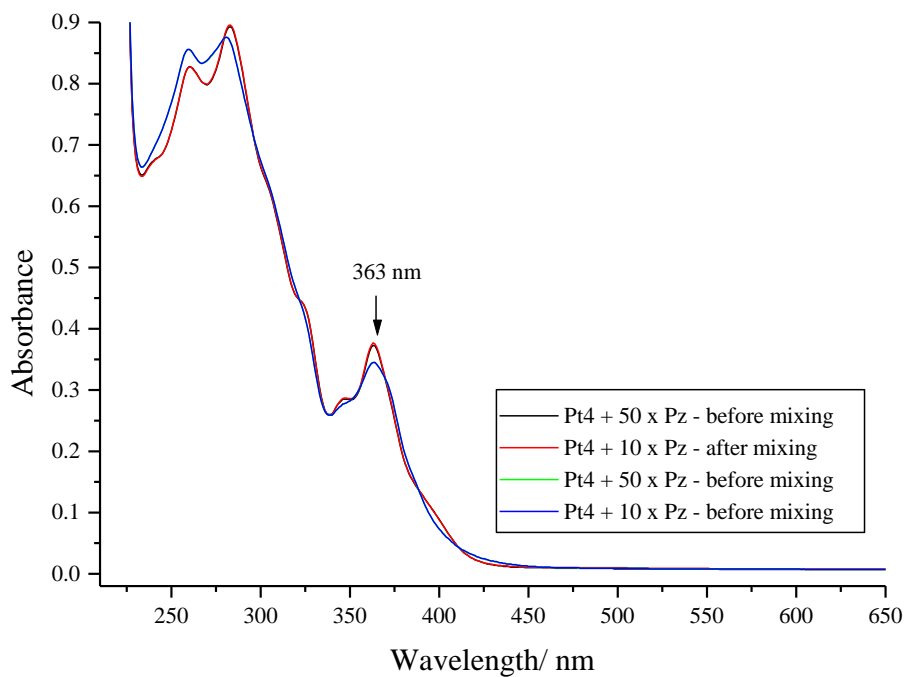


Figure B 13 Change in absorbance for the reaction of Pt4 (2.50×10^{-5} M) with pyrazole (2.50×10^{-4} M (10 fold) and 1.25×10^{-3} M (50 fold)) in methanol ($I = 0.1$ M, LiCF₃SO₃ + NaCl) at 298.15 K.

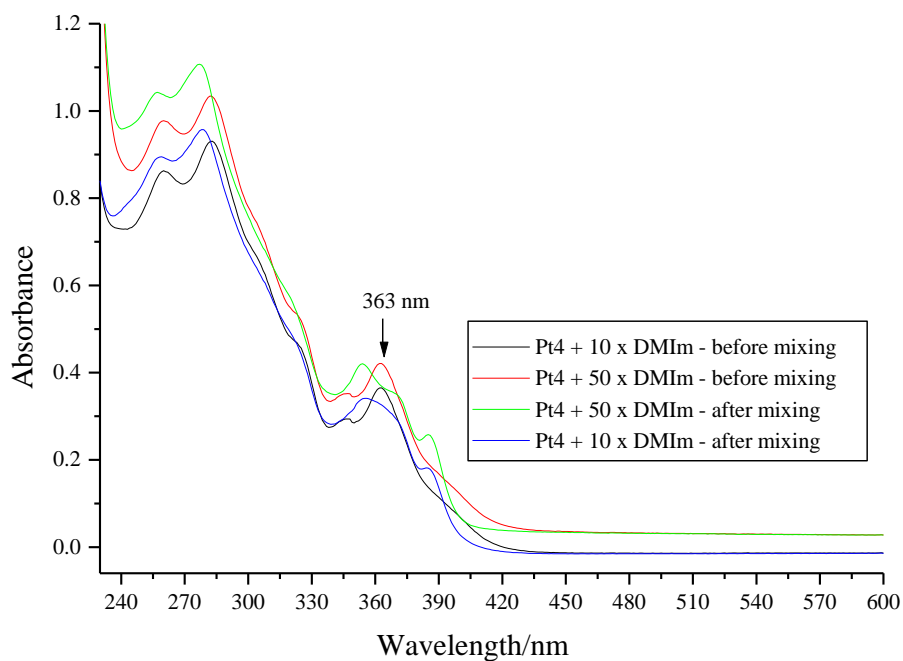


Figure B 14 Change in absorbance for the reaction of Pt4 (2.50×10^{-5} M) with 1,2-dimethylimidazole (2.50×10^{-4} M (10 fold) and 1.25×10^{-3} M (50 fold)) in methanol ($I = 0.1$ M, LiCF₃SO₃ + NaCl) at 298.15 K.

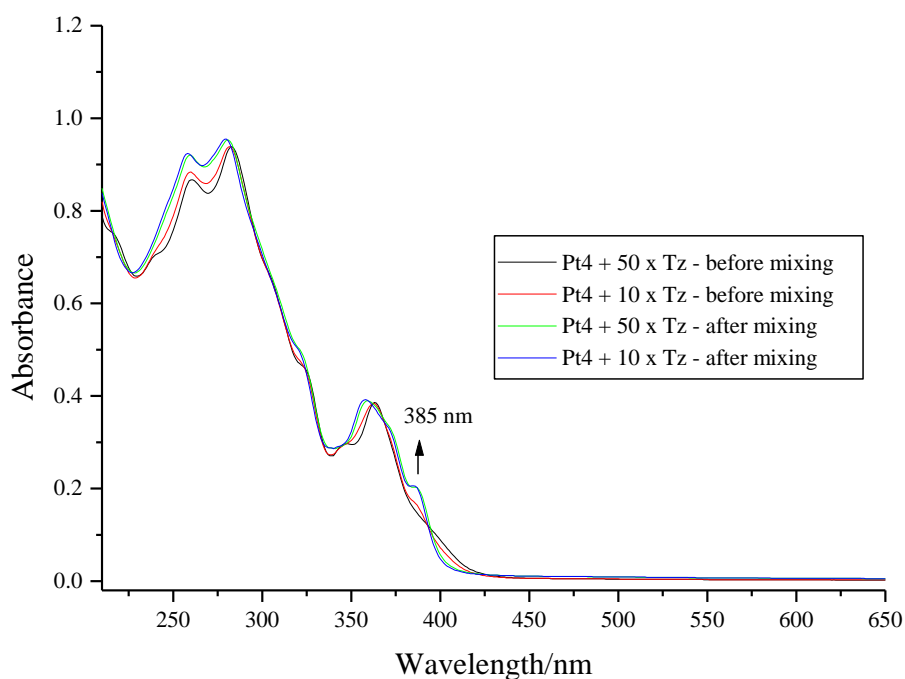


Figure B 15 Change in absorbance for the reaction of Pt4 (2.50×10^{-5} M) with triazole (2.50×10^{-4} M (10 fold) and 1.25×10^{-3} M (50 fold)) in methanol ($I = 0.1$ M, $\text{LiCF}_3\text{SO}_3 + \text{NaCl}$) at 298.15 K.

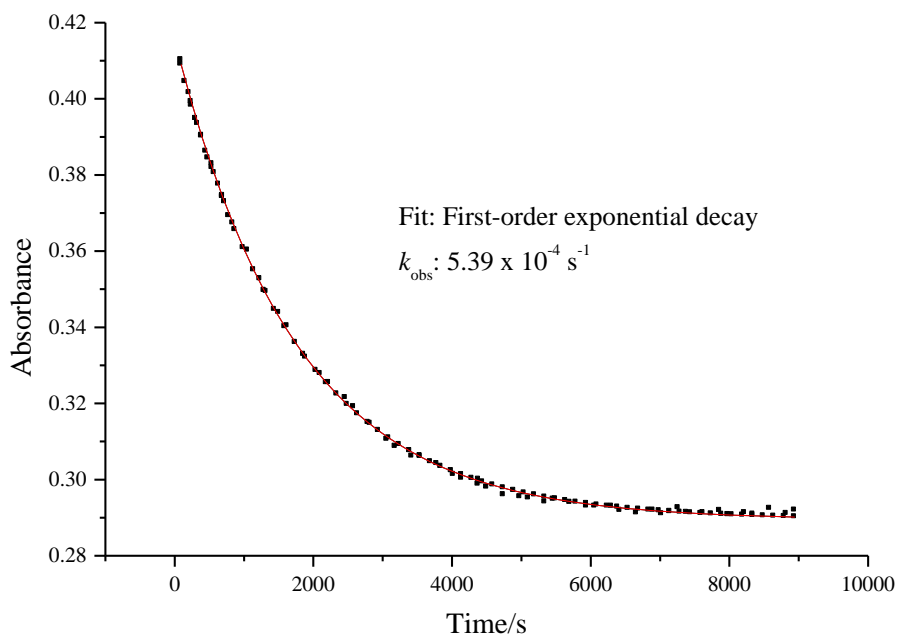


Figure B 16 Spectrum obtained from Cary UV/Visible Spectrophotometer for the reaction of Pt1 (1.51×10^{-5} M) with pyrazole (4.51×10^{-4} M (30 fold)) in methanol ($I = 0.1$ M, $\text{LiCF}_3\text{SO}_3 + \text{NaCl}$) at 298.15 K.

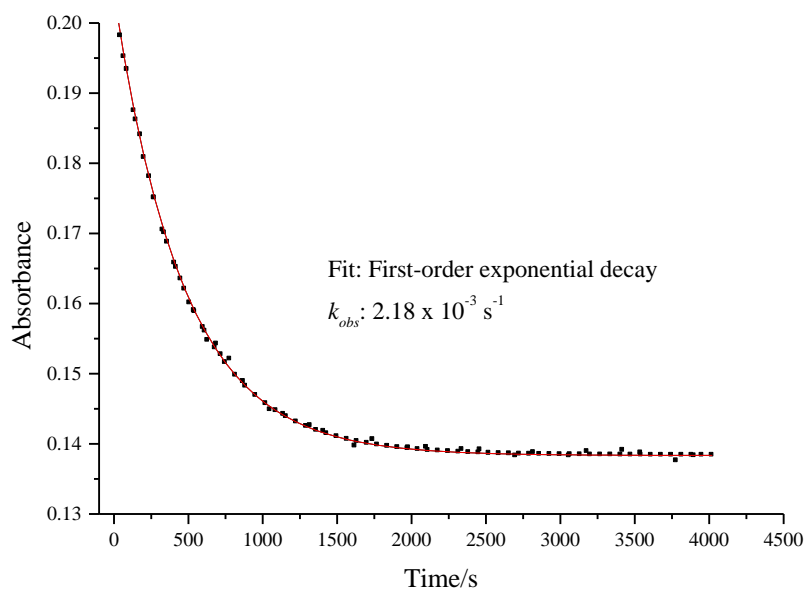


Figure B 17 Spectrum obtained from Cary UV/Visible Spectrophotometer for the reaction of Pt1 ($1.51 \times 10^{-5} \text{ M}$) with imidazole ($4.51 \times 10^{-4} \text{ M}$ (30 fold) in methanol ($I = 0.1 \text{ M}$, $\text{LiCF}_3\text{SO}_3 + \text{NaCl}$) at 298.15 K.

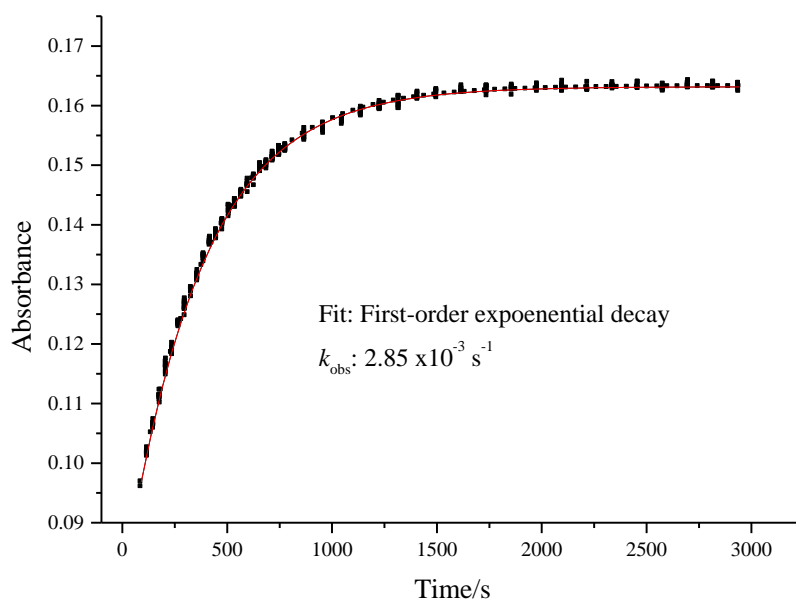


Figure B 18 Spectrum obtained from Cary UV/Visible Spectrophotometer for the reaction of Pt1 ($1.51 \times 10^{-5} \text{ M}$) with 1-methylimidazole ($4.51 \times 10^{-4} \text{ M}$ (30 fold) in methanol ($I = 0.1 \text{ M}$, $\text{LiCF}_3\text{SO}_3 + \text{NaCl}$) at 298.15 K.

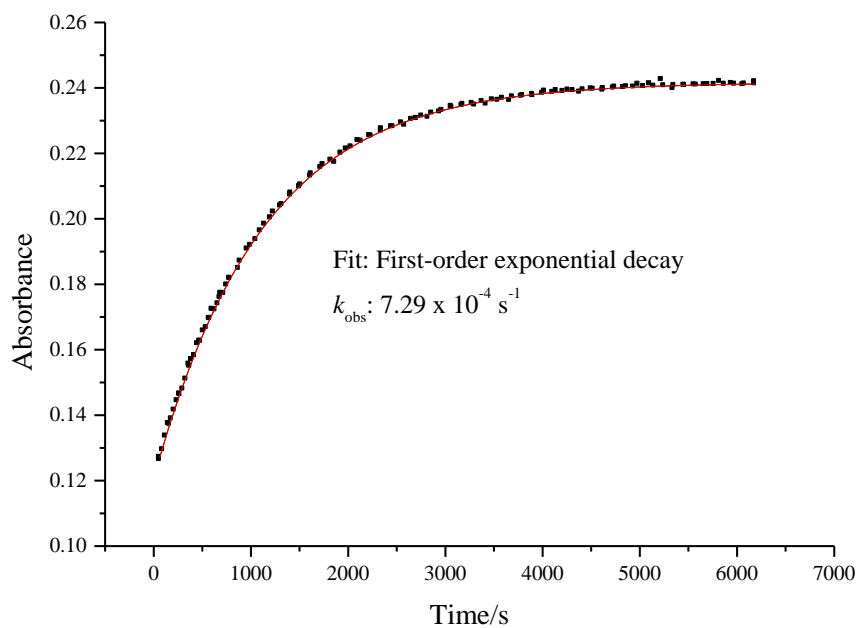


Figure B 19 Spectrum obtained from Cary UV/Visible Spectrophotometer for the reaction of Pt1 ($1.51 \times 10^{-5} \text{ M}$) with 1,2-dimethylimidazole ($4.51 \times 10^{-4} \text{ M}$ (30 fold) in methanol ($I = 0.1 \text{ M}$, $\text{LiCF}_3\text{SO}_3 + \text{NaCl}$) at 298.15 K.

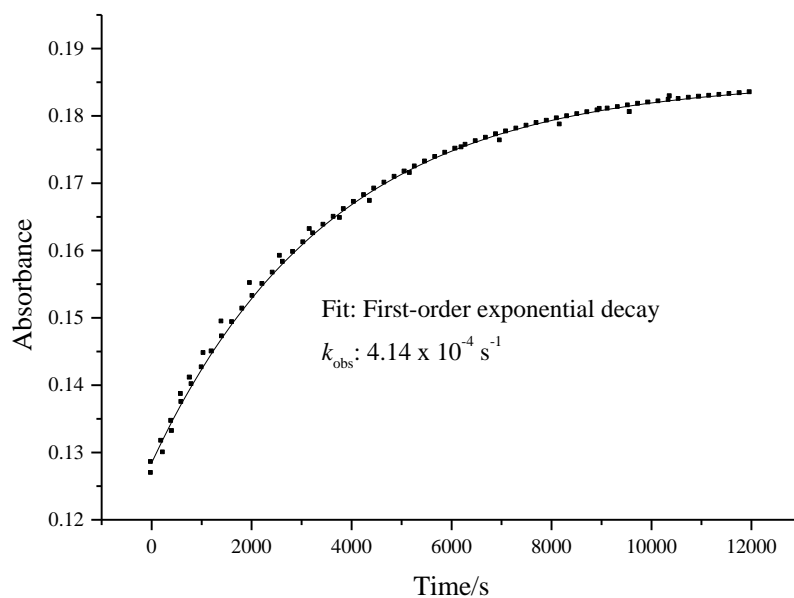


Figure B 20 Spectrum obtained from Cary UV/Visible Spectrophotometer for the reaction of Pt1 ($1.51 \times 10^{-5} \text{ M}$) with triazole ($4.51 \times 10^{-4} \text{ M}$ (30 fold) in methanol ($I = 0.1 \text{ M}$, $\text{LiCF}_3\text{SO}_3 + \text{NaCl}$) at 298.15 K.

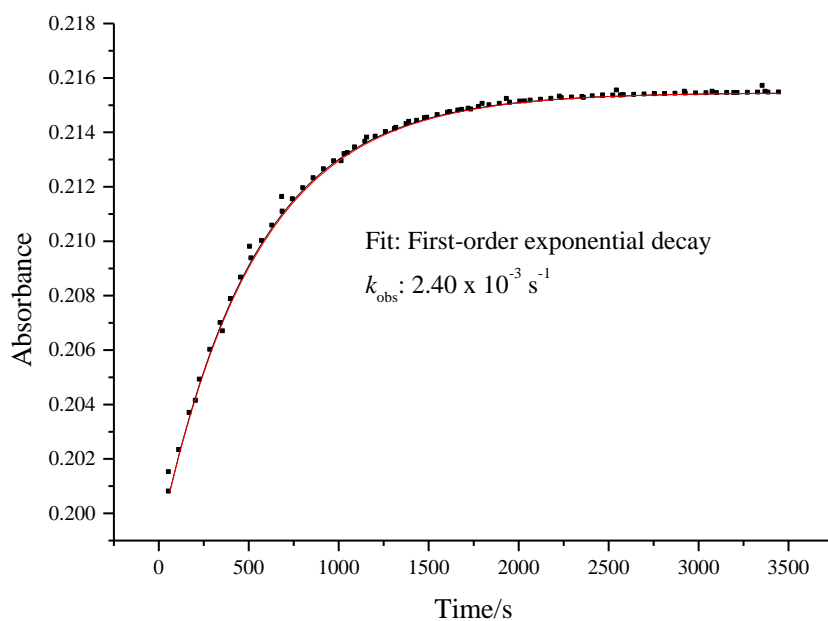


Figure B 21 Spectrum obtained from Cary UV/Visible Spectrophotometer for the reaction of Pt2 ($1.51 \times 10^{-5} \text{ M}$) with pyrazole ($4.51 \times 10^{-4} \text{ M}$ (30 fold) in methanol ($I = 0.1 \text{ M}$, $\text{LiCF}_3\text{SO}_3 + \text{NaCl}$) at 298.15 K.

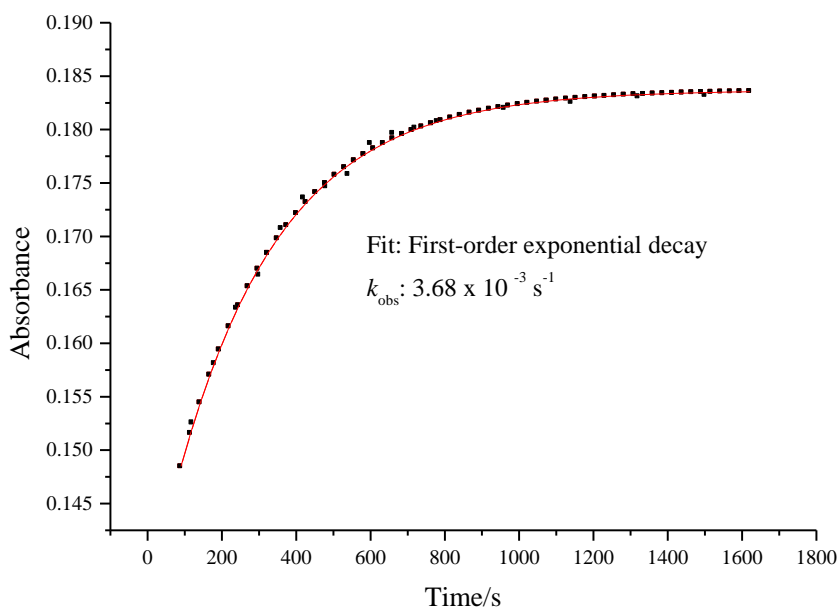


Figure B 22 Spectrum obtained from Cary UV/Visible Spectrophotometer for the reaction of Pt2 ($1.51 \times 10^{-5} \text{ M}$) with imidazole ($4.51 \times 10^{-4} \text{ M}$ (30 fold) in methanol ($I = 0.1 \text{ M}$, $\text{LiCF}_3\text{SO}_3 + \text{NaCl}$) at 298.15 K.

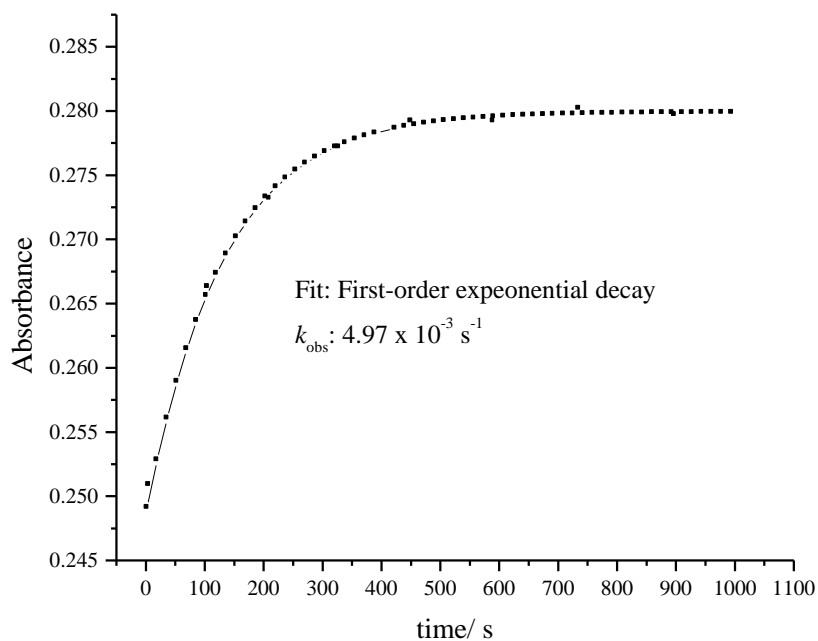


Figure B 23 Spectrum obtained from Cary UV/Visible Spectrophotometer for the reaction of Pt2 ($1.51 \times 10^{-5} \text{ M}$) with 1-methylimidazole ($4.51 \times 10^{-4} \text{ M}$ (30 fold) in methanol ($I = 0.1 \text{ M}$, $\text{LiCF}_3\text{SO}_3 + \text{NaCl}$) at 298.15 K.

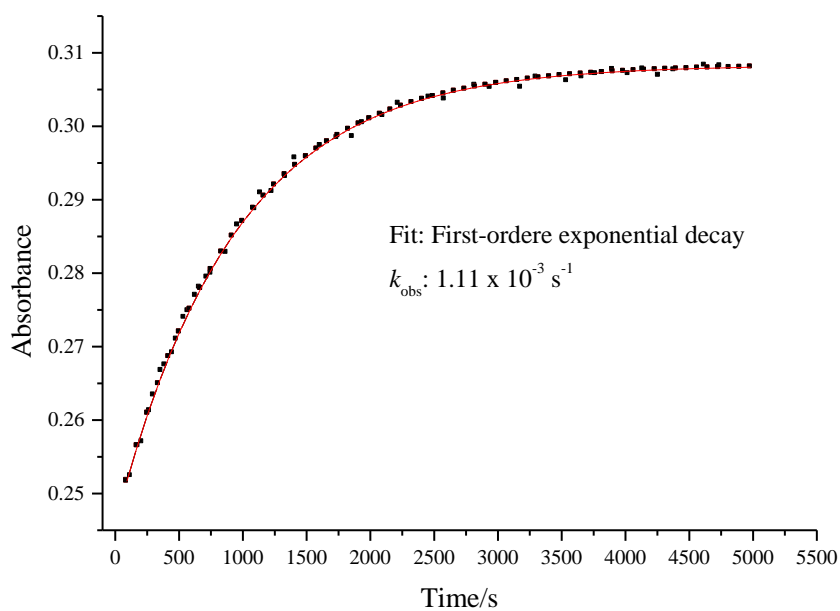


Figure B 24 Spectrum obtained from Cary UV/Visible Spectrophotometer for the reaction of Pt2 ($1.51 \times 10^{-5} \text{ M}$) with 1,2-dimethylimidazole ($4.51 \times 10^{-4} \text{ M}$ (30 fold) in methanol ($I = 0.1 \text{ M}$, $\text{LiCF}_3\text{SO}_3 + \text{NaCl}$) at 298.15 K.

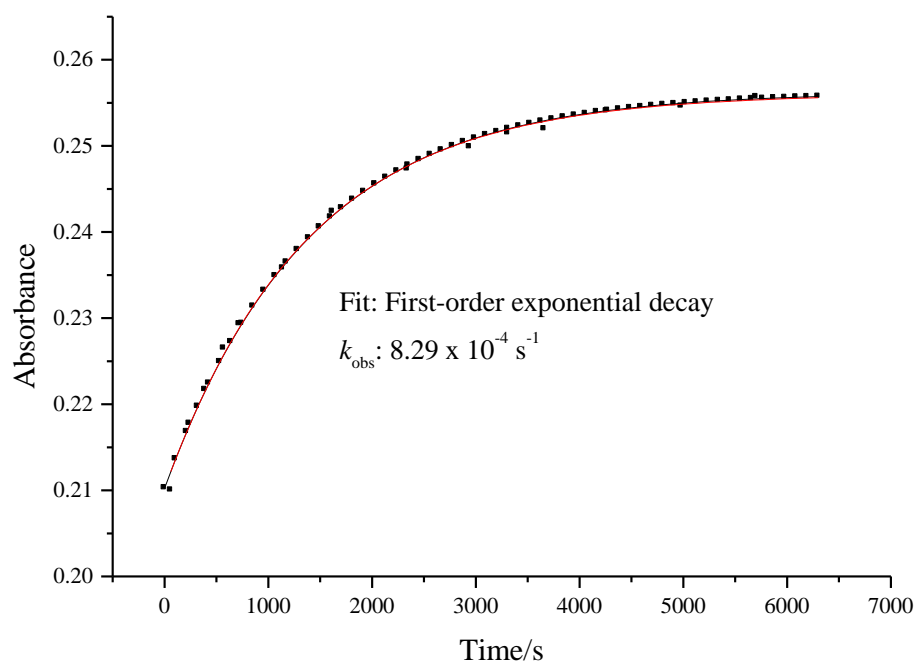


Figure B 25 Spectrum obtained from Cary UV/Visible Spectrophotometer for the reaction of Pt2 ($1.51 \times 10^{-5} \text{ M}$) with triazole ($4.51 \times 10^{-4} \text{ M}$ (30 fold) in methanol ($I = 0.1 \text{ M}$, $\text{LiCF}_3\text{SO}_3 + \text{NaCl}$) at 298.15 K.

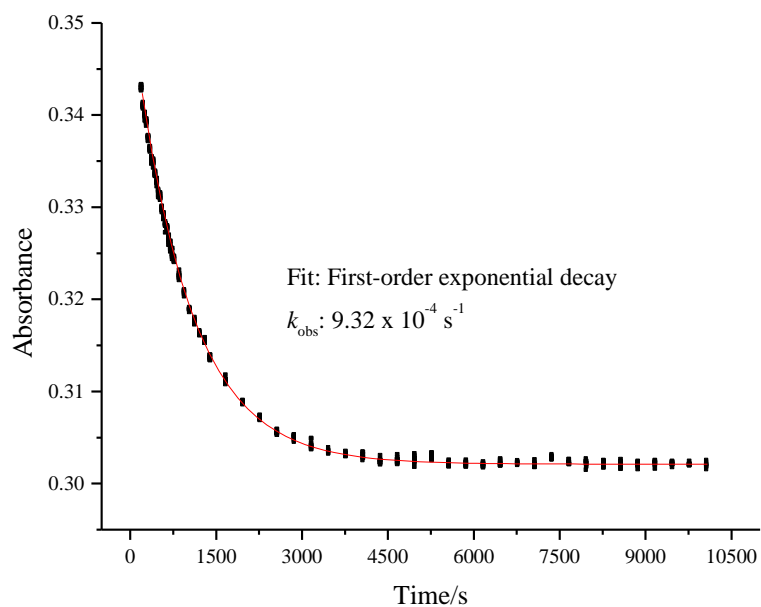


Figure B 26 Spectrum obtained from Cary UV/Visible Spectrophotometer for the reaction of Pt3 ($2.50 \times 10^{-5} \text{ M}$) with pyrazole ($7.50 \times 10^{-4} \text{ M}$ (30 fold) in methanol ($I = 0.1 \text{ M}$, $\text{LiCF}_3\text{SO}_3 + \text{NaCl}$) at 298.15 K.

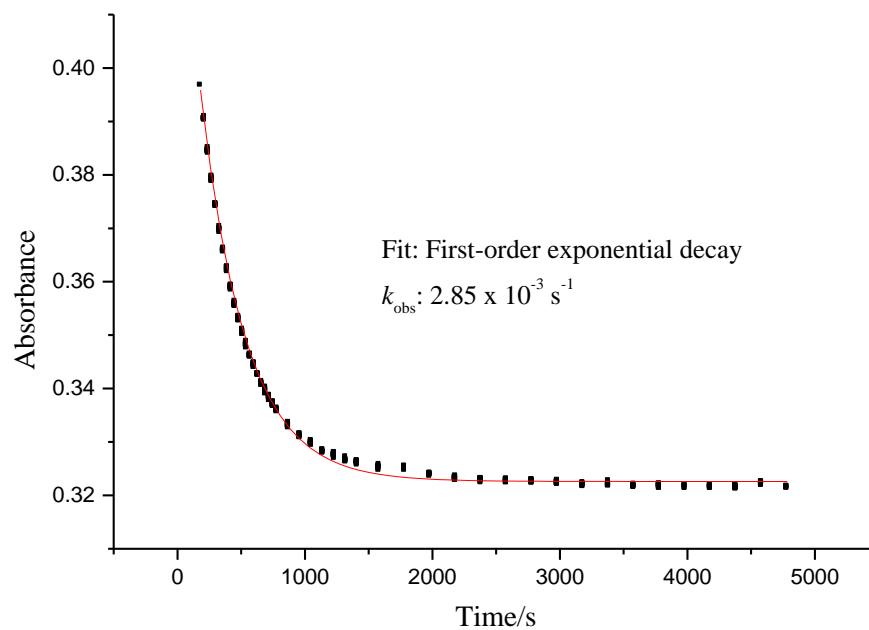


Figure B 27 Spectrum obtained from Cary UV/Visible Spectrophotometer for the reaction of Pt3 (2.50×10^{-5} M) with imidazole (7.50×10^{-4} M (30 fold) in methanol ($I = 0.1$ M, $\text{LiCF}_3\text{SO}_3 + \text{NaCl}$) at 298.15 K.

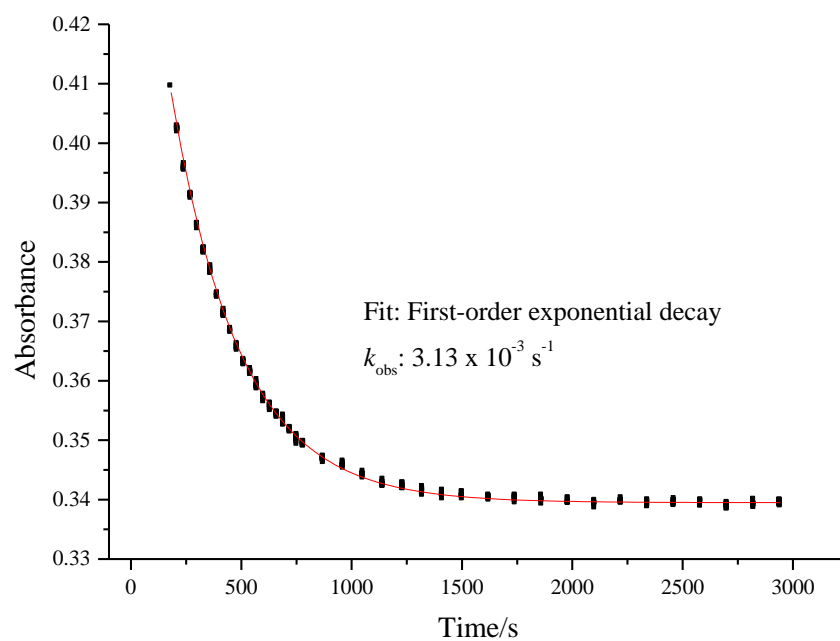


Figure B 28 Spectrum obtained from Cary UV/Visible Spectrophotometer for the reaction of Pt3 (2.50×10^{-5} M) with 1-methylimidazole (7.50×10^{-4} M (30 fold) in methanol ($I = 0.1$ M, $\text{LiCF}_3\text{SO}_3 + \text{NaCl}$) at 298.15 K.

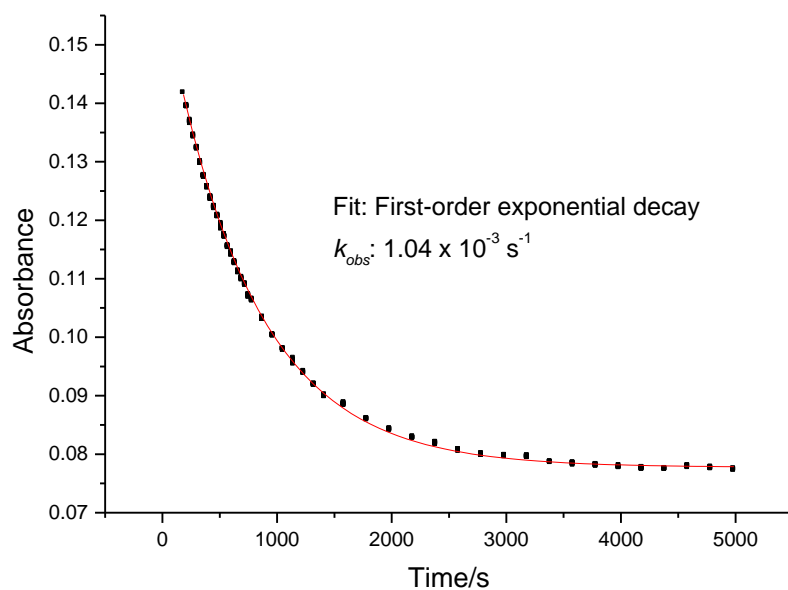


Figure B 29 Spectrum obtained from Cary UV/Visible Spectrophotometer for the reaction of Pt3 ($2.50 \times 10^{-5} \text{ M}$) with 1,2-dimethylimidazole ($7.50 \times 10^{-4} \text{ M}$ (30 fold) in methanol ($I = 0.1 \text{ M}$, $\text{LiCF}_3\text{SO}_3 + \text{NaCl}$) at 298.15 K.

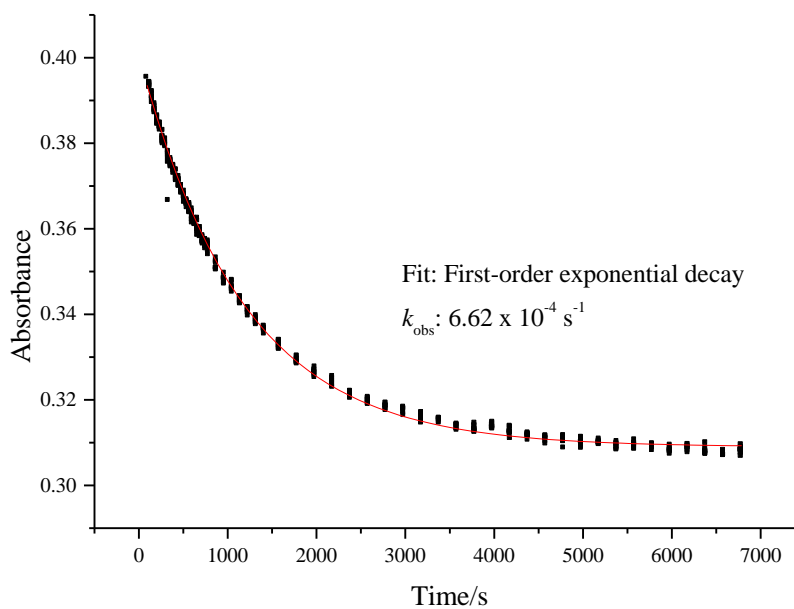


Figure B 30 Spectrum obtained from Cary UV/Visible Spectrophotometer for the reaction of Pt3 ($2.50 \times 10^{-5} \text{ M}$) with triazole ($7.50 \times 10^{-4} \text{ M}$ (30 fold) in methanol ($I = 0.1 \text{ M}$, $\text{LiCF}_3\text{SO}_3 + \text{NaCl}$) at 298.15 K.

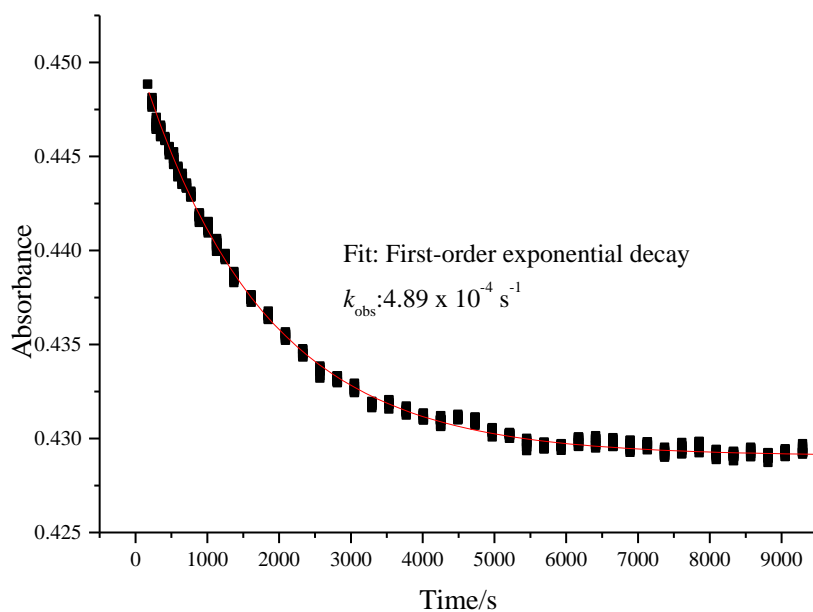


Figure B 31 Spectrum obtained from Cary UV/Visible Spectrophotometer for the reaction of Pt4 ($2.50 \times 10^{-5} \text{ M}$) with pyrazole ($7.50 \times 10^{-4} \text{ M}$ (30 fold) in methanol ($I = 0.1 \text{ M}$, $\text{LiCF}_3\text{SO}_3 + \text{NaCl}$) at 298.15 K.

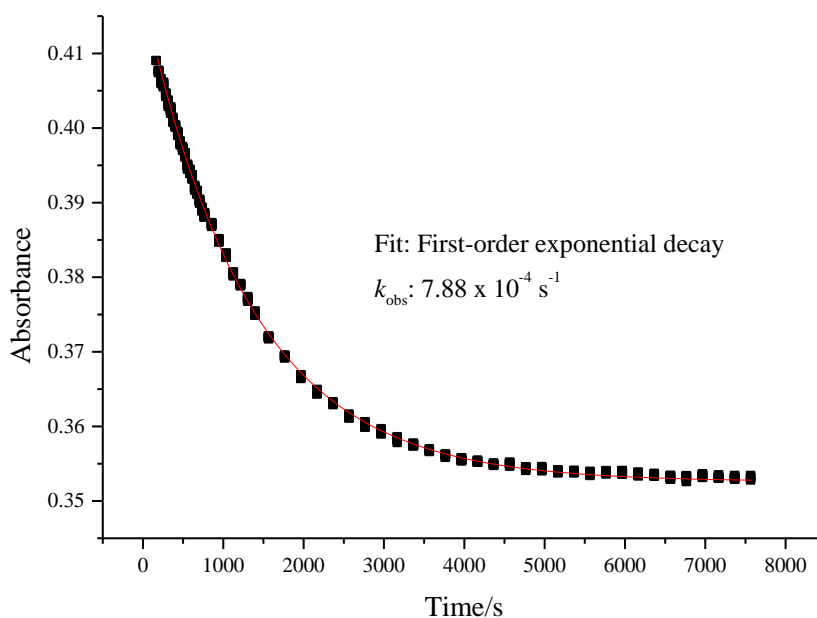


Figure B 32 Spectrum obtained from Cary UV/Visible Spectrophotometer for the reaction of Pt4 ($2.48 \times 10^{-5} \text{ M}$) with imidazole ($7.40 \times 10^{-4} \text{ M}$ (30 fold) in methanol ($I = 0.1 \text{ M}$, $\text{LiCF}_3\text{SO}_3 + \text{NaCl}$) at 298.15 K.

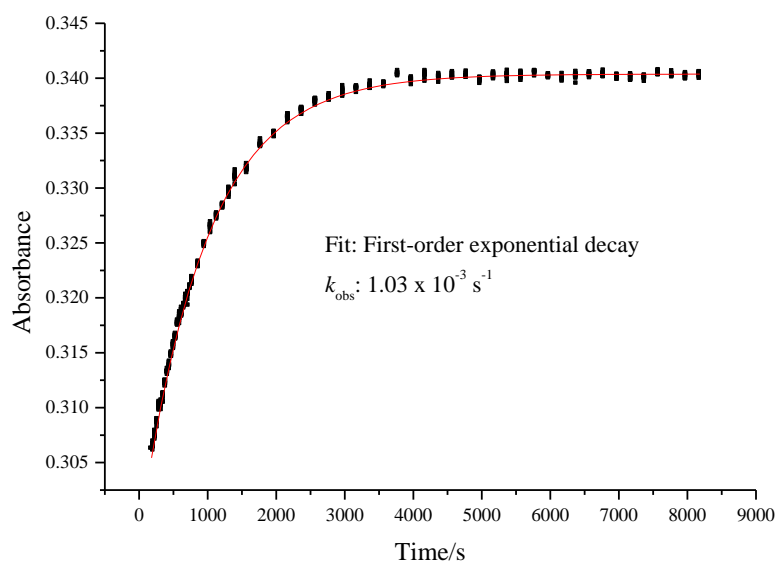


Figure B 33 Spectrum obtained from Cary UV/Visible Spectrophotometer for the reaction of Pt4 ($2.50 \times 10^{-5} \text{ M}$) with 1-methylimidazole ($7.50 \times 10^{-4} \text{ M}$ (30 fold)) in methanol ($I = 0.1 \text{ M}$, $\text{LiCF}_3\text{SO}_3 + \text{NaCl}$) at 298.15 K.

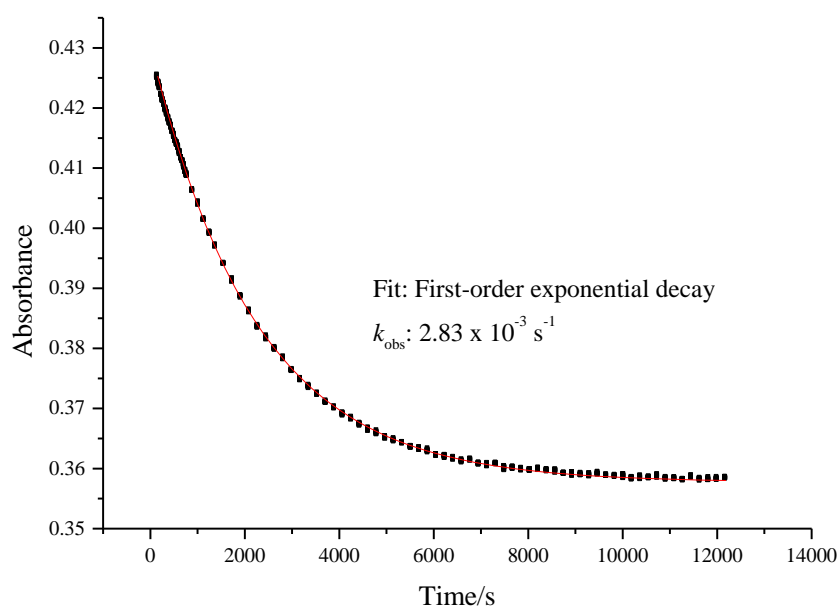


Figure B 34 Spectrum obtained from Cary UV/Visible Spectrophotometer for the reaction of Pt4 ($2.50 \times 10^{-5} \text{ M}$) with 1,2-dimethylimidazole ($7.50 \times 10^{-4} \text{ M}$ (30 fold)) in methanol ($I = 0.1 \text{ M}$, $\text{LiCF}_3\text{SO}_3 + \text{NaCl}$) at 298.15 K.

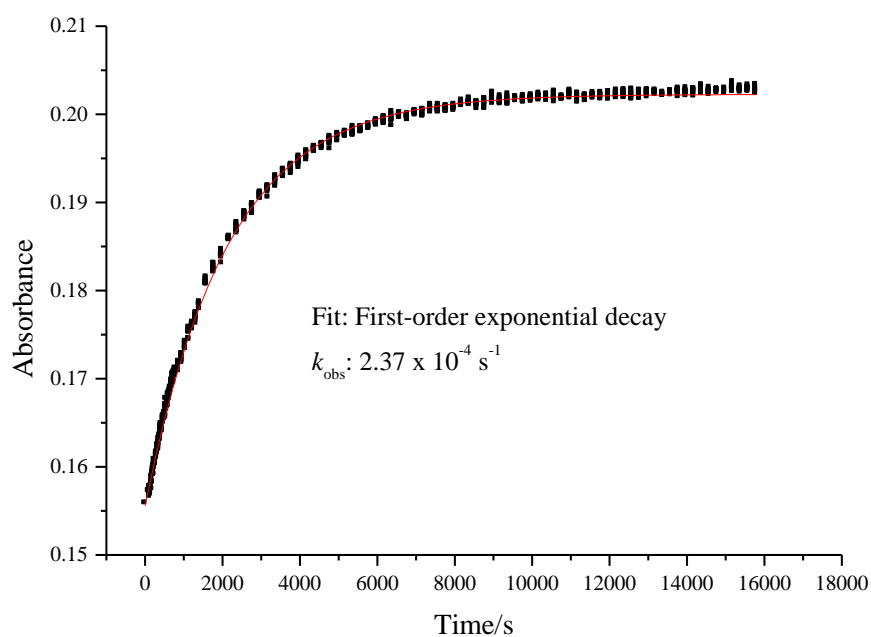


Figure B 35 Spectrum obtained from Cary UV/Visible Spectrophotometer for the reaction of Pt4 ($2.50 \times 10^{-5} \text{ M}$) with triazole ($7.50 \times 10^{-4} \text{ M}$ (30 fold) in methanol ($I = 0.1 \text{ M}$, $\text{LiCF}_3\text{SO}_3 + \text{NaCl}$) at 298.15 K.

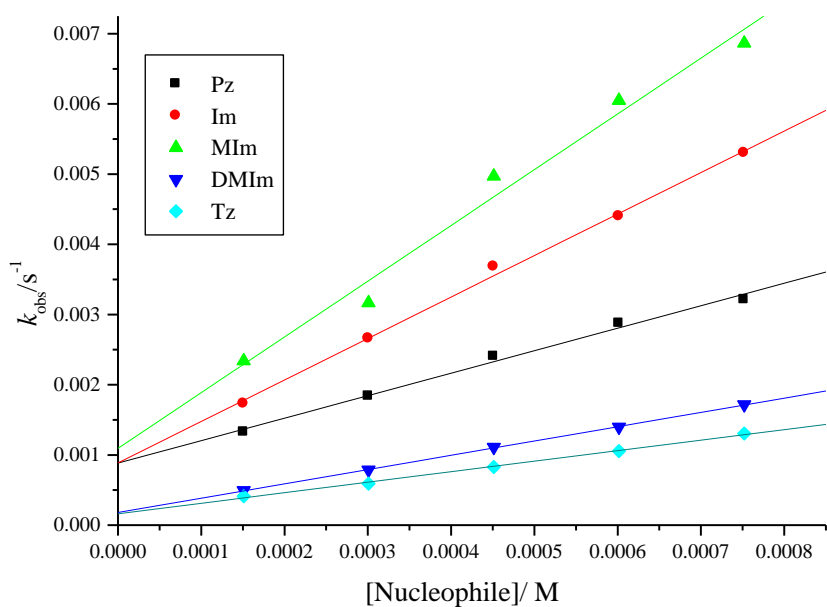


Figure B 36 Dependence of the *pseudo* first-order rate constants (k_{obs}) on the concentrations of the nucleophiles for the chloride substitution on Pt2 in methanol solution ($I = 0.10 \text{ M}$ ($\text{LiCF}_3\text{SO}_3 + \text{NaCl}$)) at 298.15 K.

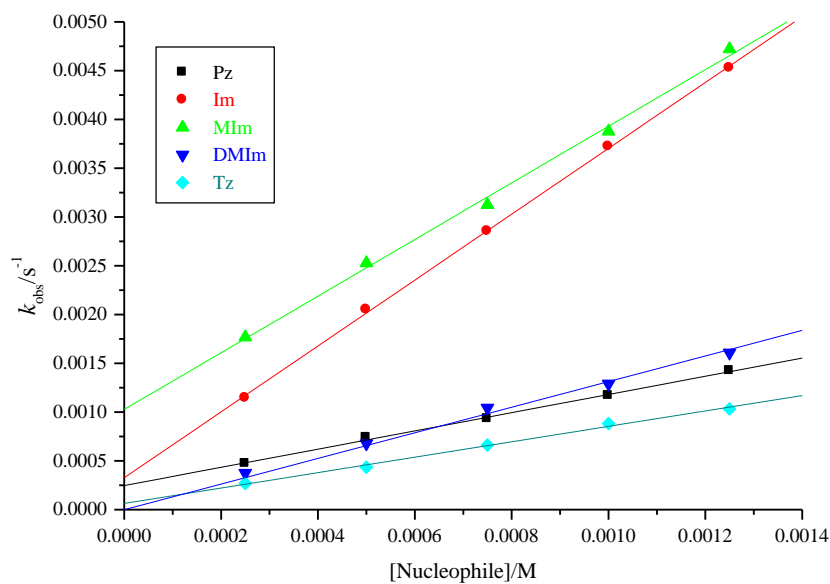


Figure B 37 Dependence of the *pseudo* first-order rate constants (k_{obs}) on the concentrations of the nucleophiles for the chloride substitution on Pt3 in methanol solution ($I = 0.10 \text{ M}$ ($\text{LiCF}_3\text{SO}_3 + \text{NaCl}$)) at 298.15 K.

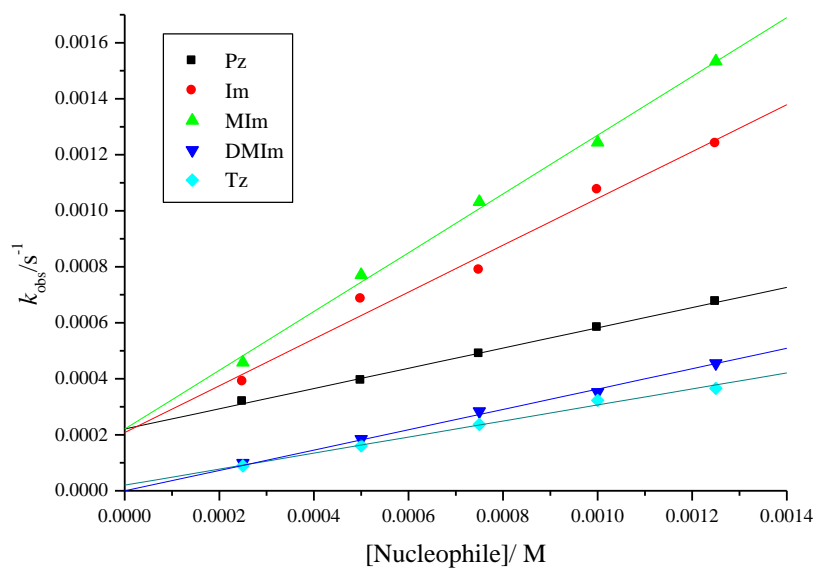


Figure B 38 Dependence of the *pseudo* first-order rate constants (k_{obs}) on the concentrations of the nucleophiles for the chloride substitution on Pt4 in methanol solution ($I = 0.10 \text{ M}$ ($\text{LiCF}_3\text{SO}_3 + \text{NaCl}$)) at 298.15 K.

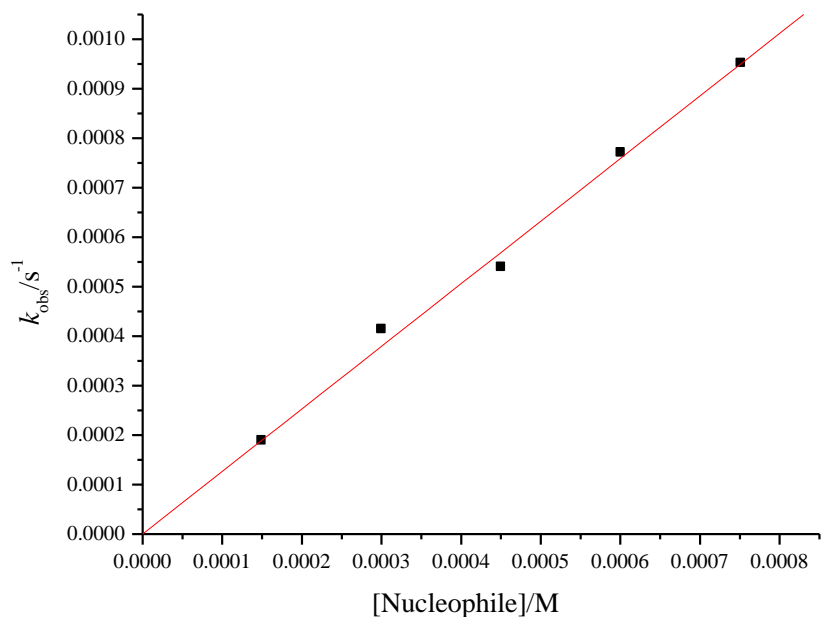


Figure B 39 Dependence of the *pseudo* first-order rate constants, (k_{obs}) on the concentration of pyrazole (0.451 mM) for the chloride substitution on Pt1 in methanol solution ($I = 0.10$ M (LiCF₃SO₃ + NaCl)) at 298.15 K.

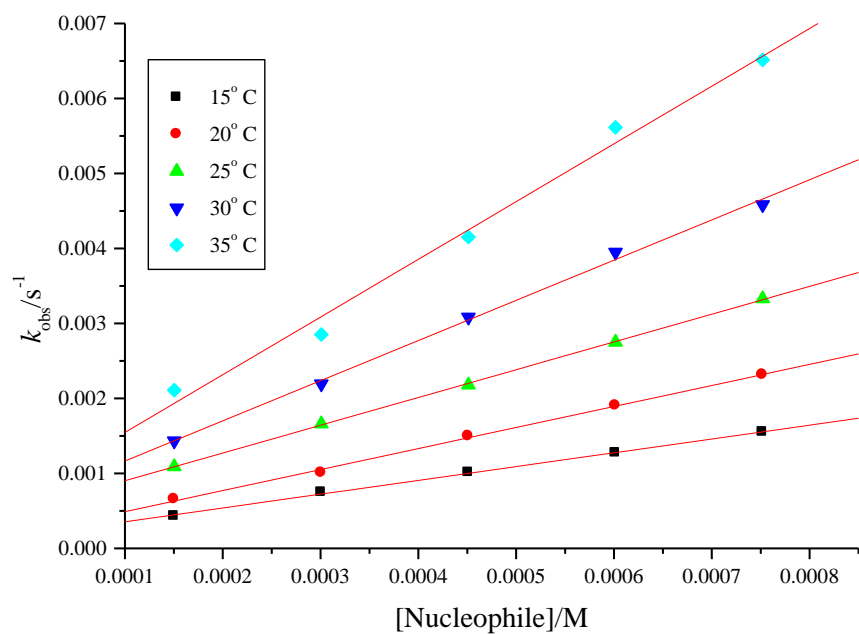


Figure B 40 Dependence of the *pseudo* first-order rate constants, (k_{obs}) on the concentrations of imidazole for the chloride substitution on Pt1 in methanol solution ($I = 0.10$ M (LiCF₃SO₃ + NaCl)) at different temperatures.

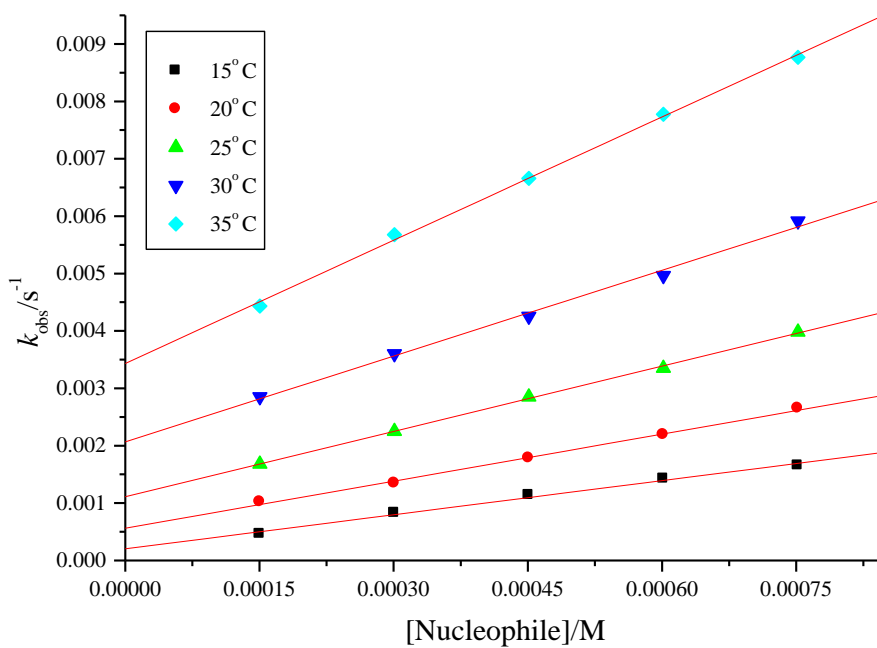


Figure B 41 Dependence of the *pseudo* first-order rate constants, (k_{obs}) on the concentrations of 1-methylimidazole for the chloride substitution on Pt1 in methanol solution ($I = 0.10 \text{ M}$ ($\text{LiCF}_3\text{SO}_3 + \text{NaCl}$)) at different temperatures.

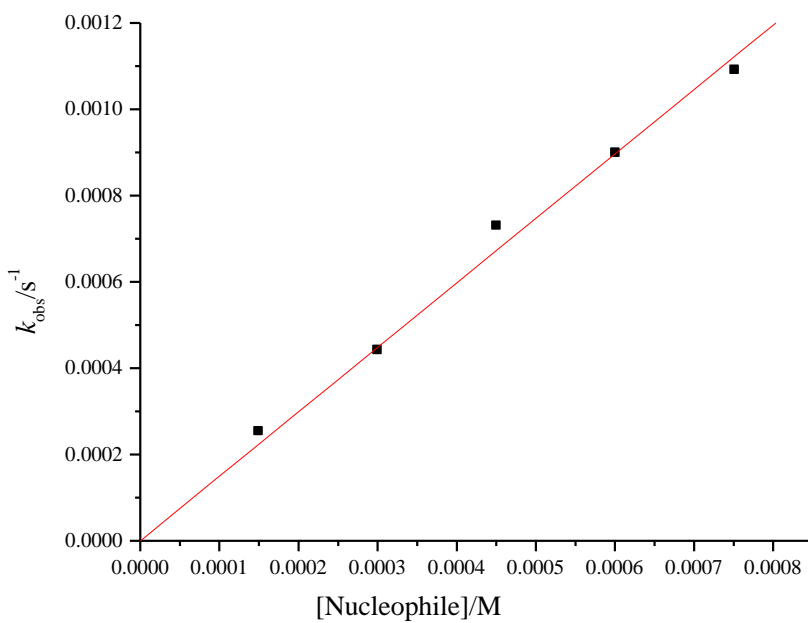


Figure B 42 Dependence of the *pseudo* first-order rate constants, (k_{obs}) on the concentration of 1,2-dimethylimidazole (0.451 mM) for the chloride substitution on Pt1 in methanol solution ($I = 0.10 \text{ M}$ ($\text{LiCF}_3\text{SO}_3 + \text{NaCl}$)) at 298.15 K.

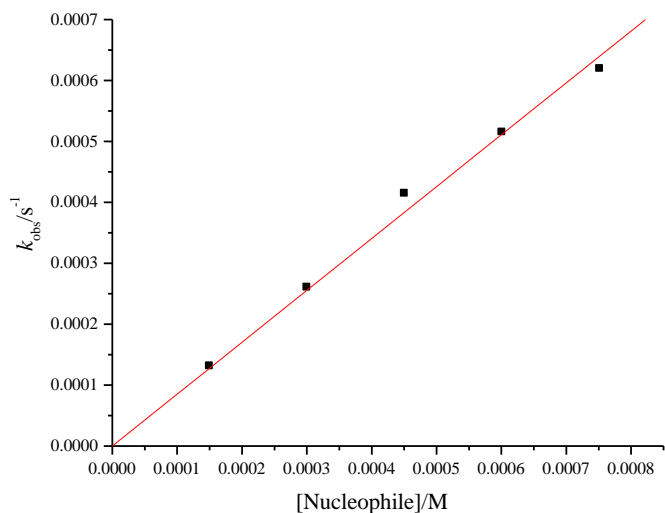


Figure B 43 Dependence of the *pseudo* first-order rate constants, (k_{obs}) on the concentration of triazole (0.451 mM) for the chloride substitution on Pt1 in methanol solution ($I = 0.10 \text{ M}$ ($\text{LiCF}_3\text{SO}_3 + \text{NaCl}$)) at 298.15 K.

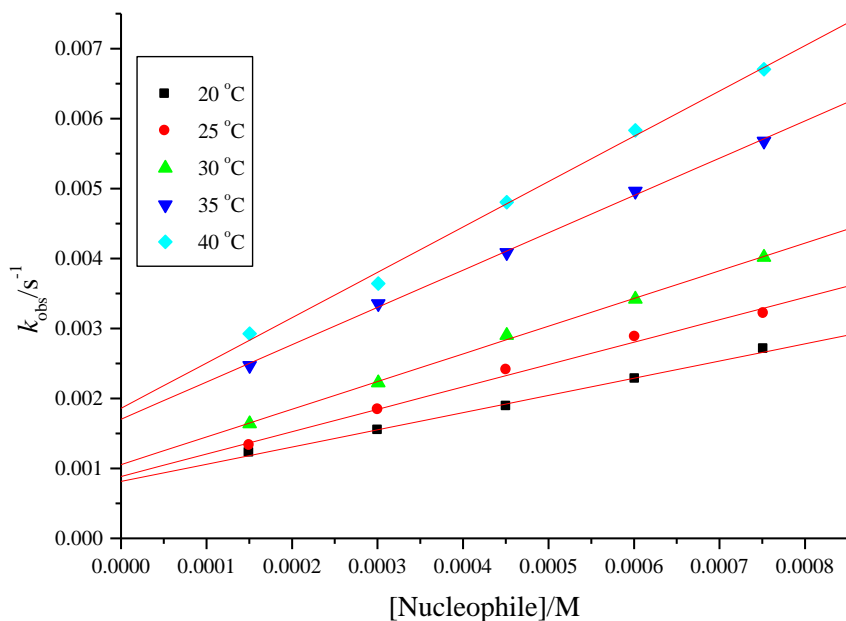


Figure B 44 Dependence of the *pseudo* first-order rate constants, (k_{obs}) on the concentrations of pyrazole for the chloride substitution on Pt2 in methanol solution ($I = 0.10 \text{ M}$ ($\text{LiCF}_3\text{SO}_3 + \text{NaCl}$)) at different temperatures.

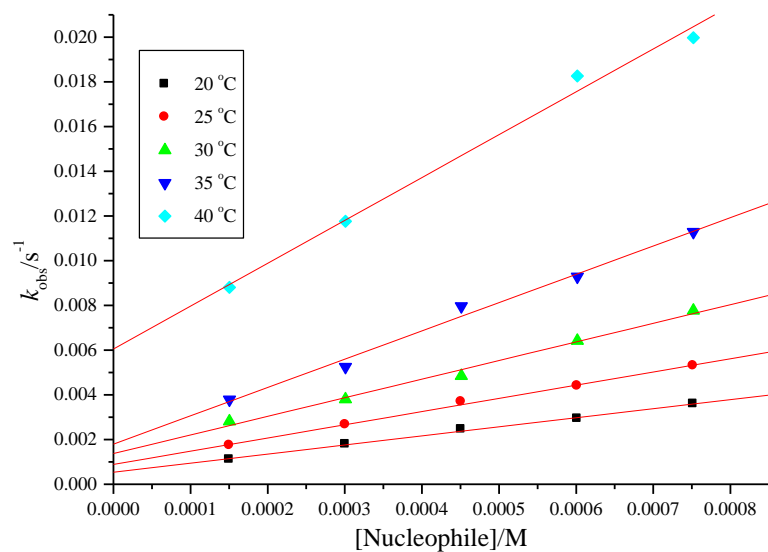


Figure B 45 Dependence of the *pseudo* first-order rate constants, (k_{obs}) on the concentrations of imidazole for the chloride substitution on Pt2 in methanol solution ($I = 0.10 \text{ M}$ ($\text{LiCF}_3\text{SO}_3 + \text{NaCl}$)) at different temperatures.

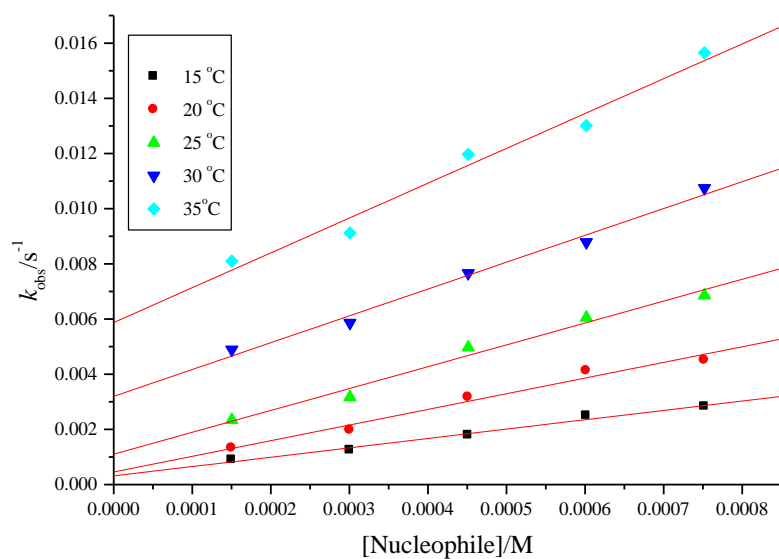


Figure B 46 Dependence of the *pseudo* first-order rate constants, (k_{obs}) on the concentrations of 1-methylimidazole for the chloride substitution on Pt2 in methanol solution ($I = 0.10 \text{ M}$ ($\text{LiCF}_3\text{SO}_3 + \text{NaCl}$)) at different temperatures.

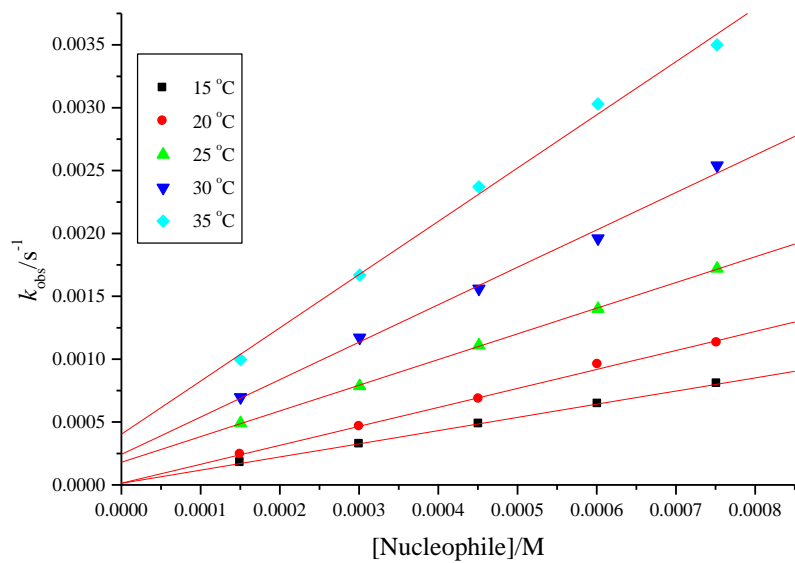


Figure B 47 Dependence of the *pseudo* first-order rate constants, (k_{obs}) on the concentrations of 1,2-dimethylimidazole for the chloride substitution on Pt2 in methanol solution ($I = 0.10 \text{ M (LiCF}_3\text{SO}_3 + \text{NaCl)}$) at different temperatures.

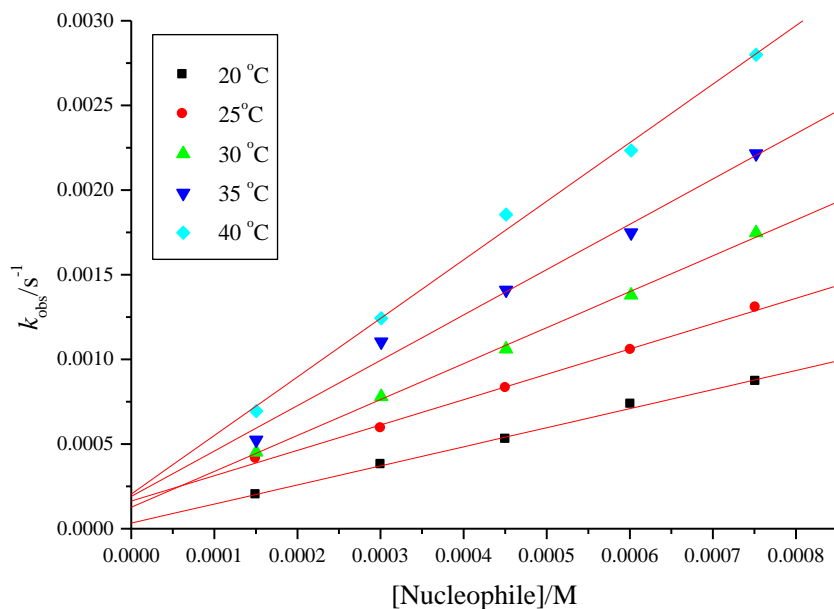


Figure B 48 Dependence of the *pseudo* first-order rate constants, (k_{obs}) on the concentrations of triazole for the chloride substitution on Pt2 in methanol solution ($I = 0.10 \text{ M (LiCF}_3\text{SO}_3 + \text{NaCl)}$) at different temperatures.

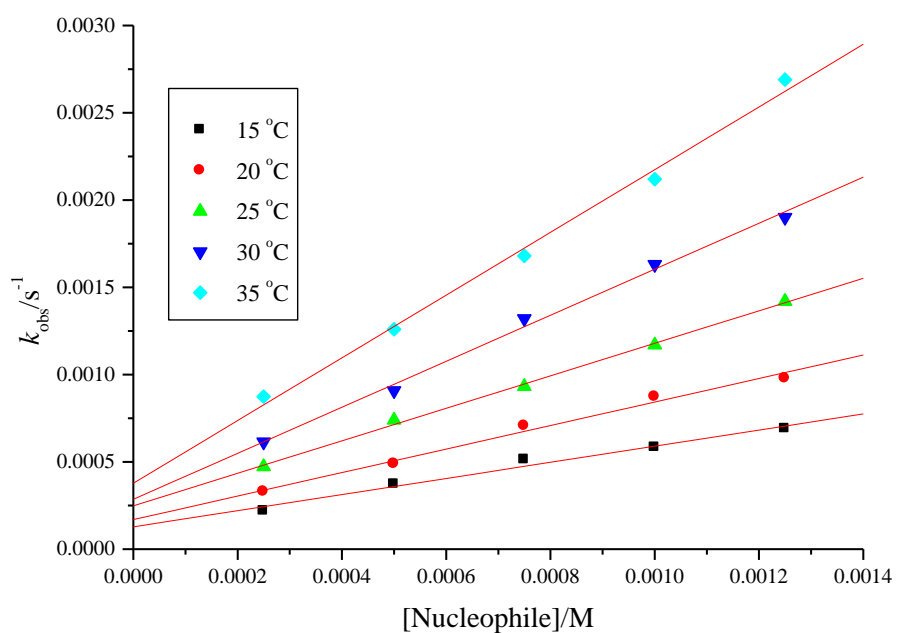


Figure B 49 Dependence of the *pseudo* first-order rate constants, (k_{obs}) on the concentrations of pyrazole for the chloride substitution on Pt3 in methanol solution ($I = 0.10 \text{ M (LiCF}_3\text{SO}_3 + \text{NaCl)}$) at different temperatures.

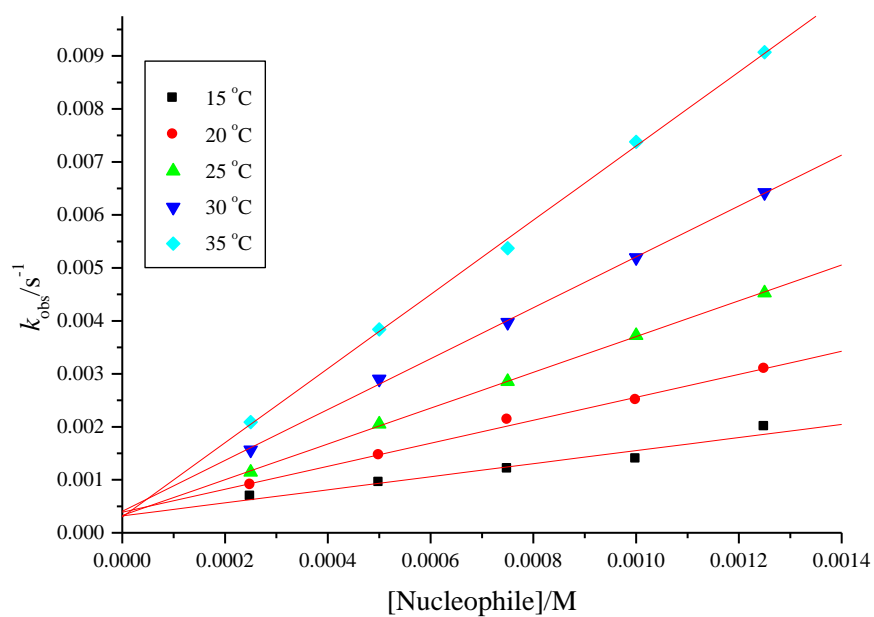


Figure B 50 Dependence of the *pseudo* first-order rate constants, (k_{obs}) on the concentrations of imidazole for the chloride substitution on Pt3 in methanol solution ($I = 0.10 \text{ M (LiCF}_3\text{SO}_3 + \text{NaCl)}$) at different temperatures.

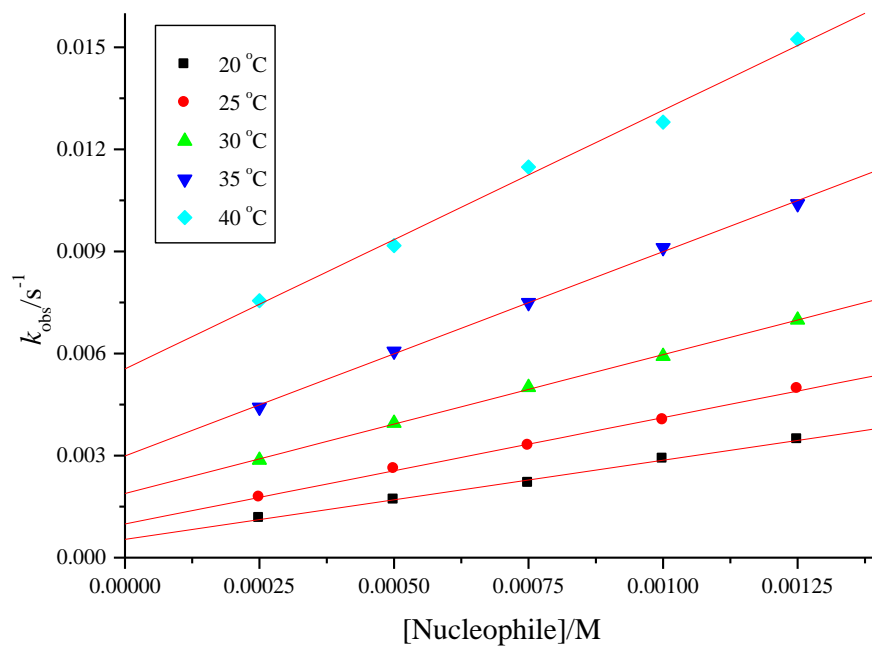


Figure B 51 Dependence of the *pseudo* first-order rate constants, (k_{obs}) on the concentrations of 1-methylimidazole for the chloride substitution on Pt3 in methanol solution ($I = 0.10 \text{ M}$ ($\text{LiCF}_3\text{SO}_3 + \text{NaCl}$)) at different temperatures.

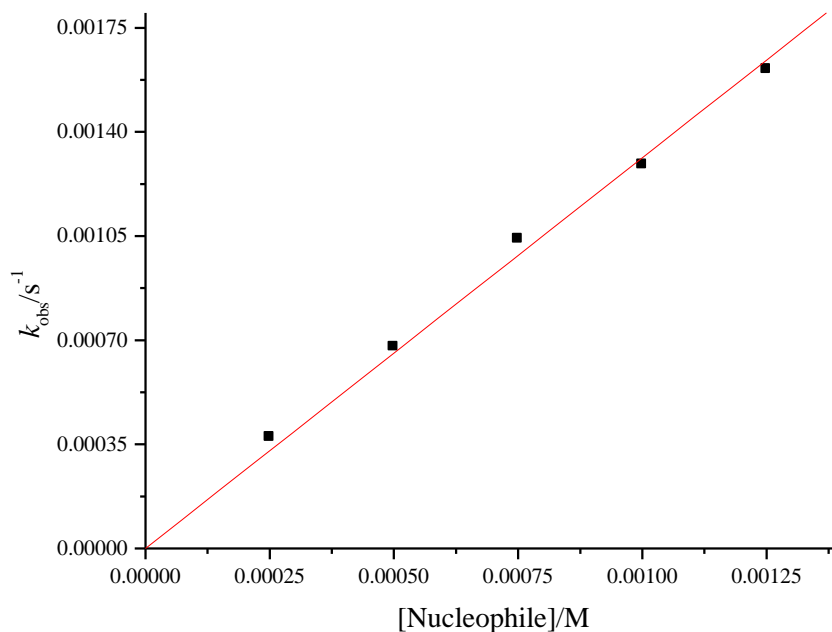


Figure B 52 Dependence of the *pseudo* first-order rate constants, (k_{obs}) on the concentration of 1,2-dimethylimidazole (0.750 mM) for the chloride substitution on Pt3 in methanol solution ($I = 0.10 \text{ M}$ ($\text{LiCF}_3\text{SO}_3 + \text{NaCl}$)) at 298.15 K.

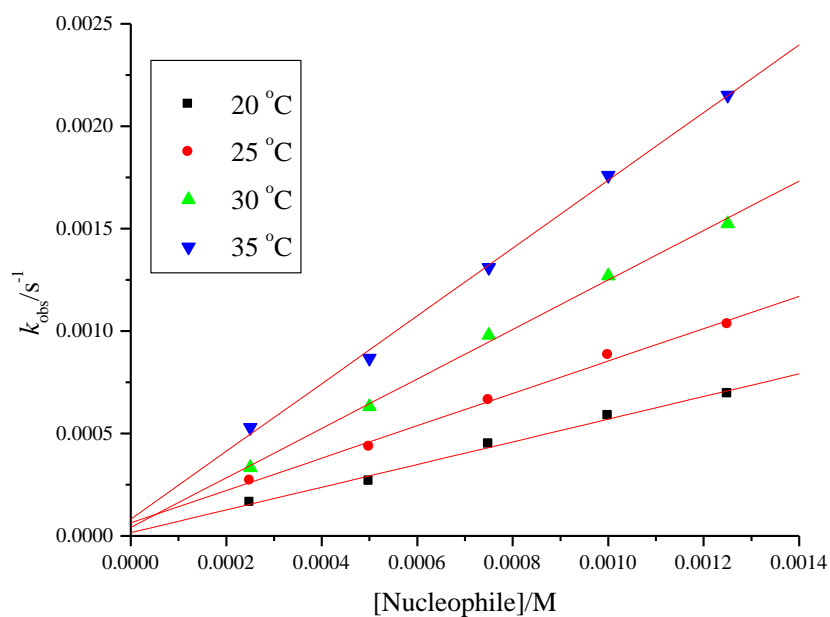


Figure B 53 Dependence of the *pseudo* first-order rate constants, (k_{obs}) on the concentrations of triazole for the chloride substitution on Pt3 in methanol solution ($I = 0.10 \text{ M}$ ($\text{LiCF}_3\text{SO}_3 + \text{NaCl}$)) at different temperatures.

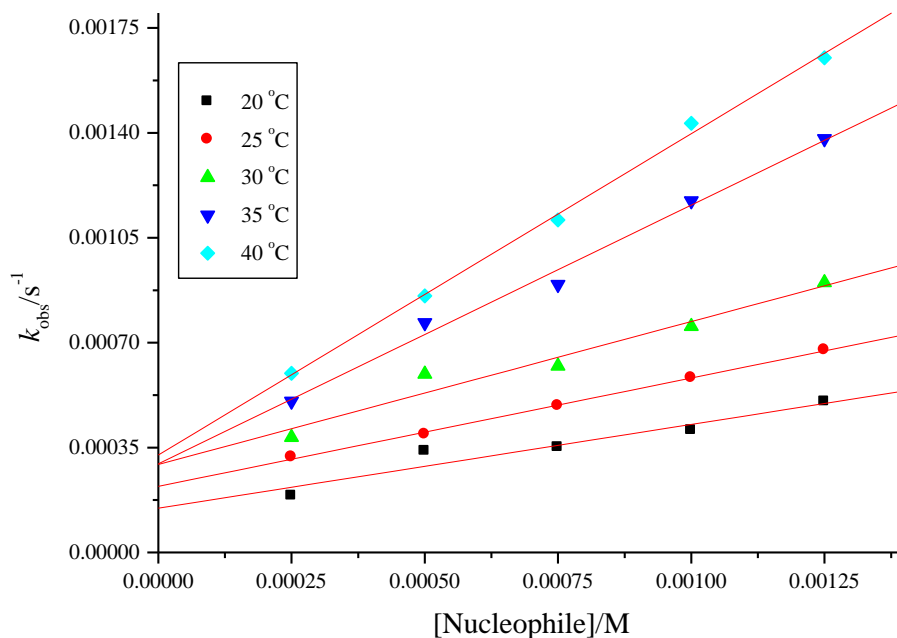


Figure B 54 Dependence of the *pseudo* first-order rate constants, (k_{obs}) on the concentrations of pyrazole for the chloride substitution on Pt4 in methanol solution ($I = 0.10 \text{ M}$ ($\text{LiCF}_3\text{SO}_3 + \text{NaCl}$)) at different temperatures.

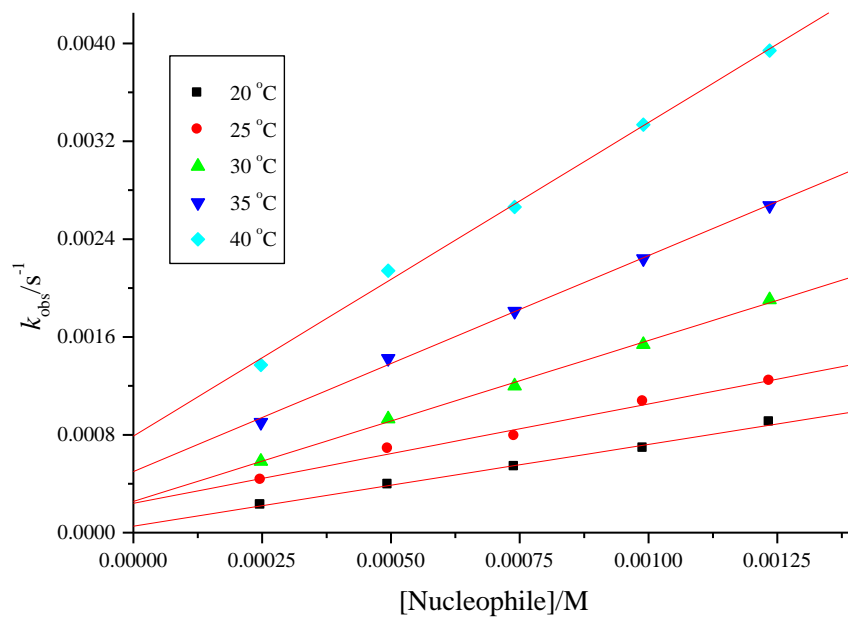


Figure B 55 Dependence of the *pseudo* first-order rate constants, (k_{obs}) on the concentrations of imidazole for the chloride substitution on Pt4 in methanol solution ($I = 0.10 \text{ M}$ ($\text{LiCF}_3\text{SO}_3 + \text{NaCl}$) at different temperatures.

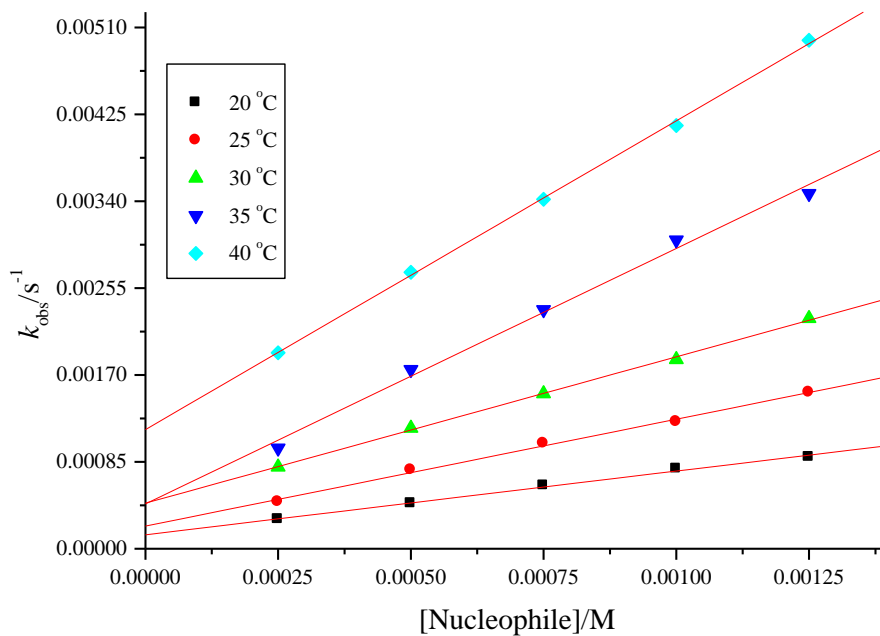


Figure B 56 Dependence of the *pseudo* first-order rate constants, (k_{obs}) on the concentrations of 1-methylimidazole for the chloride substitution on Pt4 in methanol solution ($I = 0.10 \text{ M}$ ($\text{LiCF}_3\text{SO}_3 + \text{NaCl}$) at different temperatures.

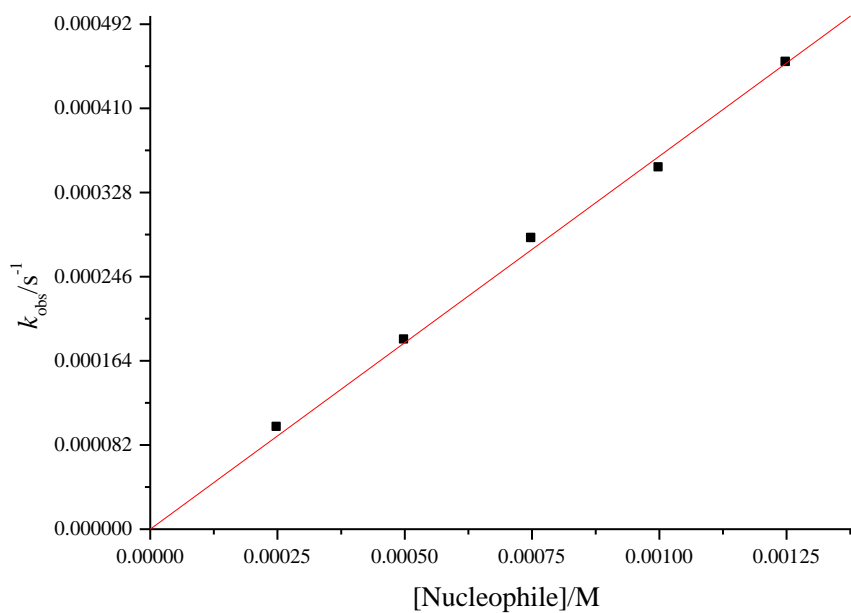


Figure B 57 Dependence of the *pseudo* first-order rate constants, (k_{obs}) on the concentration of 1,2-dimethylimidazole (0.750 mM) for the chloride substitution on Pt4 in methanol solution ($I = 0.10$ M (LiCF₃SO₃ + NaCl) at 298.15 K.

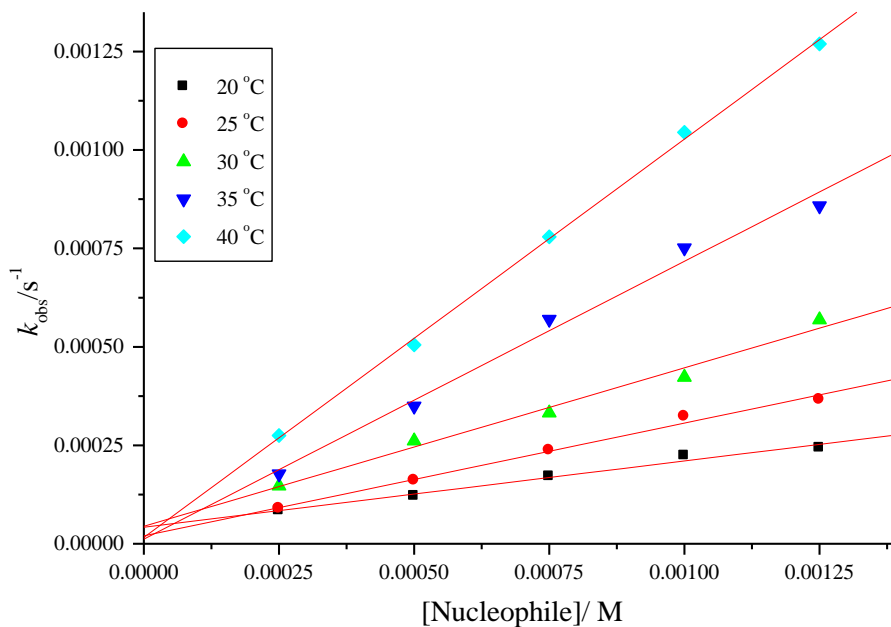


Figure B 58 Dependence of the *pseudo* first-order rate constants, (k_{obs}) on the concentrations of triazole for the chloride substitution on Pt4 in methanol solution ($I = 0.10$ M (LiCF₃SO₃ + NaCl) at different temperatures.

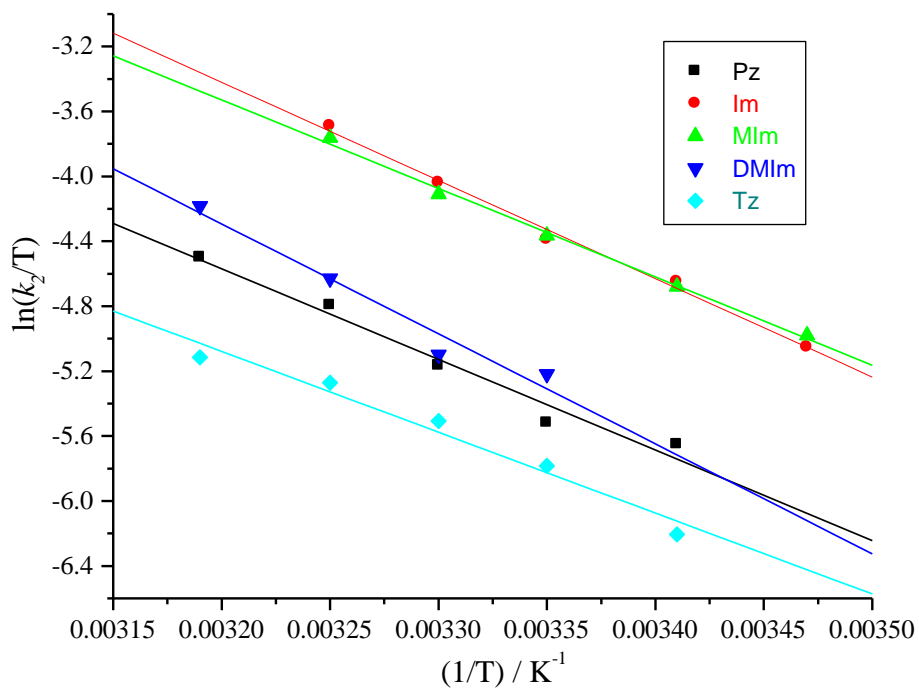


Figure B 59 Plots of $\ln(k_2/T)$ against $1/T$ for the reactions of Pt1 with the nucleophiles at various temperatures in the range 15-40 °C.

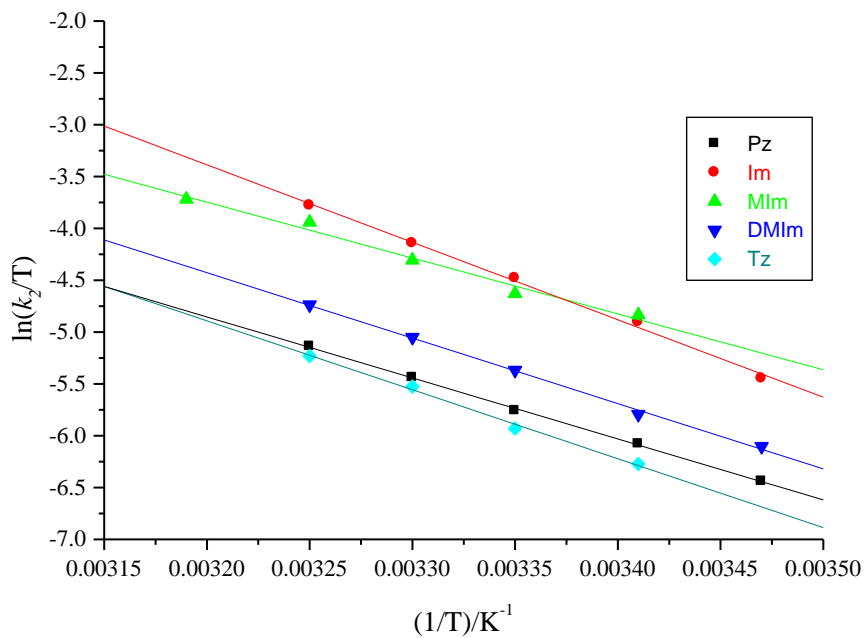


Figure B 60 Plots of $\ln(k_2/T)$ against $1/T$ for the reactions of Pt3 with the nucleophiles at various temperatures in the range 15-40 °C.

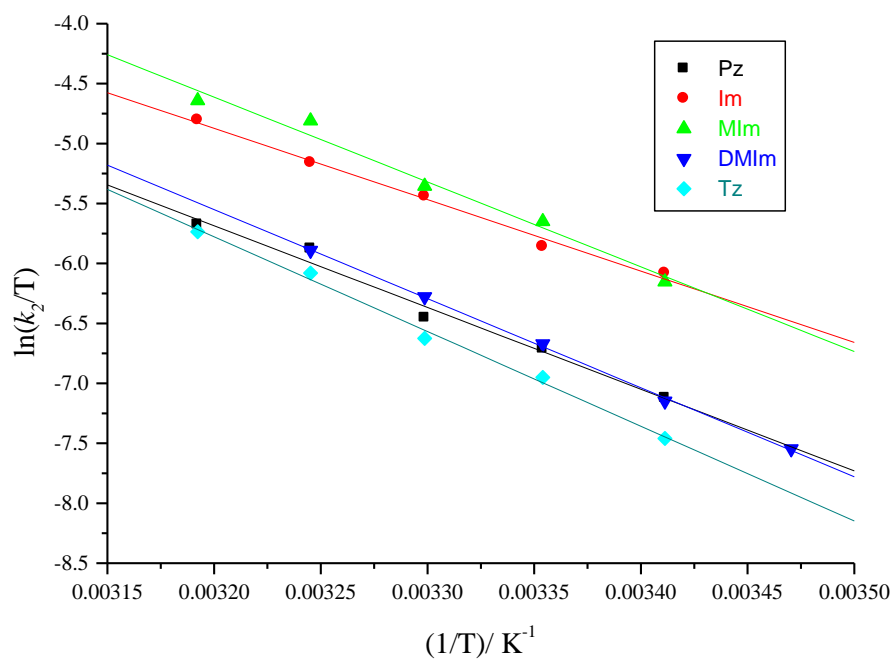


Figure B 61 Plots of $\ln(k_2/T)$ against $1/T$ for the reactions of Pt4 with the nucleophiles at various temperatures in the range 15-40 °C.

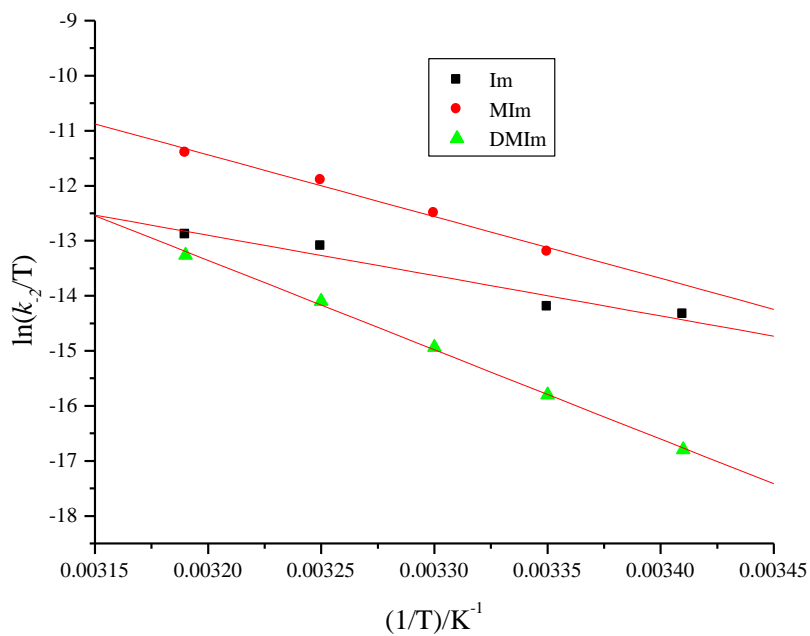


Figure B 62 Plots of $\ln(k_2/T)$ against $1/T$ for the reverse reactions of Pt1 with the nucleophiles at various temperatures in the range 20-40 °C.

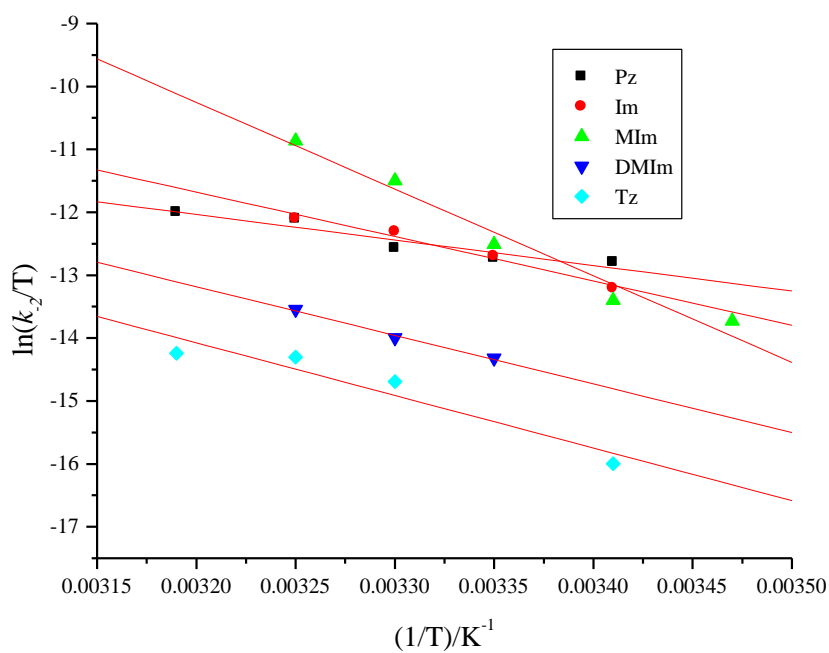


Figure B 63 Plots of $\ln(k_2/T)$ against $1/T$ for the reverse reactions of Pt2 with the nucleophiles at various temperatures in the range 15-40 °C.

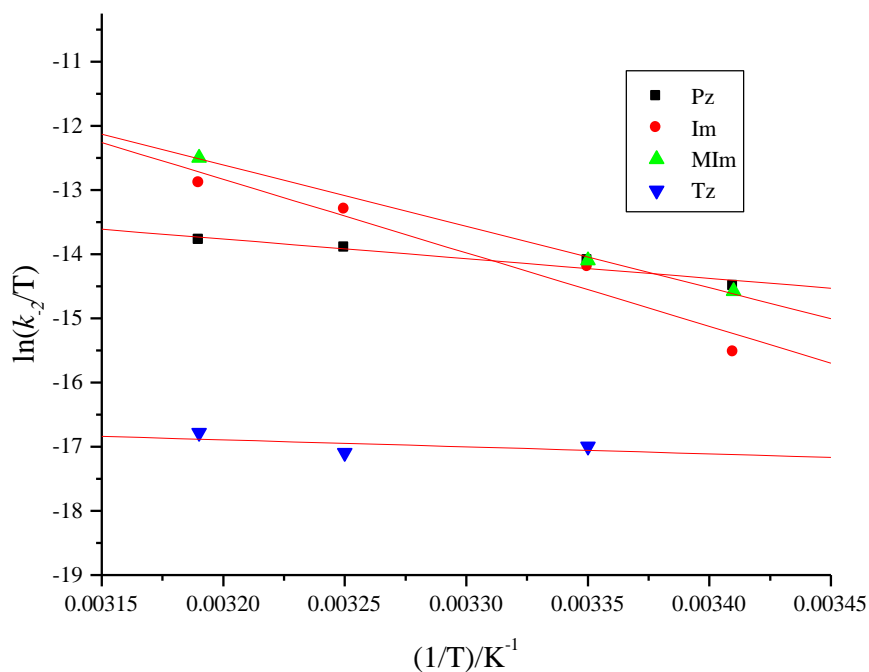


Figure B 64 Plots of $\ln(k_2/T)$ against $1/T$ for the reverse reactions Pt4 with the nucleophiles at various temperatures in the range 20-40 °C .